Assessment of an allelic series of

mouse TDP43 mutations

Thomas Ricketts (BA Oxon.)

Institute of Neurology, University College London

Mammalian Genetics Unit, Medical Research Council, Harwell

A thesis submitted for the degree of Doctor of Philosophy

May 2012

Declaration

I, Thomas Ricketts confirm that the work presented in this thesis is my own. Where information has been derived from other sources, I confirm that this has been indicated in the thesis.

Abstract

A chemical mutagenesis approach has been used to generate novel models carrying point mutations in mouse *Tardbp*, the gene encoding TDP43. TDP43 is a highly conserved protein, which in humans has been shown to be critical in amyotrophic lateral sclerosis (ALS) and frontotemporal lobar degeneration (FTLD-TDP). The aims of the work described in this thesis are to assess ten TDP43 point mutations at a behavioural, cellular and molecular level to determine whether they are functional and if they can be used as tools or models to understand TDP43 function and dysfunction in the mouse.

A comprehensive behavioural assessment of four mouse mutant lines has been completed to assess for TDP43 mutant phenotypes. Behavioural assessment has encompassed general health assessment through to motor capabilities. Tests regularly applied include SHIRPA, grip strength, rotarod and open field. All mutations have also been assessed *in vitro* using a cystic fibrosis transmembrane regulator (CFTR) add-back assay.

The data presented in this thesis characterises the nonsense mutation Q101X, and a missense mutation K160R, generated in mice. The K160R mutation lies within the first RNA recognition motif of TDP43. Compound mutants (*Tardbp*$^{Q101X/K160R}$) were also generated and assessed. Q101X causes homozygous lethality as occurs in knockout TDP43 mice. This supports the Q101X mutation as being an alternative null allele. Q101X, K160R and compound mutants (*Tardbp*$^{Q101X/K160R}$) show common neuronal associated phenotypes in the SHIRPA, including limb grasping and a softer body tone. The compound mutants (*Tardbp*$^{Q101X/K160R}$) also present novel alterations at six months as demonstrated using electron microscopy. Additionally, weight and preliminary anxiety phenotypes have been shown. Q101X heterozygotes were also crossed to transgenic SOD1^{G93A} mice to generate double mutants. Mutations in SOD1 also cause ALS. Modifying effects were assessed through behavioural characterisation with no overt interaction identified.

All missense mutations were assessed *in vitro* using a CFTR mini-gene assay. Out of ten identified point mutations, F210I, a mutation in the second RNA recognition motif of TDP43 showed deficient splicing activity. This was further confirmed *ex vivo* in mouse embryonic fibroblasts (MEFs). The F210I mutation is an RNA-binding hypomorphic allele. It shows disrupted *Tardbp* transcript regulation, supporting potential perturbations in TDP43 auto-regulation. There are also further alterations in RNA metabolism, two processes potentially

critical to ALS and FTLD-TDP. F210I demonstrates the importance of the second RNA recognition motif in RNA-binding function.

Acknowledgements

I am hugely grateful to Abraham and Lizzie for the opportunity to produce this thesis of work. There are additionally many people who I would like to thank who have contributed to my enjoyment and education during my PhD. Firstly, I would like to thank all members of Abraham's and Lizzie's labs, both past and present. I have learnt from every member of the laboratory and I have really enjoyed the discussions and interactions over the course of my PhD. I am especially grateful to Rosie and Michelle for keeping everything on track in the MLC. Thank you so much to both Silvia and Pete who have taught me many of the basics and have always been there to discuss ideas and processes. Many thanks also to Pietro and Phil for their input and contributions.

A lot of my excitement for TDP43 and the mice has been the result of the mentorship and extended discussions that I have had with Abraham over the years and I hope that I can hold on to that excitement long into the future. I would also like to express my gratitude to Lizzie for her unlimited support and expertise throughout this PhD.

I am hugely grateful to everyone at ICGEB in Trieste. In particular I am grateful to Mauricio, Emanuele and Professor Baralle ("the Prof") for their advice, guidance and friendship. I would like to acknowledge EMBO for sponsoring my short term fellowship and the MNDA for funding my PhD studentship for three years and MRC Harwell supporting my fourth year. I hope the work achieved in this PhD will lead to a strong contribution to understanding this devastating disease. These models are certainly unique and hold a lot of potential for understanding TDP43 function and dysfunction.

Finally, the work described in this thesis would not have been possible without the love and support of my family and fiancée, to whom I would like to dedicate this thesis. Their continued interest and encouragement in my studies has allowed me to fully embrace this work. Thank you to Jessica, my fiancée, for your continued advice and patience whilst we have both worked together at Harwell. I would also like to express my gratitude to my mother and brother for their continued excitement and backing. Finally I am grateful to my extended family whose support has been invaluable and for welcoming me into their home.

Contents

Figures

Tables

Glossary

ALS – amyotrophic lateral sclerosis. A form of motor neuron disease resulting in both upper and lower motor neuron degeneration.

Auto-regulation – the ability of a gene to control its own protein levels. In the case of TDP43, it binds its 3'UTR in a concentration dependent manner to regulate protein coding transcript levels. In turn this mechanism results in maintenance of steady TDP43 protein levels.

Dominant missense mutation – a change of a single nucleotide in one allele, which alters the functional output of the protein produced from that allele. This mutation causes phenotypes despite being in the presence of a wild-type allele.

ENU - *N*-ethyl-*N*-nitrosourea. A chemical mutagen which acts randomly throughout the genome causing mainly heritable point mutations.

hnRNPs - heterogeneous nuclear ribonucleoproteins. Family of proteins with extensive RNA-binding and regulation roles. They form RNA and protein complexes. TDP43 is a member of this family.

Inclusions – aggregations of proteins and other potential components in the cytoplasm or nucleus which can be stained or labelled with antibodies.

RNA metabolism – the processing of RNA through its formation (transcription), regulation, modification and degradation.

Stress granules – cytosolic aggregations of RNA bound to protein formed in cells under stressful conditions. RNA in stress granules is silenced and stabilised during the stress period.

TARDBP – Tar DNA Binding protein. Highly conserved gene encoding for the protein TDP43, located on chromosome one in humans and on chromosome four in the mouse.

TDP43 - TAR DNA Binding protein 43 kDa. Protein in which mutations cause the disease amyotrophic lateral sclerosis.

List of abbreviations

BC – backcross – term used to show the degree to which the mouse assessed has been backcrossed towards the C57BL/6J background. Figures showing the exact genetic makeup of the mice for each line are given with backcross mice being more than 50% C57BL/6J.

IVF – in vitro fertilisation – mice carrying mutations in TDP43 were rederived using stored sperm by in vitro fertilisation.

OU – outcross – term used for mice which do not have more than 50% of their genetic background belonging to a single inbred strain such as C57BL/6J.

WT – wild-type – term used for littermate control mice that do not contain any mutations in TDP43 or SOD1.

CHAPTER 1

Introduction

1.   Introduction

The work described in this thesis characterises a series of mouse TDP43 point mutations generated by chemical mutagenesis. Mice carrying a number of identified mutations have been derived and assessed to determine the functionality and impact of these mutations. Multiple TDP43 models have been published whilst undertaking this work with varying degrees of success in modelling TDP43 proteinopathies. The ENU mutants presented here provide alternative tools to understand the function and potential dysfunction of TDP43.

1.1.   ENU approach

1.1.1.   Molecular mechanism

N-ethyl-*N*-nitrosourea (ENU) is the preferred chemical mutagen because it creates stochastic heritable point mutations throughout the genome and is highly potent (Russell *et al.*, 1979). It is used to generate mutations in multiple model organisms ranging from *Drosophila melanogaster* through to *Mus musculus* and is a complementary approach to knock out strategies or transgenic modification of model organisms. The stochastic manner through which it acts on individual bases throughout the genome mean it is hypothesis generating in producing random point mutations.

ENU acts as an alkylating agent that transfers its ethyl group onto nitrogen and oxygen atoms of nucleotides. This forms a DNA adduct which during cell replication results in misreading / mutating the nucleotide at the specific base containing the adduct (Justice *et al.*, 1999). The result is an individual base change (or in rare cases a small region deletion) that creates a point mutation. In mice, spermatogonial stem cells are highly mutagenized by ENU which initially depletes these cells. Remaining stem cells repopulate by mitosis and produce sperm by meiosis (Bielas & Heddle, 2000; O'Neill, 2000). The resultant sperm each carry multiple ENU mutations, with each sperm carrying a unique array of mutations to the other. Each offspring from the original mutagenized animal therefore carries a unique array of mutations.

Depending on the location of the point mutation, many potential outcomes are possible. Within coding regions, missense mutations may change the encoded amino acid resulting in a gain or loss of function effect on the protein. Nonsense mutations will produce truncated protein products. Mutations outside coding regions can also impact on promoter activity and splicing, resulting in multiple potential mechanisms in altering gene function.

1.1.2.   Identifying mutations at MRC Harwell / RIKEN

To utilise ENU in the mouse, multiple centres around the world employ ENU mutagenesis screens. The major centre in the UK is MRC Harwell applying both forward and reverse genetic approaches to identify novel mutants generated through ENU mutagenesis. In the forward genetics approach, ENU mutagenized offspring (G1 mice) from a mutagenized male (G0 mouse) can be phenotyped for dominant mutations. Alternatively, through a breeding programme using the G1 males (G0 male is that injected with ENU, G1 are the offspring), G3 mice can be screened for recessive mutations, as reviewed elsewhere (Acevedo-Arozena *et al.*, 2008).

The work described in this thesis has adopted a complementary reverse genetics approach. At MRC Harwell a programme to generate an archive of mutations continues to run. ENU mutagenized sperm from G1 offspring of ENU mutagenized males are harvested with matching DNA samples. Over 10,000 sperm samples have been collected from males each carrying unique arrays of ENU mutations and all carrying multiple ENU mutations at a rate of approximately one mutation per one and a half mega bases (Quwailid *et al.*, 2004). The rate has been maximised through balancing the toxic effects of ENU versus that which efficiently produces the most mutations in viable mice. ENU injection produces a period of temporary sterility following treatment and is also carcinogenic. The aim is to treat males with a dose where there is a low sterility period (usually three months) with an extended period of time for the male to produce the first generation of offspring (G1 mice) which will each carry multiple unique ENU mutations. Any autosomal gene can be screened for mutations in the matching DNA samples by high resolution melting (HRM). In HRM, a polymerase chain reaction (PCR) product is heated beyond the temperature that separates the double stranded DNA. This temperature will slightly vary depending on the DNA sequence, being different between two strands with and without a mutation. This is detected using fluorescent dyes which bind the double stranded DNA and therefore will show different melt curves for DNA sequences being

separated at different temperatures. Dominant mutations on the X chromosome in female G1 mice can also be assessed, however only male sperm and tissue samples are stored in the archive. Once desired mutations are identified the matching sperm can be used to generate mice carrying these mutations through *in vitro* fertilisation (IVF).

The archive at Harwell was screened prior to the beginning of my PhD for mutations in all coding *Tardbp* exons. A non-sense and two missense mutations were identified as shown in Figure 1.1. In order to expand the allelic series, one and a half years into my PhD, all coding exons in the RIKEN (Japan) ENU archive were also screened identifying a further seven missense mutations. A summary of the mutations and the conservation of those residues are given in Figure 1.1.

Figure 1.1: TDP43 mutations. Figure showing mouse TDP43 protein domains with point mutations identified from the Harwell and RIKEN ENU archives. Protein structure domains given: NLS, Nuclear Localisation Signal, NES, Nuclear Export Signal, RRM1, RNA Recognition Motif 1, RRM2, RNA Recognition Motif 2, Glycine rich region. The mutations identified from the MRC Harwell archive are shown in red with the mutations identified from the RIKEN ENU archive in black. Residue conservation across species is given for each mutation.

1.1.3. Mutations studied as mouse lines

Whilst working to produce this thesis the timing of mutation identification has partly determined which mutations have been studied and which mice rederived. When the Harwell archive mutations were identified there were no published animal models and very little was known functionally about TDP43, so all Harwell mutations were rederived as mice for

phenotypic assessment. Sperm carrying the Q101X and K160R mutations were successfully rederived by IVF with ensuing mouse generation. These mice were partially backcrossed to remove other ENU mutations. They were not backcrossed to become fully congenic to remove all other ENU mutations for this study due to time constraints, but littermate controls were used in phenotyping tests as the most suitable control. Whilst this study has taken place, the mutant lines have been backcrossed onto a congenic C57BL/6J background. Models used to estimate mutation effects also show that despite carrying multiple mutations (in the founder mice, this is estimated at 30-50 functional mutations), phenotypes are usually the result of an individual ENU point mutation (Keays *et al.*, 2006). The T153A mutation from Harwell proved difficult to rederive by IVF (taking over one and a half years) and continues to be phenotyped. Due to this delay it is not presented in this thesis.

The expanded array of mutations supplemented by those identified at RIKEN have all been characterised *in vitro* and to early stages *in vivo* based on results. Full behavioural characterisation of these lines was not possible in the timeframe of this PhD. However, data collected warrant extensive behavioural characterisation in the future.

With nine missense and one nonsense mutation identified in *Tardbp* a large number of alleles are available to use in further understanding mouse TDP43 function. The mutations are present in all major characterised domains of TDP43 and may have partial to complete loss of function, gain of function or dominant negative effects. The aim of the work described in this thesis is to assess this functionality behaviourally and molecularly with these mice being complementary to knock out and transgenic gene overexpressing mice. They also provide a framework in which the mutations are expressed endogenously at the right time, in the right place and at the correct level providing a complementary approach to study this gene. This is particularly relevant for TDP43 as it has been shown that altering the levels of wild-type TDP43 (both increasing and decreasing) in various cellular and animal models is toxic as reviewed elsewhere (Joyce *et al.*, 2011). Complete absence of TDP43 is not permissive to survival in mammalian organisms and high overexpression is toxic. This is discussed in detail when assessing alternative models, showing that an ENU approach allows for assessment of the functional effects of mutations without being uncertain of alternative effects, such as overexpression.

1.2. Amyotrophic lateral sclerosis and frontotemporal lobar degeneration

1.2.1.   Pathology

Jean-Martin Charcot initially described amyotrophic lateral sclerosis (ALS) in 1869. Usually striking in mid-life, ALS is a rapidly progressive motor neuron disease affecting both upper and lower motor neurons. Upper motor neurons project from the motor cortex down the spinal cord and lower motor neurons project to muscle. In humans, ALS usually strikes around mid-life carrying a lifetime risk of approximately 1 in 1000. Once initial symptoms are detected and the disease diagnosed, there is a rapid progression to end stage in typically three years due to respiratory failure. During the disease course, motor neurons which control voluntary movement are lost leading to muscle weakness and atrophy resulting in paralysis and death. So far, only riluzole treatment appears to extend lifespan by a few months (Miller *et al.*, 2007). More recently, increasing clinicopathological data supports ALS being part of a spectrum of disease with frontotemporal dementia in which inclusions are ubiquitin positive and tau negative (FTLD-TDP). This is one of the two major groups of frontotemporal dementia, FTD (the other contains tau positive inclusions) which form the second most common form of young onset dementia, which classically presents with frontal and temporal atrophy as well as hyper metabolism. Distinct subtypes of the spectrum of disease include language variant semantic dementia, a behavioural variant form and progressive non-fluent aphasia which can all overlap with motor neuron disease, as reviewed (Seelaar *et al.*, 2011). Around 50% of ALS patients develop cognitive impairments (Lomen-Hoerth *et al.*, 2003) and cosegregation has been shown within families (Talbot & Ansorge, 2006). As well as clinical overlap, these disease share underlying pathology surrounding the alteration of TDP43 protein which undergoes a number of changes including mislocalisation, hyperphosphorylation, polyubiquitination, cleavage and altered solubility. These changes are discussed in depth in section 1.4.

In ALS and FTLD-TDP there are a number of hallmarks accompanying selective neuron degeneration. Within motor neurons, degeneration is accompanied by changes in axon structure. This can include disruption of neurofilaments which leads to protein accumulation and also alterations in critical components such as tubulin, dynein and dynactin in which

disruptions have been shown to result in motor disorders with altered axon transport (Hafezparast *et al.*, 2003; Puls *et al.*, 2003). Losses of synaptic vesicles have been shown to be an early event in pathogenesis as well (Hirano, 1996). The proteasome fails to function effectively due to misfolded ubiquitinated labelled proteins "clogging" up the system as well as evidence for endoplasmic reticulum stress (Petrucelli & Dawson, 2004). Critically, mitochondrial dysfunction within motor neurons, which can also promote motor neuron death, also occurs (Manfredi & Xu, 2005). Motor neurons are also hyper-activated resulting in elevated intracellular calcium which activates programmed cell death. The exact nature of the cause / effect changes within motor neurons continues to be established.

Motor neuron cell death is also marked by the elevation of stress responses in surrounding cells. Activated astrocytes have been shown to be critical in the progression of the disease producing unidentified factors which are toxic to motor neurons (Nagai *et al.*, 2007; Haidet-Phillips *et al.*, 2011). Microglia and oligodendrocytes may also be crucial in mediating disease. Within capillary endothelial cells there is also a loss of tight junctions resulting in microhaemorrhages in the spinal cord which also contribute to motor neuron degeneration. Patients also show increased levels of glutamate excitotoxicity (Shaw & Ince, 1997). Simultaneously, there is an inflammatory response (Graves *et al.*, 2004). Overall, there are multiple perturbations associated with motor neuron degeneration. A summary schematic of changes and stresses which may cause or contribute to neuronal cell death is given in Figure 1.2.

Figure 1.2: Mechanisms contributing to motor neuron dysfunction and death. Summary schematic taken from (Ilieva *et al.*, 2009) showing the environment of motor neurons and the known changes which can contribute to motor neuron death. In the example schematic, mutations in SOD1 are causative however mutations in other genes which cause ALS result in similar motor neuron changes and ultimately death.

1.2.2. Genetics

The majority of cases of ALS and FTLD-TDP present sporadically. Most of these cases show underlying TDP43 pathology, excluding a minority of cases where mutations in some known (superoxide dismutase 1, *SOD1* and fused in sarcoma, *FUS*) and unknown genes cause the disease. For familial cases of ALS and FTD, approximately 10% and 30% of cases respectively are thought to be inherited. *SOD1* was one of the first genes to be identified as having mutations causative of ALS (Deng *et al.*, 1993). More than 150 mutations have now been identified within *SOD1* accounting for around 20% of familial cases. Later in 2006, mutations in TDP43 were also found to be causative of ALS with rare mutations also causing FTLD-TDP.

TDP43 mutations cause approximately 4% of familial ALS (fALS) cases (Gitcho *et al.*, 2008; Sreedharan *et al.*, 2008). Since then, many other genes have been found to cause ALS, atypical forms of ALS and FTLD-TDP. Within FTLD-TDP, mutations in progranulin (*GRN*), as discussed elsewhere (van Swieten & Heutink, 2008) and the recently identified chromosome 9 open reading frame 72 (*C9ORF72*) account for most cases with rarer causative mutations in valosin containing protein (*VCP*), *TDP43* and other unknown factors also causing disease. Mutations in identified causal and risk factor ALS and atypical motor neuron disease genes are given in Table 1.1. In all non-*SOD1* and *FUS* cases, TDP43 is pathologically altered as described in section 1.4.

Alsin	*ALS2*	(Hadano *et al.*, 2001; Yang *et al.*, 2001)
Angiogenin (risk factor and potentially causative)	*ANG*	(Greenway *et al.*, 2006; Wu *et al.*, 2007; Gellera *et al.*, 2008; Paubel *et al.*, 2008)
Ataxin 2 (risk factor)	*ATX2*	(Elden *et al.*, 2010; Daoud *et al.*, 2011; Van Damme *et al.*, 2011)
Chromosome 9 open reading frame 72	*C9ORF72*	(DeJesus-Hernandez *et al.*, 2011; Renton *et al.*, 2011)
Dynactin 1 (risk factor)	*DCTN1*	(Puls *et al.*, 2003; Munch *et al.*, 2004; Vilarino-Guell *et al.*, 2009)
Elongator protein 3 (risk factor)	*ELP$_3$*	(Simpson *et al.*, 2009)
Fused in sarcoma	*FUS*	(Kwiatkowski *et al.*, 2009; Vance *et al.*, 2009; Corrado *et al.*, 2010; Hewitt *et al.*, 2010; Waibel *et al.*, 2010; Yan *et al.*, 2010)
Neurofilament protein, heavy polypeptide (risk factor)	*NEFH*	(Figlewicz *et al.*, 1994; Al-Chalabi *et al.*, 1999)
Optineurin	*OPTN*	(Maruyama *et al.*, 2010; Del Bo *et al.*, 2011; van Blitterswijk *et al.*, 2012)
Peripherin (risk factor)	*PRPH*	(Gros-Louis *et al.*, 2004; Corrado *et al.*, 2011)
Senataxin	*SETX*	(Chen *et al.*, 2004; Avemaria *et al.*, 2011)
Superoxide dismutase 1	*SOD1*	(Deng *et al.*, 1993; Rosen, 1993) more than 150 missense mutations identified in *SOD1*
Tar DNA binding protein 43	*TDP43*	(Kabashi *et al.*, 2008; Kuhnlein *et al.*, 2008; Sreedharan *et al.*, 2008) more than 30 missense mutations identified in *TDP43*
Ubiquilin *2*	*UBQLN2*	(Deng *et al.*, 2011)
Valosin containing protein	*VCP*	(Johnson *et al.*, 2010)
VAMP (vesicle-associated membrane protein)-associated protein B and C	*VAPB*	(Nishimura *et al.*, 2004; Landers *et al.*, 2008; Chen *et al.*, 2010)

Table 1.1: Typical and atypical ALS causative genes. Table showing the genes in which mutations increase susceptibility or that cause typical and atypical forms of ALS. Genes highlighted in blue have characterised roles in RNA processing or in the case of *C9ORF72*, may disrupt RNA processing due to a hexanucleotide repeat expansion.

Mutations in genes with a variety of known functions may increase the risk or directly result in atypical-ALS, ALS and FTLD-TDP. Genes in which mutations may increase the risk of ALS include *ANG*, *ATX2*, *DCTN1*, *ELP₃*, *NEFH*, and *PRPH*. *ANG* mutations have been identified in familial and sporadic ALS cases, although there is no conclusive proof that the variants segregate with disease as the families studied were not large enough. Several mutations have also been shown to increase the risk of ALS particularly in Irish and Scottish populations (Greenway *et al.*, 2006). *ANG* is a member of the pancreatic ribonuclease A superfamily with RNase activity of *ANG* being important for its angiogenic activity. *ATX2* has been shown as a strong modifier of TDP43 mediated toxicity in yeast and animal models with the two proteins binding in an RNA-binding dependent manner (Elden *et al.*, 2010). Several studies have shown that an intermediate number of CAG repeat expansions in *ATX2* (around 29 repeats) is associated with increased risk of ALS. *DCTN1* is a subunit of dynactin, a macromolecular complex binding both microtubules and cytoplasmic dynein and as such, impacts on multiple cell processes via axonal transport. Mutations in *DCTN1* are rare, however can increase susceptibility to ALS (Munch *et al.*, 2004) with mutations having been identified in sporadic and familial cases of ALS. *ELP₃* has a characterised role as the catalytic subunit of the histone acetyltransferase elongator complex with a multistage association study for ALS across three populations showing linkage to this locus (Simpson *et al.*, 2009). Disrupted neurofilament processing is a prevalent feature of ALS, and *NEFH* motif deletions are rare but can be risk factors for ALS (Al-Chalabi *et al.*, 1999). Considering the rare nature of mutations in *NEFH*, disrupted neurofilaments and altered structure may modify disease. Furthermore, a deletion identified in *PRPH*, a type III intermediate filament protein similar to neurofilaments also supports increased susceptibility to ALS, (Gros-Louis *et al.*, 2004). Independent mutations have been identified in two sporadic cases (Gros-Louis *et al.*, 2004) however further data is required to rule out these being rare polymorphisms. Overall, there are a variety of genes in which mutations appear to enhance the risk of ALS. However, it can be difficult to determine whether mutations cause disease outside of individual cases unless there is additional data such as familial segregation supporting this effect.

As well as mutations increasing ALS susceptibility, mutations in *ALS2*, *C9ORF72*, *FUS*, *OPTN*, *SETX*, *SOD1*, *TDP43*, *UBQLN2*, *VCP* and *VAMP* cause various forms of ALS. When considering known gene function, *ALS2* is a guanine nucleotide exchange factor for the small GTPase *RAB5* with established roles in endosomal trafficking, as shown in *ALS2* deficient mice (Devon *et al.*, 2006). Mutations have been shown to cause juvenile onset ALS in multiple studies. In autosomal dominant frontotemporal dementia and / or ALS families, two studies have very

recently identified a heterozygous expanded intronic hexanucleotide repeat (GGGGCC) in *C9ORF72*. This gene has not yet been functionally characterised, however the identified repeat expansion is the most common causal variant of ALS and FTLD-TDP identified to date, causing almost 40% of familial ALS cases as well as sporadic cases. Like *C9ORF72*, mutations in *FUS* cause both ALS and FTLD (however with FUS positive, TDP43 negative inclusions). FUS protein is highly similar to TDP43 with multiple established roles in RNA metabolism, with the two proteins having been shown to function in the same pathways in *D. melanogaster* (Lanson *et al.*, 2011; Wang *et al.*, 2011). Rare mutations in *OPTN* also cause ALS. *OPTN* interacts with a variety of proteins with anticipated roles in cellular morphogenesis, membrane trafficking, vesicle trafficking, and transcription activation (Faber *et al.*, 1998; Hattula & Peranen, 2000; Moreland *et al.*, 2000). Mutations in *SETX* have been found to be causative of juvenile ALS (Chen *et al.*, 2004) as rare autosomal dominant mutations. SETX protein contains a helicase domain and has been shown to interact with transcription and RNA processing proteins (Suraweera *et al.*, 2009). More recently, five mutations in X-linked *UBQLN2* have been identified as causative of familial forms of ALS (Deng *et al.*, 2011). *UBQLN2* is a member of the ubiquitin-like protein family. Similarly, heterozygous mutations have been identified in ALS families using exome sequencing in *VCP*, a member of the AAA+ ATPase family of proteins. Mutations in VCP also cause FTLD-TDP and inclusion body myopathy with paget disease of bone (IBMPD), in both cases causing TDP43 pathology. Finally, rare mutations have also been identified in *VAPB* protein which has known roles in the unfolded protein response (Nishimura *et al.*, 2004).

Genes associated with ALS and FTLD-TDP have multiple known and unknown functions. Furthermore, many genes which contribute towards and cause ALS and FTLD-TDP remain to be identified. This is further being addressed through genome wide association studies which aim to provide a tool to identify critical loci or provide a reference point for investigation (Schymick *et al.*, 2007). There are limitations in the ability to identify causative alleles using this approach which include phenotypically variable syndrome presentation, different disease causing alleles within a gene, optimal statistical analysis and the importance of rare variants. However, despite the variation in known and unknown genes associated with disease, there is convergence of multiple pathways in selective neuronal degeneration with TDP43 pathology. Broadly, current data supports many characterised functions appearing to show RNA metabolic roles or protein stability / degradation functions. For those genes with central roles within RNA metabolism multiple potential perturbations may occur. In *C9ORF72*, a hexanucleotide expansion drives disease and this is the most common identified causal variant

of familial and sporadic ALS (Majounie *et al.*, 2012; Rademakers, 2012). Outside of *C9ORF72*, *FUS* and *TDP43* have been shown to interact in the same pathways with *TDP43* acting upstream of *FUS* in having multiple roles in RNA metabolism (Wang *et al.*, 2011). This has extended the data for a subset of ALS and FTLD-TDP causative genes that RNA biology may be critical to pathology with mutations potentially altering these RNA roles in driving disease. Alternative genes in which mutations cause pathology such as *VCP* and *UBQLN2* also have established roles in protein folding and degradation pathways. With clusters of genes in which causative mutations surround various known functions further understanding is required. There is emerging support for RNA metabolism being critical to TDP43 perturbations which is pathologically altered in nearly all ALS and FTLD-TDP cases irrespective of the causative gene in which the mutation resides. This may be anticipated considering the extensive interaction between TDP43 and the transcriptome.

1.3. TDP43 biology pre 2006

1.3.1. *Tardbp* encoding transcripts

The protein TDP43 is encoded for by the gene *TARDBP*. In humans, this gene lies on chromosome 1. However, in the mouse it is on chromosome 4. Its RNA expression profile is given in Figure 1.3 showing that its transcripts are ubiquitously expressed.
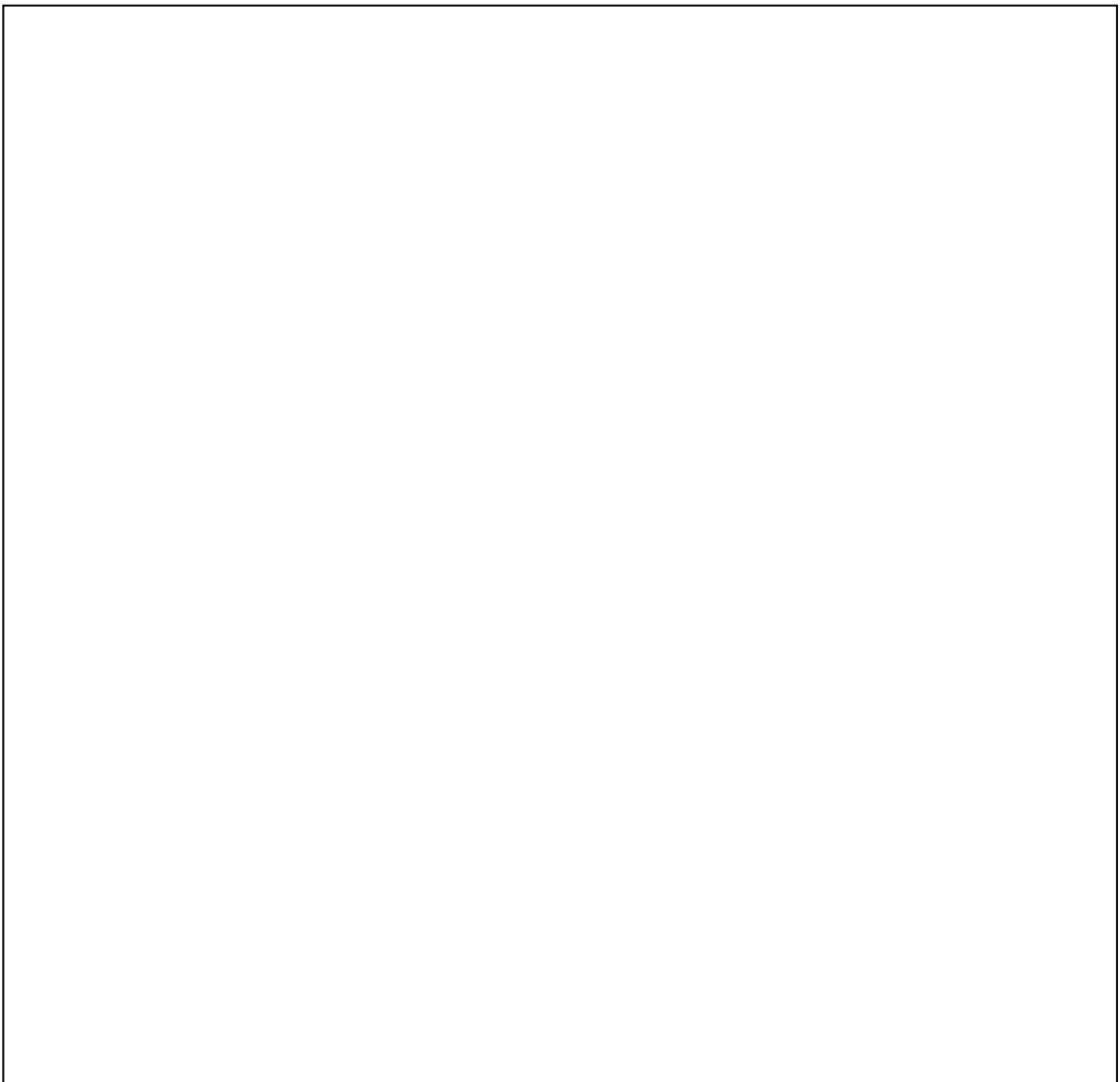
Figure 1.3: *Tardbp* **expression profile**. Left panel shows human adult tissue expression and right panel shows mouse adult tissue expression, as taken from (biogps.org). Colours show tissue type. Values have been normalised showing that TDP43 encoding transcripts are widely expressed in both human and mouse tissue.

Multiple annotated transcripts are present for TDP43 in human and mouse tissue indicating that there is significant complexity in *TARDBP / Tardbp* RNA processing. This is shown in Figure 1.4.

Figure 1.4: *Tardbp* **transcripts**. Figure taken from www.ensembl.org showing *Tardbp* annotated human and mouse transcripts. In both cases *Tardp*-001 encodes for full length TDP43 however multiple alternate transcripts exist with significant variation for both species in the 3' UTR.

TDP43 protein was first identified for its role in repressing HIV1 transcription (Ou *et al.*, 1995). TDP43 was found to bind the Tar DNA sequence and repress transcription through an unknown mechanism. Tar is an HIV1 element required for its transcription, with this role providing TDP43's name: Tar DNA binding protein – 43 kDa. Being identified for this role prior to its protein structure being characterised, it was later found structurally to belong to the family of heterogeneous nuclear ribonucleoproteins (hnRNPs). These are RNA-binding proteins involved in multiple aspects of RNA metabolism. They affect processing through localisation, transport and translation of mRNAs but also impact on non-coding RNAs (Dreyfuss *et al.*, 2002; Chaudhury *et al.*, 2010). As a result, TDP43 is normally localised to euchromatic regions such as nuclear speckles and perichromatin fibrils which are regions where splicing and transcription occur.

The characterised protein domains of TDP43 reflect these hnRNP functions as shown in Figure 1.5 for mouse TDP43.
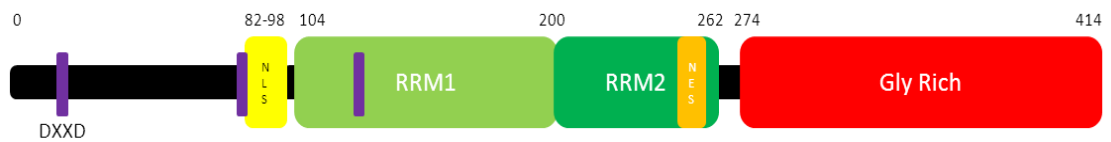
Figure 1.5: Structural domains of mouse TDP43. TDP43 is a 414 amino acid protein. It contains three caspase cleavage motifs (purple boxes), DXXD at positions 10, 86 and 119. It also contains a nuclear import (yellow box) and export signal (orange box) at positions 82-89 and 239-250 respectively. Two RNA recognition motifs that bind both single stranded DNA and RNA are shown (green boxes) with overlapping positions in the mouse, RRM1 at 104-200, RRM2 at 192-262. A glycine rich domain is present (red box) at position 274 - 413. Domains defined from www.uniprot.org.

TDP43 is highly conserved across species. Amino acid conservation between human and mouse protein is 96%. Across multiple species, the poorly defined N-terminal region (all amino acids up to the first RNA recognition motif) is highly conserved as are the RNA recognition motifs. The N-terminal region was recently shown to mediate a protein-protein interaction with P65. However, its high conservation (100% between mouse and human) supports further critical roles for TDP43 function (Swarup *et al.*, 2011b).

RNA recognition motif 1 (RRM1) is necessary and sufficient for RNA-binding (Buratti *et al.*, 2001; Giordana *et al.*, 2010). TDP43 has a high affinity for binding UG_6 and TG repeats with increasing affinity as the number of repeats increases (Buratti & Baralle, 2001; Acharya *et al.*, 2006; Kuo *et al.*, 2009). Deletion studies suggest that RRM2 is not critical for RNA-binding with very little known about its functions. It has been proposed to be involved in chromatin reorganisation (Ayala *et al.*, 2008b) and has also been shown to interact with single-stranded DNA (Kuo *et al.*, 2009).

The C-terminal (glycine rich region) mediates major protein interactions with other hnRNPs and proteins (Wang *et al.*, 2004; Buratti *et al.*, 2005; D'Ambrogio *et al.*, 2009). This region has also been shown through deletion experiments to be critical for completing RNA-binding functions requiring protein interactions. The C-terminal region is not as highly conserved as other domains and modelling supports it being relatively unstructured. It has been shown to be a prion-like domain (Udan & Baloh, 2011) which is speculated to play an important role in aggregation and pathology as discussed later. The unstructured C-terminal domain may provide functional flexibility to enable alterations and multiple protein interactions. TDP43

itself functions as a dimer and is predominantly localised to the nucleus. However, it has been shown to shuttle to and from the cytoplasm.

Prior to 2006, TDP43's identification in binding the TAR DNA sequence was followed by its characterisation as a splicing factor for the cystic fibrosis transmembrane regulator (CFTR) and apo-A-II genes (Buratti & Baralle, 2001; Buratti *et al.*, 2001; Buratti *et al.*, 2004; Ayala *et al.*, 2005; Buratti *et al.*, 2005; Mercado *et al.*, 2005). In 2006, it was discovered that TDP43 is a major component of ubiquitinated inclusions in ALS and FTLD-TDP (Arai *et al.*, 2006; Neumann *et al.*, 2006). Since then, over 600 papers have been published regarding what has emerged as the TDP43 proteinopathies (Kwong *et al.*, 2008; Geser *et al.*, 2009; Neumann, 2009). The TDP43 proteinopathies consist of ALS and FTLD-TDP where TDP43 pathological changes are seen in cases with and without TDP43 causative mutations. Secondarily, in other neurodegenerative diseases including some tauopathies, α-synucleinopathies and poly Q disorders, pathological alterations in TDP43 are also observed. A large diversity of approaches and techniques have been applied to model and modify TDP43 disease. Despite the significant progress that has been made, the primary roles of TDP43 in neurons susceptible to neurodegeneration are poorly characterised as is the extent to which human mutations are gain versus loss of function (both elements are thought to be important and this is discussed below when reviewing existing TDP43 models).

1.3.2.   TDP43 functions

The diversity of roles for TDP43 in RNA metabolism continues to be established. A characterisation by RNA sequencing and exon arrays has established that TDP43 affects around 30% of the murine transcriptome (Polymenidou *et al.*, 2011). Discussed in more detail in Chapter 5, this study was one of the first to show the impact of TDP43 down regulation in adult mouse striatum on the transcriptome. With hundreds of mRNA transcript level and splicing changes upon TDP43 knock down, TDP43 plays a central role in multiple aspects of RNA metabolism, which is anticipated to be relevant to pathology. Disease models and TDP43 alteration in human pathology are discussed in the next section. Results since 2006 driven by TDP43's roles in neurodegeneration have shown that TDP43 has central roles in general RNA metabolism as shown in Figure 1.6.

mRNA stability

TDP43

TIA1

Cytoplasm

TDP43

Nucleus

Splicing

TDP43

hnRNPs

RNA editing

TDP43

TDP-43

Stress Granules

ssDNA Promoter
Silencing

Pre-miRNA

Drosha

TDP43

TDP43

RNA translocation
Transport granules
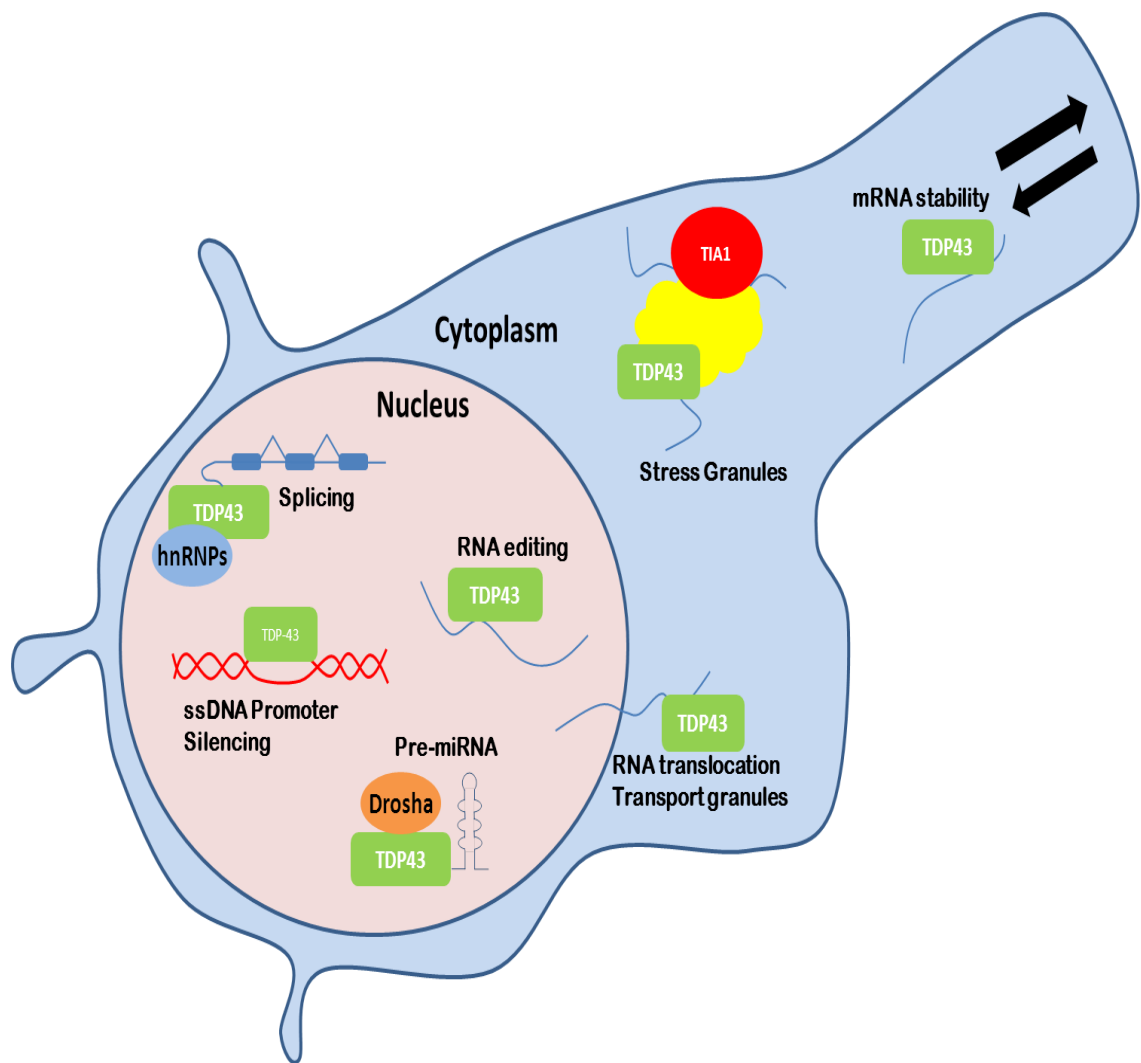
Figure 1.6: TDP43 known roles. Image of a cell showing some of the known functions of TDP43 relating to RNA metabolism. Within the nucleus, TDP43 has published roles for interacting with hnRNP family members to affect splicing of target RNAs (Buratti *et al.*, 2001; Mercado *et al.*, 2005; Bose *et al.*, 2008; Dreumont *et al.*, 2010), editing RNA (Aizawa *et al.*, 2010) and playing roles in pre-miRNA formation by interacting with DROSHA (Buratti *et al.*, 2010; Kocerha *et al.*, 2011; Kawahara & Mieda-Sato, 2012). As characterised with HIV1 Tar, TDP43 can bind single stranded DNA and through unknown mechanisms promote transcription silencing. Inside and outside of the nucleus, TDP43 is involved in mRNA stability and RNA transport (Ayala *et al.*, 2008a; Wang *et al.*, 2008; Fiesel *et al.*, 2010; Godena *et al.*, 2011). Under stress conditions, stress granules form which are thought to silence non-essential RNAs and store them during the stress. TDP43 associates with stress granules potentially silencing multiple RNAs (Colombrita *et al.*, 2009; Moisse *et al.*, 2009a; Liu-Yesucevitz *et al.*, 2010; Dewey *et al.*, 2011; Parker *et al.*, 2012).

Alongside TDP43's established roles in RNA metabolism, it has emerged that TDP43 auto-regulates its own protein levels (Ayala *et al.*, 2011; Polymenidou *et al.*, 2011). The mechanism continues to be characterised however there is *in vivo* data in this thesis and published knock out mouse models (Kraemer *et al.*, 2010; Sephton *et al.*, 2010; Wu *et al.*, 2010) for TDP43 auto-

regulation. TDP43 binding to its own 3' UTR has been established as critical for auto-regulation. Data from various models also shows that TDP43 levels are tightly regulated and that both significantly reduced and increased levels results in toxicity. Alongside TDP43's role in RNA metabolism, levels of TDP43 protein are also speculated to be important in TDP43 human pathology, although conclusive data of this remains to be presented.

Finally, assessment of TDP43 function has shown that the first RRM is necessary and sufficient for RNA-binding with the C-terminal glycine rich region being critical for major protein-protein interactions. Little information regarding the roles of the highly conserved N-terminal region or the second RRM is available. As part of the work described in this thesis, mutations from all major domains are functionally assessed to determine their importance in potentially establishing the roles of these domains in TDP43 function.

1.4. TDP43 pathology

1.4.1. TDP43 mutations which cause ALS

Mutations in *TARDBP* are causative of ALS. In rare cases they are also causative of FLTD-TDP and these two diseases are part of a clinicopathological spectrum (Geser *et al.*, 2010). They are the core of the TDP43 proteinopathies in which TDP43 is pathologically mislocalised and modified irrespective of whether the causative mutation is within TDP43.

Mutations in TDP43 shown to be causative of ALS are given in Figure 1.7. More than thirty mutations have been identified clustering in the C-terminal glycine rich region. All mutations are dominant causing both familial and sporadic ALS cases. The mutations are reviewed in more detail elsewhere (Da Cruz & Cleveland, 2011).
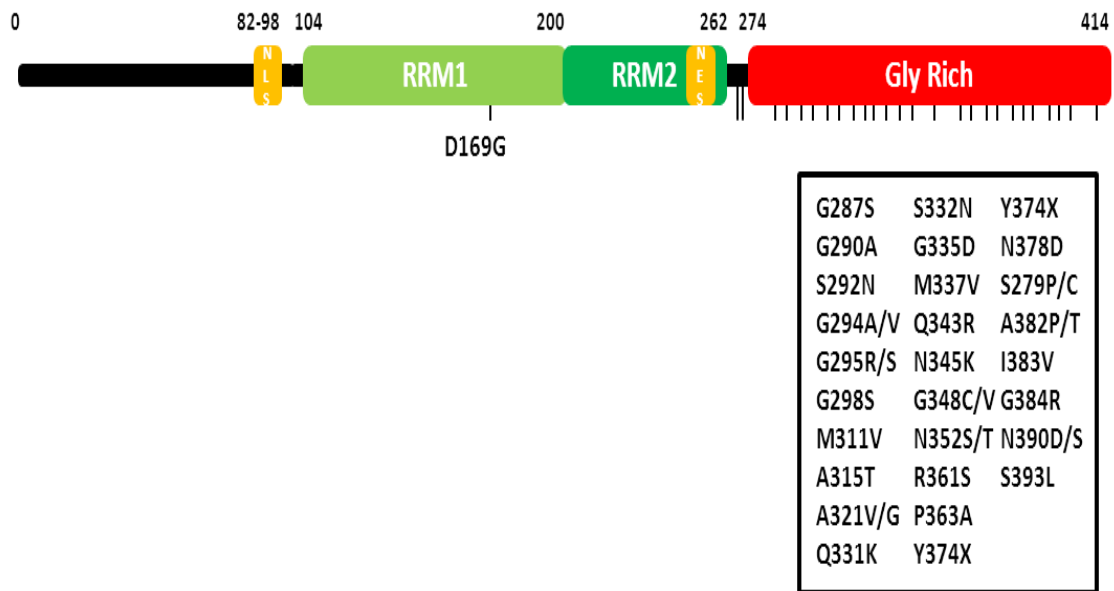
Figure 1.7: TDP43 mutations which cause ALS. Figure showing the functional domains of TDP43 and where human causative mutations have been identified. Nearly all mutations cluster in the C-terminal glycine rich region. All mutations are dominant missense mutations except Y374X which is a nonsense mutation. The mutation D169G was identified in a sporadic case and is located in the first RRM, however no other mutations have been identified in this region.

It is unknown whether TDP43 mutations cause loss or gain of function with extensive data from cell culture and animal models (discussed below) showing both elements as being critical to TDP43 pathology. The result in human patients is TDP43 aggregates in neurons and glia in the central nervous system (Neumann *et al.*, 2006). Pre-inclusions have been observed, thought to form at early disease stages (Mori *et al.*, 2008; Sreedharan *et al.*, 2008). This is followed by dense inclusions in motor neuron axoplasm, as well as filamentous skeins. In FTLD-TDP, pathology is seen as inclusions in nuclei, axoplasm and neurites of forebrain neurons (Mackenzie *et al.*, 2006; Sampathu *et al.*, 2006; Mackenzie *et al.*, 2011) reflective of the disease phenotypes in the patient. Most, but not all inclusions are ubiquitinated (Giordana *et al.*, 2010). These changes are primary hallmarks of pathology in these TDP43 proteinopathies. In ALS and FTLD-TDP, spinal cord inclusions are labelled with both N- and C-terminal antibodies, but only C-terminal antibodies recognise inclusions in brain (Igaz *et al.*, 2008) showing cleaved fragments in disease.

1.4.2.   TDP43 pathological changes

TDP43 undergoes a series of molecular changes in TDP43 proteinopathies. The cause / effect of each of these continue to be investigated to find the critical alterations which are the drivers of pathology. The pathological changes are listed below.

Hyperphosphorylation and polyubiquitination

TDP43 protein is hyperphosphorylated (at multiple residues including S409 / 410) correlating with a shift towards insoluble protein. These residues are not detected as being hyperphosphorylated in a non-ALS context. This has been shown in patients and replicated in animal models (Wegorzewska *et al.*, 2009; Shan *et al.*, 2010; Stallings *et al.*, 2010). Hyperphosphorylation appears as an early event and is hypothesized to affect protein degradation and toxicity, although it is not required for TDP43 cleavage, toxicity and aggregation in cell culture models (Dormann *et al.*, 2009; Zhang *et al.*, 2009). TDP43 is also poly-ubiquitinated (both hyperphosphorylated and polyubiquitinated forms are not readily detected in normal brain tissue).

Solubility changes

TDP43 is sequestered in predominantly cytoplasmic sarkosyl insoluble inclusions (intranuclear inclusions can also occur). There is a shift towards increased insolubility occurring in glia and neurons (Neumann *et al.*, 2006; Sampathu *et al.*, 2006). This correlates with nuclear clearance, hyperphosphorylation, polyubiquitination and mislocalisation. There is data for mislocalised TDP43 in forming pre-aggregate structures (Mori *et al.*, 2008; Giordana *et al.*, 2010) which are speculated to be the precursors of inclusions. This may link in to TDP43's role in stress granules. As discussed above, TDP43 naturally localises to stress granules potentially silencing and protecting its RNA bound targets during stress. Stress coupled with the effects of TDP43 mutations may alter this process in contributing towards aggregate formation although in models, TDP43 aggregation itself appears not necessary for toxicity, as discussed later. TDP43 solubility change and mislocalisation is also hypothesised to affect TDP43 auto-regulation (Polymenidou *et al.*, 2011).

Protein cleavage

TDP43 is cleaved into smaller 35 and 20-25 kDa C-terminal fragments (these are not detected in wild-type brains and have been shown at different lengths, seen particularly in the cerebral cortex). These cleavage products are labelled in inclusions (Igaz *et al.*, 2008). TDP43 contains caspase 3 motifs at locations which have been suggested as being able to produce the 35 and 25 kDa fragments (Zhang *et al.*, 2007). Overexpressing the C-terminal fragments results in hyperphosphorylated and poly-ubiquitinated C-terminal fragments (Caccamo *et al.*, 2009; Nishimoto *et al.*, 2010). Data in models without C-terminal fragments indicates that toxicity can also occur without their presence (Shan *et al.*, 2010; Igaz *et al.*, 2011).

The pathological changes within TDP43 protein correlate highly with each other and continue to be investigated to determine the nature of which occur early / late and which are cause / effect. This ultimately results in ALS or other TDP43 proteinopathies. The sequence of changes that occur and which are protective versus those that are toxic has yet to be shown. Modelling approaches with animals and cells have begun to show the order of changes that occur, for example, hyperphosphorylation is thought to be an early event with polyubiquitination occurring later. Further data is required to assess the impacts of these changes on known functions of TDP43, with particular focus on how they impact on TDP43's RNA metabolism functions including splicing and other transcript processing roles.

1.4.3.   TDP43 models

In order to understand TDP43 biology and deconstruct the disease process, multiple cell and animal models have been generated. The consensus from loss and gain of function modelling approaches has shown that levels of TDP43 are critical to survival and neuronal health. A significant reduction or increase in protein levels results in toxic consequences with data supporting both reduced and enhanced TDP43 levels impacting on neuronal function and survival. Within humans, it is not known whether mutations result in a loss or gain of function, however animal modelling approaches support both mechanisms contributing to disease.

Loss of function models

Knock out TDP43 lines have been generated in *Caenorhabditis elegans* (worm), *D. Melanogaster* (fruit fly)*, Danio rerio* (zebra fish) and *M. musculus* (mouse*)*. In worms, knockout of *tdp-1*, the *Tardbp* ortholog, does not result in overt defects (Liachko *et al.*, 2010). However, worm *tdp-1* contains a poorly conserved glycine rich region whose lack of conservation may contribute to the absence of overt phenotypes. In the fly, knocking out *TBPH* (the *Tardbp* homolog) is lethal or results in severe phenotypes. In fly *TBPH* knockouts, survival through hatching from the pupal developmental stage is significantly reduced with those flies able to hatch displaying shortened lifespan and strong motor phenotypes (Feiguin *et al.*, 2009). These fly *TBPH* knockouts can be rescued by ectopic expression of the wild-type human TDP43 transgene. Alternative fly knock out models also show semi-lethality and neuronal phenotypes including abnormal neuromuscular junctions and reduced dendritic branching (Feiguin *et al.*, 2009; Lu *et al.*, 2009; Fiesel *et al.*, 2010). Likewise knockdown of fish *TARDBP* results in motor neurons that are shorter and display abnormal branching (Kabashi *et al.*, 2010).

Within the mouse, three knock out models have been made (Kraemer *et al.*, 2010; Sephton *et al.*, 2010; Wu *et al.*, 2010). In all three cases, homozygous embryonic lethality is observed between embryonic day E3.5-8.5 days post coitum (dpc) due to inner cell mass growth defects. An attempt to surpass this developmental lethality through the generation of a tamoxifen inducible knock out TDP43 has also been made (Chiang *et al.*, 2010). Once the knock out was activated a rapid lethality resulted. A further loss of function approach from Professor Zuoshang Xu (UMass) was presented at the American Society for Neuroscience conference 2011. These results have not been published at the time of writing this thesis. In this approach, a transgenic RNAi mouse has been generated modelling partial loss of TDP43 function. The transgenic RNAi knocks down *Tardbp* RNA levels to 50% and TDP43 protein levels to 80% of that of non transgenic controls. This results in a progressively "wobbly" gait which progresses to paralysis by 9 weeks. There is around 60% motor neuron loss with TDP43 negative, ubiquitin positive inclusions. In parallel to these mouse models at a cellular level, knockdown of TDP43 in HeLa, U2OS and Neuro-2a cell lines results in cell death and in the Neuro-2a cells affects neurite growth (Iguchi *et al.*, 2009).

Complete loss of TDP43 across cell lines and various animal models is generally not conducive with survival. Where fly and fish survive, neuronal defects in branching and size are observed. This indicates that TDP43 plays critical roles in multiple neuronal processes that are significantly altered in the absence of TDP43. In the mouse, Professor Xu's transgenic RNAi

approach does show selective neuronal degeneration that matches human selective degeneration in progressive motor neuron loss. But the model does not contain TDP43 in inclusions, TDP43 mislocalisation from the nucleus or C-terminal fragments as seen in human patients. This shows that through a loss of function mechanism, the output of motor neuron loss can occur in mice, but the pathological hallmarks are not identical to those in humans. Purely through loss of function, the mouse as a model may not be able to recapitulate certain elements of human pathology. The data from across species is that pathology and neuronal dysfunction are associated with loss of function and this will be critical to human pathology. It may also be associated with gain of function and possible dominant negative effects. This is outside of TDP43's overtly important role in development in multiple species, where it is unknown whether these roles at this stage are relevant to neuronal pathology.

Transgenic models

A vast number of transgenic models across species have been generated. They have been reviewed previously (Joyce *et al.*, 2011). In nearly all cases, overexpression of wild-type or mutant TDP43 is toxic with a dose dependent effect. Transgenic models with various TDP43 alterations (sequence deletions or human pathogenic mutations) have also been generated, showing overall that multiple alterations in TDP43 can impact on the pathological outcome.

Saccharomyces cerevisiae*, *Danio rerio*, *Caenorhabditis elegans* and *Drosophila melanogaster

Overexpression of human TDP43 in yeast results in toxicity that is dependent partly on mitochondrial dysfunction and oxidative stress. Overexpression of both wild-type and mutant forms is toxic (Braun *et al.*, 2011). In fish overexpressing wild-type human TDP43, the result is a motor axonopathy with shorter axon length and abnormal branching phenotypes (Laird *et al.*, 2010). Both wild-type and mutant overexpressed TDP43 localise to cell nuclei. Injecting TDP43 constructs also results in motor deficits and deletion experiments show that the C-terminus of TDP43 is required for pathogenicity (Kabashi *et al.*, 2010). In worms, wild-type and mutant overexpression models have been generated with both being pathogenic. Overexpressing wild-type TDP43 is toxic requiring RNA-binding and the C-terminal region (Ash *et al.*, 2010). Multiple models including worms show GABAergic deficits and interestingly, mutating serines 409 / 410, that are hyperphosphorylated residues in human pathology, ameliorates the motor deficits (Liachko *et al.*, 2010).

In the fly, models have been generated overexpressing *TBPH* and human TDP43. *TBPH* overexpression causes a sensory neuron branching axonopathy (Lu *et al.*, 2009). Human mutant TDP43 overexpression (Q331K and M337V) also causes dendritic branching phenotypes (Lu *et al.*, 2009). Overexpression of wild-type TDP43 in flies causes retinal degeneration, axonal loss in mushroom bodies and motor neuron death. It has pathogenic effects on axonal branching and neuromuscular junctions (NMJs) (Hanson *et al.*, 2010; Li *et al.*, 2010). Mutating phenylalanines at positions 147 / 149 which are necessary for RNA-binding reduces overexpression induced toxicity producing mild motor deficits (Voigt *et al.*, 2010). Full length overexpressing TDP43 mutants show that TDP43 localises to the nucleus to induce pathogenicity so there is no nuclear depletion as seen in human patients. Mild abnormalities in the eye are also worsened when mutating the nuclear localisation signal (NLS) (Miguel *et al.*, 2011). Considering full length TDP43 and modified forms, there are no aggregates or cytoplasmic mislocalisation phenotypes. However, there is toxicity. Overexpressing full length TDP43 in flies is toxic to neuronal cells, but overexpressing C-terminal fragments has been shown as less toxic (Li *et al.*, 2010; Voigt *et al.*, 2010). These overexpression models overall show significant motor axonopathy with wild-type overexpression localising more to nucleus and TDP43 mutant forms localising slightly more to the cytoplasm. This is also reflected in rodent models discussed below, showing that pathogenicity in neuronal systems in these models does not occur through identical mechanisms seen in human patients and that overexpression is toxic.

Rodent models (*Rattus norvegicus* and *Mus musculus*)

Multiple transgenic mouse models overexpressing TDP43 have been generated. A variety of wild-type and mutant forms of TDP43 have been expressed with different neuronal and promoters with ubiquitous expression. These have been reviewed (Joyce *et al.*, 2011) and show that overexpression of either wild-type or mutant TDP43 forms (such as A315T) generally results in dose dependent toxicity. Various motor and cognitive phenotypes are also observed in different models. Mice overexpressing TDP43 with a deleted nuclear localisation signal (Igaz *et al.*, 2011) show behavioural abnormalities and neurodegeneration, however endogenous TDP43 is still expressed in the nucleus. With overexpression of TDP43 over a certain threshold of exogenous protein production the endogenous protein is downregulated by auto-regulation. Overexpression models may support a gain of function model however when

considering individual models, the degree of endogenous protein down regulation (due to TDP43 auto-regulation) must be considered as this may confer elements of loss of function.

In transgenic rats wild-type and mutant (M337V) overexpressers have been generated (Zhou *et al.*, 2010). Wild-type transgenic rats do not show early paralysis but overexpressing TDP43 M337V results in an early paralysis phenotype. This supports increased mutant TDP43 toxicity, which is not always reflected in other models / species. In rodent models, overexpressed TDP43 localises to the nucleus and is toxic. In both the mouse and rat, endogenous protein in all of the rodent models has not been completely depleted from the nucleus. Despite this, some transgenic rodents do show TDP43 positive inclusions but they are rarely seen (Wegorzewska *et al.*, 2009; Shan *et al.*, 2010; Stallings *et al.*, 2010; Wils *et al.*, 2010; Xu *et al.*, 2010; Igaz *et al.*, 2011). Some transgenic mice also contain TDP43 negative mitochondrial aggregates (Wegorzewska *et al.*, 2009; Shan *et al.*, 2010; Stallings *et al.*, 2010; Wils *et al.*, 2010; Xu *et al.*, 2010), suggesting abnormal alterations in metabolic pathways. When overexpressing truncated TDP43 (C-terminal fragments) this results in cytoplasmic aggregates that are hyperphosphorylated and polyubiquitinated (Dormann *et al.*, 2009; Igaz *et al.*, 2009; Nonaka *et al.*, 2009; Zhang *et al.*, 2009). Rodent models overexpressing TDP43 have also been shown to have lower molecular weight TDP43 fragments (Wegorzewska *et al.*, 2009; Shan *et al.*, 2010; Stallings *et al.*, 2010; Tsai *et al.*, 2010; Wils *et al.*, 2010; Xu *et al.*, 2010). Levels of these lower molecular weight fragments increase with disease progression in some models (Wegorzewska *et al.*, 2009; Stallings *et al.*, 2010; Wils *et al.*, 2010). TDP43 C-terminal fragments are also soluble when extracted from tissue (Wegorzewska *et al.*, 2009; Tsai *et al.*, 2010; Wils *et al.*, 2010; Xu *et al.*, 2010) and are in the nuclear fraction, which does not reproduce what is seen in human ALS patients (Wils *et al.*, 2010). Furthermore not all transgenic rodents show C-terminal fragments (Shan *et al.*, 2010; Igaz *et al.*, 2011) but still show selective neurodegeneration. An alternative approach using a bacterial artificial chromosome (BAC) to express wild-type TDP43 in all mouse tissues has been completed replicating many of the major pathological hallmarks of human TDP43 ALS (Swarup *et al.*, 2011a). With this more subtle overexpression approach, mice showed age dependent TDP43 positive ubiquitinated inclusions, C-terminal fragment production, axonopathy and neuroinflammation. Despite these features, overt motor neuron degeneration was not present. Overall, TDP43 transgenic rodents in many cases do recapitulate aspects of the phenotypes observed in human TDP43 proteinopathies although few show progressive motor neuron degeneration. Transgenic overexpressing mice show selective motor neuron degeneration and motor phenotypes accurately reflecting motor

changes in human patients. The complexity of the underlying pathology driving these changes in humans are not all observed, however multiple aspects are recapitulated.

Non-human primate model

More recently a non-human primate model of ALS has been generated (Uchida *et al.*, 2012). By overexpressing wild type human TDP43 in cynomolgus monkey (*Macaca fascicularis*) spinal cord through viral injection of a transgene, these monkeys develop progressive motor weakness. They show muscle atrophy and distal hand fasciculation. At a molecular level there are cystatin C positive cytoplasmic aggregates and TDP43 mislocalisation from the nucleus of specific motor neuron subsets (lateral nuclear group). This study did not see cleavage fragments or recapitulate all features of human ALS; however they argue that this model is "superior" to mouse models because they recapitulate aspects of the human condition not seen in rodent models. This model is further support that overexpressing wild-type TDP43 protein is toxic.

1.4.4.   Summary of models and disease

The overall picture from TDP43 models across cells and species is that TDP43 plays a critical role in survival and neuronal function. Too little or too much TDP43 results in toxic outcomes indicating that TDP43 auto-regulation may be a critical factor in pathology. Within TDP43 proteinopathies and specifically ALS, multiple hallmarks of pathology are present. Expression levels of TDP43 encoding RNA are upregulated in human ALS / FTLD-TDP one and a half fold as measured by quantitative real time PCR (Mishra *et al.*, 2007; Gitcho *et al.*, 2009) and there are a series of modifications to TDP43 protein. It is unknown whether TDP43 protein levels are upregulated, although one study has shown increased levels in cerebrospinal fluid of ALS patients (Kasai *et al.*, 2009). If so, it is not known if that protein is available for normal function, or whether the amount of functional TDP43 is downregulated (potentially sequestered in inclusions). It is also yet to be determined whether many TDP43 modifications cause aggregate formation and toxicity or are normal responses to pathology. Within models that show selective neuronal vulnerability or relevant phenotypes, aspects of the human condition are recapitulated. For example hyperphosphorylation, which is seen in human ALS, is not required

for toxicity in some models, with TDP43 cleavage or aggregation in cells (Dormann *et al.*, 2009; Zhang *et al.*, 2009). Furthermore, cytoplasmic inclusions can form when overexpressing C-terminal fragments or an NLS TDP43 mutant (Igaz *et al.*, 2009; Nonaka *et al.*, 2009). But toxicity often occurs without these features in many models, where overexpressing both nuclear and cytoplasmic TDP43 is toxic. Data from models supports both loss and gain of function mechanisms leading to neuronal abnormalities and degeneration. Dissecting species differences in TDP43 function will be necessary to delineate whether models can accurately reproduce the human condition. The high degree of conservation of TDP43 and the consistent axonopathy phenotypes show that existing models are very useful tools. They can be used to understand TDP43 function and dysfunction in human pathology and alongside alternative models must be used to address hypotheses behind TDP43 pathology.

1.4.5.   Hypotheses for TDP43 pathology

Importance of TDP43 levels in toxicity

Across animal models, toxicity is generally increased as a dosage response effect rather than wild-type versus mutant TDP43 overexpression. Higher expression levels in transgenic mice can also downregulate endogenous mouse TDP43 (Xu *et al.*, 2010; Igaz *et al.*, 2011) which correlates highly with neurodegeneration. This shows *in vivo* the impacts of TDP43 on auto-regulation / down regulation of TDP43 protein, potentially causing or contributing to neuronal phenotypes. When TDP43 is removed or highly downregulated in various models, neuronal health and survival are compromised.

TDP43 auto-regulation is thought to occur in the nucleus (Polymenidou *et al.*, 2011). TDP43 regulates its own RNA transcript by binding to its 3' UTR (Ayala *et al.*, 2011; Polymenidou *et al.*, 2011; Tollervey *et al.*, 2011). There is emerging evidence that a disruption of TDP43 auto-regulation may be important in pathology with models linking auto-regulation disruption and pathology having been proposed (Lee *et al.*, 2012). Both loss and gain of auto-regulation models rely on a disruption of TDP43 in regulating its transcript levels. Further characterisation in various cell and animal models is required to determine the relevance of different proposed auto-regulation mechanisms (Ayala *et al.*, 2011; Polymenidou *et al.*, 2011) with assessment of whether human pathogenic mutations directly alter the dynamics of this process.

Importance of RNA metabolism

Alongside the potential importance of auto-regulation, there is emerging data that TDP43's roles in RNA metabolism may be crucial to TDP43 proteinopathies. A variety of genes are associated with ALS and atypical motor neuron disease with roles in RNA metabolism. Shortly after the identification that mutations in TDP43 cause ALS, mutations in FUS were identified (Kwiatkowski *et al.*, 2009; Vance *et al.*, 2009). FUS is structurally highly similar to TDP43 and has since been shown to directly bind TDP43 (Ling *et al.*, 2010) and act downstream of TDP43 in common pathways (Wang *et al.*, 2011). This further enhanced the potential importance of perturbations in RNA metabolism potentially being responsible for diseases such as ALS. Overall, TDP43 is part of an extensive RNA metabolic network, as would be expected with it being an hnRNP. Down regulation of TDP43 has been shown to alter 30% of the murine transcriptome (Polymenidou *et al.*, 2011). With such extensive interactions with RNA and a diversity of functions (as shown in Figure 1.6) mutations in TDP43 may disrupt RNA metabolism through multiple proposed mechanisms. Assessment of this is a viable hypothesis to being a causal mechanism behind TDP43 proteinopathies (Johnson *et al.*, 2009; Lagier-Tourenne *et al.*, 2010; Strong & Volkening, 2011).

Emergence of the prion hypothesis

TDP43 has a C-terminal prion like domain (Johnson *et al.*, 2009; Fuentealba *et al.*, 2010; Gitler & Shorter, 2011; Guo *et al.*, 2011) and in cell culture this promotes features such as aggregation. *In vitro* TDP43 is naturally prone to aggregation (Johnson *et al.*, 2009) and a novel hypothesis has emerged regarding TDP43 being prion-like. In the case of diseases such as ALS, there is a focal initiation of disease with symptoms progressing. Under this hypothesis, TDP43 spreads in a prion-like manner sequestering wild-type protein and steadily progressing through specific neural pathways. A human pathogenic change has been shown to increase aggregation ability (Guo *et al.*, 2011) potentially supporting human mutations altering the properties of TDP43 in the prion hypothesis context.

1.5.   ENU approach (considering pathology): An allelic series of *Tardbp* mutations to understand TDP43 biology

TDP43 is a widely expressed protein with extensive roles in RNA metabolism. These roles continue to be focused on in driving forward TDP43 proteinopathy research. TDP43 is likely to have critical roles in other aspects of biology that are yet to be defined. With such diverse roles already characterised, it remains a major challenge to determine how these roles relate to human pathology. Understanding this will provide a clear understanding of the mechanisms driving TDP43 proteinopathies and ultimately provide the targets for effective treatments and a potential cure for these devastating diseases.

Loss of function and transgenic overexpressing models have been discussed and show across species that both elements may be relevant to neuronal health and pathology. Of those presented, various aspects of human pathology have been recapitulated but no model has shown all the major hallmarks of ALS or FTLD-TDP.

Although the aim is to replicate human conditions as best as possible, models that recapitulate certain aspects of disease remain powerful tools for understanding elements of pathology as well as normal protein function. For example, in the case of rodent transgenic models TDP43 positive inclusions are rare yet some lines of mice still show selective motor neuron degeneration and many changes relevant to the human condition, such as inflammatory changes and astrogliosis (Wegorzewska *et al.*, 2009; Wils *et al.*, 2010; Zhou *et al.*, 2010).

For the work described in this thesis, one nonsense and nine missense mutations have been identified in mouse *Tardbp*. These are endogenous mutations that are expressed in an identical fashion to human pathogenic mutations. The nonsense mutation (Q101X) acts in a similar fashion to the knockouts and is characterised alongside the K160R mutation, which may also show a partial loss of function. These mutations were originally re-derived due to their identification from the MRC Harwell archive. They represent the first mice of a potential allelic series for deconstructing the biology of TDP43 in the mouse. They are complementary models to knockouts and transgenic mice asking questions that these alternative models are less able to at an endogenous level.

Alongside the Q101X and K160R mutations all alleles were functionally assessed with F210I showing a strong deficit in RNA-binding and RNA functions. It is a strongly hypomorphic allele

with its identification and characterisation presented in this thesis. This provides an alternative loss of function allele particularly relevant to addressing auto-regulation and TDP43's roles in RNA metabolism. All of the animal models generated and hypotheses proposed in reviews may support auto-regulation and RNA metabolism alterations as being key processes in TDP43 proteinopathies. Certainly at an endogenous level in the mouse, F210I is a hypomorphic allele that can contribute to evaluating this. It will also provide a model in which to determine the impact of loss of function on post mitotic neurons, which has yet to be assessed. There is data for loss of function being critical to pathology and the F210I allele in the mouse provides an ideal tool to assess the relevance of loss of RNA-binding function and its impacts in disease.

Outside of the data for mutations presented in this thesis, recent data from the laboratory on the M323K mutation supports it being a gain of function allele. This result is not a component of this thesis, but it shows how an allelic series provides an array of mutations that can show multiple effects, whether they are complete loss, gain, hypomorphic or dominant negative effects.

By being completely random, ENU is hypothesis generating and has no *a priori* assumptions. The generation of multiple random mutations in TDP43 requires an assessment of each of these mutations which is the aim of the work of this thesis. This provides novel alleles that can be used as tools to deconstruct TDP43 biology, and this is needed to further understand TDP43 function. A complementary approach is to generate knock-ins. However, this can be difficult and lengthy in process. The allelic series has been characterised and mutations in previously uncharacterised residues show clear effects, providing a series of mutations that will be useful to understanding TDP43 biology in the future. Characterisation of a number of lines continues with the aim of deconstructing TDP43 biology and potentially modelling pathology.

1.6.   Aims of the work presented in this thesis

The aims of the data presented in this thesis are to utilise an allelic series of endogenous mouse TDP43 mutations as a complementary approach to knock-out and transgenic overexpression mouse lines. Ten point mutations spanning all major domains of mouse TDP43 were identified with the aim to determine their functionality in deconstructing TDP43 biology and potential dysfunction in pathology. In order to address this, the Q101X and K160R mutations, which were the first mutations identified, have been derived as mice without *a priori* data on their functionality, which has been assessed longitudinally at the behavioural level. Once all ten mutations were identified, an *in vitro* CFTR mini-gene assay was used to assess all mutations in order to guide further work during the PhD. F210I, a mutation in the second RNA recognition motif was shown as having deficient splicing activity of the CFTR mini-gene and the degree of loss of function was further characterised *in vivo*. The bullet points below summarise the aims assessed.

- To rederive and generate mice harbouring TDP43 Q101X and K160R mutations and assess animal viability

- To perform a longitudinal behavioural characterisation of Q101X and K160R mice. Phenotypic tests include: SHIRPA, grip strength, rotarod, startle response and open field

- To generate compound ($Tardbp^{Q101X/K160R}$) mutants and perform a behavioural characterisation to assess for additive or interactive effects and to assess *in vivo* the ability of K160R to auto-regulate

- To molecularly characterise mutant TDP43 using both RNA and protein analysis

- To assess *in vitro* whether any of the mutations identified from the MRC Harwell and RIKEN ENU archives show any functional alterations (loss or gain of function) using the CFTR mini-gene assay (of which the mutant F210I was deficient)

- To determine the mechanism of F210I CFTR mini-gene splicing functional deficits

- To rederive and generate mice harbouring TDP43 F210I and confirm altered functionality *in vivo*

CHAPTER 2

Materials and Methods

2. Materials and Methods

2.1. Behavioural phenotyping

2.1.1. License

All mice were phenotyped in accordance with conditions stated on Home Office project license 30/2758, held by Professor Elizabeth Fisher. My personal license in completing this work is 30/8612 (L285). Mice were maintained at MRC Harwell, following all Home Office conditions as specified in project and personal licenses. All mice that were sick were assessed by the Named Animal Care and Welfare Officer (NACWO). All procedures were recorded for Home Office records.

All behavioural tests were completed blind. This was achieved through applying a numbering system for every mouse on the reverse of the card where the genotype was hidden. This allowed staff to continue to maintain the colonies whilst simultaneously allowing the assessor to be blind to the genotype when completing tests. All tests were individually completed at approximately the same time of the day to minimise behavioural variation associated with circadian rhythms.

2.1.2.   SHIRPA

SmithKline Beecham, Harwell, Imperial College, Royal London Hospital, phenotype assessment (SHIRPA) was used as a first line screening test. Mice were assessed using the SHIRPA set up shown in Figure 2.1.
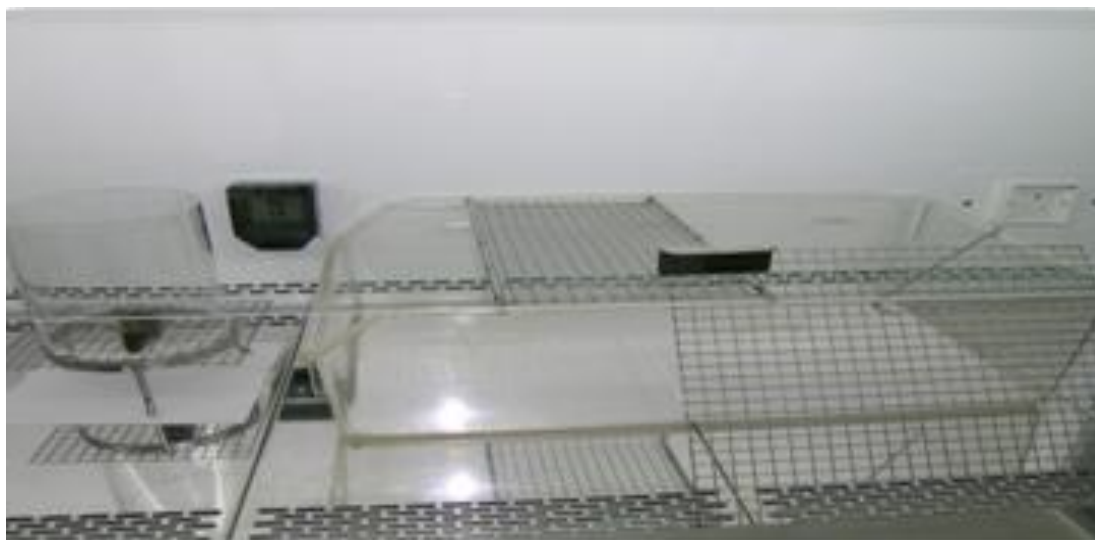
Figure 2.1: Photograph of SHIRPA equipment. To the left is a viewing jar on an elevated platform. The mouse is then transferred to the main arena for a series of tests before being assessed on a grid shown in front of the SHIRPA arena.

The SHIRPA equipment consists of:

- Clear perspex cylindrical viewing jar (14 cm diameter, 18 cm height)
- Tripod (7.5 cm height).
- Plastic sheet [sandpapered down to create a surface that is not smooth] (20 cm x 20 cm)
- Clear perspex arena (60 cm length, 37 cm width and 18 cm height). In the floor of the arena is a perspex sheet. A grid (40 cm x 20 cm) with 12 mm mesh (approximate) is secured across the top of the width of the box
- Institute of hearing research (IHR) click-box (generates a brief 20 KHz tone at 90 dB)
- Clear perspex tube (3 cm diameter, 20 cm length)

2.1.3.   Modified SHIRPA procedure

Mice were placed in the assessment room and allowed to acclimatize to the room for more than fifteen minutes. The area was wiped clean with alcohol and allowed to dry before use to prevent any smell being detected by the mice. Under a biological safety cabinet, the viewing jar was placed upright on top of the plastic sheet. The mouse was removed from its home cage and placed into the viewing jar where highlighted behaviours were recorded without disturbing the mouse. These behaviours included body position, respiration rate and tremors. The mouse was then transferred to the centre of the arena inside the viewing jar, using the plastic sheet underneath the jar to contain the mouse. The plastic sheet was removed from underneath the viewing jar at approximately 25 cm above the arena floor. A sequence of further behaviours were then scored including locomotor activity, gait and startle response.

The mouse was then removed from the arena gripping the tail between the thumb and forefinger. It was suspended 20 cm above the arena to identify whether the mouse struggled when held by its tail. The colour gradations of the plantar surface and digits of forelimbs were noted as well as forward curling (i.e. head to abdomen) of the mouse when held by the tail. The mouse grasping its limbs when held by the tail was also scored. It was then placed on the grid above the arena allowing front paws to grip bars. Whilst holding rear paws elevated, the body tone of the mouse was assessed. The mouse was then scruffed to assess limb tone. Limb grasping when suspended by the tail and body tone are shown in Figure 2.2 and Figure 2.3.
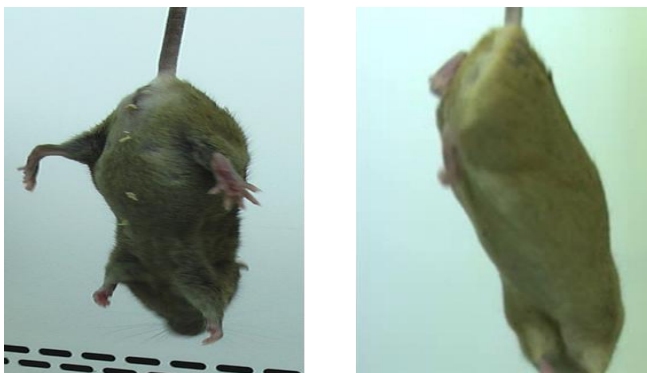
Figure 2.2: Limb grasping. Photograph showing normal (left) response by a wild-type mouse when suspended by the tail. Limbs and digits on paws are extended. Limb flapping when suspended is also normal. Right panel (a compound heterozygote *Tardbp*$^{Q101X/K160R}$ mouse) shows rear limb grasping when suspended. Rear limbs are not continuously splayed, with foot and digit curling. Limb grasping is also seen in front paws which instead of being extended outwards grasp each other.
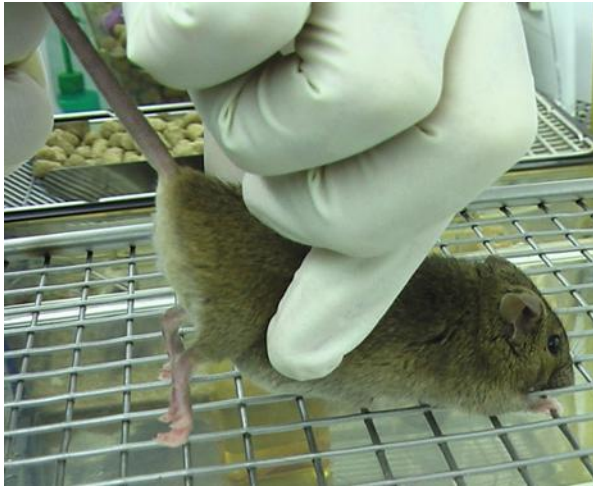
Figure 2.3: Body tone assessment. Photograph showing mouse spread on grid above SHIRPA arena. Thumb and index finger are used to feel rear body tone. There is a basal muscular tone with an elicited response. The mouse must be calm as it may reflexively hunch its rear body completely which is not a body tone response.

The mouse was then placed into the clear perspex plastic tube with the tube rolled slowly until the mouse inside it was upside down to observe the righting reflex. The grid was then placed vertically on top of the SHIRPA arena with the mouse placed at the top of grid to assess its ability to climb down the grid to the horizontal base. The mouse was made to travel down vertically and straight or replaced at top of grid if it tried to turn sideways or upwards. At the end of the SHIRPA, scores were made for whether or not the mouse bit during the screen and whether the mouse was vocal during the screen.

The basis of the SHIRPA protocol has been adapted from the EMPRESS phenotyping screen (empress.har.mrc.ac.uk). This protocol has been modified to match the protocol completed by myself. A scoring sheet for all scored behaviours is given in the Figure 2.4 with typical scores and explanations given.

MAMMALIAN GENETICS UNIT Harwell, UK.				COMMENTS
				Date
Operator				
Date of Birth (dd/mm/yy)				
Animal				
Sex				
Weight				
VIEWING JAR				
Body Position	0-5	3	Sitting or standing	
Spontaneous Activity	0-4	2	Vigorous scratch, moderate movement	
Respiration Rate	0-3	2	Moderate	
Tremor	0-2	0	Absent	
Defecation	n	1	Number	
Urination	n	1	Size - small	
Bizarre Behaviour etc.(comments)				
ARENA				
Transfer Arousal	0-6	3	Brief freeze then active movement	
Locomotor activity	n	6	Movement around arena	
Palperebral Closing	0-2	0	Eyes wide open	
Piloerection	0-1	0	None	
Gait	0-3	0	Fluid movement	
Pelvic Elevation	0-3	2	Normal (3mm)	
Tail Elevation	0-2	1	Elevated, not stiff	
Startle Response	0-3	2	Jumps less than 1 cm	
Touch Escape	0-3	2	Flees prior to touch	
Positional Passivity	0-4	0	Struggles when held by tail	
TAIL SUSPENSION				
Limb Grasp	0-1	0	None	
Limb Grasp-OTHER	0-1	0	None	
Visual Placing	0-4	2	Upon vibrissae contact	
Grip strength	0-4	2	Moderate grip, effective	
Body Tone	0-2	2	Extreme resistance	
Pinna Reflex	0-2	-		
Corneal Reflex	0-2	-		
Toe Pinch	0-4	-		
Abnormal big toe	0-1	-		
Wire Manoeuvre	0-4	0	Active grip with hind legs	
SUPINE RESTRAINT				
Body Length (mm)	n			
Heart Rate	0-2	1	Normal	
Limb Tone	0-4	2	Moderate resistance	
Abdominal Tone	0-2	1	Slight resistance	
Provoked Biting	0-1	0	None	
TEST AREA				
Righting Reflex	0-3	0		
Contact Righting Reflex	0-1	0	Normal, lands on four legs	
Catelepsy(-ve geotaxis)	0-4	0	Normal grip	
Fear	0-1	0	None	
Irritabiity	0-1	0	None	
Aggression	0-1	0	None	
Vocalization	0-1	0	None	

Figure 2.4: SHIRPA sheet. SHIRPA sheet components scored with normal values for a wild-type mouse given. Explanation of the normal value is also provided. Additional comments are noted during SHIRPA for any other abnormal behaviour.

2.1.4.   Rotarod

The accelerating rotarod test assesses balance and motor coordination. An accelerating rotating rod (UgoBasile, France) starting at four revolutions per minute (rpm) increased to 40 rpm over 300 seconds with the time that each mouse could stay on recorded.

Equipment:

Commercially available rotarod apparatus modified with rubber foam coating. Dimensions of the apparatus: rotating rod diameter is 5 cm, made of hard plastic material covered by grey rubber foam (cut from insulation material to provide better grip for the mice); lane width is 5 cm with five lanes.

Protocol:

Mice were acclimatised in the test room for 15 minutes. Up to five mice from the same cage only were placed on the rotarod with a steady speed of 4 rpm. All mice were stably on the rotarod before beginning the run. The programme was then started which steadily increased the rotation speed. If a mouse held on to the rod and spun rather than running, three spins were allowed then the time was stopped for that mouse. Times were recorded as mice fell off, up to 300 seconds. Once completed mice were returned to their cages and the rotarod cleaned with 70% ethanol, which was allowed to dry before a repeat run with the next cage. All mice were tested then repeated from the first tested cage again (once more than 15 minutes had passed). Three measurements per mouse per day over three days were recorded, using the average of all nine values for analysis.

2.1.5.   Grip strength

Grip strength (Coupan, BioSeb) is used to measure muscle strength. Forelimb strength is measured twice with an average value recorded, followed by total limb (fore and hind) measurements.

Grip strength equipment:

A BioSeb grip strength meter was used. The system is supplied with a single grid (400 x 180 x 200 mm), which connects to the sensor, shown in Figure 2.5.

Figure 2.5: Forelimb grip strength assessment.

Protocol:

The unit of measurement of the sensor was delivered in grams mode. The mouse was removed from its cage, gripping the base of the tail between the thumb and the forefinger. It was gently lowered over the top of the grid so that only its front paws could reach and grip the grid. Keeping the torso horizontal the mouse was pulled back steadily (not jerking) until the grip was released down the complete length of the grid. When the animal released the grid, the maximal grip strength value of the animal was displayed on the screen, which was recorded. This procedure was repeated to obtain a second forelimb grip strength measurement, taking the average of the two values for analysis. Then all four limbs were assessed.

This protocol has been edited from EMPRESS phenotyping (empress.har.mrc.ac.uk).

2.1.6.   Startle and pre-pulse inhibition

Startle response requires normal hearing to detect the startle tone which elicits a sensorimotor jump response, which is measured relative to weight. Pre pulse inhibition assesses sensory inhibition. A series of pre-pulses which are weaker acoustic stimuli precede the startle tone. These pre-pulses should dampen the startle response.

Equipment:

Med Associate startle boxes were used. Twelve sound proof boxes allowed assessment of twelve mice per run. The experimental apparatus is an outer chamber containing a sound proofed acoustic chamber with a load cell platform and an amplifier. A sound generator and the appropriate software regulate pulses from the amplifier (Med Associates Inc equipment).

Protocol:

Sound calibration and movement sensor calibration were completed monthly. Test animals were transported to the phenotyping room and left undisturbed for 30 minutes prior to the test to acclimatise. The computer was switched on setting up the experimental design to complete the following:

- An initial acclimation period of 5 minutes without a pre-pulse stimulus, an inter-trial interval of 50 msec and a pulse of white noise 110 (dB) / 40 msec.

- A pre-pulse inhibition session of 10 different trial types:

- A trial in which only an acoustic startle pulse is presented as white noise 110 dB / 40 msec. Pulses should be presented ten times in pseudorandom order with an inter-trial delay varying between 20 and 30 seconds.

- Eight different pre-pulse trials, of 10 msec duration, of 70, 80, 85, or 90 dB white noise stimuli presented alone or preceding the pulse by 50 msec.

- A trial in which only background noise 65 dB is presented to measure baseline movement of the animal in the chamber. Pulses should be presented ten times in pseudorandom order with an inter-trial delay varying between 20 and 30 seconds.

- Startle response recorded every millisecond for 65 msec after the onset of startle.

Each mouse was removed from its home cage and placed onto the load cell platform inside the acoustic chamber and then the door closed. Additional mice in the remaining boxes were then loaded before running the experimental session. Once complete, each mouse was carefully removed from the acoustic chamber and placed into its home cage. The acoustic chamber was wiped clean with 70% alcohol following each session and allowed to dry before subsequent sessions were run. The recorded data was saved for analysis.

This protocol has been modified from EMPRESS phenotyping (empress.har.mrc.ac.uk).

2.1.7.   Open field

Mice were placed in an empty arena and ambulation was assessed. A camera from above was used to measure ambulation for interpretation as locomotor activity, exploratory drive, neophobia and agoraphobia. Aspects of fear and anxiety were also measured. If locomotor activity was the same between mice then alterations were interpreted as being driven by fear or increased exploratory drive.

Equipment:

The open field is a 44 x 44 cm square arena. The walls are opaque (so that animals cannot see the room) and approximately 50 cm high. The arena floor is not completely smooth allowing the mice to move freely. The base colour of the open field is light grey. Light grey (RAL 7035) compensates for various coat colours, for Ethovision Noldus software video tracking.

Procedure:

Mice were moved into the testing room and left for 30 minutes, to acclimatise. Ethovision software was opened and the programme loaded. A mouse was placed into each arena and the door to the room closed before starting the trial. A standard trial run was 30 minutes. After 30 minutes video tracking the trial was saved and the mice returned to their cages. All arenas were cleaned with 70% ethanol allowing the arena to dry before beginning the next run. Four mice were analysed at the same time, always using mice from the same cages.

2.2.   Genotyping mice

For the *Tardbp* mutations, genotyping assays were completed for Q101X, K160R and F210I mutations. For SOD1^{G93A}, the transgene was genotyped as described below. Q101X and K160R samples were genotyped using a Qiagen Pyro Sequencer. F210I was genotyped using an Idaho® LightScanner and SOD1 ^{G93A} was genotyped by PCR band assessment on an agarose gel.

For all genotyping methods DNA was extracted from tissue using the following protocol. Ear clips (or other tissue) were placed in a microcentrifuge tube with 200 µl TENS buffer (amounts

were scaled to tissue size). 10 µl Proteinase-K (20mg / ml) (P6556, SIGMA) was added, mixed and incubated overnight at 55°C. The microcentrifuge tube was centrifuged for 5 minutes at maximum speed (>13,200 x g) at 4°C to pellet non-digested tissue. The supernatant was passed to a new tube and 200 µl isopropanol (BP2618-212, Fisher) was added, the tube capped and shaken. The tube was the centrifuged for 10 minutes, maximum speed (>13,200 x g) at 4°C. The supernatant was carefully discarded and then left for 1 hour to allow excess alcohol to evaporate leaving a pellet. The pellet was then resuspended in an appropriate volume of H_2O (100 µl). The recipe for TENS buffer is given in Table 2.1.

Components	Final Concentration
Tris 1M (pH 8) (BP-12-5 Fisher)	100 mM
EDTA (BP1339-1 Fisher)	5 mM
NaCl (AC42429-0050 Fisher)	200 mM
SDS (BP166-100 Fisher)	0.20%

Table 2.1: TENS buffer recipe

2.2.1. Q101X and K160R

DNA at 5 ng / µl was prepared for PCR using primers, mix and PCR as outlined in Table 2.2, Table 2.3 and Table 2.4. Following the PCR the sample was run on a Qiagen Pyro Sequencer. During this process the PCR product is added to a mixture of enzymes, DNA polymerase, ATP sulfurylase, luciferase, and apyrase as well as the substrates adenosine 5' phosphosulfate (APS) and luciferin. The mix is heated to separate the template double strand and anneal the sequencing probe. A dNTP is then added and if it matches the template strand it binds releasing pyrophosphate (PPi) which is converted by ATP sulfurylase to ATP. This drives conversion of luciferin to oxyluciferin generating light which is detected by the machinery. Apyrase then degrades the free dNTP and the next one is added, slowly sequencing from the probe. Deoxyadenosine α-thio triphosphate (dATP·S) is used as a substitute for the natural deoxyadenosine triphosphate (dATP).

Primer ID	Sequence 5' – 3'
K160R-II-F-biot	AAGGGTTTGGCTTTGTTCG
K160R-II-R	GCCCATCTATCATATGTCGTTGT
K160R-II-Seq-R	CATATGTCGTTGTGACATT
Q101X-F	CAAAAGGAAAATGGATGAGAC
Q101X-R-Biot	AGTTGTTTTCCAGGGGAGAC
Q101X-Seq-F	GAAAGTGAAAAGAGCAGTC

Table 2.2: Pyro sequencing primers and probes. Primers and probes for Q101X and K160R genotyping. Sequencing primer contains "Seq" in name.

Components	Q101X (µl)	K160R (µl)
Qiagen PCR mix (201445, Qiagen)	5	5
H_2O	2.6	2.4
Forward Primer (10 µM)	0.2	0.2
Reverse Primer (10 µM)	0.2	0.2
DMSO (D159-4 Fisher)	0	0.2
DNA (5 ng / µl)	2	2

Table 2.3: PCR set-up for pyro sequencing Q101X and K160R.

Temp (°C)	Time
95	5 minutes
Cycle 44 times	
95	30 seconds
55	30 seconds
72	15 seconds
End cycle	
72	5 minutes

Table 2.4: Pyro PCR conditions for Q101X and K160R.

2.2.2.　　　F210I

The F210I SNP was genotyped using the Idaho ® system, which uses high resolution melting for sample genotyping. The primers used, mix for PCR and PCR conditions are shown in Table 2.5, Table 2.6 and Table 2.7. The PCR was run in an Idaho® LightScanner compatible PCR plate (4ti-0771, 4ti). Following the PCR the plate was placed in the LightScanner and the samples were melted from 55 to 98°C, where the high resolution melt curve was assessed for genotyping. The temperature at which the probe falls off the wild-type and mutant alleles varies (giving different melt curves) to distinguish wild-type, heterozygous and homozygous F210I samples.

Primer ID	Sequence 5' – 3'
TDP43_F210I_F	GAAAGGTGTTTGTTGGACGTT
TDP43_F210I_R	TCTGAATGGTTTGGGAATGAAGAC
TDP43_F210I_PrF	GCTTCAGCAGATTTTCTGTCAGTATGGAG

Table 2.5: F210I primers and probe. Table showing sequence for forward and reverse primers, with the third panel showing the probe sequence. The probe was manufactured with an amino C3 modification at the 3' end. This works the same as a 3' phosphate (but lasts longer) and blocks extension of the probe.

Components	μl
HotShot master mix (HRLS-ASY- 0002 Idaho Tech)	5
LCGreen (BCHM-ASY- 0005 Idaho Tech)	1
TDP43_F210I_F (20ng / μl)	0.1
TDP43_F210I_R (20ng / μl)	0.5
TDP43_F210I_PrF (20ng / μl)	0.5
DNA (5ng / μl)	2
ddH$_2$O	0.9

Table 2.6: F210I PCR mix. Table showing the reagents used to set up the F210I genotyping PCR reaction.

Temp (°C)	Time
95	2 minutes
Cycle 55 times	
95	30 seconds
60	30 seconds
72	30 seconds
End cycle	
95	30 seconds
25	30 seconds
15	30 seconds

Table 2.7: F210I PCR programme. PCR programme used to amplify F210I fragment for analysis.

2.2.3.   SOD1^{G93A}

All mice carrying the SOD1^{G93A} transgene underwent a mating regime that maintained the transgene in heterozygosis (such that SOD1^{G93A} mice were not inter-crossed). The primers, PCR mix and normal PCR programme run are shown in Table 2.8, Table 2.9 and Table 2.10. Amplification was from genomic DNA and band products were assessed on an acrylamide gel.

Primer ID	Sequence 5' – 3'	Amplicon Length
IMR113	CATCAGCCCTAATCCATCTGA	236 bp
IMR114	CGCGACTAACAATCAAAGTGA	
Snca4R	AGAAGACCAAAGAGCAAGTGACA	130 bp
Snca4L	ATCTGGTCCTTCTTGACAAAGC	

Table 2.8: SOD1^{G93A} primers. Primers used to detect SOD1^{G93A} (IMR113 / 114) amplify a product of 236 base pairs when the transgene is present. *Snca* primers are control primers for mouse *Snca* amplifying a 130 base pair fragment. PCR product was loaded on a 2% agarose gel and run at 120 V (60 mA) for 30 minutes or until complete band separation. Samples with 2 bands are SOD1^{G93A} heterozygotes.

Components	µl
H_2O	16.8
10X buffer	2.5
DMSO	2.5
dNTPs (2.5 mM)	2
Primers (25 µM)	1
Taq polymerase	0.2
DNA	1

Table 2.9: SOD1^{G93A} genotyping PCR mix. Mix used to set up SOD1^{G93A} transgene genotyping PCR.

Temp (°C)	Time
94	3 minutes
Cycle 35 times	
94	30 seconds
60	30 seconds
72	45 seconds
End cycle	
72	10 minutes

Table 2.10: SOD1^{G93A} PCR conditions. PCR conditions to amplify SOD1^{G93A} fragment.

2.3. Constructs

2.3.1.   pcDNA 3.1 V5 / HIS constructs

All V5 / HIS mammalian expression vectors were pcDNA 3.1 (K4800-01 Invitrogen). They contain mouse TDP43 encoding cDNA inserted using BamHI / XbaI restriction sites. The backbone and *Tardbp* cDNA insert is 6.688 kilo bases (kb), as mapped in Figure 2.6.

Figure 2.6: Schematic representation of pcDNA3.1 vector containing *Tardbp* cDNA. Note that this is a mammalian expression vector with a CMV promoter in advance of the T7 promoter, not indicated on the map. Map generated using Ape software.

The V5 / HIS plasmids containing mouse TDP43 encoding cDNA were generated by Dr Peter Joyce who also generated the allelic series of point mutations through site directed mutagenesis (SDM). Two additional mutant constructs were generated by myself through site directed mutagenesis (protocol at end of section) using the primers shown below (Table 2.11). Highlighted regions show the mutant residues for the respective encoding amino acid changes.

Primer ID	Sequence 5' – 3'
TDP_D169G_F	cgacatatgatag<mark>G</mark>tgggcgatggtg
TDP_D169G_R	caccatcgccca<mark>C</mark>ctatcatatgtcg
TDP_F147L / F149L_F	CTCGAAAGGG<mark>ctt</mark>ggc<mark>ctt</mark>GTTCGATTTACAG
TDP_F147L / F149L_R	CTGTAAATCGAAC<mark>aag</mark>gcc<mark>aag</mark>CCCTTTCGAG

Table 2.11: Site directed mutagenesis primers for TDP43 point mutations. Table showing the primer sequences to generate the point mutations D169G and F147L / F149L in mouse *Tardbp* cDNA.

2.3.2.   Human TDP43 construct and CFTR mini-gene

Human TDP43 was gifted from Dr Emanuele Buratti. The construct was pFLAG TDP43 siRNA-resistant wild-type cloned HindIII / KpnI pFLAG-CMV2. Silent mutations were introduced using standard PCR procedure (SDM) in order to make them resistant to anti-TDP43 siRNA. The primers used to achieve this are shown below (Table 2.12). The CFTR mini-gene construct C155T TG11T5 was also gifted by Dr Emanuele Buratti.

Primer ID	Sequence 5' – 3'
siTDP_KOFW	taattctaagcagtcccaggatga
siTDP_KOREV	tcatcctgggactgcttagaatta

Table 2.12: Human TDP43 silent mutation primers. Primers used by the Buratti / Baralle laboratory to generate silent mutations in order to allow the construct to express human TDP43 protein despite siRNA treatment which downregulates endogenous cellular protein.

2.3.3.   GST tagged constructs - pGEX5X3 GST fusion vectors

GST tagged mouse TDP43 constructs were sub cloned from the pcDNA 3.1 vectors. pcDNA constructs containing wild-type and each of the TDP43 mutant alleles were sub cloned into pGEX5X3 GST fusion vectors. These are the bacterial expression vectors used to purify wild-type and F210I mouse TDP43 protein.

2.3.4. Generation of TDP43 D169G, F147L / F149L by site directed mutagenesis

Site directed mutagenesis was performed as per the manufacturer's conditions (200519, Stratagene). The procedure was carried out on ice. The PCR was set up on ice as shown below in Table 2.13, with the PCR run as shown in Table 2.14.

Reagent	µl
10 X Buffer	5
10 – 50 ng plasmid DNA	X
125 ng FW primer	1
125 ng REV primer	1
dNTPs	1
Quick Solution	3
PFU Turbo DNA Polymerase	1
Up to 50 µl H2O	X

Table 2.13: Stratagene SDM mix for PCR.

Temperature (°C)	Time
95°C	1 minute
Cycle 18 times	
95 ^{o}C	50 seconds
60 ^{o}C	50 seconds
68 ^{o}C	1 minute
End cycle	
68 ^{o}C	7 minutes
Store at 4 ^{o}C	

Table 2.14: SDM PCR cycling conditions.

Following the PCR, 1 µl DpnI enzyme was added and incubated at 37°C for 1 hour. Transformation of the mutagenized plasmid followed using 45 µl XL competent cells provided. 2 µl β-mercaptoethanol (M3148 Sigma) was added and incubated on ice for 10 minutes flicking

the tube to mix every 2 minutes. 2 µl reaction product was added to the cells and incubated on ice for 30 minutes. The cells were heat shocked at 42°C for 30 seconds before returning to ice for 2 minutes. 500 µl pre warmed (37°C) SOC medium (15544-034 Invitrogen) was then added and the mix was incubated at 37°C for 1 hour in the shaking incubator. 250 µl transformed cells was spread on a pre-warmed Lysogeny Broth / Ampicillin (LB-Amp plate) (100 µg / ml ampicillin, 11593-027 Invitrogen) and incubated overnight at 37°C. Individual colonies were picked the following day, grown overnight in LB-Amp and the following day mini prepped (27104, Qiagen). Plasmids (pcDNA 3.1) were sequenced using the following primers to confirm SDM (Table 2.15).

Primer Name	Sequence 5' – 3'
T7	TAATACGACTCACTATAGGG
Pj23	GAAAGTGAAAAGAGCAGTCCAG
Pj24	CTTCATTCCCAAACCATTCAGAG
Pj25	CATGTTAGCCAGCCAGCAGAAC

Table 2.15: Primers used to sequence insert region for pcDNA 3.1 TDP43 vectors. These primers are designed to sequence the full length of the TDP43 encoding cDNA transcript inserted into the V5 / HIS plasmid. There is significant sequence overlap from the T7 sequence to beyond the C-terminal tags and STOP site.

2.3.5.   Plasmid amplification and extraction

Plasmids were extracted using Qiagen mini / midi / maxi (endotoxin free) kits (27106, 12143, 12362 Qiagen). When working in the Buratti / Baralle laboratory, plasmids were grown up using JetStar (210025 Gmbh) mini / midi / maxi kits. The JetStar protocol is outline below.

E coli DH5α (18263-012, Invitrogen) cells were thawed on ice and 3 µl plasmid (10ng / µl) was added to 30 µl cells. The cells were incubated on ice for 20 minutes, then placed at 42°C for 2 minutes in a water bath and returned to ice for 5 minutes. All 30 µl of the cells were spread on pre-warmed agar plates (at 200 µg / ml Ampicillin) and left to incubate overnight at 37°C, agar side up. The following day, single, isolated colonies were selected and put into 500 ml LB + 500 µl of 1000 X ampicillin stock. This was incubated at 37°C on a shaker (speed 140) for 16 hours. The bacterial cells were then pelleted at >3700 *x g* for 20 minutes and frozen at -20°C until required.

Mini / Midi / Maxi preps were completed using the JetStar Plasmid purification system (210025, GENOMED Gmbh). Jet Star purification solutions (provided by the manufacturer) are given below with solutions 2-6 stored at room temperature.

Solution 1 – (cell resuspension) 50 mM Tris + 10 mM EDTA + HCl to pH 8 (add extra RNAse and store at 4°C)

Solution 2 – (cell lysis) 200 mM NaCl + 5% SDS (w / v)

Solution 3 – (Neutralization) 3.1 M potassium acetate + acetic acid to pH 5.5

Solution 4 – (Column equilibration) 600 mM NaCl + 100 mM sodium acetate + 0.015% Triton X-100 + acetic acid to pH 5.5)

Solution 5 – (column washing) 800 mM NaCl + 100 mM sodium acetate + acetic acid to pH 5.0

Solution 6 – (DNA elution) 1500 mM NaCl + 100 mM sodium acetate + acetic acid to pH 5.0

Midi preps were carried our as per the manufacturer's instructions. A column was equilibrated with 10 ml solution 4, which was allowed to flow through by gravity. Bacterial cells were harvested by pelleting for 20 minutes at 3700 x g and removing all traces of medium (completed at the end of plasmid amplification step). Cells were suspended in 4 ml solution E1. 10 µg / ml of extra RNAse inhibitor (50 µl to 4 ml) was added. Solution 2 (4 ml) was then added and mixed gently by inversion until a homogeneous lysate formed. The lysate was incubated at room temperature for 5 minutes before adding solution 3 (4 ml) and mixing immediately by multiple inversions until a homogeneous lysate formed. This was filtered through thin filter paper and then the supernatant was added to the equilibrated JetStar column. The column was washed with 10 ml solution 5 twice and the DNA then eluted with solution 6 (5 ml). The DNA was precipitated with 0.7 volumes isopropanol (3.5 ml) and then centrifuged at 4°C at 12,000 x g for 30 minutes. The pellet was washed with 70% ethanol and centrifuged at 12,000 x g. The pellet was then air dried for 10 minutes and re dissolved in 200 µl H$_2$O.

2.4. Culturing cells, transfections, add-back assay and labelling

All cells were grown in Heraeus Cell culture incubators at 37°C in humidified conditions with 5% CO_2. All media used were pre-warmed to 37°C before cell exposure unless otherwise stated. All cell culture work was completed in class two biological safety cabinet.

2.4.1. HeLa cells

HeLa cells were grown using standard cell culture practise. Cells were grown in complete media containing DMEM (31966, Gibco) supplemented with 10% FBS (10082147, Invitrogen) and 1% pen / strep (10378016, Invitrogen). Cells were split at 80-90% visual confluence (being split 1:5) and maintained following standard practise in 10 cm dishes (664160 Greiner).

2.4.2. Mouse Embryonic Fibroblasts (MEFs)

Complete medium for MEFs was identical to that used for HeLa cells but was also supplemented with 3 ml Ultraglutamine II (BE04-684E Lonza). MEFs were obtained from embryos using the following protocol.

PBS-Gelatin (0.1%) (Gelatin, S-006-100 Invitrogen) was added to a 10 cm (664160 Greiner) cell culture dish, with 10 ml in one dish per embryo. Dishes were pre warmed (37°C) in cell culture incubators until needed. Embryos were harvested from E14.5 dpc pregnant females. The female was culled by schedule one procedure and embryos were removed and stored in PBS on ice. Each embryo was dissected from the maternal sac and assessed for visual defects. The head, limbs and organs were removed from each embryo. Individual carcasses were then processed in parallel in separate dishes. From this step, all work was completed in a class two biological safety cabinet. Each carcass was transferred to a 5 cm dish (628160 Greiner) with 3 ml pre-warmed trypsin (25300062, Invitrogen). The carcass was roughly chopped using two 10a sterilised scalpel blades (Swan Morton). The trypsin / cell solution was homogenised by

pipetting up and down ten times with a 5 ml pipette and then transferred to a 50 ml Falcon tube (352070, BD). Each Falcon tube was incubated at 37°C in a water bath with agitation for 5 minutes. Following incubation, the trypsin / cell solution was returned to the 5 cm dish and syringed up and down five times (using a 10 ml syringe). Pre warmed cell culture dishes were taken from the incubator and 7 ml of PBS-Gelatin was removed. 10 ml pre warmed (37°C) complete media was then added to the dish. The trypsinized cell mix was then added drop wise and the plate swirled gently. The presence of cells was confirmed under a light microscope and the cells were left in the culture incubator overnight (5% CO_2, 37°C).

Once cells reached 80% visual confluence, which was usually after one to two days, the cells were passaged at a 1:3 ratio. In between passages, cells were washed with PBS and fresh growth media added.

2.4.3.   Transfection with Effectene

Effectene (1008430, Qiagen) was used for HeLa cell transfections. The following solutions were made for each transfection: 300 µl EC buffer, 3 µg plasmid and 16 µl enhancer. The samples were then vortexed for 10 seconds and left to incubate for 5 minutes at room temperature. 20 µl Effectene was then added and vortexed for 20 seconds followed by incubation for 10 minutes at room temperature. During this time, the cells were washed with 10 ml PBS and 9 ml complete medium was added (cells were in 10 cm dishes, at 80% confluence). After the 10 minute incubation, 600 µl complete medium was added to the mix. The mix was then added to the cells drop wise and the cell culture dish was swirled to distribute evenly. After 24 hours the cells were harvested. This was scaled down for six well dishes in the add-back assay as described later.

2.4.4.   Electroporation (CFTR mini-gene)

Electroporation was used to insert the CFTR mini-gene into MEFs. Wild-type and F210I mutant P1 MEFs were grown to 80% confluence (in a 10 cm dish) and then split into a T75 flask (658975 Greiner). Once at 80% confluence (normally up to two days), the MEFs were

electroporated with 4 µg maxi prepped CFTR mini-gene plasmid using the Lonza Amaxa system (DPD-1005, Lonza), programme T20, solution one. For MEFs, a choice of two programs and solutions were available, with T20 / solution one providing a transfection efficiency for a GFP control plasmid of 50%. Electroporation was completed following the manufacturer's instructions. MEFs were grown to 80% confluence in a T75 flask. They were washed once in PBS and trypsinized for 3 minutes at 37°C. Cell detachment was confirmed and the cells were centrifuged at 200 x g for 10 minutes. The cell pellet was resuspended in 100 µl nucleofector solution (room temperature). 100 µl cell solution was combined with 4 µg CFTR plasmid. The cell / DNA suspension was transferred into a certified cuvette and the cap closed. Programme T20 was selected and the cuvette inserted into the holder before applying the programme. Once complete the cuvette was removed (approximately 3 seconds) then 500 µl complete medium was added to the cuvette. The contents were transferred to a 10 cm dish and 9 ml complete media was added. The MEFs were grown overnight and harvested after 24 hours. Control electroporation of no CFTR plasmid, or no solution one was also run alongside samples.

MEFs were harvested by being washed in 10 ml PBS and then trypsinized in 3 ml trypsin in the cell culture incubator. Following detachment, 7 ml complete media was added to deactivate the trypsin and the cells were pelleted in a 15 cm Falcon tube at 1000 x g, for 5 minutes. The supernatant was removed and the cell pellets snap frozen.

2.4.5. Add-back assay

To prevent interference with the transfection reagent (Effectene) antibiotic was not added to the complete medium used to culture the HeLa cells. All solutions were pre-warmed to 37°C including complete medium, trypsin (R-009-50, GIBCO) PBS, optimem (S1985, GIBCO) and EC buffer (Qiagen). A four day protocol was completed as described below:

Day 1: HeLa cells were plated into 6 well plates (3516, Costar) at 180 000 cells per well.

Day 2: First day of siRNA against endogenous human TDP43. The following mix per well was prepared: 13 µl optimem + 3 µl oligofectamine (Qiagen). This was incubated at room temperature for 5 minutes. In another tube 180 µl optimem + 2.5 µl siRNA (40 mM, GCAAAGCCAAGAUGAGCCUdTdT, ThermoSci Dharmacon) was prepared and after five minutes

was mixed with the first tube. The combined solutions were resuspended and then incubated for 20 minutes. While waiting, cells were washed in PBS (2 ml) and then suspended in 1.5 ml optimem. The siRNA solution was then added to the wells drop wise with gentle plate swaying to ensure even distribution. 4-6 hours after this 200 µl of FBS was added.

Day 3: Repeated day 2 (this was the second round of siRNA against endogenous TDP43).

Day 4: Transfection of plasmid. EC buffer was pre-warmed (Qiagen). For each well 150 µl EC buffer, 0.5 µg Plasmid, 0.5 µg CFTR mini-gene and 4 µl enhancer (Qiagen) were added to an microcentrifuge tube. Following a 2 second vortex the mix was then incubated for 5 minutes at room temperature. 5 µl Effectene was then added, the mix vortexed again for 10-15 seconds and then incubated for 10 minutes at room temperature. While waiting, cells were washed with PBS (2 ml) and then 1.5 ml complete medium was added. After 10 minutes, 600 µl complete medium was added to the microcentrifuge tube with the plasmid mix, resuspended with a pipette and then added drop wise to the plate. The plate was then swirled to ensure even distribution.

The following day cells were washed in PBS (2 ml) before adding trypsin (300 µl). They were incubated for 5 minutes at 37°C. Once detached, 700 µl complete medium was added to the cells, which were then resuspended and divided into two microcentrifuge tubes equally. The microcentrifuge tubes were centrifuged at 200 x g for 10 minutes at room temperature; the supernatant removed with the cell pellet frozen either for Western blotting or reverse transcription PCR (one microcentrifuge tube for each).

2.4.6.   Nuclear / Cytoplasmic fractionation

Following HeLa cell transfection with wild-type and F210I V5 / HIS tagged plasmids using Effectene, two 10 cm dishes of HeLa cells were harvested. Solutions needed for nuclear / cytoplasmic fractionation are given in Table 2.16.

Buffer N	Buffer N + NP40	Solution 1	Solution 2
15 mM Tris HCl pH7.5	Buffer N + 0.6% NP40 (NC9807780 Fisher)	10 mM Hepes pH 7.9 (AC21500-1000 Fisher)	10 mM Hepes pH 7.9
60 mM KCl (AC19677-0010 Fisher)		10 mM KCl	10 mM KCl
15 mM NaCl		1.5 mM $MgCl_2$	1.5 mM $MgCl_2$
5 mM $MgCl_2$ (AC41341-5000 Fisher)		0.1 mM EGTA (ICN213293 MP Bio)	0.1 mM EGTA
1 mM $CaCl_2$ (AC34961-0250 Fisher)		0.1 mM DTT	0.1 mM DTT
1 mM DTT (AC32719-0010 Fisher)		0.5 mM PMSF	5% glycerol (AC15892-2500 Fisher)
250 mM sucrose (AC17714-0050 Fisher)			400 mM NaCl
2 mM sodium vanadate (S454-50 Fisher)			0.5 mM PMSF
1 mM PMSF (AC21574-0500 Fisher)			
1X Protease Inhibitor (Roche)			

Table 2.16: Nuclear / Cytoplasmic fractionation solutions. Recipes for all components required for nuclear / cytoplasmic fractionation.

2.4.7.   Fractionation protocol

HeLa cells (in 10 cm dishes) were washed twice with PBS. 5 ml PBS was added and the cells were then scraped and transferred to a microcentrifuge tube which was centrifuged at 200 x g for 5 minutes at 4°C. The cells were resuspended with buffer N (five times the volume of the pellet – 500 µl). Then the same volume of buffer N + NP40 (to break the cytoplasmic membrane) was added. This was mixed using a tip (with the end cut off) and incubated on ice for 5 minutes. The mix was centrifuged for 5 minutes at 200 x g, 4°C. The supernatant was stored at -80°C (cytoplasmic fraction). The nuclei (pellet) were resuspended in 1 ml solution 1 using a tip with a cut off end. This was then centrifuged for 5 minutes at 4°C, 200 x g. The supernatant was discarded and the pellet resuspended in solution 2 (1X the volume of the

pellet – 100 µl was added). Solution 2 breaks the nuclear membrane and extracts nuclear proteins. The solution was mixed (with a cut tip end) and incubated for 30 minutes on ice, swirling every 5 minutes. This was followed by 30 minutes centrifugation at maximum speed at 4°C, taking the supernatant for storage at -80°C (nuclear fraction). Everything was done at 4°C and when mixed this was done gently to avoid causing damage that could ruin the fractionation process. 20 µl of each fraction was then loaded on an acrylamide gel with 5 µl SDS 5X loading buffer. This stage is described later.

2.4.8. Immunofluorescence

MEFs were cultured as previously described. On the penultimate passage, cells were trypsinized and split into dishes containing sterile glass coverslips to which the cells adhere. MEFs were grown for 24-48 hours to achieve a desirable visual degree of confluence. Cells were washed twice with an appropriate volume of PBS to the culture dish size, before PBS removal and 4% PFA (fix) (158127 Sigma) addition for 10 minutes at room temperature. Following incubation, the PFA was removed and the fixed cells were washed in PBS to remove PFA traces. All cells were then permeabilized. PBS was removed and the cells submerged in ice cold methanol (A456-212 Fisher) for 15 minutes at room temperature. Methanol removal was followed by a PBS wash. The cells were then put in blocking (PBS, 5% BSA BP617-10 Fisher) for one hour. After blocking, an appropriate volume of blocking per coverslip was prepared with primary antibody added at the desired concentration (1:200). The primary antibody in blocking was added as a drop on parafilm (S37441 Fisher), placing the coverslip with cells face down on the drop to cover the surface of the coverslip. Incubation for 1 hour at room temperature was followed by removing the coverslip and face up, washing in PBS for 3 X 5 minutes. The cover slip with cells was then incubated with fluorescently tagged secondary antibodies in blocking, as completed with the primary antibody. Incubation took place in the dark and then PBS washes were repeated. The slide was then prepared with DAPI self-hardening mounting medium (H1500, Vector Labs). The coverslip was placed face down on mounting medium to cover the surface completely. Coverslip edges were sealed with nail varnish or DPX. This was allowed to air dry in the dark for more than three hours at room temperature then stored at 4°C. Samples were visualized on a confocal microscope (SP5 Leica) for up to two weeks, although the signal faded through time. The antibody used is shown in Table 2.17.

Primary antibody	Primary Concentration	Secondary antibody	Secondary Concentration
anti-TDP43 (Protein Tech)	1:200	Alexa488 anti-rabbit (A-11008, Invitrogen)	1:500

Table 2.17: Immunofluorescence antibody conditions. Primary and secondary antibodies used for immunofluorescence with concentrations used.

2.5. RNA

2.5.1. Extracting RNA from MEFs, embryo head and adult brain

RNA extraction was completed using TRIzol. RNAse free filter tips (732-2223 VWR) were used and all bench space and equipment were sterilised using 70% ethanol. Cells or tissue were homogenised in 1 ml TRIzol (15596-026 Invitrogen) per 50 – 100 mg tissue. This was incubated at room temperature for 5 minutes, before adding 0.2 ml chloroform (AC42355-0040 Fisher). The microcentrifuge tube was capped and shaken for 15 seconds before incubation at room temperature for 25 minutes. The microcentrifuge tube was centrifuged for 15 minutes at 12,000 $x g$ at 4°C. The aqueous top phase was transferred to a new microcentrifuge tube. 500 µl isopropanol (AC41279-0025 Fisher) was added and incubated for 10 minutes at room temperature. This was then centrifuged for 10 minutes at 12,000 $x g$ at 4°C. The supernatant was removed and the RNA pellet washed with 1 ml 75% ethanol. The microcentrifuge tube was vortexed briefly at low intensity and then centrifuged for 5 minutes at 7,500 $x g$ at 4°C. The supernatant was removed and the pellet air dried briefly (1-3 minutes) and then re dissolved in 50 µl RNAse free water. The RNA concentration was measured on a N8000 spectrophotometer (Thermo) with a ratio of absorbance at 260 nm and 280 nm of approximately two.

2.5.2. Quantifying RNA and converting to cDNA

1 μg RNA was DNAse treated using the Invitrogen DNAse I kit (18068-015, Invitrogen). A mix of 1 μg RNA sample, 1 μl 10X DNAse reaction buffer and 1 μl DNAse (up to 10 μl with H_2O) was prepared. The mix was incubated for 15 minutes at room temperature then 1 μl 25 mM EDTA was added and heated for 10 minutes at 65°C (to deactivate the DNAse).

Following DNAse treatment, cDNA was generated using the Invitrogen Superscript 3 First strand cDNA Synthesis kit (18080-200 Invitrogen). A mix of 1 μg RNA, 2 μl RT enzyme mix, 10 μl 2 X RT reactions mix (containing Oligo dT) was made up to 20 μl with H_2O. The mix was run on the thermo programme given below in Table 2.18. The cDNA was then stored at -20°C until required.

Temp (°C)	Time
25 ^{o}C	10 minutes
50 ^{o}C	30 minutes
85 ^{o}C	5 minutes
1 μl of E. Coli RNAse H was added and mixed	
37°C	20 minutes

Table 2.18: cDNA thermo programme.

2.5.3. Splicing reactions and band separation by agarose gel electrophoresis

cDNA was generated from MEFs, embryonic head and adult brain. For splicing primer reactions, 1 μl of cDNA was used in the PCR. The PCR was set up and run as indicated in Table

75

2.19, Table 2.20 and Table 2.21. PCR product was run on Tris-acetate-EDTA / Tris-Borate-EDTA (TAE / TBE) agarose gels. TAE and TBE gels were made and run in their respective buffers. 10X TAE buffer (48.4 grams of Tris base [tris(hydroxymethyl)aminomethane], 11.4 ml of glacial acetic acid (17.4 M), 3.7 grams of EDTA disodium salt, deionized water up to 1 L) was diluted to 1X in ddH$_2$O. For a 100 ml gel, 100 ml of TAE was added to the appropriate amount of agarose (T4382 Sigma) or NuSieve 3:1 (4618727 Fisher) to make the desired percentage gel (for example 2 grams for a 2% gel). The mix was heated in a microwave for approximately 2 minutes until the powder dissolved. It was allowed to cool then 4 µl ethidium bromide (AC17096-0050 Fisher) or gel red (BT41001 Biotium) was added. Once cool the mix was poured into a sealed mould and gel combs added. Once the gel had solidified in the biological safety cabinet it was placed in a tank and submerged in 1X TAE buffer. Loading buffer added (B7022S, NEB) to the PCR product followed by loading an appropriate volume in the gel. NEB 100 bp or 1 kb ladder (N3231 / N3232, NEB) was also loaded to estimate the product size. The gel was run at 100 - 120 volts (50 mA) for an appropriate time to achieve band separation and visualised on a BioRad chemidoc. In order to quantify bands, photos saved as tif images were opened using ImageJ software and measured (which measures pixel intensity to show band intensity). For quantification purposes, PCRs were completed with fewer cycles to avoid producing saturated bands which would skew the results interpreted by the ImageJ software. Splicing primer gels were 3.5% NuSieve 3:1 agarose gels. The PCR mix, programme and primers used are given in Table 2.19, Table 2.20 and Table 2.21.

Reagent	µl
Qiagen Mix (201445)	5
H$_2$O	3.6
Primer-F (10 µM)	0.2
Primer-R (10 µM)	0.2
cDNA	1

Table 2.19: Mix for splicing reactions.

Temp (°C)	Time
94	3 minutes
Cycle 34 times	
94	45 seconds
55	45 seconds
72	45 seconds
End cycle	
72	10 minutes

Table 2.20: PCR for splicing reactions.

Gene	Primer ID	Primer Sequence 5' – 3'	Exon
Dnajc5	Dnajc5-F_SPLI_DC	CTCTATGTGGCGGAGCAGTT	3
	Dnajc5-R_SPLI_DC	GCTGTATGACGATCGGTGTG	5
Pdp1	Pdp1-F_SPLI_DC	GTGCTGAGTGAGGGAAGGAC	5' UTR
	Pdp1-R_SPLI_DC	TGCAGTGCCATAGATTCTGC	2
Poldip3	Poldip3-F_SPLI_DC	CATTGGGACTGTAACCCCAG	2
	Poldip3-R_SPLI_DC	TGCAAACTTCATCTGCTTGG	4
Sort1	Mouse Sort1-F	CAGGAGACAAATGCCAAGGT	17
	Mouse Sort1-R	TGGCCAGGATAATAGGGACA	19
TDP43	TDP43-NMD2-L:	AAGAAGTGGAAGATTTGGTGGT	6
	TDP43-NMD2-R:	GCGTGATGACGAATTCTTGG	3' UTR

Table 2.21: Primers used for splicing reactions.

2.5.4.   Add-back assay reverse transcription PCR

Reverse transcription PCR was used to assess exon 9 mini-gene splicing. This protocol was completed in the Buratti / Baralle laboratory. Once RNA was extracted the concentration was measured and the RNA was converted to cDNA. For each sample a mix was made (Table 2.22). The mix was heated at 70°C for 5 minutes and then left on ice for 5 minutes. While waiting a separate mix per sample was made (Table 2.23). The second mix was added to the first mix with the RNA and incubated for 1 hour at 37°C. Following the 1 hour incubation the cDNA was ready for PCR. The following mix per tube was made (Table 2.24), 23 µl mix + 2 µl cDNA were added together for PCR (Table 2.25). Following PCR, 5 µl sample + 1 µl loading dye were loaded onto a TBE agarose gel (1.8%) with ethidium bromide in 1X TBE. 3 µl ladder (1 kb, N3232 NEB) was also loaded. Once the gel had run (at 100 volts / 60 mA, until sufficient band separation), the product was photographed and quantified using ImageJ software as previously described.

Components	µl
1 µg RNA (make up to 10 µl with H_2O)	10
Random primers (100ng / µl) (C118A 28320210 Promega)	1
dNTPs (5 mM)	1

Table 2.22: Part 1 of cDNA generation in Buratti / Baralle laboratory.

Components	µl
5X reaction buffer (Y02321 Invitrogen)	4
0.1mM DTT	2
Reverse Transcriptase Mlv (RT) (28025-013 Invitrogen)	0.5

Table 2.23: Part 2 of cDNA generation in Buratti / Baralle laboratory.

Components	µl
Buffer (NEB Biolab)	2.5
α23 primer (20 µM) CAACTTCAAGCTCCTAAGCCACTGC	1
Bra primer (20 µM) TAGGATCCGGTCACCAGGAAGTTGGTTAAATCA	1
dNTPs (5 mM)	1
Taq (M0273L NEB)	0.52
H_2O	17.435

Table 2.24: CFTR mini-gene PCR set up.

Temp (°C)	Time
94	5 minutes
Cycle 20 times	
94	30 seconds
55	30 seconds
72	30 seconds
End cycle	
72	7 minutes
4	hold

Table 2.25: CFTR mini-gene PCR cycling conditions.

2.5.5. Real time PCR using cDNA

Real time PCR was used to quantify RNA transcripts using primers designed to produce a product spanning exons. Real time PCR used SYBR Green Fast mix (4385616, Applied Bio) with an ABI 7500 Fast Real Time System, using the cycling programme, mix and primers shown in Table 2.26, Table 2.27 and Table 2.28. Primer amplification efficiency was optimized and the control gene used was *S16,* with the amplification efficiency between target and control genes being confirmed as not being significantly different. For this, the difference between the amplification slopes was less than 0.1. This confirms that control and target gene primers amplify equally efficiently. Levels were measured through calculating ΔΔCT showing fold change normalized to the reference gene *S16*. The amount of target gene normalised to *S16* is represented in the formula $2^{-\Delta\Delta C_T}$. All samples per plate were then normalised to a reference sample.

Temp (°C)	Time
95°C	20 seconds
Cycle 40 times	
95°C	3 seconds
60	30 seconds
End cycle	

Table 2.26: PCR programme for real time PCR.

Component	µl
Fast SYBR Green Master Mix (2X) (4309155 ABI)	10
Forward Primer (2 µM)	1
Reverse Primer (2 µM)	1
H_2O	5
cDNA (1 / 10 dilution)	3

Table 2.27: PCR mix for real time PCR.

Gene	Primer ID	Primer Sequence 5' – 3'
Cdk6	Cdk6_p4_SyGr_F	CCAGCAGTGGACAGATAAAGC
Cdk6	Cdk6_p4_SyGr_R	CTGGACTGGAGCAGGACTTC
Grn	PGRN_F_2_M_SyGr	AAGCCTCAAGGGAAGTTGG
Grn	PGRN_R_2_M_SyGr	ACGGGAGGCTGGATAAAATC
Fus	FUS_F_1_SyGr	GTTTTGGCCCTGGCAAGAT
Fus	FUS_R_1_SyGr	CTGGGTACAGGAAGAGTTCCA
Cadps	Cadps_FW_ex28_SyGr	TGCAGCTCCACATTTACCAG
Cadps	Cadps_RV_ex29_SyGr	CCTCCACAGTGAGACGGTTT
TDP43	tdp_exon2_F	GGAATCCCGTGTCTCAGTGT
TDP43	tdp_exon3_R	AGGAAGCATCTGTCTCATCCA

Table 2.28: Primers used for real time PCR.

2.6. Protein

2.6.1. Protein extraction

To extract protein from cells, embryonic head or adult brain, cells / tissue were obtained from -80°C storage or freshly extracted. Cells were placed in an appropriate amount of RIPA buffer (Table 2.29) containing 1X protease inhibitor (11873580001 Roche) and if required, phosphatase inhibitor (04906837001 Roche). For tissue, samples were placed in RIPA within a lysis column (116540434, MP Bio) containing beads and homogenised until all tissue was gone, using a sample homogenizer. With cells, homogenization was achieved by pipetting up and down on ice. Following homogenization samples were transferred to a microcentrifuge tube and centrifuged at >14,000 x g for 15-30 minutes. The supernatant was removed into a new microcentrifuge tube (RIPA soluble fraction) and the pellet stored (RIPA insoluble). Soluble extract was kept on ice and aliquoted. To measure concentrations a Bradford assay was completed as described below.

Components	Amount
1M Tris pH 7.5	10 ml
NaCl	1.753 grams
10% SDS	2 ml
10% Sodium-Deoxycholate (AA B2075914 Fisher)	10 ml
NP-40	2 ml
H_2O	176 ml

Table 2.29: RIPA buffer recipe.

2.6.2.   Bradford assay

The Bradford assay was completed using 1:5 diluted RIPA, as RIPA affects the Bradford reagent. Bradford reagent (B6916 Sigma) was mixed gently and incubated on the bench to get to room temperature (from 4°C storage). BSA standards were prepared: 2 µg, 1 µg, 0.5 µg, 0.25 µg and 0.125 µg. 20 µl BSA (10 mg / ml 90001, NEB) was added to 80 µl 1:5 diluted RIPA. This was vortexed for 10 seconds and centrifuged, giving the 2 µg standard. 50 µl of this was added to 50 µl RIPA (1:5), vortexed and centrifuged. The serial dilution was then continued. Having made the standards, the samples were diluted 1:5 in ddH$_2$O. The Bradford assay was prepared by loading the standard curve in triplicate, 5 µl per well in a 96 well plate (265302 NUNC). RIPA 1:5 and H$_2$O controls were also loaded. The samples were then loaded in triplicate. Following sample loading 200 µl Bradford reagent was added to every well. The plate was mixed on a rocker for 5 minutes then read on a KC Junior plate reader (Biotek). Results were exported to excel (which accounted for the dilution). Bradford standard curves always had an R greater than 0.98 to be acceptably accurate. Also, if sample concentrations were significantly higher than 2 µg per µl, in not matching curve values, the sample was diluted further and re-measured.

2.6.3.   Western blotting

Protein samples were run by SDS Page using Invitrogen Novex BisTris gels, either 4-12% or 10% (WG1401A / NP0301PK2 Invitrogen). Either mini or midi gels were run with varying numbers of combs providing flexibility in sample volumes and numbers that were loaded per gel. All samples were run under reduced conditions and prepared as indicated below using a mini gel example.

Samples were prepared by adding X µl of protein, 2.5 µl NuPage LDS sample buffer (4X) (NP0007 Invitrogen), 1 µl NuPage Reducing agent (10X) (NP0004 Invitrogen) and made up to 10 µl with ddH$_2$O. Samples were heated at 70°C for 10 minutes, or 95°C for 5 minutes (to denature the protein). The gel was submerged in 1X SDS running buffer in the tank (prepared by adding 50 ml 20X NuPage MOPS buffer (NP0001 Invitrogen) to 950 ml deionized water). For reduced samples, 500 µl NuPage antioxidant (NP0005 Invitrogen) was added to the inner

chamber. Samples were loaded into wells alongside the See Blue plus 2 ladder (LC5925 Invitrogen). The gel was electrophoresed at 200 volts (60- 125 mA) for 55 minutes.

Following the run the gel was semi-dry blotted. Two thick filter papers (3030-6185, Whatman) were pre-soaked in transfer buffer (Table 2.30) and the PVDF membrane (IPFL00010 Millipore) was activated in methanol for 5 seconds before also being placed in transfer buffer. A thick filter paper, the PVDF membrane, the gel and then a final thick filter paper were layered as a "sandwich". The chamber was closed for the semi dry blotter and protein transferred from the gel to the membrane at 15 volts (100 mA) for 90 minutes. At the end of the run, the membrane was removed and placed into 10 ml blocking (PBS, 0.2% tween, 5% milk powder) (tween is BP337-100 Fisher, Milk powder is Marvel).

Component	Amount
Tris	11.64 grams
Glycine (G48-12 Fisher)	5.88 grams
10% SDS solution	7.5 ml
100% Methanol (A456-212 Fisher)	400 ml
H_2O	1 592.5 ml

Table 2.30: Transfer buffer recipe.

For antibody labelling the membrane was initially blocked (PBS, 0.2% tween, 5% milk) for 1 hour at room temperature shaking, or at 4°C overnight. This blocking reduces non-specific antibody labelling. The membrane was then incubated in 10 ml blocking with primary antibody (at a defined concentration) for 1 hour at room temperature shaking. After primary antibody incubation, the membrane was washed for 3 X 20 minutes on the belly dancer platform (in PBST – PBS 0.2% tween), then the secondary was added (at a defined concentration) in blocking with shaking for 1 hour. During fluorescent secondary antibody incubation the membrane container was covered in foil to block light bleaching the secondary fluorophore. Following secondary incubation, 3 X 20 minutes washes on the belly dancer ensued (in PBST 0.2%). The membrane could then be stained for ECL visualisation (with secondary HRP antibodies) or dried for Li-Cor odyssey visualisation.

Where secondary HRP antibodies were used, the membrane was removed from wash solution and placed on film, tipping of excess wash solution. Pierce ECL (32106 Pierce) was added and the membrane covered. It was incubated for 3 minutes and then excess ECL was tipped off. A

top seal of film was placed over the membrane for visualisation with a Chemi Doc (UVP). Complete band quantification used ImageJ software.

Where fluorescent secondary antibodies for the Li-Cor Odyssey visualisation system were used, the membrane was dried in a dark box on white tissue. The membrane was then placed in the Li-Cor Odyssey machine and visualized accordingly. Band quantification was completed using Odyssey software.

For both visualisation methods, membranes were stripped and re labeled with alternative antibodies. Stripping was completed by shaking the membrane in 10 ml stripping solution (21059, Thermo) (for 10-20 minutes), then washing for 3 X 10 minutes in PBST, re blocking for 1 hour and repeating antibody labelling.

2.6.4.   Alternative Western blotting protocol

When working in the Buratti / Baralle laboratory, Western blotting was completed using individually cast gels rather than the pre-cast Invitrogen system. This technique is presented in detail below. Acrylamide gels were run at 80-100 volts (100 mA) through stacking, then at 150 V (80 mA) for the remainder of the run. Gel components are shown in Table 2.31, Table 2.32, Table 2.33 with loading buffer in Table 2.34. Following antibody staining and ECL visualisation membranes were stripped using the solution in Table 2.35, to allow for further antibody labelling.

Acrylamide / bis 40% 29:1	Catalogue details	%
Acrylamide	1138 Gerbu	38.7
N,N'-Methylenebisacrylamide	1138 Gerbu	1.33
Water		60

Table 2.31: Making acrylamide / bis 40%.

Components	8%	10%	12%
Acrylamide / bis (40%) - 29:1	4 ml	5 ml	6 ml
Tris HCl 1.5 M pH 8.8	5 ml	5 ml	5 ml
H_2O distilled	11 ml	10 ml	9 ml
SDS 10%	200 μl	200 μl	200 μl
APS 10% (AC40116-0250 Fisher)	200 μl	200 μl	200 μl
TEMED (BP150-20 Fisher)	20 μl	20 μl	20 μl

Table 2.32: Making acrylamide gels for Western blotting.

Stacking	Volume
Acrylamide / bis (40%)	0.42 ml
Tris HCl 0.5M pH 6.8	2.5 ml
H_2O	2 ml
SDS 10%	50 μl
APS 10%	50 μl
TEMED	10 μl

Table 2.33: Making stacking gels for Western blotting.

Component	Final Concentration
Tris-HCl pH6.8	250 mM
SDS	10%
Glycerol	30%
β-mercaptoethanol (or 0.5 M DTT)	5%
Bromophenol blue (AC40315-1000 Fisher)	0.02%

Table 2.34: 5X SDS loading sample buffer.

Component	Volume
β-mercaptoethanol	175 μl
Tris pH 6.8	3.125 ml
SDS 10%	5 ml
H_2O	16.7 ml

Table 2.35: Stripping solution.

Membrane transfer to PVDF membranes was completed in a wet tank blotter. 10X transfer solution: 30g Tris, 147g glycine in 1 litre of H_2O was made. For a 1X solution, 100 ml of 10X stock was added to 800 ml H_2O and 100 ml methanol. A "sandwich" was made containing a spacer material, the PVDF membrane, the gel and another spacer material. The sandwich was placed in a chamber containing 1X transfer solution, with the current passing through the gel and then membrane to transfer the protein to the membrane. Proteins were transferred onto PVDF Hybond C membrane (RPN303E Amersham Biosciences).

Visualisation of gels without transfer was completed by staining with Coomassie blue staining solution (B-0149 SIGMA) (50% H_2O, 40% methanol, 10% acetic acid, 0.2% Coomassie powder). The gel was left in Coomassie solution shaking at 65°C for 2 hours and then destained with the same solution without the Coomassie, shaking at room temperature.

2.6.5.   EMSA gels / Band shift

The band shift experiment was completed using an electrophoretic mobility shift assay (EMSA). The EMSA gel (5% acrylamide) was made up of 2.5 ml acrylamide / bis (40%), 200 µl APS, up to 20 ml in 0.5X TBE with 20 µl TEMED. The gel was run at 4°C and was pre chilled in a cold room for a minimum of 2 hours. It was electrophoresed in 0.5 X TBE, with different concentrations of TBE affecting how the gel runs. SDS was prevented from contacting any equipment or buffers. Band shift samples of 20 µl were loaded per well using the binding buffer, EMSA mix and loading buffer shown in Table 2.36, Table 2.37 and Table 2.38.

Component	Final Concentration
HEPES pH 7.5	200 mM
EDTA	2 mM
DTT	5 mM
Glycerol	60%

Table 2.36: B10X Binding Buffer.

Components	Volume
UG_6	1 µl (0.5ng / µl)
B10X binding buffer	2 µl
Purified protein	0.25, 0.5, 1, 2 µg
H_2O	Up to 20 µl

Table 2.37: EMSA mix.

Component	Amount
TBE 0.5X	700 µl
Glycerol	300 µl
Bromophenol blue	0.0025%

Table 2.38: Loading buffer 3X (used 1X).

The binding buffer was mixed with the purified protein and water, followed by incubation on the bench for 5 minutes. Labelled RNA (by $\gamma^{32}P$ as described below) was then added with 1 µl loading dye. The contents were mixed and loaded immediately on the pre-cooled gel (2 hours at 4°C) which had been pre-run for 30 minutes. The gel was run at 100 volts (up to 60 mA) at 4°C. After the run was complete the gel was placed on a thick 3MM Whatman filter paper and covered in cling film. It was dried for 1 hour 30 minutes (583 Gel Dryer BioRad) and visualized using X-OMAT film or auto radiographic XAR film (F5763 Sigma / Kodak).

The radioactive labelling of the RNA solution was completed by Dr Mauricio Budini. For oligonucleotide preparation he used 2 µl oligonucleotide (0.1µg / µl) – total 200 ng. 2 µl PNK buffer 10X and 1 µl T4-PNK was then added. 2 µl radioactive γ-ATP was then added on top of 13 µl H_2O. This was left at 37°C for 1 hour before adding 2 µl sodium acetate 3M pH 5 and 80 µl 100% ethanol to precipitate the RNA. This was left on dry ice for 20 minutes then centrifuged at maximum speed for 30 minutes. The supernatant was carefully removed and the pellet washed in 100 µl ethanol (100%). This was then centrifuged at maximum speed for 5 minutes and then resuspended in 400 µl ddH₂0 (giving a concentration of 0.5ng / µl). The labelled RNA was used within one month accounting for the radioactive half-life decreasing through time. Oligonucleotides were labelled by phosphorylation with ($\gamma^{32}P$) ATP and T4 polynucleotide

kinase (PNK, Stratagene) for 1 hour at 37°C and then precipitated with 0.3 M sodium acetate pH 5.2, and three volumes of ethanol.

2.6.6.   GST overlay / Far Western

For the GST overlay experiment 10% acrylamide gels were used. 20 µl HeLa nuclear extract and 20 µl cytoplasmic extract were loaded into 10% acrylamide gels. The gels were run as in normal Western blots: 80- 100 volts (100 mA) through stacking and 150 volts (60 mA) afterwards. Transfer onto PVDF membrane was completed in the same way. The membrane was stained with 10 ml Ponceau solution (P7170 Sigma) for 10 minutes, at room temperature whilst shaking. The Ponceau was then washed off using water followed by 10 minutes shaking with PBST (0.2%). This was to confirm protein extract presence. The membrane was then blocked overnight at 4°C shaking. The following day the membrane was cut to split nuclear and cytoplasmic fractions for exposure to wild-type or F210I GST-TDP43 purified proteins and to probe the membranes. The membrane was placed in 10% milk in PBST and 2 µg GST purified protein added (wild-type TDP43 or F210I) with incubation at room temperature, shaking for 1 hour. This was followed by four washes in PBST 0.2%, 10 minutes per wash, shaking at room temperature, then incubation for 1 hour at room temperature shaking with primary anti-GST (27-457701 Health care) 1:2000, in blocking solution. After primary incubation, four more washes were completed, each 10 minutes at room temperature in PBST 0.2% followed by incubation in anti-Goat HRP 1:2000 in blocking for 1 hour, room temperature. Finally, washes for 10 minutes (four times) at room temperature in PBST were completed, before 5 minutes ECL exposure.

2.6.7.   Antibodies

A summary of all antibodies used is given below (Table 2.39).

Antibody	Conc	Incubation	Source	Species	Used
Anti-TDP43	1:2000	1hr RT	In house, Baralle lab	Rabbit	Add-back assay, Nuclear Cytoplasmic localisation
Anti-V5	1:2000	1hr RT	Invitrogen, R960-25	Mouse	Add-back assay, Nuclear Cytoplasmic localisation
Anti-p84	1:2000	1 hr RT	Abcam, Ab487	Mouse	Nuclear Cytoplasmic localisation
Anti-Tubulin	1:80000	1hr RT	In house, Baralle lab	Mouse	Add-back assay, Nuclear Cytoplasmic localisation
Anti-GST	1:2000	1hr RT	Healthcare, 27-457701	Goat	GST Overlay
Anti-TDP43	1:5000	1hr RT	Cosmo, CAC-TIP-TD-P07	Rabbit	Q101X fragment
Anti-TDP43	1:1500	1hr RT	Protein Tech, 10782-2-AP	Rabbit	Immunofluorescence, HeLa auto-regulation
Anti-TDP43	1:2000	1hr RT	Abcam N term, ab50930	Rabbit	Q101X fragment
Anti-Sort1	1:50	1hr RT	Alomone, ANT-009	Rabbit	MEFs localisation
Anti-Actin	1:80000	1hr RT	AC-15, Abcam	Mouse	HeLa auto-regulation

Anti-rabbit	1:2000	1hr RT	Dako, P0448		HRP secondary
Anti-mouse	1:2000	1hr RT	Dako, P0448		HRP secondary
Anti-goat	1:2000	1hr RT	GE Healthcare, P0448		HRP secondary
Anti-mouse	1:10000	1hr RT	Li-Cor IRDye 680RD / 800CW		Fluorescent secondary
Anti-rabbit	1:10000	1hr RT	Li-Cor IRDye 680RD / 800CW		Fluorescent secondary

Table 2.39: Antibodies. List of antibodies used and conditions.

2.6.8.   GST purification

GST purification was required for band shift and GST overlay experiments. GST plasmids (wild-type and F210I mouse TDP43) were transformed into BL21 DE3 *E. Coli* cells, provided by the Buratti / Baralle laboratory. Cells (50 µl) were left on ice for 20 minutes after adding 1 µl of plasmid (10ng / µl), heated at 42°C for 2 minutes, placed back on ice for 5 minutes and then streaked onto plates with 75 µg / ml ampicillin. To express the protein the following day, a colony was picked and put in a solution at room temperature of 500 ml "terrific" broth + 50 ml SOL TB (KH_2PO_4-K_2HPO_4) + 500 µl ampicillin (from 1000 X stock). This was placed in a conical flask and grown at 37°C on a shaker at 140 rpm. After 8 hours 150 µl IPTG (1M) (AB-0481, Fisher) was added to induce protein production and left on a shaker overnight at room temperature (IPTG protein induction was checked by running 25 µl on a gel with loading buffer before and after IPTG addition). The next day, the bacterial cells were pelleted in a Sorvall 500 ml tube at 3500 x g / room temperature (at this stage the pellet was frozen). The pellet was then resuspended in 45 ml PBS-triton 1% (by vortexing and pipette mixing) (triton, AC21568-0010 Fisher). One proteinase inhibitor pellet (M0273L Roche) was then added. The resuspended pellet was left on ice for 30 minutes. To purify the protein, the solution was then

sonicated, in cycles of 30 seconds on, 30 seconds off at 100% amplitude for 10 cycles. Following centrifugation, the supernatant was transferred to a new Falcon tube. Glutathione Sepharose 4B beads were then prepared (17-0756-01 Amersham Biosciences / 635610 Clonetech beads) by taking 500 µl, washing in cold PBS-triton 1% (10 ml), centrifuging briefly, and then adding beads to the supernatant. The supernatant was then placed with beads on a rotator at 4°C for 2 hours. The supernatant was then centrifuged for 10 minutes at 500 x g at 4°C. The beads were washed with bound protein three times in cold PBS-triton 1% (20 ml per wash) and centrifuged for 10 minutes, 500 x g at 4°C after each wash. Before the third and final wash, the beads were put with PBS-triton 1% on the rotator in the cold room for 10 minutes. Then after the final wash, when removing the PBS-triton 1%, 1 ml was left and the beads were moved into a 2 ml microcentrifuge tube. This tube was centrifuged for 5 minutes at room temperature followed by removal of as much of the supernatant as possible. During the washes the following elution buffers given in Table 2.40 and Table 2.41 were made.

Component	µl	Preparation
Glutathione 250 mM	30	Prepare in warm water at 37°C. Store at -20°C
DTT 1 M	1.5	Should be stored at -20°C
Protease Inhibitor (25X)	120	1 tablet in 2 ml H_2O is 25X (store -20°C)
Tris 100 mM pH 8.8	1350	

Table 2.40: 5 mM elution buffer.

For 10 ml solution (1 sample)	µl
Glutathione 250 mM	400
DTT 1M	10
Protease Inhibitor (25X)	800
Tris 100 mM pH 8.8	8800

Table 2.41: 10 mM elution buffer.

For protein elutions 1 ml 5 mM elution buffer was added to the beads, with 5 minutes incubation on a rotator at 4°C, followed by a 5 minute centrifugation at 500 x g at 4°C. For elutions two and three, 1 ml 10 mM elution buffer was added and rotated for 20 minutes at 4°C, then centrifuged for 10 minutes at 500 x g at 4°C. For elutions four and five the same process was completed but incubated on the rotator for 10 minutes. Then 1 ml elution buffer

was added and the microcentrifuge tube rotated overnight for the sixth elution by centrifugation for 10 minutes 500 x *g* at 4°C. The next morning the final protein elution was stored at -80°C (all previous elutions were frozen when obtained). 20 μl per elution was run on a gel (with 5 μl 5X SDS loading dye) to check that protein had been successfully extracted and to quantify against BSA. A representative image of the protein elutions is shown in Figure 2.7.
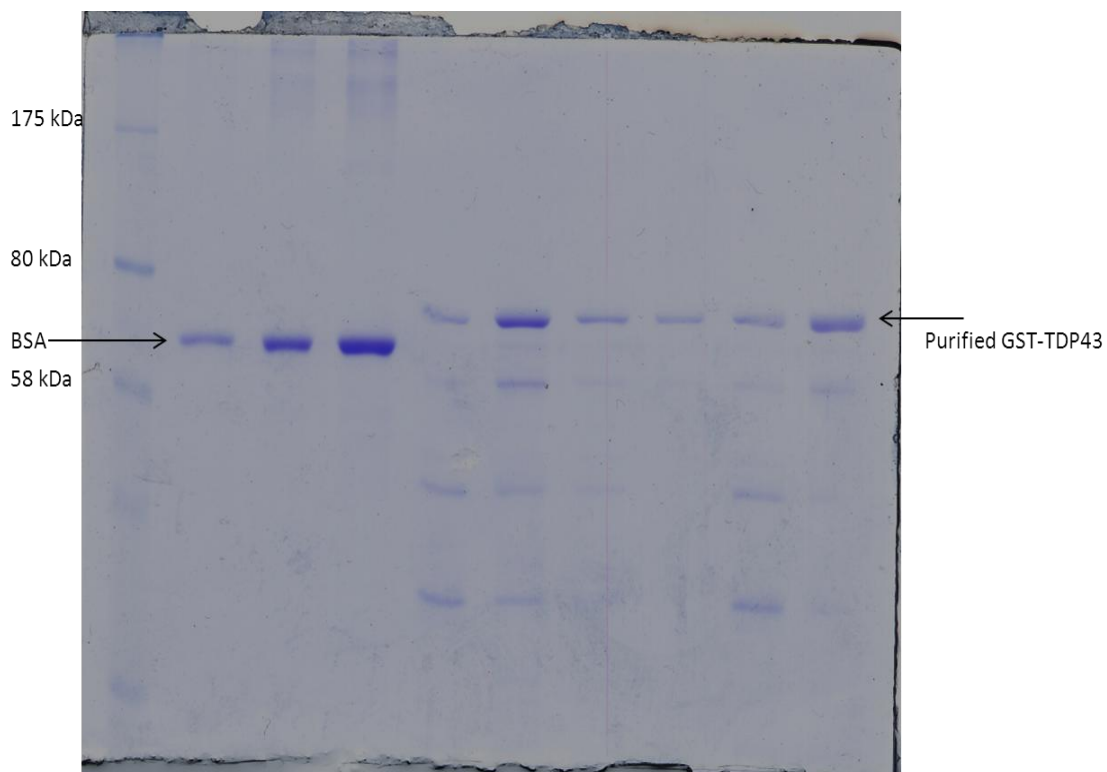
Figure 2.7: Purified TDP43 protein stained by Coomassie. Image showing a typical run of GST-purified TDP43. Protein has been loaded on a 12% acrylamide gel and stained with Coomassie blue. First three lanes contain BSA (66.5 kDa) and following six lanes contain TDP43 elutions. GST-TDP43 runs at a height of 69 kDa as the mass of GST is 26 kDa. This image can also be used to quantify protein amounts as comparing band intensity to known loaded amounts of BSA allows for protein concentration calculation.

CHAPTER 3

Results: Q101X and K160R mutations identified from the MRC Harwell ENU archive

3. Results: Q101X and K160R mutations identified from the MRC Harwell ENU archive

3.1. Mouse lines and genetics

All coding exons of the MRC Harwell archive were screened for mutations in *Tardbp*. A nonsense and two missense mutations were identified. They are Q101X, K160R and T153A shown in Chapter 1, Figure 1.1. These mutations were found prior to the beginning of my PhD when there were no published TDP43 models in September 2008. The aim was to re-derive mice carrying each of the mutations for phenotypic assessment. These mice were behaviourally assessed to determine whether the mutations were functional and whether they resulted in pathology relevant to known TDP43 proteinopathies.

At TDP43 amino acid position 101, glutamine is mutated to a stop codon (Q101X). This truncates the protein producing a potential null allele. The two missense mutations T153A and K160R lie in the first RNA recognition motif (RRM), which is a domain that is necessary and sufficient for RNA-binding (Buratti *et al.*, 2001; Giordana *et al.*, 2010). At residue 153, a threonine is mutated to an alanine (T153A). Threonine is a neutral polar amino acid with the change to a neutral non-polar amino acid. The phosphorylation of this threonine may be important in TDP43 function however this residue is not highly conserved across species (Figure 1.1), but it does appear to be phosphorylated (Hasegawa *et al.*, 2008). At position 160, there is a lysine to arginine change. This lysine is more highly conserved than the threonine at position 153 (although it is not conserved in Drosophila, where TDP43 is generally not highly conserved in this species).

The first lines to be re-derived from the sperm archive by IVF were Q101X and K160R. The initial IVF to rederive the T153A mutant failed and therefore resulted in a delay for these mice to be generated. These mice continue to be phenotyped and are not presented as part of the work in this thesis. The genetic backgrounds of the phenotyped Q101X and K160R mice are given in Figure 3.1.
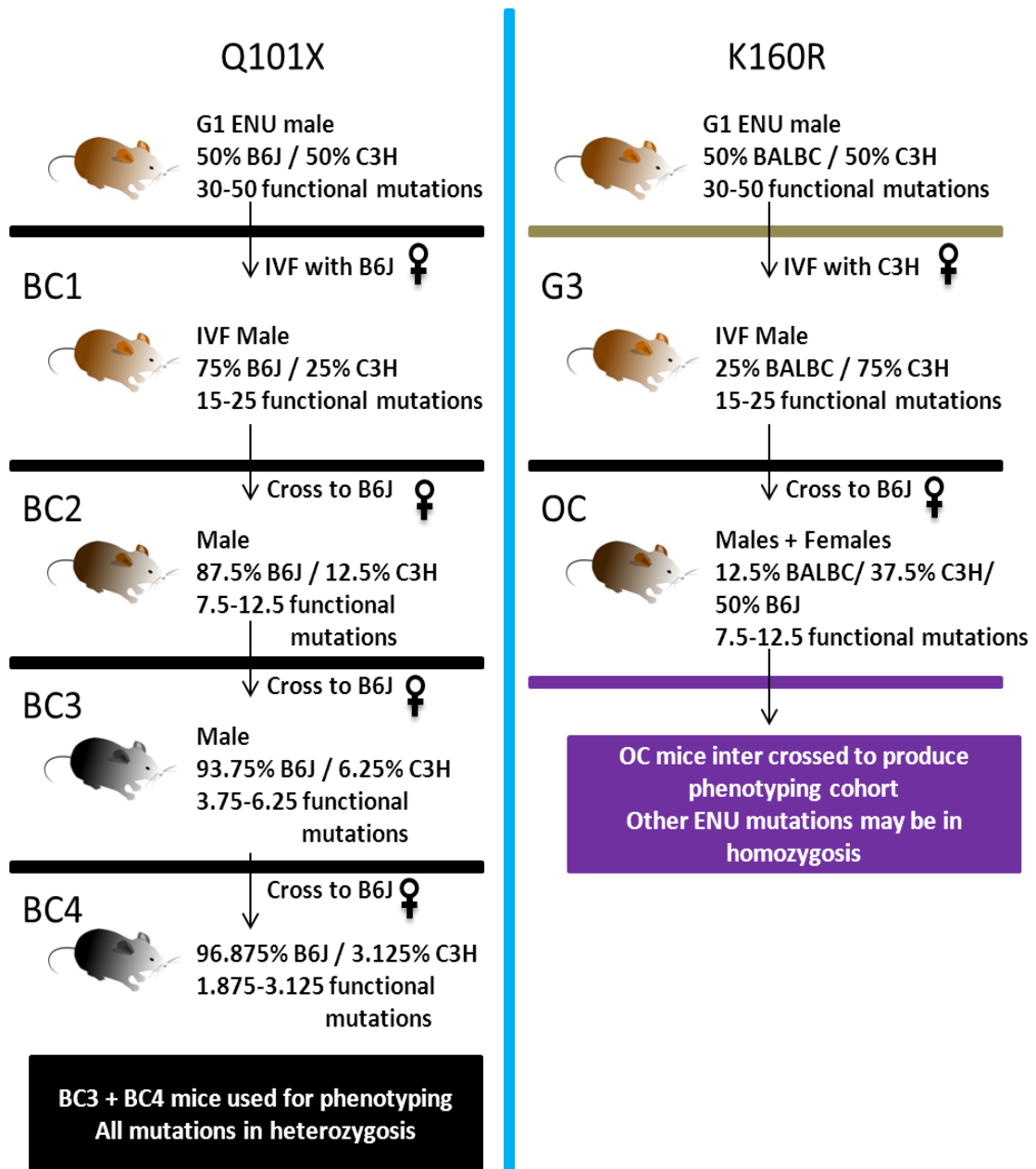
Figure 3.1: Q101X and K160R mice. Schematic showing the genetic background and ENU mutations carried by the Q101X and K160R phenotyping cohorts. Q101X cohorts were a mixture of BC3 and BC4 C57BL/6J mice, carrying all ENU mutations in heterozygosis as they were generated through a backcross. This is because Q101X homozygotes are not viable. K160R mice are OC mice with a more mixed genetic background than Q101X mice. There may be other ENU mutations in homozygosis as the phenotyping cohort was generated though inter cross matings. The starting genetic makeup of the Q101X and K160R mice is different because the mutagenesis regime changed through time as the Harwell centre progressed. Overall, the aim with all lines is to get the mutations congenic on a C57BL/6J background as this is the background in which the group studies most mutations.

Following generation of the initial Q101X and K160R cohorts, further crosses were used to produce compound and double mutants. Q101X heterozygotes were crossed to K160R heterozygotes to generate compound heterozygotes ($Tardbp^{Q101X/K160R}$). Q101X heterozygotes

were also crossed to low copy SOD1[G93A] transgenic mice to generate double mutants. Figure 3.2 summarises the genetic makeup of each of the lines with the number of backcrosses completed.
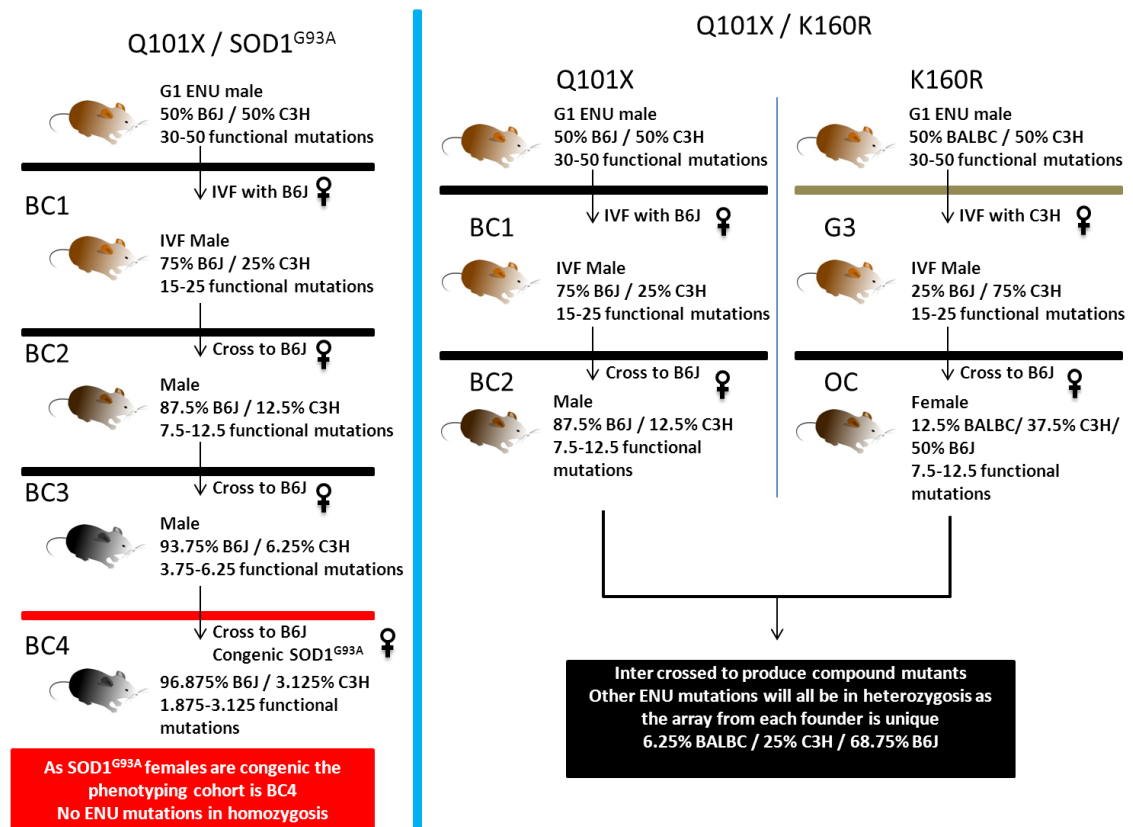
Figure 3.2: Q101X double and compound mutants. Schematic showing the generation of Q101X/ SOD1[G93A] double mutants and compound *Tardbp*[Q101X/K160R] TDP43 compound mutants. The Q101X / SOD1[G93A] double mutants are BC4 C57BL/6J mice crossing Q101X heterozygous mice to SOD1[G93A] transgenic heterozygous mice. SOD1[G93A] transgenic mice were congenic, therefore in this schematic this mating is considered as a backcross. Compound *Tardbp*[Q101X/K160R] double mutants were generated through crossing Q101X male BC2 C57BL/6J mice to K160R OC females. Note that as these mice carry unique arrays of ENU mutations, no other ENU mutations are in homozygosis.

The cross to generate compound mutants (*Tardbp*[Q101X/K160R]) was used to assess the impact of having one full length encoding K160R allele versus two in K160R homozygotes (*Tardbp*[K160R/K160R]). The aim was to assess whether there were any effects at a behavioural level when comparing one and two full length encoding alleles. Q101X heterozygotes were also crossed to SOD1[G93A] low copy transgenic mice to assess for modifying effects on SOD1[G93A] induced phenotypes. Both males and females were aged to end stage which due to the SOD1[G93A] transgene is 31-38 weeks (Alexander *et al.*, 2004; Acevedo-Arozena *et al.*, 2011). In

this SOD1^{G93A} model, the disease course is highly consistent with onset from 22- 24 weeks progressing to death by humane endpoint. The SOD1^{G93A} mice are a well characterised model of ALS, overexpressing around 8-10 copies of the human SOD1^{G93A} transgene. They recapitulate many of the major hallmarks of SOD1 induced ALS seen in humans showing a progressive motor neuron degeneration disease course. Mutations in both SOD1 and TDP43 cause ALS. SOD1 induced ALS results in TDP43 negative inclusions and when mutations in TDP43 as well as other causative genes cause ALS they result in SOD1 negative inclusions. Despite this lack of overlap in these misfolded proteins aggregating, there is convergence of the effects of mutations in both genes resulting in ALS and therefore there could be commonality in the mechanism through which selective neurodegeneration occurs. Considering the well characterised nature of the SOD1^{G93A} model, these mice were crossed to Q101X heterozygotes to assess for potential interactive effects up to end stage. A summary of the crosses for the compound (*Tardbp*$^{Q101X/K160R}$) and SOD1^{G93A} double mutants is given in Figure 3.2 with a summary schematic of all lines phenotyped shown in Figure 3.3.
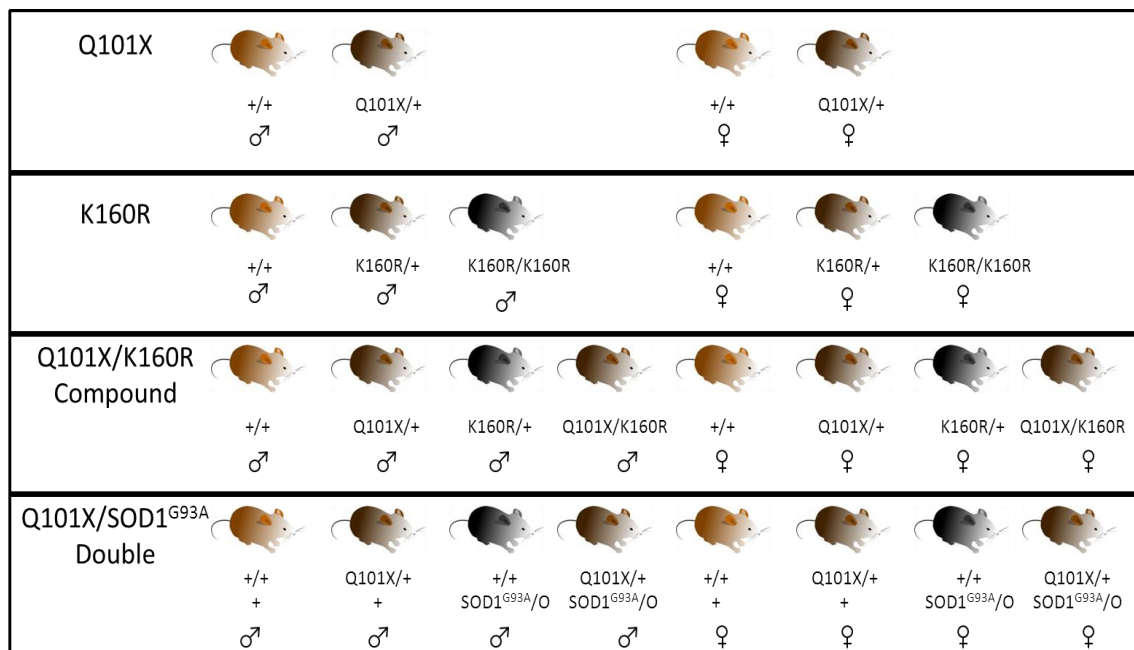

Figure 3.3: Mouse lines phenotyped. Schematic showing genotypes of mice phenotyped for each mutant line with littermate controls. Q101X homozygotes are not viable as presented below. More than ten mice per sex per genotype were assessed for all tests where possible.

A phenotyping regime containing a variety of behavioural assessments was developed to characterise the mutant mice. For the Q101X, K160R and compound ($Tardbp^{Q101X/K160R}$) lines this included SHIRPA, grip strength and rotarod as well as other tests aimed at providing a comprehensive assessment of mouse health and behaviour with a focus on motor capabilities. For the first six months, phenotyping was carried out on a monthly basis. Once initial phenotypes were detected, the programme was revised. Due to the subtle nature of the phenotypes observed, the phenotyping continued on a two to three monthly basis. Most tests have been completed every two to three months. The aim was to complete a comprehensive behavioural assessment characterising health, cognitive and motosensory ability. The phenotyping tests applied were focused on assessing motor capabilities, considering TDP43's central role in amyotrophic lateral sclerosis (ALS). Mouse cohorts of more than ten mice per sex per genotype were generated in order to provide cohorts with significant numbers to assess phenotypes and potential sex differences. The generation of each mouse cohort was staggered for phenotypic assessment in order to allow for a comprehensive phenotypic assessment of large numbers of animals.

For the Q101X, K160R and compound ($Tardbp^{Q101X/K160R}$) mice, based on the phenotypic characterisation throughout the first year, it was decided that at one year the male mice from each cohort would be culled to assess for pathology. These males were perfused or had tissue snap frozen to use for pathology or biochemical assessment. Behavioural characterisation of the female cohorts continued to end stage or two years of age, before harvesting tissues for further assessment.

Results are presented for the Q101X, K160R and compound ($Tardbp^{Q101X/K160R}$) lines together. The Q101X cross to SOD1^{G93A} is presented separately.

3.2. Viability

Following the IVF for Q101X and K160R mice, Q101X heterozygote inter crosses were set up to determine homozygote viability. No Q101X homozygotes were present from the original inter cross matings using BC2 and BC3 mice (Figure 3.1). Inter cross matings were set up to determine at what stage during development Q101X homozygotes could be identified (Table 3.1). No homozygous Q101X mice were identified at the developmental stages assessed indicating early embryonic lethality.

		Genotype			
Timed mating (dpc)	N	+/+	-/+	-/-	Resorptions
E7.5 - 11.5 dpc	47	12	21	0	14
E6.5 dpc	25	9	11	0	5

Table 3.1: Q101X homozygote viability. Table showing genotyped embryos from selected developmental time points. No homozygous Q101X embryos were identified at any time point. Resorptions were at a stage where they were unable to be genotyped. At 6.5 dpc $\chi2$ = 8.3, p = 0.0158 versus an expected 1:2:1 WT: heterozygote: homozygote ratio.

Following this result, three independent TDP43 knock out studies showed that knockout mice are not viable in homozygosis, dying between E3.5- 8.5 dpc (Kraemer *et al.*, 2010; Sephton *et al.*, 2010; Wu *et al.*, 2010) supporting Q101X being a null allele. Crosses to generate K160R homozygotes (*Tardbp*$^{K160R/K160R}$) and compound mutants (*Tardbp*$^{Q101X/K160R}$) were successful in producing genotypes at the expected Mendelian ratio.

3.3. Phenotyping regime

A comprehensive pipeline of tests has been applied to phenotype all mutant lines. In order to avoid bias, all mice were phenotyped blind to their genotype. Additionally, all mice phenotyped were weighed on a two weekly schedule until mice were culled for tissue or at end stage. Following complete characterisation, survival of each mouse cohort was also analysed.

The phenotyping tests used were SHIRPA, grip strength and rotarod. SHIRPA is a first line phenotyping screen consisting of multiple elements. Mice were scored for behavioural activity as well as being assessed physically. An example SHIRPA sheet is included in Figure 2.4 in Chapter 2.

All elements of the SHIRPA were assessed. However, data analysis has focused on: gait, startle response, limb grasp, grip strength, body tone and negative geotaxis. The SHIRPA set up is shown in Figure 2.1. One week after the SHIRPA test, rotarod and grip strength were assessed as described in methods.

At selected time points, startle response and open field were also measured. Startle response assesses motosensory response gating and open field measures aspects of locomotor activity and fear. Startle response is measured in the SHIRPA, with a score given for the jump response to a 90 dB tone. This semi-quantitative assessment was also completed using Minnesota medical development Inc (MMDI) boxes to a give a fully quantitative readout, providing an arbitrary value. Startle response to a 110 dB tone was measured in the quantitative system. Pre-pulse inhibition (PPI) was also measured, where pre tones of varying intensity are used which should dampen the mouse's response to a successive startle tone. This test models sensorimotor gating with PPI deficits being linked to schizophrenia and psychosis (Geyer, 1999; Geyer *et al.*, 1999; Ouagazzal *et al.*, 2001a; Ouagazzal *et al.*, 2001b). In applying this test the assessment aims were twofold, to determine normal sensorimotor gating in the startle response as well as any PPI deficits. As well as startle, mice were assessed in the open field arena. Mice were placed in a grey arena for 30 minutes and their activity was recorded using Noldus Ethovision software. Parameters analysed included total distance moved, duration moving, velocity, rearing frequency and time near the edge or centre of the arena. This data can represent features such as locomotor activity, neophobia, agoraphobia, exploratory drive and aspects of anxiety and fear (Crawley & Paylor, 1997; Choleris *et al.*, 2001). The software itself measures ambulation.

3.4. *Tardbp*$^{Q101X/+,}$ *Tardbp*$^{K160R/K160R}$, *Tardbp*$^{Q101X/K160R}$ phenotypes

3.4.1. Survival

Female cohorts from all lines were aged to end stage to assess survival. End stage was defined by 20% weight loss from maximum weight, mice being found dead or if the animal was sick as defined by the Named Animal Care and Welfare Officer (NACWO). Mice that were injured due to wounds from handling or fighting with other mice were not included in this study. Q101X heterozygous (*Tardbp*$^{Q101X/+}$) mice show no significant differences in survival (Figure 3.4).
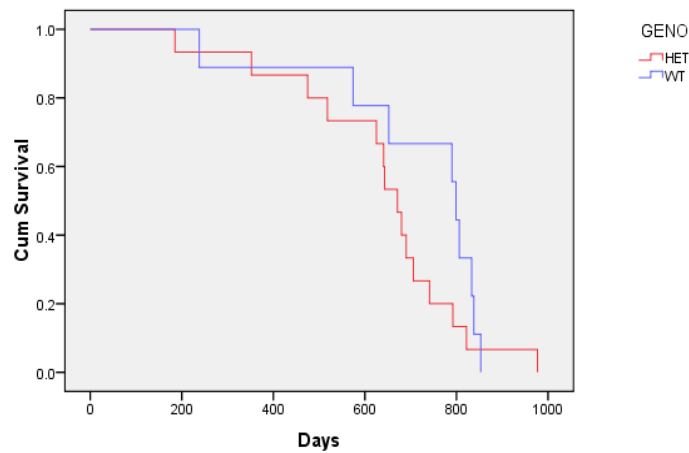
Q101X Survival Females

Figure 3.4: Q101X survival. Plot showing the Q101X phenotyping cohort survival. Animals included were those that died for health or severe weight loss reasons. Mice that were culled due to reasons such as fight wounds from other mice were not included. Only female cohort aged to end stage n = 9 WT, 15 HET. Mean survival was WT = 709 days, HET = 643 days. No significant differences in survival observed p = 0.235 Log rank statistic, Kaplan Meier Analysis.

In the K160R line, wild-type, heterozygote (*Tardbp*^K160R/+^) and homozygote (*Tardbp*^K160R/K160R^) female survival was approximately two years (Figure 3.5). No significant differences in survival were observed between genotypes.

K160R Survival Females
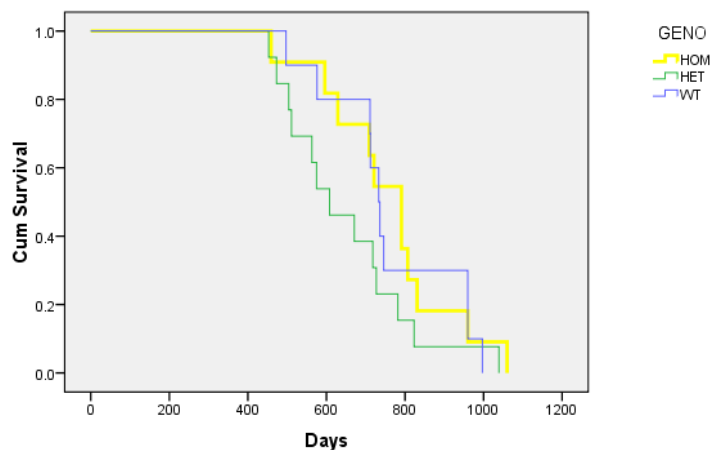
Figure 3.5: K160R survival. Survival plot showing the K160R phenotyping cohort. Animals included were those that died for health or severe weight loss reasons. Mice that were culled due to reasons such as fight wounds from other mice were not included. Only female cohort aged to end stage, n = 10 WT, 13 HET, 11 HOM. No significant differences in survival observed. Mean survival was WT = 762 days, HET = 649 days, HOM = 759 days. No significant differences between genotypes observed p > 0.05 Log rank statistic, Kaplan Meier Analysis. Overall p = 0.245 (log rank).

Significant differences in survival were observed in the compound heterozygote ($Tardbp^{Q101X/K160R}$) line. Q101X heterozygotes and compound heterozygotes reached end stage significantly earlier (Figure 3.6) than littermates. Mean wild-type ($Tardbp^{+/+}$) survival was 749 days, Q-Het ($Tardbp^{Q101X/+}$) was 693 days, K-Het ($Tardbp^{K160R/+}$) was 642 days and Q/K-Comp ($Tardbp^{Q101X/K160R}$) was 689 days. Mice that reached end stage earlier due to weight loss or poor health condition were perfused for full pathological assessment which continues to be assessed. So far, there appear to be no genotype specific causes of death indicating that as mice naturally reach end stage the $Tardbp^{Q101X/K160R}$ and $Tardbp^{Q101X/+}$ mice in this cohort were more susceptible to natural causes of death at an earlier age.

Q101X/ K160R Survival Females
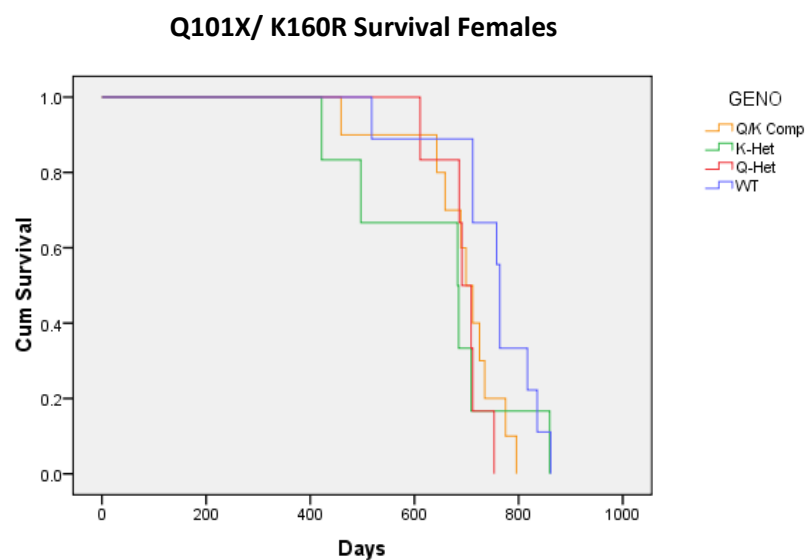
Figure 3.6: Compound $Tardbp^{Q101X/K160R}$ survival. Survival plot showing the compound $Tardbp^{Q101X/K160R}$ phenotyping cohort survival plot. Animals included were those that died for health or severe weight loss reasons. Mice that were culled due to reasons such as fight wounds from other mice were not included. Only female cohort aged to end stage n = 10 WT, 6 Q-Het, 6 K-Het, 9 Q/K-Comp. Mean survival was WT = 749 days, Q-Het = 693 days, K-Het = 642 days, Q/K-Comp = 689 days. WT versus Q-Het p = 0.007, WT versus K-Het p = 0.133, WT versus Q/K-Comp p = 0.049, Log rank statistic, Kaplan Meier Analysis. Overall p = 0.134 (log rank statistic).

3.4.2. Weights

Weight measurements were taken from between five and seven weeks, on a two weekly basis as shown in Figure 3.7, Figure 3.8 and Figure 3.9. No significant differences in weight are seen in the Q101X and K160R lines (Figure 3.7 and Figure 3.8). There is increased variability in

weight in the compound heterozygote line, potentially due to the mixed genetic background of the mice. Through time female compound heterozygotes are significantly smaller. This is significant by repeated measures ANOVA (overall $p = 0.025$) from 28 weeks in females using the least significant difference (LSD) test statistic (Figure 3.9). Repeated measures analysis up to one year shows no significant differences in males.
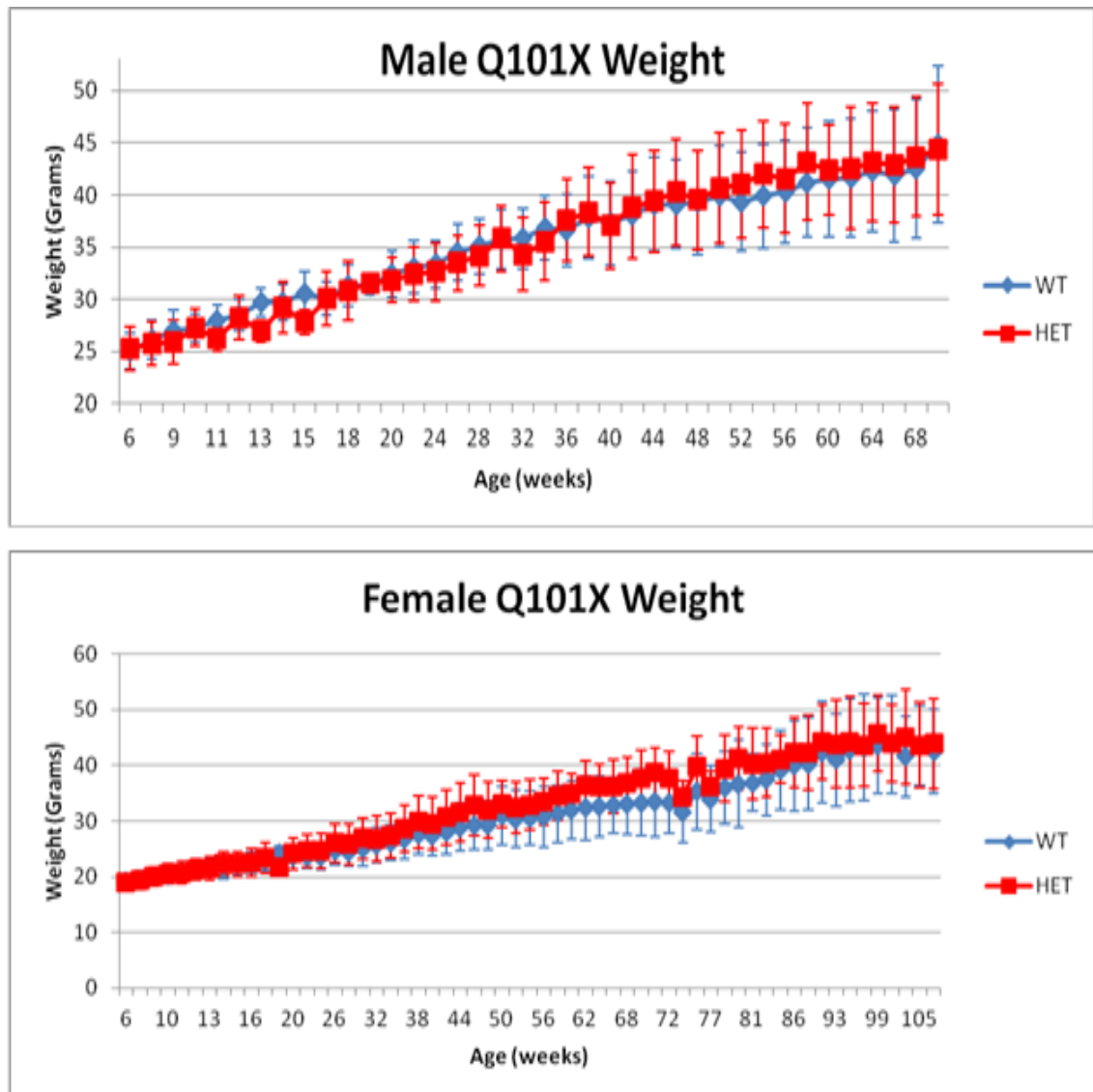
Figure 3.7: Q101X weights. Graphs showing male and female Q101X weights through time. N is more than ten per sex per genotype, until individual mouse end stage for female cohort. No significant differences in weight are observed through repeated measures (where possible) or 1 way ANOVA analysis ($p > 0.05$). Error bars show standard deviation.
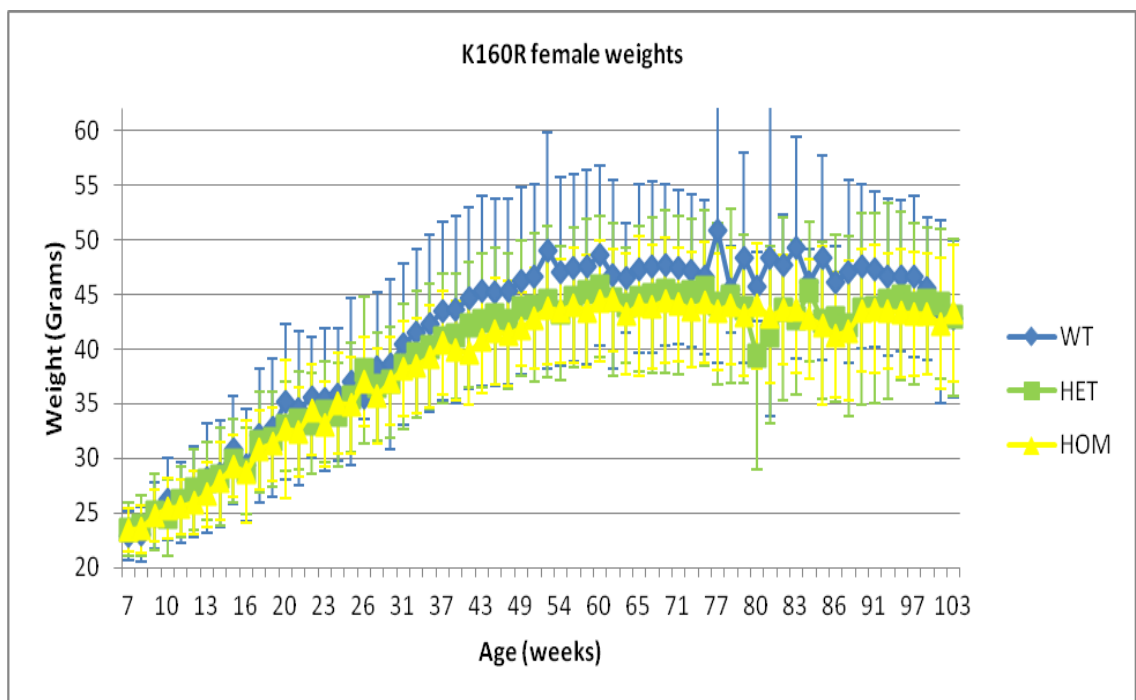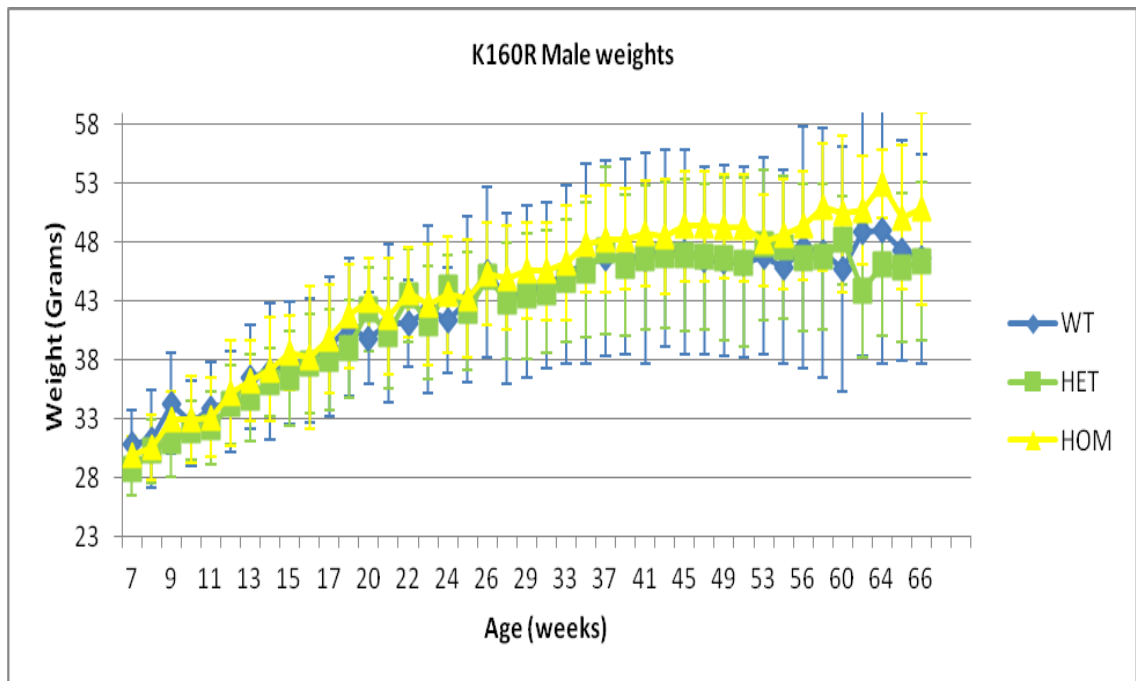
Figure 3.8: K160R weights. Graphs showing male and female K160R weights through time. N is more than ten per sex per genotype, until individual mouse end stage for female cohort. No significant differences in weights are observed through repeated measures (where possible) or 1 way ANOVA analysis Bonferroni post hoc analysis (p = 0.05). Error bars show standard deviation.
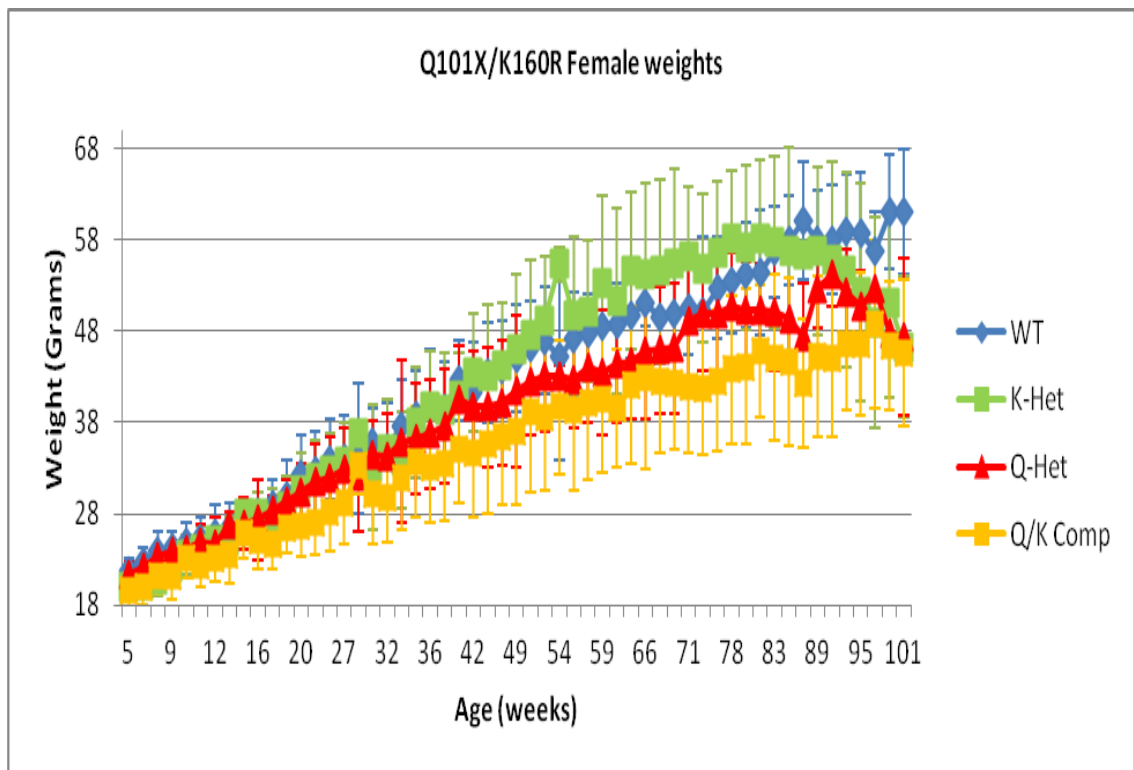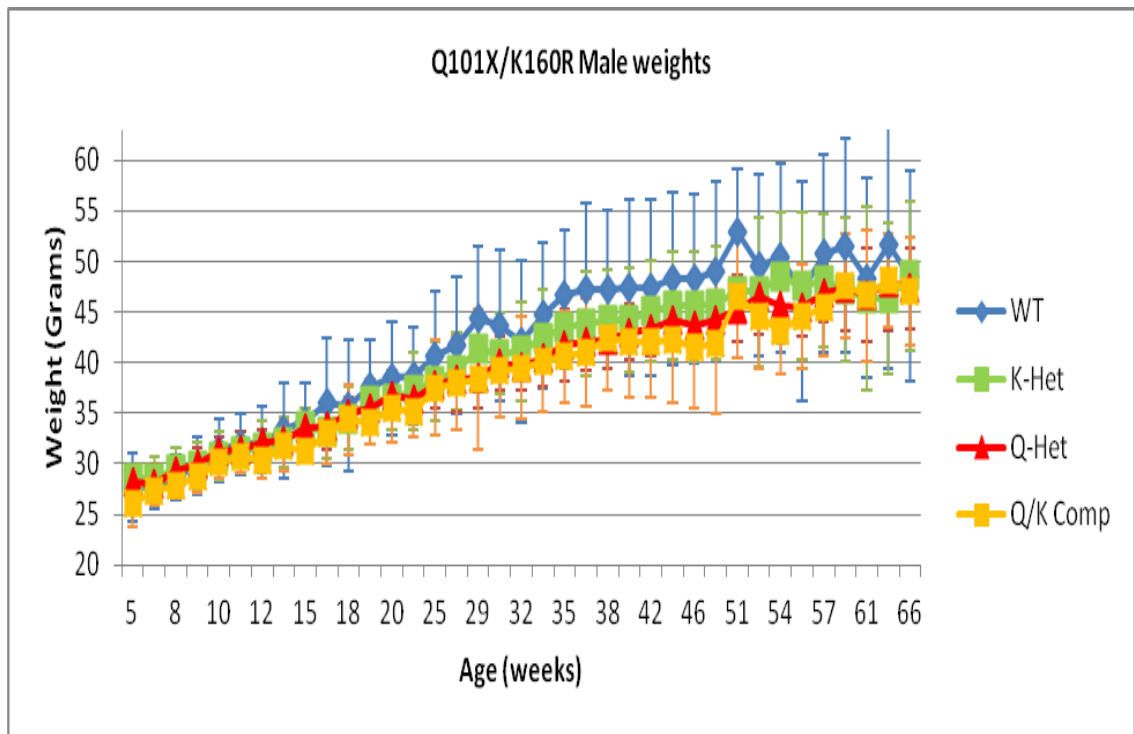
Figure 3.9: Compound *Tardbp*^Q101X/K160^R weights. Weights (grams) measured approximately every two weeks. No significant differences are observed in male compound *Tardbp*^Q101X/K160R^ mice. Female compound *Tardbp*^Q101X/K160R^ mice are significantly smaller than wild-type littermate controls from 28 weeks onwards (repeated measures ANOVA up to one year, followed by multivariate GLM with LSD test statistic). From 28 weeks, wild-type versus *Tardbp*^Q101X/K160R^ $p < 0.05$. Repeated measures GLM could not be used for analysis at end stage due to mice dying resulting in uneven data point collection. Error bars show standard deviation.

105

3.4.3. SHIRPA

SHIRPA was completed every two months in all lines. All lines show significant differences in a number of SHIRPA endophenotypes. Male mice were assessed by SHIRPA up to one year of age, starting from seven weeks. Female cohorts were assessed up to two years of age. There were significant differences in a number of SHIRPA endophenotypes as detailed below. Male mice were culled for pathological assessment and protein / RNA analysis at one year.

3.4.4. Gait

In the SHIRPA arena, a small proportion of Q101X heterozygote mice showed a more pronounced and less fluid gait compared to littermate controls. The lack of motion fluidity was subtle but consistantly present in mice showing the phenotype. This was observed through time at a mean age of 67 weeks, with no wild-type mice showing an abnormal gait. The combined proportion of heterozygous mice showing an abnormal gait across sexes was over 20% in both sexes (Figure 3.10).

Q101X Gait - Females   Q101X Gait - Males
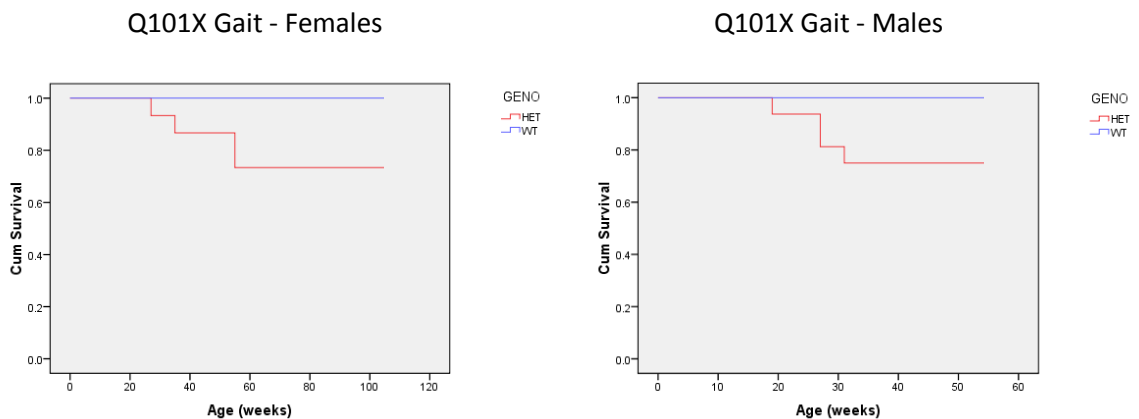
Figure 3.10: Q101X Gait. Onset plots showing the presence of abnormal gait observed in the SHIRPA arena, through time, plots shown by sex. Y axis shows proportion of mice with lines for each genotype decreasing from 1, where no mice show the phenotype. N = female WT 12, HET 15. N = male WT 16, HET 16. Mean age at which gait was shown for both sexes combined was WT = no phenotype, HET = 67. WT versus HET p = 0.014, Kaplan Meier Log Rank Statistic. Overall p = 0.014 (log rank) with no significant differences between sexes p = 0.954.

Abnormal gait was also observed in the compound heterozygote line. Wild-type males up to one year showed normal gait as did nearly all wild-type females up to two years. More than 50% Q101X heterozygotes and compound homozygote males showed abnormal gait (versus

wild-type p = 0.001 Log rank statistic), with 25% female compound mutants showing abnormal gait (Figure 3.11).

Q101X/ K160R Gait Females   Q101X/ K160R Gait Males
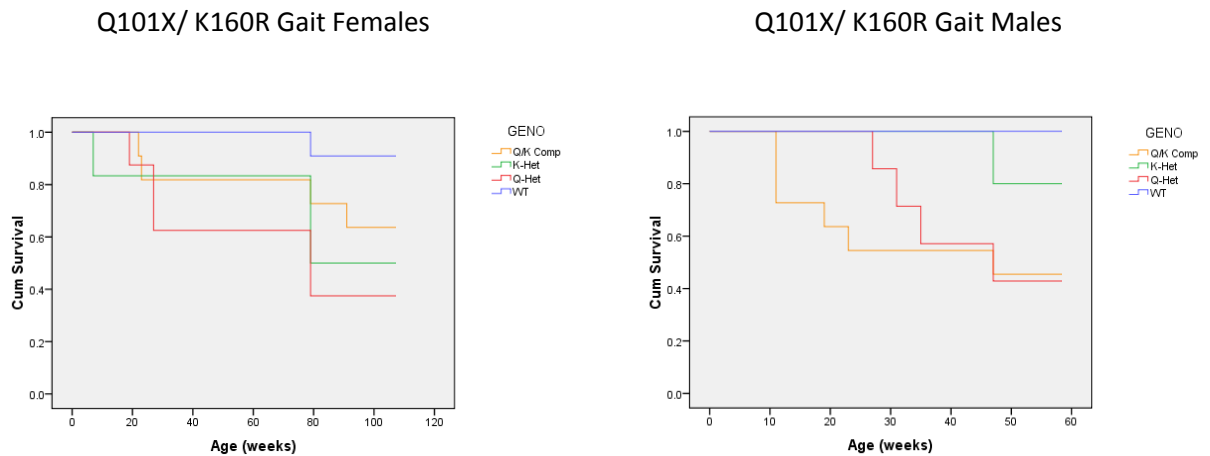
Figure 3.11: Compound *Tardbp*^{Q101X/K160R} Gait. Onset plots showing the presence of abnormal gait observed in the SHIRPA arena through time. Plots shown by sex. Y axis shows proportion of mice with lines decreasing from 1 where no mice show the phenotype. N = female WT 11, Q-Het 8 , K-Het 6, Q/K Comp 11 . N = male WT 12, Q-Het 7, K-Het 10, Q/K Comp 11. Mean age at which gait was shown for both sexes combined was WT = no phenotype, Q-Het = 58 (more than 50% females), K-Het = 66 (more than 50% females), Q/K Comp = 63 (more than 50% males). WT versus Q-Het p < 0.0001, WT versus K-Het p = 0.013, WT versus Q/K Comp p = 0.001, Kaplan Meier Log rank statistic. Overall p = 0.002 with no sex differences by genotype up to one year of age (p > 0.05). There was a trend in a compound heterozygote sex difference (p = 0.07).

3.4.5. Limb grasp

Limb grasping was assessed when the mouse was suspended by the tail or hanging from a wire In the Q101X line, heterozygous males were culled at one year and did not overtly show this phenotype. In females the phenotype developed at a mean age of 61 weeks, which was not observed in the littermate controls (p = 0.002, Log Rank Statistic, Kaplan Meir Analysis) shown in Figure 3.12.

Q101X Limb grasp Females   Q101X Limb grasp Males

Figure 3.12: Q101X Limb grasp. Onset plots showing the presence of limb grasp observed in the SHIRPA arena, through time. Plots shown by sex. Y axis shows proportion of mice with lines decreasing from 1, where no mice show the phenotype. N = female WT 12, HET 15. N = male WT 16, HET 16. Mean age at which limb grasp was shown for both sexes combined was WT = no phenotype, HET = 61. WT versus HET p = 0.002, Kaplan Meier Log Rank Statistic. Overall p = 0.002 with a significant difference in Q101X heterozygote sex up to one year, p = 0.046.

In the K160R line, more than 50% K160R homozygotes limb grasped in both sexes (Figure 3.13). Beyond 60 weeks, almost 80% K160R homozygote females were limb grasping when suspended by the tail (wild-type versus homozygote limb grasp p < 0.0001 Kaplan Meier Log rank statistic). There is a trend for K160R heterozygotes in limb grasping, with almost 50% females showing this phenotype however it is not significant.

K160R Limb grasp Females

K160R Limb grasp Males
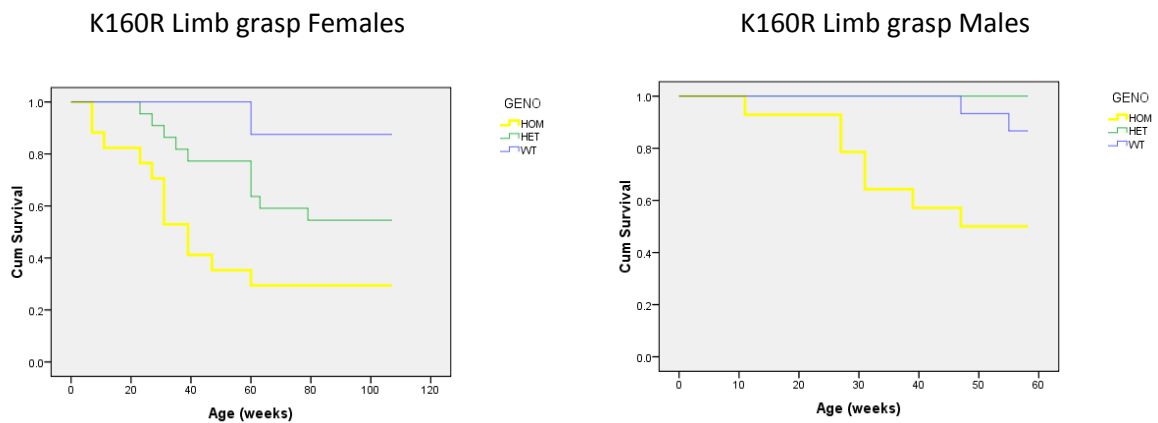
Figure 3.13: K160R Limb grasp. Onset plots showing the presence of gait observed in the SHIRPA arena, through time. Plots shown by sex. Y axis shows proportion of mice and each with lines decreasing from 1 where no mice show the phenotype. N = female WT 16, HET 22, HOM 17. N = male WT 14, HET 15, HOM 15. Mean age at which limb grasp was shown for both sexes combined was WT = no phenotype, HET = no phenotype, HOM = 49 (more than 50% females). WT versus HET p = 0.136, WT versus HOM p < 0.0001, Kaplan Meier Log rank statistic. Overall p < 0.0001 with no sex differences within genotypes. A trend towards a difference in K160R heterozygotes up to one year was seen, p = 0.052.

Limb grasping was also present in the compound heterozygote line. More than 50% of Q101X heterozygote and compound heterozygote mice showed a limb grasping reflex (wild-type versus Q-Het p = 0.019, wild-type versus Q/K Compounds p = 0.001, Kaplan Meier Log rank statistic). This is shown in Figure 3.14.

Q101X/ K160R Limb grasp
Females

Q101X/ K160R Limb grasp
Males

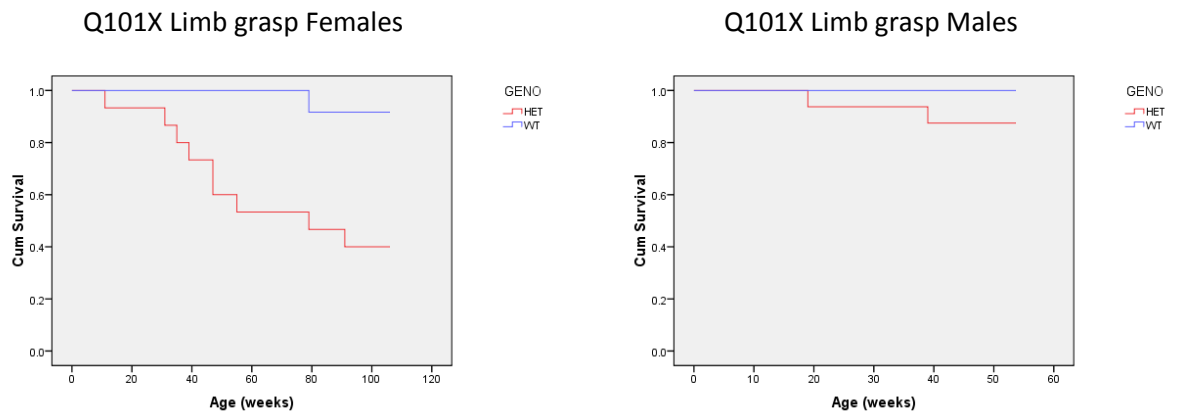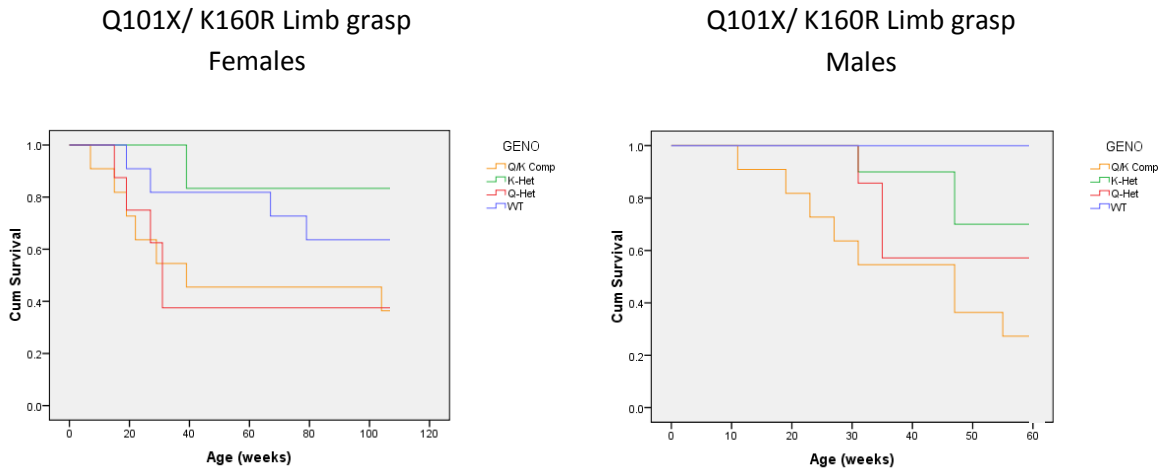**Figure 3.14: Compound** *Tardbp*^{Q101X/K160R} **Limb grasp**. Onset plots showing the presence of abnormal limb grasp observed in the SHIRPA arena through time. Plots shown by sex. Y axis shows proportion of mice with lines decreasing from 1 where no mice show the phenotype. N = female WT 11, Q-Het 8 , K-Het 6, Q/K Comp 11 . N = male WT 12, Q-Het 7, K-Het 10, Q/K Comp 11 . Mean age at which limb grasp was shown for both sexes combined was WT = no phenotype, Q-Het = 52 (more than 50% females), K-Het = no phenotype, Q/K Comp = 50 (more than 50% both sexes). WT versus Q-Het p = 0.019, WT versus K-Het p = 0.551, WT versus Q/K Comp p = 0.001, Kaplan Meier Log rank statistic. Overall p = 0.001, with no sex differences within genotypes (p > 0.05).

3.4.6. Body tone

Softer rear abdominal body tone was assessed by pressing the rear body (abdomen) of the mice with the thumb and index finger as described in methods. Body tone was scored as normal (0), soft (1) or severely soft (2). A score of zero was a firm normal tone. A score of 1 was a significantly soft tone with no elicited tonal reflexive response and a score of 2 was a severely soft and flaccid tone with almost absent basal tone with no elicited response. In the Q101X line, a softer body tone developed in all genotypes and sexes, but was more prevalent with an earlier onset in Q101X heterozygous mice. Up to 20 weeks of age, the body tone in all mice remained firm with an elicited response. This progressed into a softer body tone in heterozygotes at a mean age of 45 weeks, versus less than 50% having a softer body tone in littermate controls. 80% of heterozygous Q101X mice show the soft body tone phenotype with only 30% of controls showing this phenotype (Figure 3.15).

Q101X Body tone Females

Q101X Body tone Males

Figure 3.15: Q101X Body tone. Onset plots showing the presence of softer body tone observed in the SHIRPA arena, through time. Plots shown by sex. Y axis shows proportion of mice and with lines decreasing from 1, where no mice show the phenotype. N = female WT 12, HET 15. N = male WT 16, HET 16. Mean age at which body tone was shown for both sexes combined was WT no phenotype, HET 90 (more than 50% in both sexes). WT versus HET $p < 0.001$, Kaplan Meier Log Rank Statistic. Overall $p < 0.0001$, with a trend in sex differences within Q101X heterozygotes up to one year, $p = 0.07$

As well as scoring for body tone, a score for severe softness of body tone was given (2). In this score, the previously soft body tone becomes significantly softer such that there is no muscular tone felt with a clear ability to feel internal structures and organs. More than 50% of Q101X females displayed this and it was increasingly prevalent with age (Figure 3.16).

Q101X Severe body tone
Females

Q101X Severe body tone
Males

Figure 3.16: Q101X Severe reduction in body tone. Onset plots showing the presence of severely softer body tone observed in the SHIRPA arena, through time. Plots shown by sex. Y axis shows proportion of with lines decreasing from 1, where no mice show the phenotype. N = female WT 12, HET 15. N = male WT 16, HET 16. Mean age at which severe body tone was shown for both sexes combined was WT no phenotype, HET 66. WT versus HET p = 0.003, Kaplan Meier Log Rank Statistic. Overall p = 0.003 with no significant differences in Q101X heterozygotes by sex up to one year (p = 0.621).

In the K160R line, increasing numbers of mice displayed softer body tone through time in both males and females (Figure 3.17). Nearly all K160R homozygotes (more than 90%) showed a soft body tone through time in the SHIRPA assessment, which was not seen to the same degree in wild-type and heterozygote littermates. As with Q101X, body tone was scored as 0, 1 or 2. Significantly more heterozygote and homozygote K160R mice showed a severely softer body tone (scored as 2) compared to wild-type controls (Figure 3.18). This occurred with a higher prevalence in females, beyond the final age to which males were assessed.
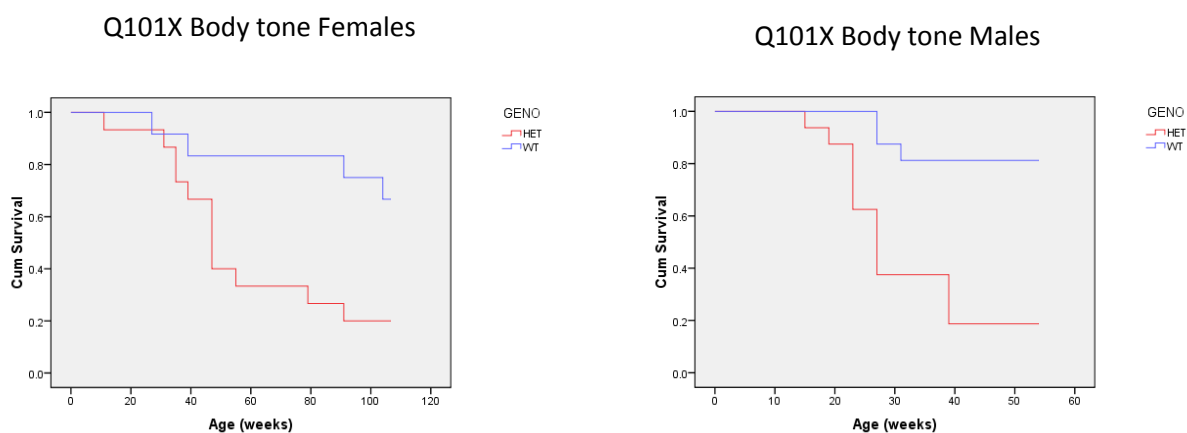
K160R Body tone Females

K160R Body tone Males

Figure 3.17: K160R Body tone. Onset plots showing the presence of soft body tone observed in the SHIRPA arena, through time. Plots shown by sex. Y axis shows proportion of mice with lines decreasing from 1, where no mice show the phenotype. N = female WT 16, HET 22, HOM 17. N = male WT 14, HET 15, HOM 15. Mean age at which body tone was shown for both sexes combined was WT= 62, HET = 59, HOM = 38. WT versus HET p = 0.605, WT versus HOM p < 0.0001, Kaplan Meier Log rank statistic. Overall p < 0.0001 with no significant differences by sex within genotype (p > 0.05).

K160R Severe body tone Females
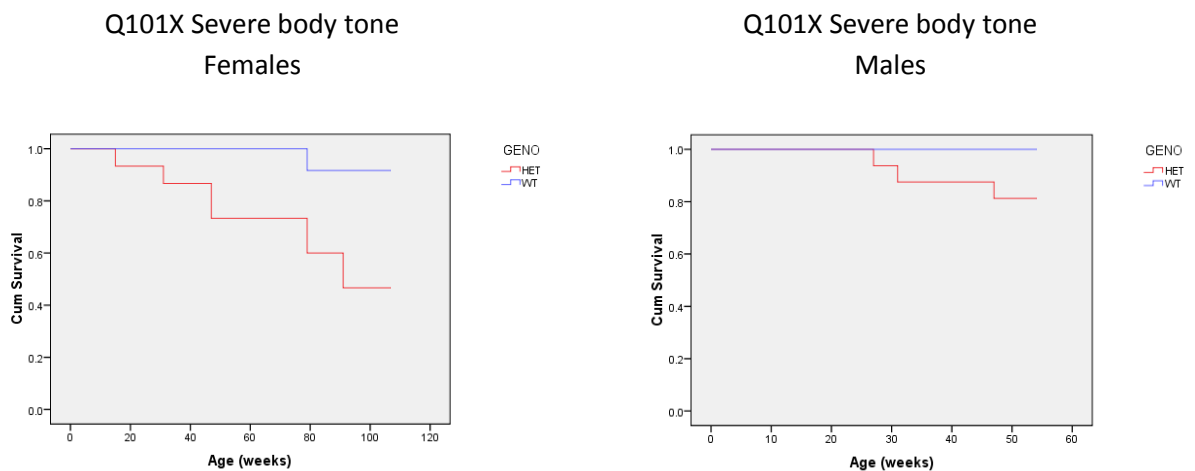
K160R Severe body tone Males

Figure 3.18: K160R Severe reduction in body tone. Onset plots showing the presence of severely softer body tone observed in the SHIRPA arena through time. Plots shown by sex. Y axis shows proportion of mice with lines decreasing from 1 where no mice show the phenotype. N = female WT 16, HET 22, HOM 17. N = male WT 14, HET 15, HOM 15. Mean age at which severe body tone was shown for both sexes combined was WT = no phenotype, HET = no phenotype, HOM = 62 (more than 50% for both sexes). WT versus HET p = 0.018, WT versus HOM p = 0.001, Kaplan Meier Log rank statistic. Overall p = 0.003 with no differences within genotype by sex up to one year.

As with Q101X and K160R lines, in the compound heterozygote line loss of body tone firmness was progressive in all genotypes. In wild-type mice assessed, the number of mice showing softer body tone was less than 50% (Figure 3.19). More than 50% K160R heterozygotes, Q101X

heterozygotes and compound heterozygotes showed softer body tone. The compound mutants showed an earlier onset, particularly in males, versus K160R heterozygotes and wild-type controls. There is also a trend towards an earlier onset than Q101X heterozygote littermate controls. When scoring for a severely soft body tone, Q101X heterozygotes and compound heterozygotes showed severely softer body tone. This was most prevalent in female mice, where 90% compound heterozygotes showed a severely soft body tone compared to less than 40% wild-type controls, p < 0.001 (Figure 3.20).
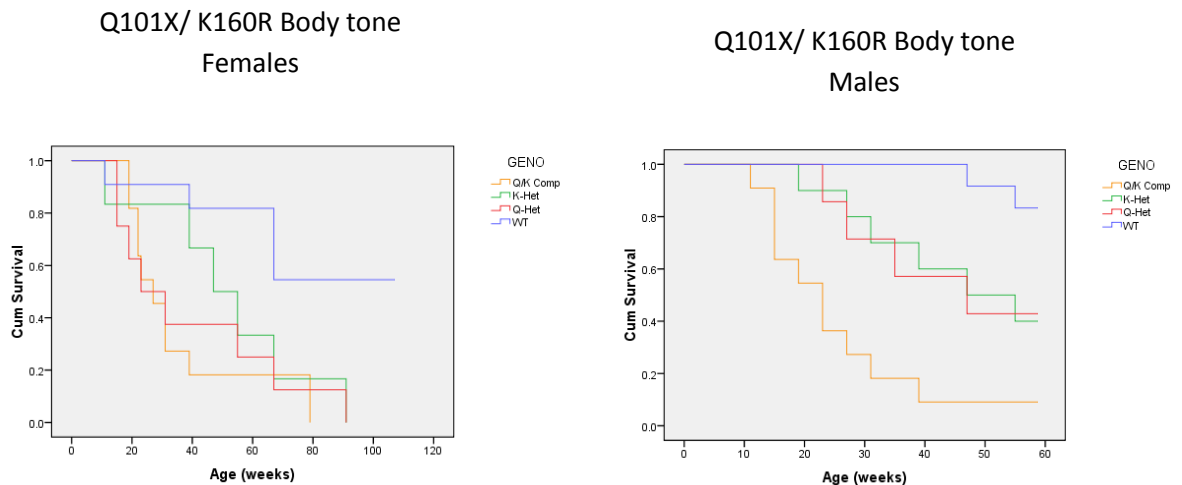
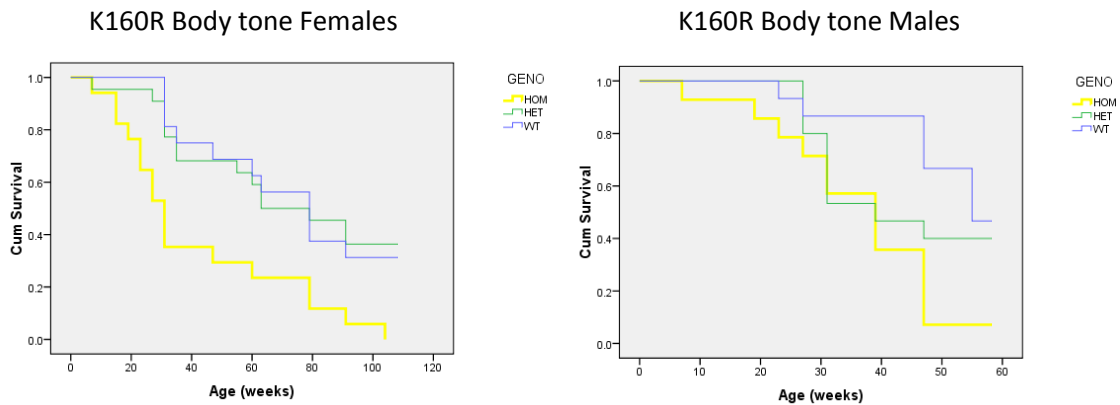**Figure 3.19: Compound *Tardbp*[Q101X/K160R] Body tone**. Onset plots showing the presence of soft body tone observed in the SHIRPA arena through time. Plots shown by sex. Y axis shows proportion of mice and each with lines decreasing from 1 where no mice show the phenotype. N = female WT 11, Q-Het 8 , K-Het 6, Q/K Comp 11 . N = male WT 12, Q-Het 7, K-Het 10, Q/K Comp 11. Mean age at which body tone was shown for both sexes combined was WT = less than 50%, Q-Het = 41 (more than 50% both sexes), K-Het = 47 (more than 50% both sexes), Q/K Comp = 30 (more than 50% both sexes). WT versus Q-Het p < 0.0001, WT versus K-Het p = 0.001, WT versus Q/K Comp p < 0.0001, K-Het versus Q/K Comp p = 0.009, Q-Het versus Q/K Comp p = 0.105, Kaplan Meier Log rank statistic. Overall p < 0.0001, with no differences by sex within genotype (p > 0.05).

Q101X/K160R Severe body tone Females
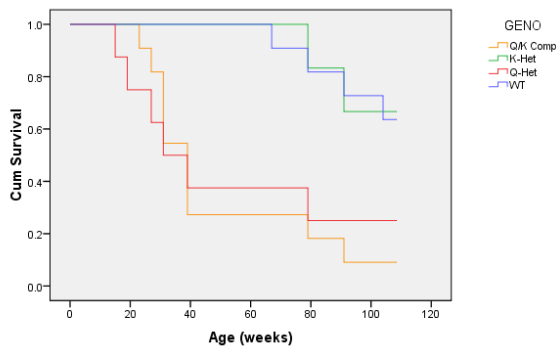
Q101X/K160R Severe body tone Males

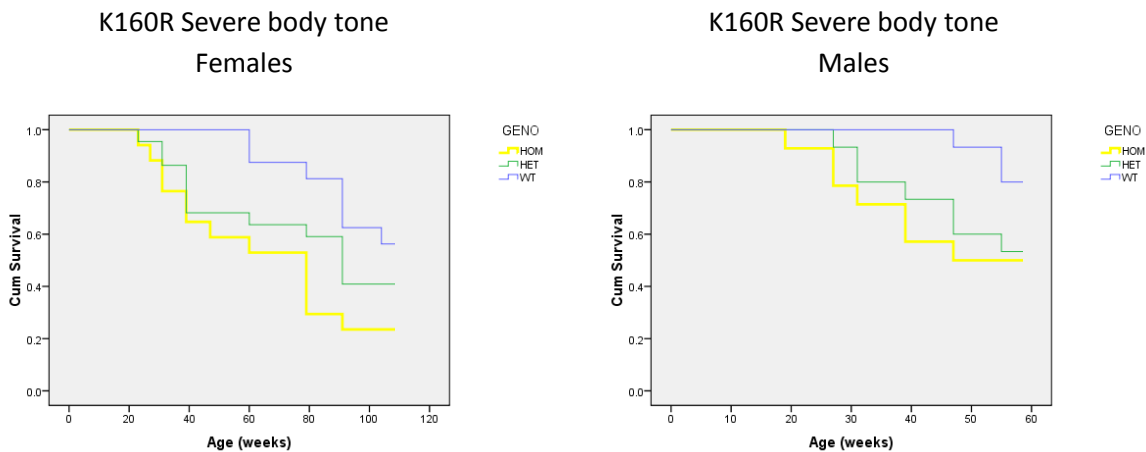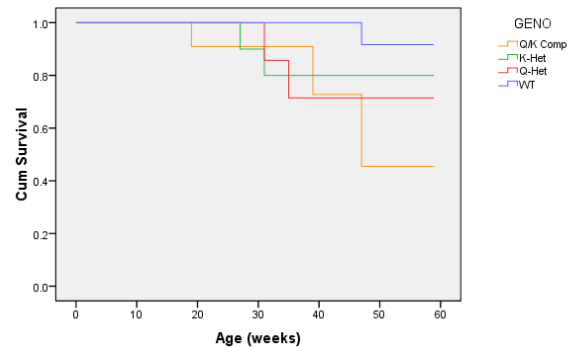**Figure 3.20: Compound** *Tardbp*[Q101X/K160R] **Severe reduction in body tone**. Onset plots showing the presence of severely softer body tone observed in the SHIRPA arena through time. Plots shown by sex. Y axis shows proportion of mice with lines decreasing from 1, where no mice show the phenotype. N = female WT 11, Q-Het 8 , K-Het 6, Q/K Comp 11 . N = male WT 12, Q-Het 7, K-Het 10, Q/K Comp 11. Mean age at which body tone was shown for both sexes combined was WT = no phenotype, Q-Het = 52 (more than 50% of females), K-Het = no phenotype, Q/K Comp = 48 (more than 50% both sexes). WT versus Q-Het p = 0.009, WT versus K-Het p = 0.692, WT versus Q/K Comp p < 0.001, Q-Het versus Q/K Comp p = 0.514, K-Het versus Q/K Comp p = 0.004. Kaplan Meier Log rank statistic. Overall p < 0.0001, with no differences by sex within genotype (p > 0.05).

3.4.7. Negative geotaxis

Negative geotaxis was assessed by placing the mouse on a vertical grid and assessing how effectively the mouse was able to climb down to the floor and to what degree the mouse slips. Negative geotaxis is a challenge to wild-type mice with increased slipping progressing as the mice aged. In the Q101X line, slipping was observed in both sexes however there was a higher penetrance and earlier onset (Figure 3.21) in Q101X heterozygotes, age of onset (wild-type less than 50%, Q101X heterozygotes was 44 weeks).

Q101X Negative geotaxis
Females

Q101X Negative geotaxis
Males

Figure 3.21: Q101X Negative geotaxis. Onset plots showing the presence of negative geotaxis slipping observed in the SHIRPA arena, through time. Plots shown by sex. Y axis shows proportion of mice with lines decreasing from 1, where no mice show the phenotype. N = female WT 12, HET 15. N = male WT 16, HET 16. Mean age at which negative geotaxis was shown for both sexes combined was WT less than 50%, HET = 44. WT versus HET $p < 0.0001$, Kaplan Meier Log Rank Statistic. Overall $p < 0.0001$ with significant difference by sex within genotype. Wild-type females versus males $p = 0.02$, Q101X heterozygote females versus males $p < 0.001$).

In the K160R line, the mean age at which mice began to slip in the task was significantly younger in homozygote mice versus controls. Wild-type mice slipped at 42 weeks, heterozygote mice on average at 36 weeks with homozygous mice slipping at 24 weeks (Figure 3.22).

K160R Negative geotaxis
Females

K160R Negative geotaxis
Males
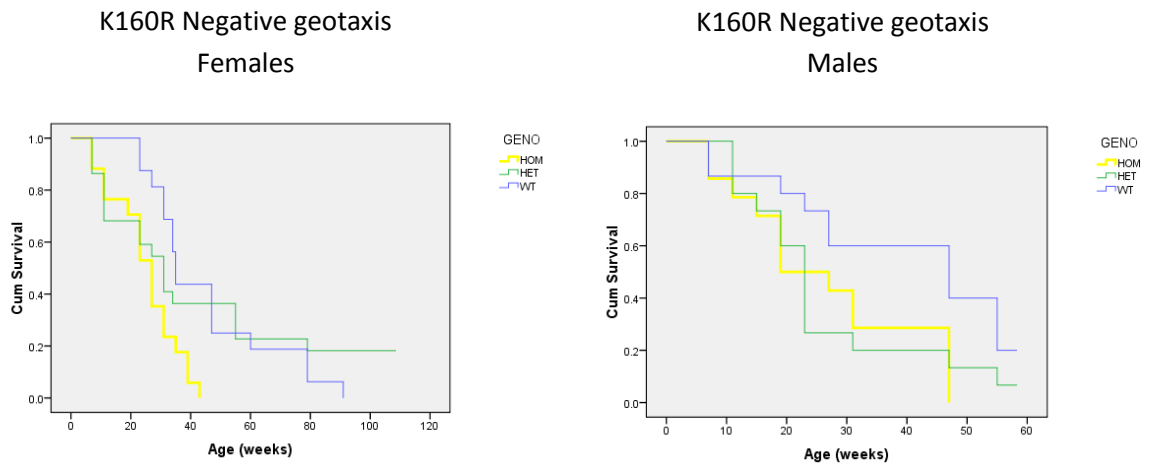
Figure 3.22: K160R Negative geotaxis. Onset plots showing the presence of slipping on the negative geotaxis observed in the SHIRPA arena through time. Plots shown by sex. Y axis shows proportion of mice with lines decreasing from 1, where no mice show the phenotype. N = female WT 16, HET 22, HOM 17. N = male WT 14, HET 15, HOM 15. Mean age at which negative geotaxis was shown for both sexes combined was WT = 42, HET = 36, HOM = 24. WT versus HET p = 0.204, WT versus HOM p < 0.001, Kaplan Meier Log rank statistic. Overall p = 0.003 with no differences by sex within genotype up to one year of age.

More than 50% of mice from every genotype significantly slipped in the negative geotaxis challenge in the compound heterozygote line. The frequency and prevalence of slipping was significantly higher with an earlier onset in compound heterozygotes mice versus WILD-TYPE controls (Figure 2.3).

Q101X/K160R Negative geotaxis Females

Q101X/K160R Negative geotaxis Males

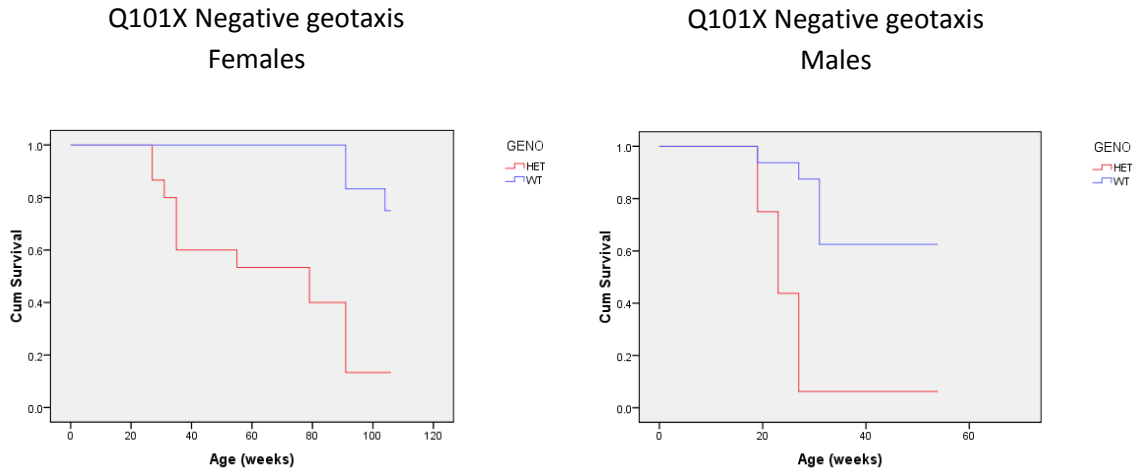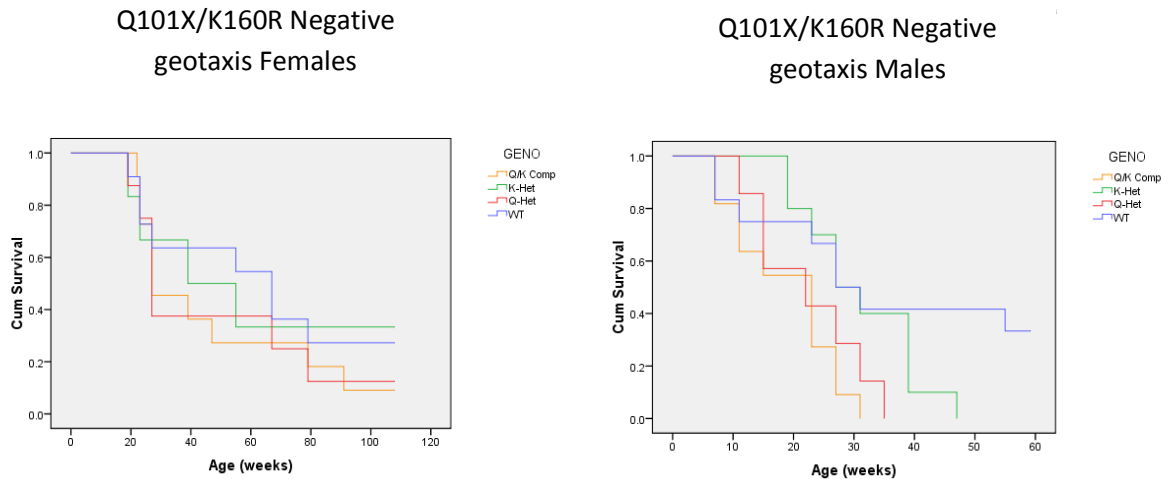**Figure 3.23: Compound** *Tardbp*^Q101X/K160R **Negative geotaxis**. Onset plots showing the presence of negative geotaxis slipping observed in the SHIRPA arena through time. Plots shown by sex. Y axis shows proportion of mice with lines decreasing from 1 where no mice show the phenotype. N = female WT 11, Q-Het 8 , K-Het 6, Q/K Comp 11 . N = male WT 12, Q-Het 7, K-Het 10, Q/K Comp 11. Mean age at which negative geotaxis slipping was shown for both sexes combined was WT = 47 (more than 50% both sexes), Q-Het = 35 (more than 50% both sexes), K-Het = 41 (more than 50% both sexes), Q/K Comp = 32 (more than 50% both sexes). WT versus Q-Het p = 0.135, WT versus K-Het p = 0.402, WT versus Q/K Comp p = 0.027, K-Het versus Q/K Comp p = 0.016, Q-Het versus Q/K Comp p = 0.488, Kaplan Meier Log rank statistic. Overall p = 0.029 with significant sex differences within genotypes. There were trends for significant differences between male and female Q101X and K160R heterozygotes (p = 0.078 and 0.073 respectively) and a significant difference between sexes in compound heterozygotes (p = 0.004) up to one year.

3.4.8. SHIRPA summary

SHIRPA assessment of Q101X, K160R and compound heterozygote lines showed significant differences in a number of endophenotypes, common to all lines. The commonality of phenotypes in K160R and Q101X lines, despite each line carrying different alternative ENU mutations, supports these phenotypes being caused by the TDP43 mutations. A summary of all SHIRPA phenotypes is given below, in Table 3.2, with comparisons by sex up to one year shown in Table 3.3.

	Q101X Line	K160R Line	Compound (*Tardbp*$^{Q101X/K160R}$) line
Gait	< 50%, p = 0.014	No phenotype	> 50% Q-het + Q/K Compounds (all mutants significant), Q/K Comp p = 0.001
Limb grasp	> 50% (females), p = 0.002	> 50% homozygotes only, Het p = 0.136, Hom p < 0.001	> 50% Q/K Compounds (Q-Het and compounds significant), Q/K Comp p = 0.001
Body Tone	> 50%, p < 0.001	> 50% all genotypes, Het p = 0.605, Hom p < 0.001	> 50% Q/K Compounds (all mutants significant), Q/K Comp p < 0.001
Severe Body tone	> 50% (females), p = 0.003	> 50% homozygotes only, Het p = 0.018, Hom p = 0.001	> 50% Q/K Compounds (Q-het and compounds significant), Q/K Comp p < 0.001
Negative geotaxis	> 50%, p < 0.001	> 50% all genotypes (homozygotes only significant), Het p = 0.204, Hom p < 0.001	> 50% all genotypes (compounds significant) Q/K Comp p = 0.027

Table 3.2: SHIRPA phenotype summary. Table showing the proportion of mice from each line showing the SHIRPA endophenotypes and which genotypes are significantly different from littermate controls.

		Q101X Line	K160R Line	Compound (*Tardbp*$^{Q101X/K160R}$) line
Gait	Male	No sex differences	No phenotype	no sex differences
	Female			
Limb grasp	Male	Significantly in females	No sex differences	No sex differences
	Female			
Body Tone	Male	Trend to earlier onset with increased prevalence in males	No sex differences	No sex differences
	Female			
Severe Body tone	Male	No sex differences	No sex differences	No sex differences
	Female			
Negative geotaxis	Male	Significantly earlier onset in males	No sex differences	Significantly earlier and more prevalent in compound males with trends in heterozygote mutants
	Female			

Table 3.3: SHIRPA sex differences. Table showing significant differences by sex within genotype for those endophenotypes were differences were observed.

3.4.9. Startle response and open field

Startle response was used to measure the sensorimotor jump response to a tone stimulus. This was tested alongside pre-pulse inhibition to assess sensory inhibition. Open field was also used to measure mouse behaviour and locomotor activity in an arena. Both tests were used to characterise reflexive and behavioural responses, with both tests potentially assessing motor deficits.

Startle response and pre-pulse inhibition were assessed at 10 and 22 weeks of age in all lines (number greater than ten mice per sex per genotype). No significant differences in startle response or pre-pulse inhibition were present in the Q101X heterozygote line ($p > 0.05$, Multivariate general linear model - GLM). Open field was assessed at 14 and 30 weeks, with no significant differences observed ($p > 0.05$ for all endophenotypes, Multivariate GLM). The results for startle response and pre-pulse inhibition are shown in Figure 3.24 and Figure 3.25. There were no significant differences between sexes either ($p > 0.05$, Multivariate GLM).
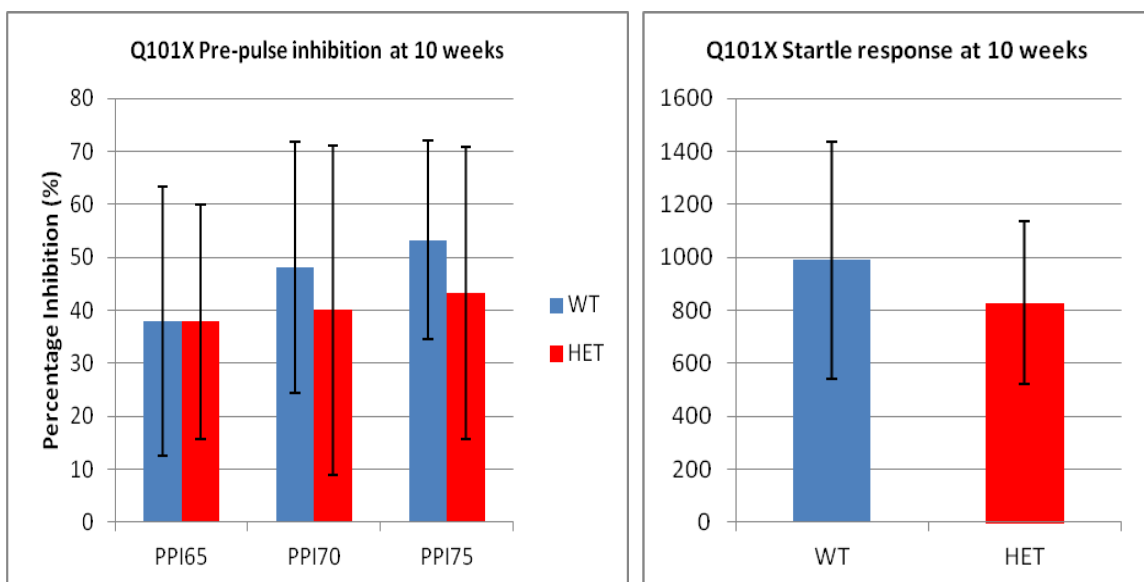
Figure 3.24: Q101X Startle response and pre-pulse inhibition at 10 weeks. N = WT 23, HET 27. Average startle response is WT = 989, HET = 829, $p < 0.05$ Univariate GLM. With no significant difference in startle indicating normal hearing and sensorimotor gating, pre pulse inhibition can be analysed. Tones at 65, 70 and 75 dB played before the 110 dB startle should increasingly dampen the startle response. This occurs for control and mutant mice, with no significant differences observed. Error bars represent standard deviation.
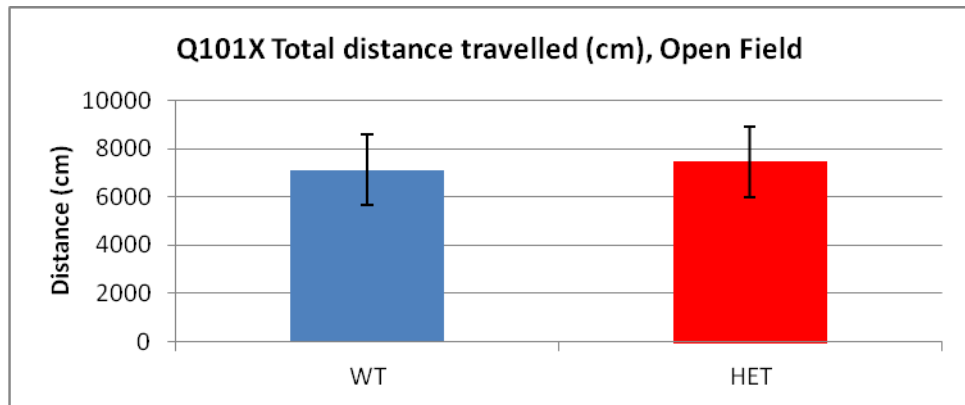
Figure 3.25: Q101X Open field 14 weeks. Graph showing total distance travelled in Q101X mice and littermate controls. N = WT 21, HET 24. Mean distance travelled: WT = 7115.12 cm, HET = 7448.32 cm. p = 0.841 Univariate GLM. Error bars represent standard deviation.

No significant differences in startle response were seen at 10 and 22 weeks of age in the K160R line. At 10 weeks, 14 wild-type, 16 heterozygote and 10 homozygote K160R mice were assessed. At 22 weeks, 25 wild-type, 33 heterozygous and 22 homozygous mice were assessed. Startle response was not significantly different. With a normal startle response, pre-pulse inhibition can be assessed, which was also not significantly different (in all cases p > 0.05, Univariate GLM, post hoc Bonferroni analysis). Open field activity was assessed at 14 and 30 weeks. There was a trend to reduced movement duration in K160R heterozygotes versus littermate controls at 14 weeks (Figure 3.26). However at 30 weeks, with 17 wild-type, 19 heterozygous and 18 homozygous mice assessed, no significant differences were present and this trend was also absent. For startle response there were no significant differences between sexes (p > 0.05) but in the open field females had significantly reduced movement duration across genotypes (p = 0.044 Multivariate GLM, Bonferroni post hoc).
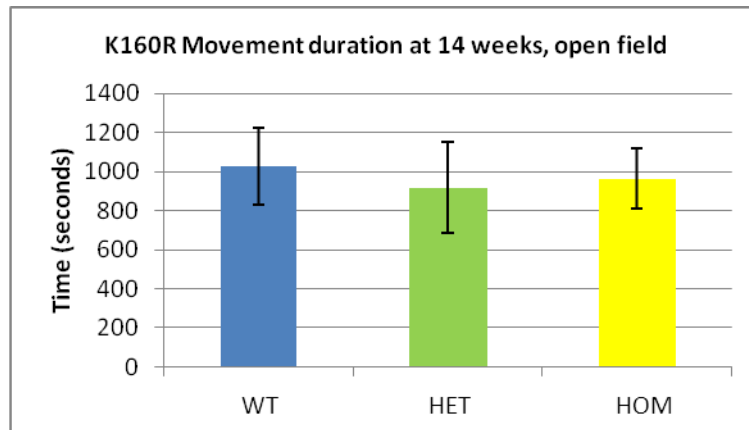
Figure 3.26: K160R Open field at 14 weeks. Bar chart showing the movement duration (seconds) from a total of 1800 seconds in the arena, measured using Noldus Ethovision software. Error bars represent standard deviation. N = WT 25, HET 30, HOM 42. Movement duration average was WT = 1029.02, HET = 916.32, HOM = 963.11. WT versus HET p = 0.06, WT versus HOM p = 0.509, Multivariate GLM, Bonferroni post hoc.

In the compound heterozygote line, startle response was assessed at 10 and 22 weeks. At 10 weeks there was a significant difference between K160R heterozygotes (1360) and Q101X heterozygotes (830), p = 0.025 Univariate GLM, Bonferroni post hoc analysis. The number of mice tested was wild-type 19, K-Het 11, Q-Het 12, Q/K Compounds 18, with an equal male to female ratio. At 22 weeks, there was no significant difference between heterozygotes (Figure 3.27). There was a trend to reduced startle response in compound heterozygotes (versus wild-type p = 0.06 Univariate GLM, Bonferroni post hoc analysis). Open field activity was assessed at 14 and 30 weeks. At 14 weeks, no significant differences were observed (n = WT 24, Q-Het 14, K-Het 14, Q/K Comp 24). Analysing the data before it was fully complete at 30 weeks, showed trends in the movement duration endophenotype. Based on this measurements were taken at 42 weeks, before the 30 week data set was complete. Once all results at 30 weeks were collected no significant differences were observed (n = WT 22, Q-Het 13, K-Het 14, Q/K Comp 21). As a result the 42 week time point was not completed by all mice however significant differences due to K160R heterozygote activity were observed (Figure 3.28). Overall for both startle and open field tests no significant differences by sex were observed (p > 0.05 in all cases).
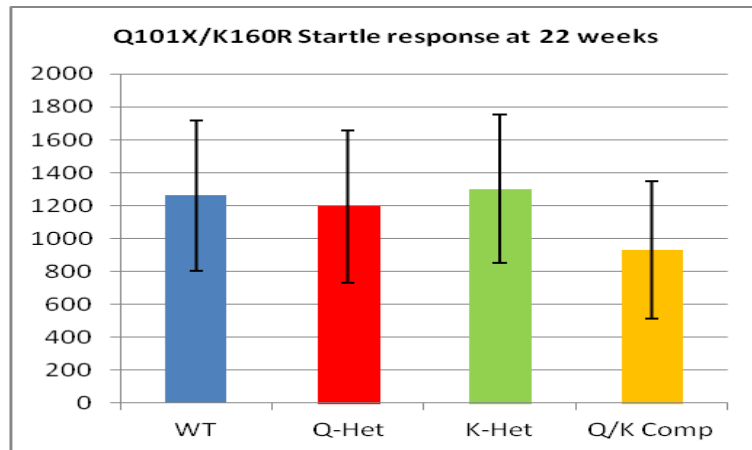
Figure 3.27: Compound *Tardbp*$^{Q101X/K160R}$ Startle response at 22 weeks. Bar chart showing the relative startle response to a 110 dB tone, quantitatively measured. Error bars represent standard deviation. N = WT 23, Q-Het 14, K-Het 13, Q/K Comp 22. Average startle response was WT = 1260.70, Q-Het = 1195.70, K-Het = 1302.58, Q/K Comp = 932.64. WT versus Q/K Comp p = 0.06, K-Het versus Q/K Comp p = 0.078, Multivariate GLM Bonferroni post hoc.
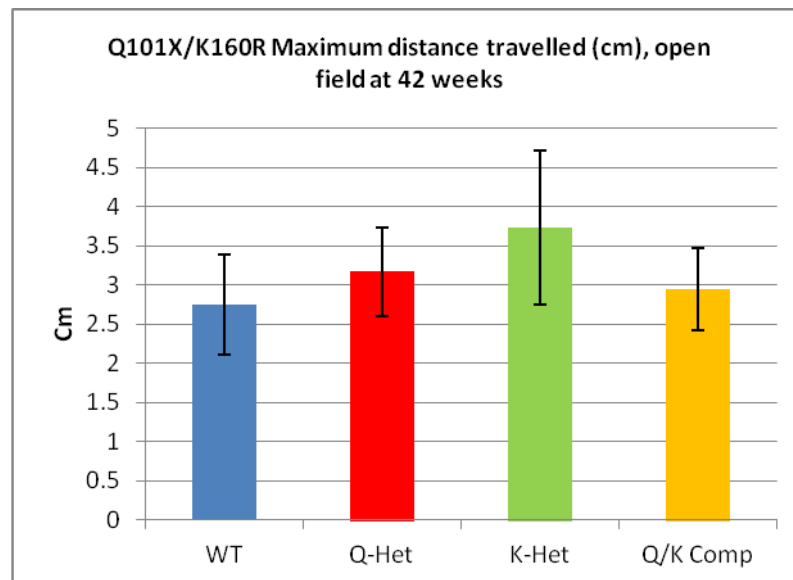
Figure 3.28: Compound *Tardbp*$^{Q101X/K160R}$ Open field at 42 weeks. Bar chart showing the maximum distance travelled in a directed movement, measured using Noldus Ethovision software. Error bars represent standard deviation. N = WT 16, Q-Het 9, K-Het 10, Q/K Comp 17. Average distance moved was WT = 2.74, Q-Het = 3.17, K-Het = 3.73, Q/K Comp = 2.94. WT versus Q/K Comp p = 1, WT versus K-Het = 0.002, Q/K Comp versus K-Het p = 0.02, Multivariate GLM Bonferroni post hoc.

3.4.10.   Rotarod and grip strength

Rotarod was assessed at time points indicated in Figure 3.29, Figure 3.31 and Figure 3.33, initially once per month and later every two months. No significant differences in overall performance were seen up to 64 weeks of age in the Q101X heterozygote line with no significant differences due to sex ($p > 0.05$) (Figure 3.29).

Figure 3.29: Q101X longitudinal rotarod. Graph showing average WT and HET time on the accelerating rotarod, with error bars representing standard deviation. Rotarod measurements were taken in triplicate over three days (nine values per mouse), with the average of total performance recorded. There are no significant differences in rotarod performance between WT and Q101X HET mice observed up to 64 weeks ($p > 0.05$, Repeated measures ANOVA wherever possible and Standard GLM).

Grip strength analysis followed the rotarod assessment in the same week. No significant differences were observed in Q101X male cohorts up to one year and female cohorts up to two years, as summarised in Figure 3.30. Mean force generated in mutants and controls remained around 200 grams, slightly decreasing in later age beyond 80 weeks. Weight was not accounted for in the analysis as there were no significant differences in weight between genotypes up to one year of age, with no significant differences by sex ($p > 0.05$, Multivariate GLM).
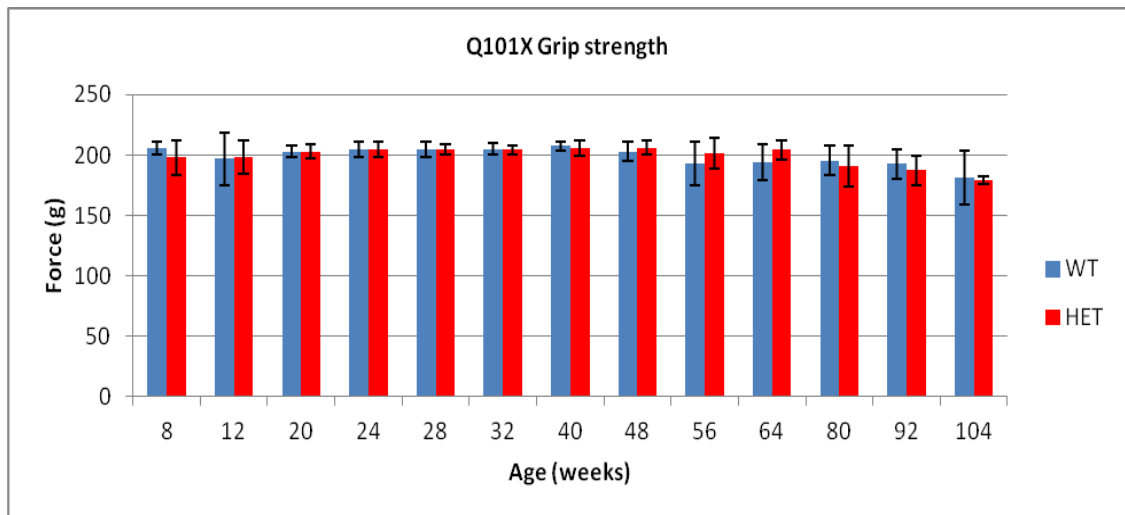
Figure 3.30: Q101X longitudinal grip strength. Graph showing average WT and HET grip strength, with error bars representing standard deviation. Measurements represent average force (g) generated in duplicate over four limbs. There are no significant differences in grip strength between WT and Q101X HET mice observed up to 64 weeks with males and females, or up to 104 weeks with females ($p > 0.05$, Repeated measures ANOVA wherever possible and Standard GLM).

As with the Q101X heterozygote line, in the K160R line no significant differences in rotarod performance were seen at any point by genotype or sex ($p > 0.05$). Because of a low average time spent on the rod and large variation, only major differences would have been detected (Figure 3.31). Grip strength was assessed at selected time points up to 92 weeks as shown in Figure 3.32. Data includes male and female strength up to 54 weeks of age, with only female results up to 92 weeks of age. No consistently significant differences in grip strength were seen in male and female mice.
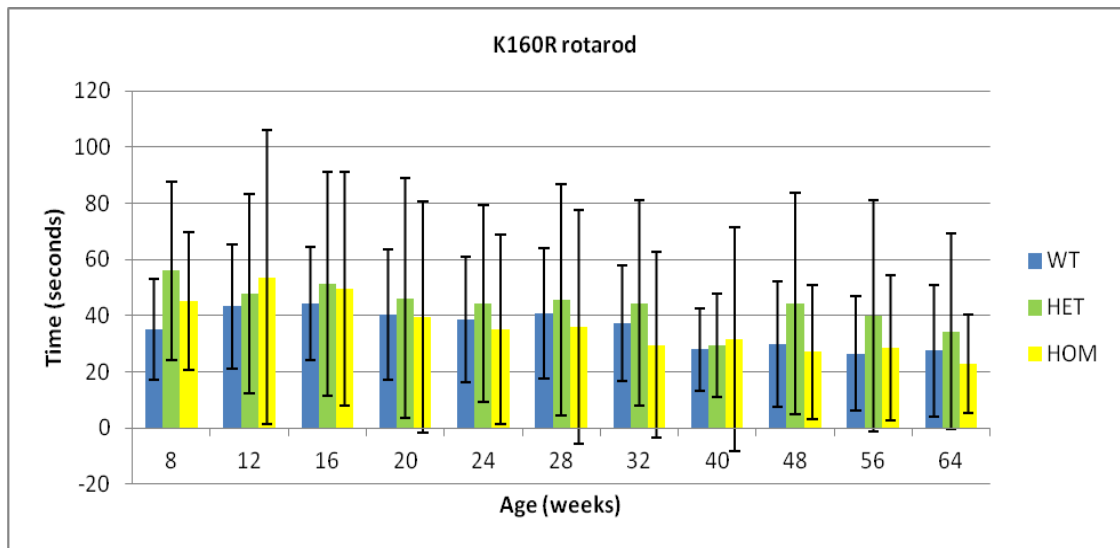
Figure 3.31: K160R longitudinal rotarod. Graph showing average WT, HET and HOM time on the accelerating rotarod, with error bars representing standard deviation. Rotarod measurements were taken in triplicate over three days (nine values per mouse) with the average of total performance taken. There are no significant differences in rotarod performance between WT , HET and HOM K160R mice observed up to 64 weeks ($p > 0.05$, repeated measures ANOVA wherever possible and Standard GLM, Bonferroni post hoc).
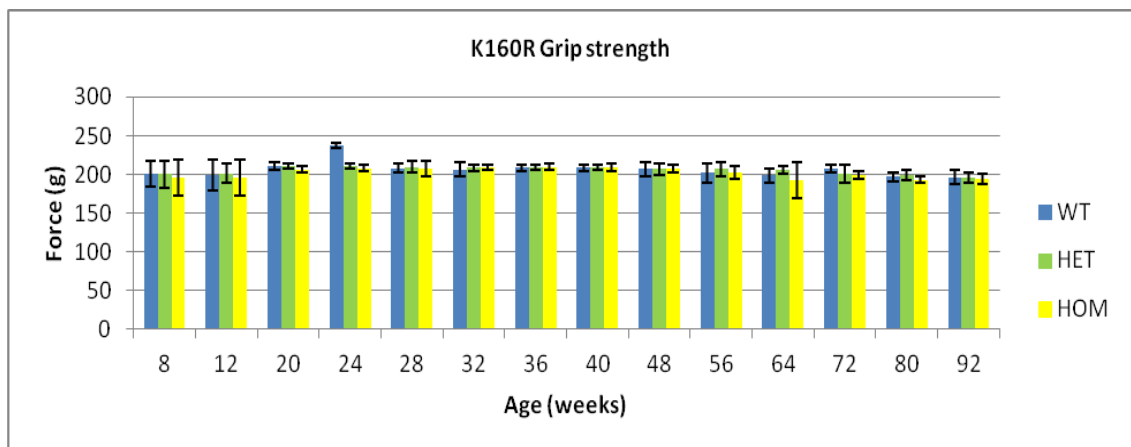
Figure 3.32: K160R longitudinal grip strength. Graph showing average grip strength, with error bars representing standard deviation. Measurements represent force (g) generated in duplicate over four limbs. There are no consistent significant differences in grip strength between genotypes observed up to 64 weeks with males and females, or up to 104 weeks with females ($p > 0.05$, repeated measures ANOVA wherever possible and Standard GLM Bonferroni post hoc). At 24 weeks, WT grip strength is significantly higher than mutants ($p < 0.05$) but this is not repeated. Error bars represent standard deviation.

No significant differences were seen in either rotarod and grip strength in the compound heterozygote line, by sex or genotype as shown in Figure 3.33 and Figure 3.34.
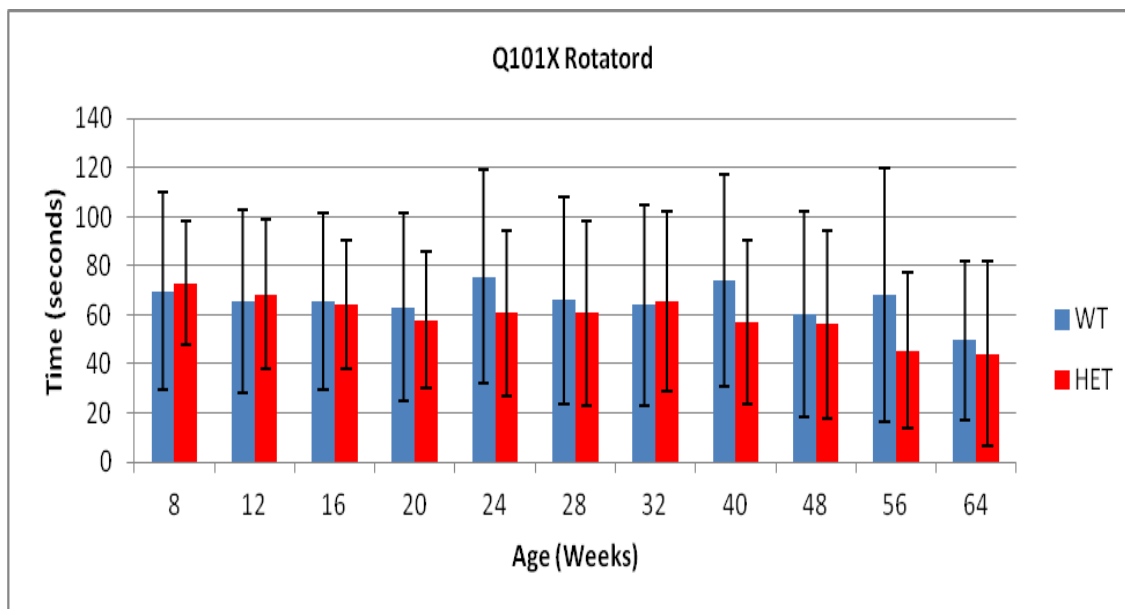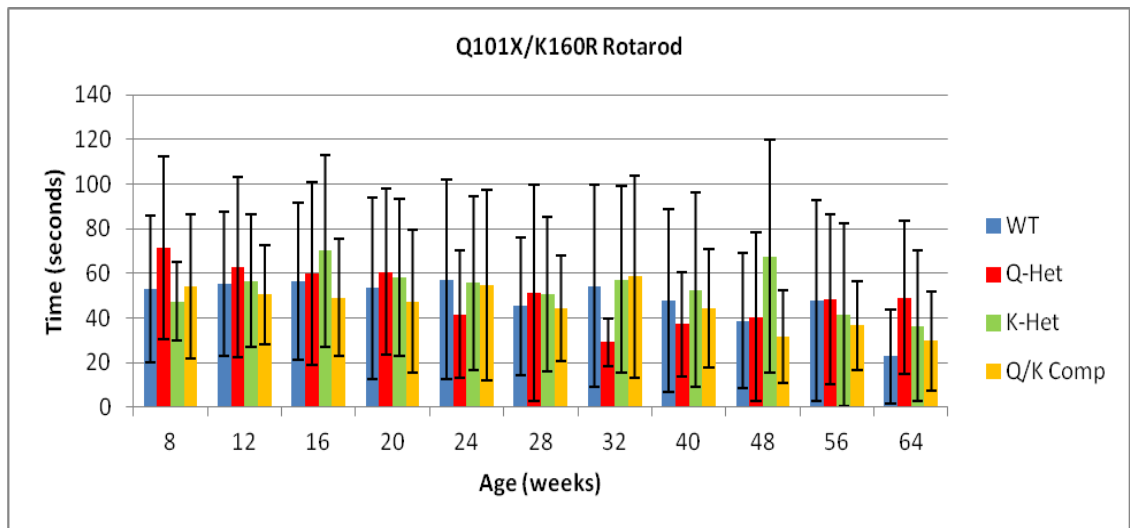
Figure 3.33: Compound *Tardbp*[Q101X/K160R] longitudinal rotarod. Graph showing average time on the accelerating rotarod, with error bars representing standard deviation. Rotarod measurements were taken in triplicate over three days (nine values per mouse), with the average of total performance measured. There are no consistently significant differences in rotarod performance between genotypes observed up to 64 weeks (p > 0.05, repeated measures ANOVA wherever possible and Standard GLM).
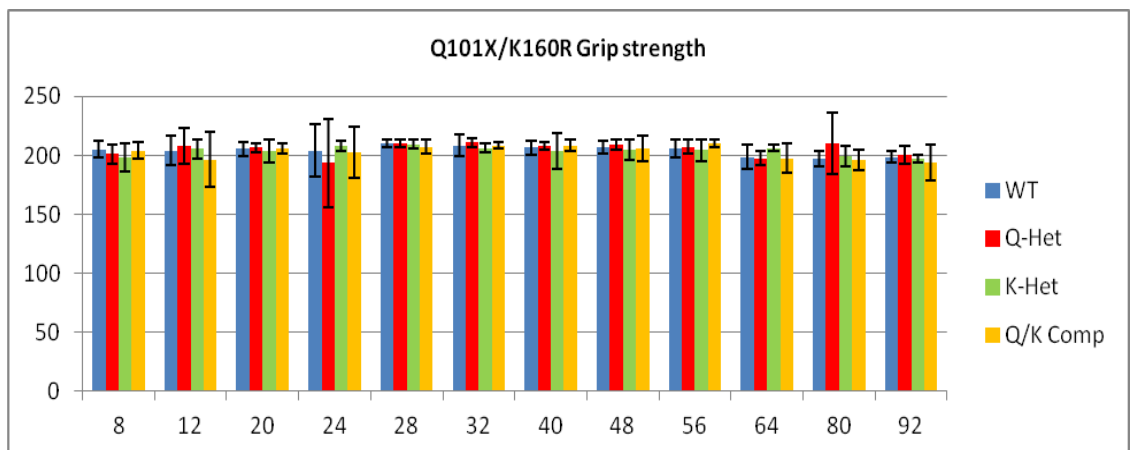
Figure 3.34: Compound *Tardbp*[Q101X/K160R] longitudinal grip strength. Graph showing average grip strength, with error bars representing standard deviation. Measurements represent average force (g) generated in duplicate over four limbs. There are no significant differences in grip strength between genotypes observed up to 64 weeks with males and females, or up to 92 weeks with females (p > 0.05, repeated measures ANOVA wherever possible and Standard GLM).

3.5. Q101X and K160R cognitive assessment

A separate cohort of female compound ($Tardbp^{Q101X/K160R}$) and K160R ($Tardbp^{K160R/K160R}$) homozygote mice were generated, with respective littermate controls. These mice were sent to the Department of Psychology, Oxford University for cognitive assessment. Dr Sam Line and Dr Rob Deacon assessed these mice with a pipeline of cognitive tests. The aims of these experiments were based on FTLD-TDP being part of a spectrum of disease with ALS (Liscic *et al.*, 2008). The aim was to determine if there were deficits in multiple aspects of cognition in these mice, indicative of the changes seen in dementia.

Significant differences were seen in two cognitive tests, the light-dark box test and the black-white alley test. The light dark box test and black white alley test both measure multiple aspects of anxiety based phenotypes. In the light-dark box test, a smaller dark box is adjacent to an illuminated box with the mouse having the ability to move between the boxes. Mice have an aversion to the illuminated box and the activity of the mice starting from the dark or light box over time is measured. The test is used to predict anxiolytic and anxiogenic-like behaviours through measuring time in each compartment and transitions. Similarly, in the black-white alley test, a long alley box which is half black and half white is used. The mouse is placed facing the black wall which is less aversive and it is timed to enter the white half of the alley. In both tests the white area represents a mild stressor to the mice.

Compound heterozygotes ($Tardbp^{Q101X/K160R}$) in the light-dark box test spend more time in the dark versus littermate controls (Figure 3.35). Overall, the significant differences observed in these two tests indicate that the compound heterozygotes are more anxious and show lower emotionality. This is not seen in heterozygous mutants or K160R homozygotes when compared to their littermate controls. The numbers of mice assessed were approximately ten per genotype, so this result is preliminary. A second cohort is being aged to re-assess whether these mutations result in anxiety related phenotypes.
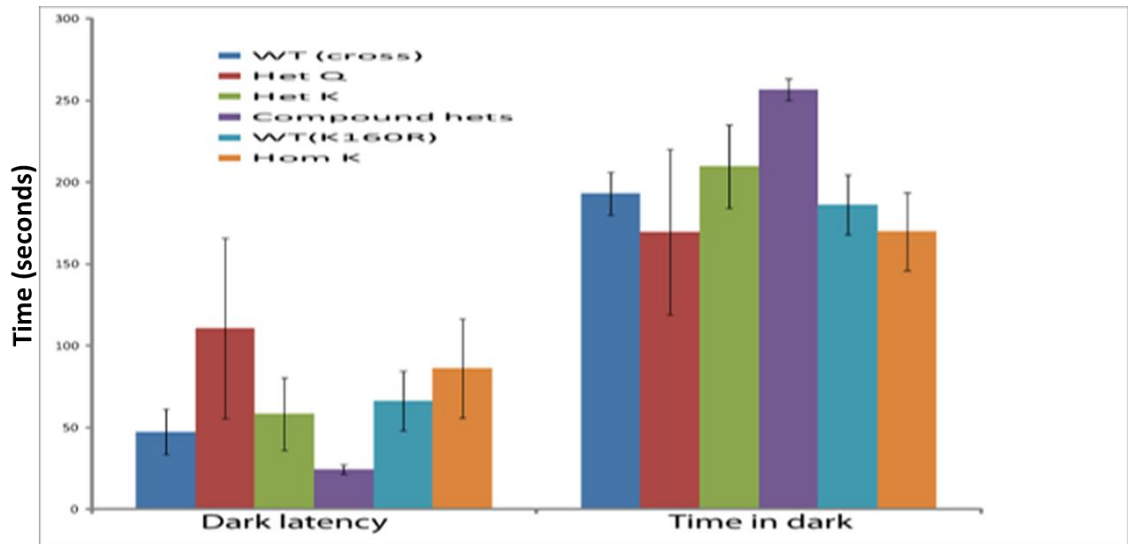
Figure 3.35: Compound *Tardbp*^{Q101X/K160R} cognitive assessment. Cohorts of mice (n = WT 8, Q/K Comp 7, all other genotypes 9) were generated for cognitive assessment. Compound *Tardbp*^{Q101X/K160R} mice in the light dark box showed increased time in the dark: p = 0.001 versus WT, a trend in dark latency: p = 0.105 versus WT, and reduced transits: p = 0.010 versus WT.

3.6. Pathology

Pathology was assessed at one year of age for all mutant lines. Pathological assessment was required as it often precedes behavioural abnormalities where subtle alterations may not be detected at a behavioural level. One year old males were perfused and brains were harvested for analysis. Three brains per genotype for the compound (*Tardbp*^{Q101X/K160R}) and K160R (*Tardbp*^{K160R/K160R}) cohorts were sent to Dr Sebastian Brandner (UCL) for this assessment. Following a standard staining regime including hematoxylin and eosin stain, no overt alterations at the light microscopy level was seen in brain at this stage. Brains from two year old (end stage) samples are yet to be analysed.

Pathological assessment showed no overt alterations in the brain at one year of age at the light microscope level. At eight months, spinal cords from two wild-type, two Q101X heterozygotes and two compound heterozygotes (*Tardbp*^{Q101X/K160R}) were harvested for electron microscopy (EM) analysis. This was completed by Constandina Vasiliou in Dr Julian Thorpe's laboratory at the University of Sussex. Spinal cord sections were analysed by transmission EM. Immunogold labelling using anti-TDP (ProteinTech) showed small aggregate

structures exclusively seen in the cytoplasm of *Tardbp*^{Q101X/K160R} compound neurons (Figure 3.36). These were not seen in Q101X heterozygote or littermate controls.
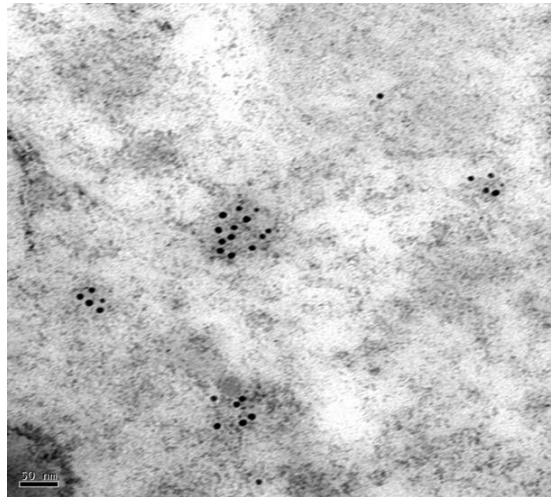
Figure 3.36: Compound *Tardbp*^{Q101X/K160R} EM pathology. Image taken in the cytoplasm of a spinal cord neuron from a compound mutant. Black dots show anti-TDP43 (ProteinTech) labelled structures which are not seen in control samples. Image taken from tissue harvested at eight months.

3.7. Compound *Tardbp*^{Q101X/K160R} molecular characterisation

3.7.1. Q101X auto-regulation

Q101X heterozygous animals only have one full length functional TDP43 allele. Whilst phenotyping the Q101X cohort, published knock out papers showed that in heterozygous knock outs, protein levels are equivalent to wild-type controls (Kraemer *et al.*, 2010). This confirmed *in vivo* that in heterozygote knock outs TDP43 auto-regulates its protein levels equivalently to having two functional alleles. This was initially assessed in the Q101X heterozygotes with Westerns blots for six wild-type and six heterozygotes from twelve week harvested adult brain. Protein levels normalised to actin were not significantly different. This has since been assessed in one and a half year old TDP43 mice, with an equivalent level of protein detected when normalised to actin (Figure 3.37). This confirms that *in vivo* in Q101X heterozygous mice, there is TDP43 protein auto-regulation as in knock out heterozygotes. This data supports the Q101X mutation being a null allele, alongside the homozygote lethality phenotype occurring at the same time as published knockouts.
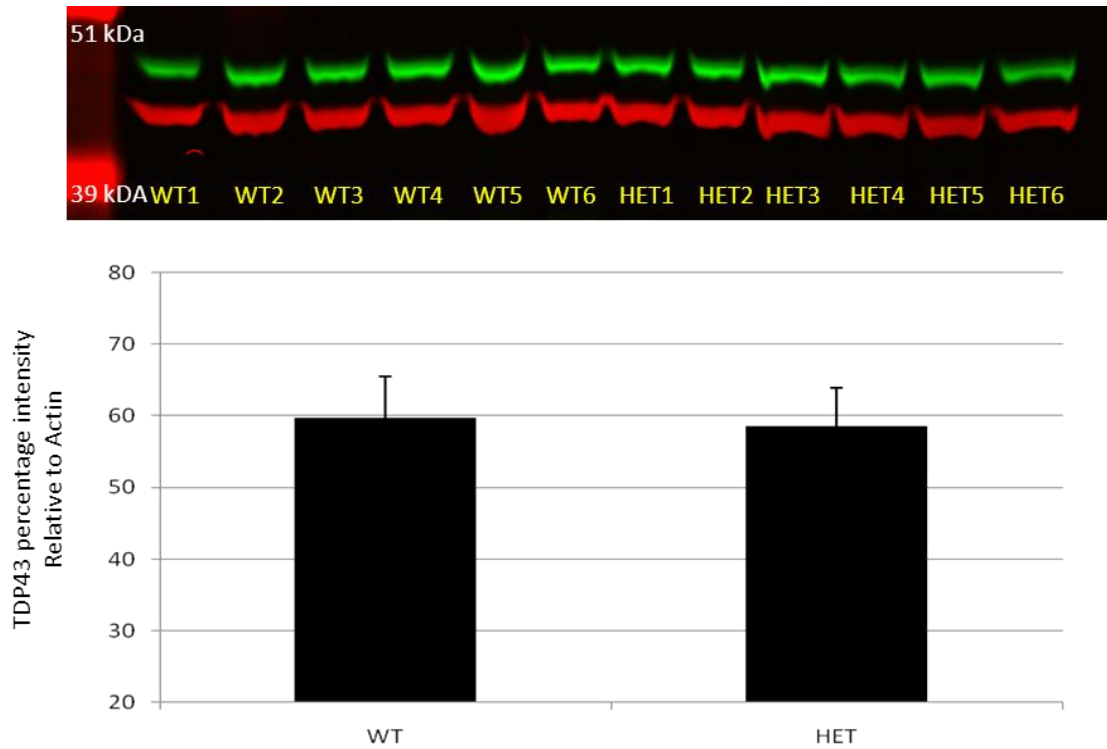
Figure 3.37: TDP43 Q101X levels from mouse brain. N = WT 6, HET 6. Brains were collected for protein and RNA analysis. Protein was extracted from half brain and quantified using anti-TDP (ProteinTech) with anti-actin control (Abcam). Fluorescent Leica secondary antibodies were used with Leica Odyssey visualisation and quantification software. TDP43 is green and actin is red. TDP43 levels were calculated as percentage intensity relative to actin. Error shows standard deviation.

Two N-terminally targeted antibodies (Ab50930 Abcam, CAC-TIP-TD-P07 Cosmo) were used to detect whether the Q101X allele is expressed at the protein level. Western blots were unable to detect the band expected at approximately 18 kDa. This indicates that the Q101X protein is either not produced or is rapidly degraded.

The Q101X encoding RNA transcript was quantified to compare the relative levels against the full length protein encoding transcript. Using the same pyro-sequencing assay for genotyping Q101X, RNA levels were quantified. RNA was extracted from brain tissue and cDNA generated. The Q101X genotyping assay was run and the area under the curve for the wild-type and mutant peaks was measured. DNA serves as a control with Q101X heterozygotes having a 1:1 ratio of wild-type (C) and mutant (T) alleles. From the cDNA, the wild-type allele is highly expressed (C = 83.9%) whereas the Q101X encoding transcript relative to the wild-type allele is lowly expressed (T = 16.1%). This is shown in Figure 3.38. This was repeated from three

independent samples and confirms that the Q101X encoding transcript is reduced and is likely to be degraded with minimal protein produced.
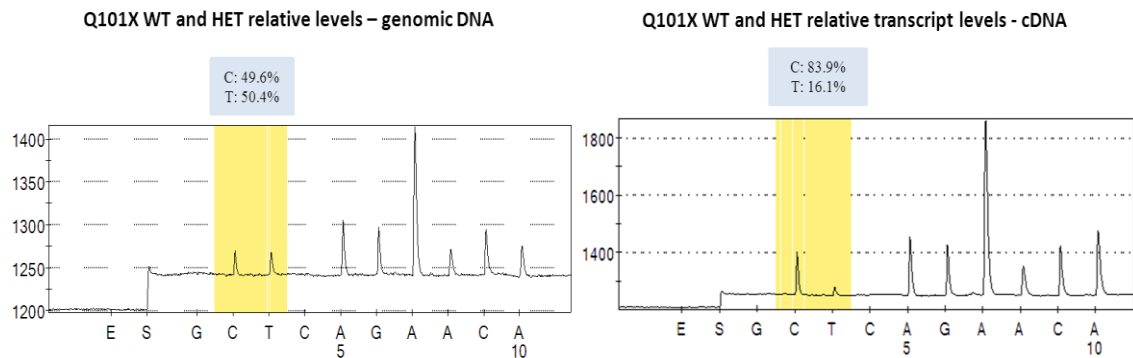
Figure 3.38: Q101X transcript ratio. Pyro-sequencer result from the assay used normally to genotype Q101X mice. The WT base is a C and the Q101X mutated base is a T. Genotyping from genomic DNA produces an approximate 50 / 50 ratio for each allele (left panel). Down regulation of the Q101X allele from RNA converted to cDNA is shown in the right panel. The pyro sequencer measures the relative areas under each curve, which can be used as a quantified measurement to compare expression levels of the two transcripts to each other.

3.7.2. Protein levels

Data for protein levels has been collected from mouse brain at various time points. There is a trend towards reduced TDP43 levels in compound heterozygotes versus wild-type controls. Relative to actin, TDP43 levels decrease by a third in compound heterozygotes, from 12 week adult brain (Figure 3.39). This Western blot has been repeated. However, there is no significant reduction in the protein levels between genotypes.
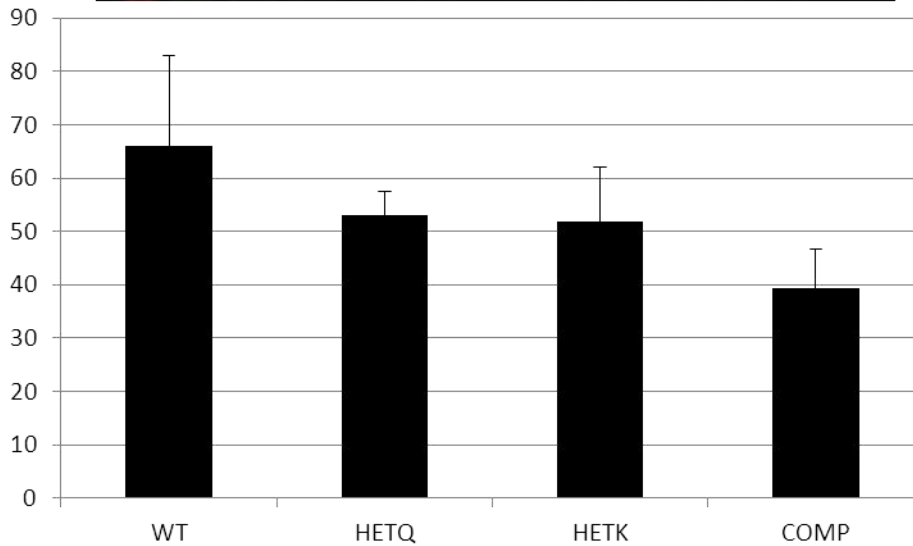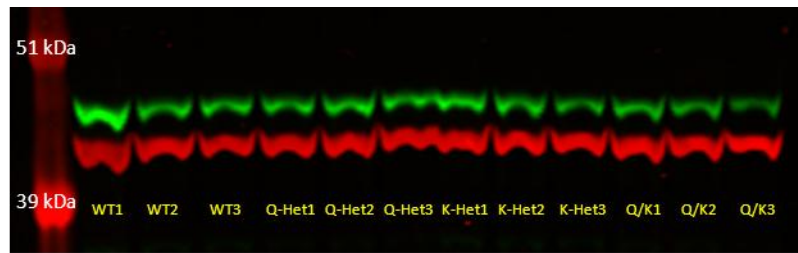
Figure 3.39: Compound *Tardbp*^{Q101X/K160R} three month protein levels. Western blot of protein extracted from compound *Tardbp*^{Q101X/K160R} half brain with littermate controls. TDP43 (ProteinTech) is the green band (Li-Cor Rabbit secondary) and actin (Invitrogen) is the red (Li-Cor Mouse secondary). Bands quantified using Li-Cor Odyssey software. As a mean percentage of actin band intensity, WT = 66.05%, Q-Het = 53.02%, K-Het = 51.75%, Q/K Comp = 39.25%. WT versus Q/K Comp p = 0.097, 1 way ANOVA Bonferroni post hoc. Error bars show standard deviation.

Westerns were also run using samples from one year old male brain. wild-type, Q101X heterozygous and compound heterozygous samples were run (3:3:3 per genotype). Figure 3.40 shows that there is a trend towards reduced Q101X heterozygote protein levels with a trend to decreased levels in compound heterozygote protein levels. This matches the trend seen in young brain harvested at three months.
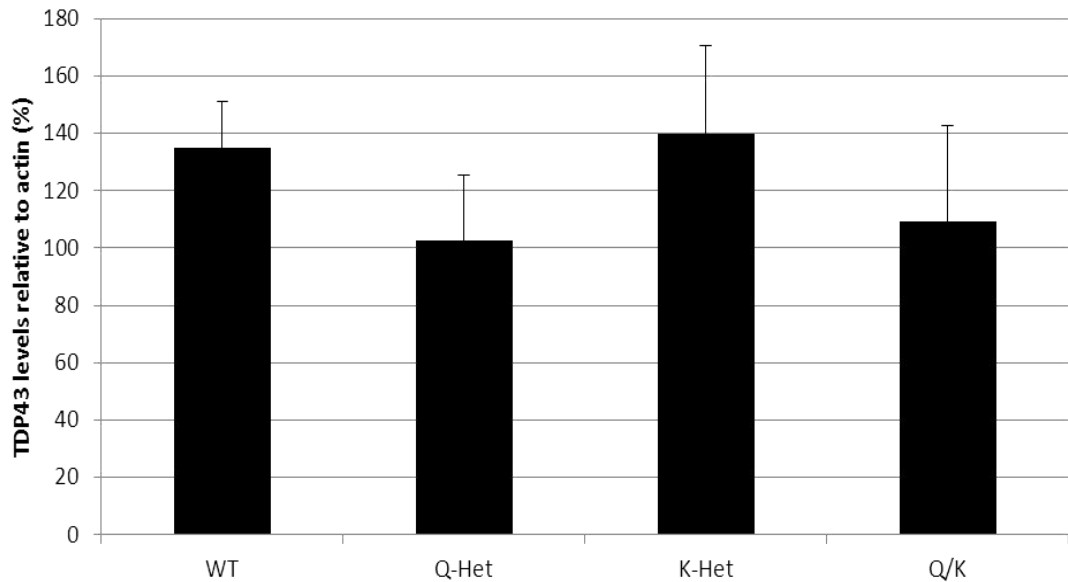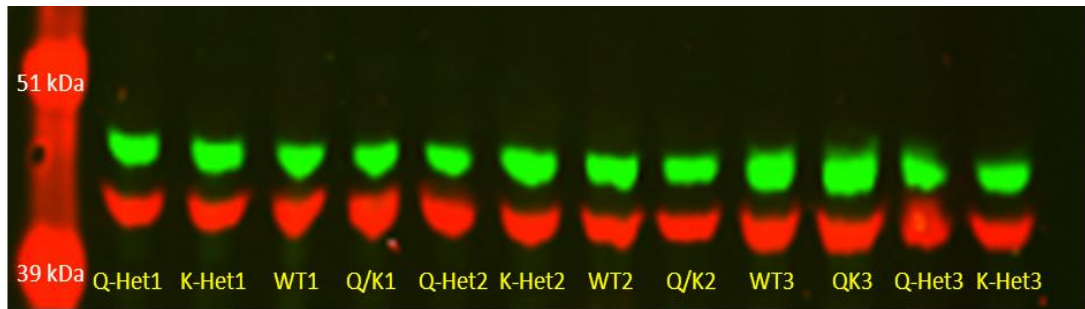
Figure 3.40: Compound *Tardbp*[Q101X/K160R] one year Western blot. Top panel shows Western blot using protein extracted from one year old snap frozen half brain. TDP43 (ProteinTech) and actin (Invitrogen) were labelled with green and red secondaries respectively (Li-Cor rabbit and mouse). Levels were quantified relative to actin and plotted in a bar chart. WT versus Q-Het p = 0.11, WT versus Q/K compound p = 0.29 (ANOVA Bonferroni post hoc). Error bars show standard deviation.

As well as the samples assessed at one year of age, males were aged to 18 months. Protein was extracted from half brain and assessed by Western blotting (Figure 3.41).There is a trend towards significantly reduced protein levels in compound heterozygotes verses wild-type. This Western blots were repeated technically as well as from re-extracted samples in order to determine whether this difference was significant, however significance was not consistently achieved and in some repeats the trend was lost.
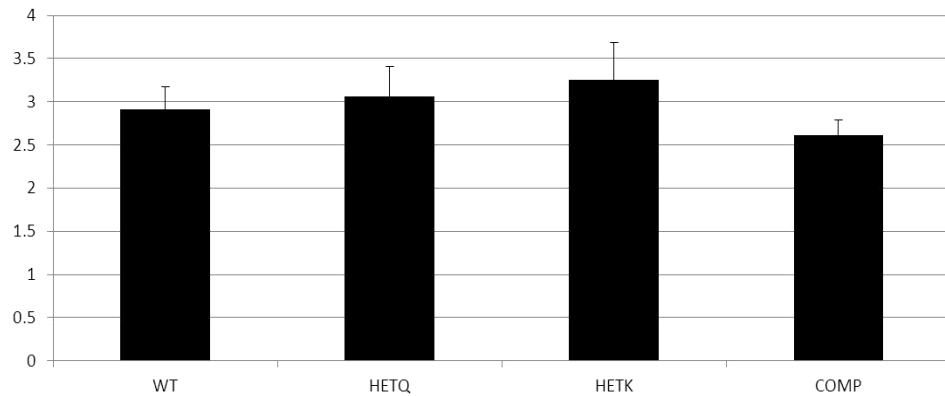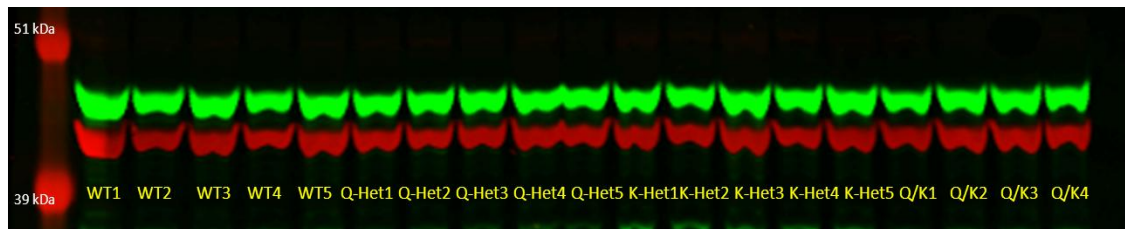
Figure 3.41: Compound *Tardbp*[Q101X/K160R] eighteen month Western blot. Top panel shows Western blot using protein extracted from 18 month old snap frozen half brain. TDP43 (ProteinTech) and actin (Invitrogen) were labelled with green and red secondaries respectively (Li-Cor Rabbit and Mouse). Levels were quantified relative to actin and plotted on a bar chart. All other comparisons p > 0.05 (1 way ANOVA Bonferroni post hoc). Error bars show standard deviation.

3.7.3. Endogenous splicing target

Alongside characterisation of protein levels, the levels of splicing were assessed in aged adult brain. TDP43 has extensively characterised roles in splicing. *Sortilin1* (*Sort1*) exon 18 is spliced by TDP43 (Polymenidou *et al.*, 2011). This is discussed in more detail in Chapter 5. RNA was extracted from harvested mouse brain and cDNA generated. *Sort1* exon 18 spliced and non-spliced transcripts were amplified and the ratio of band intensity was measured. Promotion of exon 18 skipping in Q101X brain and compound heterozygous brain was significantly reduced, compared to littermate controls (Figure 3.42 and Figure 3.43). No significant differences were seen in K160R homozygous brain (Figure 3.44).

Sortilin1 Exon 18 inclusion in compound one year old brain
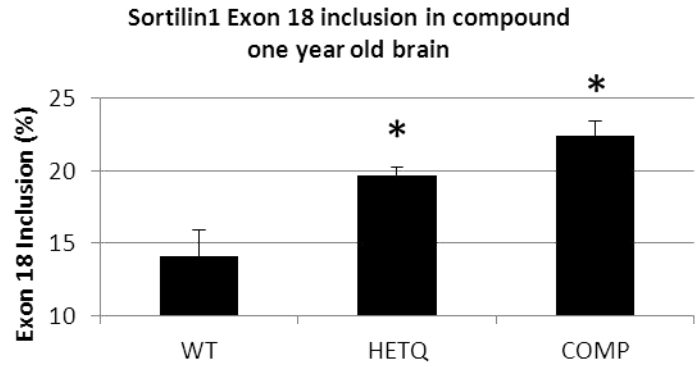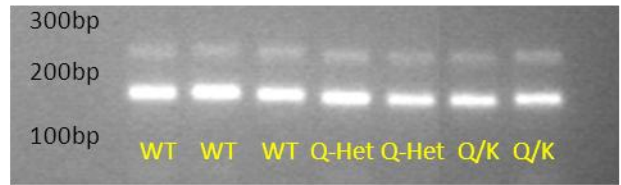
Figure 3.42: Compound *Tardbp*^{Q101X/K160R} ***Sort1* splicing from one year brain**. Top panel shows *Sort1* spliced (bottom band) and unspliced (top band) transcripts. Bar chart shows quantified percentage of top band relative to total band intensity. N = WT 3, Q-Het 2, Q/K Comp 2. WT versus Q-Het p = 0.038, WT versus Q/K Comp p = 0.009, Q-Het versus Q/K Comp p = 0.396, 1 way ANOVA Bonferroni post hoc. Error bars show standard deviation.

Sortilin1 Exon 18 inclusion in Q101X one and a half year old brain
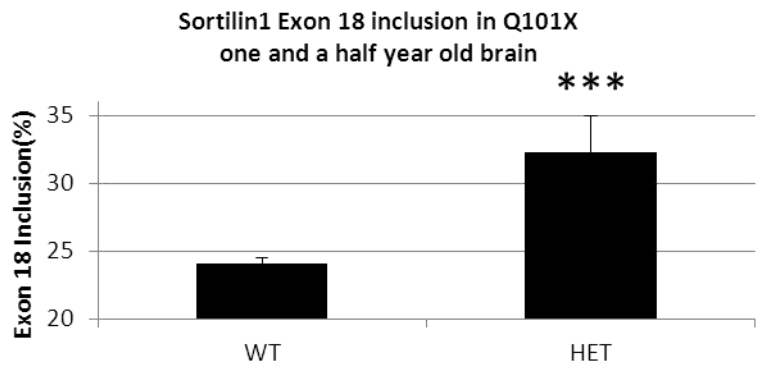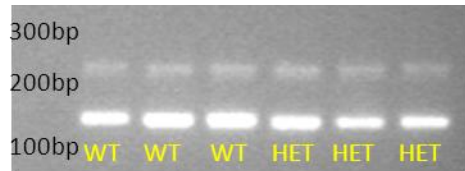
Figure 3.43: Q101X *Sort1* splicing from one and a half year brain. Top panel shows *Sort1* spliced (bottom band) and unspliced (top band) transcripts. Bar chart shows quantified percentage of top band relative to total band intensity. N = WT 3, HET 3. WT versus HET p = 0.006, students two tailed T test. Error bars show standard deviation.
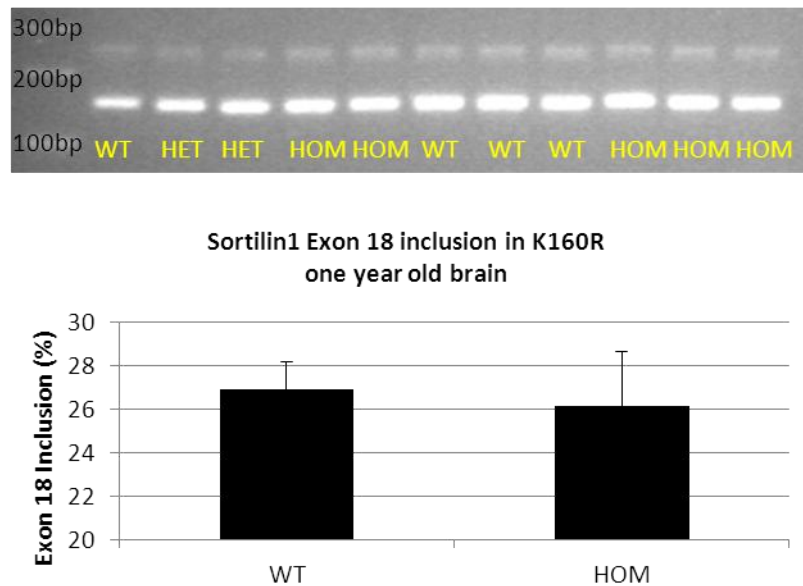
Figure 3.44: K160R *Sort1* splicing from one year brain. Top panel shows *Sort1* spliced (bottom band) and unspliced (top band) transcripts. Bar chart shows quantified percentage of top band relative to total band intensity. N = WT 4, HET 1, HOM 5. WT versus HOM p = 0.813, students two tailed T test. Error bars show standard deviation.

3.8. Q101X / SOD1^{G93A} double mutant

Q101X heterozygotes (*Tardbp*$^{Q101X/+}$) were crossed to SOD1^{G93A} transgenic low copy mice, to generate double mutants. At the time of generating this cross, the aim was to assess whether the Q101X TDP43 mutation could modify the disease of this characterised mouse model of ALS (Gurney *et al.*, 1994; Acevedo-Arozena *et al.*, 2011) and vice versa. Mutations in both TDP43 and SOD1 cause ALS, however the pathological signature between the two induced disease courses is different. In SOD1 induced ALS, misfolded SOD1 is found in aggregates without TDP43, whereas in TDP43 induced ALS and most forms with mutations in other genes, TDP43 is localised to inclusions without SOD1. Despite this independence, mutations in both genes result in motor neuron disease supporting potential interactions (Mackenzie *et al.*, 2007; Robertson *et al.*, 2007; Turner *et al.*, 2008).

The low copy transgenic SOD1^{G93A} mice are a well characterised model of ALS. They have been characterised previously and within the laboratory (Acevedo-Arozena *et al.*, 2011), with a clear understanding of disease onset and progression in the model. By crossing to Q101X, as shown

in Figure 3.2, the aim was to phenotype the mice to look for potential modifying effects. Carrying 8-10 human copies of SOD1^{G93A}, disease onset begins at approximately 22 weeks, with end stage by paralysis or more than 20% weight loss (as defined in the Home Office license conditions) between 31-38 weeks. This provided a clear model with a well characterised phenotype in which to search for modifying effects. The phenotypes induced by the transgene are only discussed here where potential modification occurs.

3.8.1. Survival and weights

SOD1^{G93A} induced paralysis typically occurs at 31-38 weeks (217-266 days). When comparing Q101X WT / SOD1^{G93A} mice to Q101X HET / SOD1^{G93A} mice, there were no significant differences in survival (Figure 3.45). Being heterozygous for Q101X in both sexes does not enhance or decrease SOD1^{G93A} induced survival.

Q101X / SOD1^{G93A} Survival
Females

Q101X / SOD1^{G93A} Survival
Males
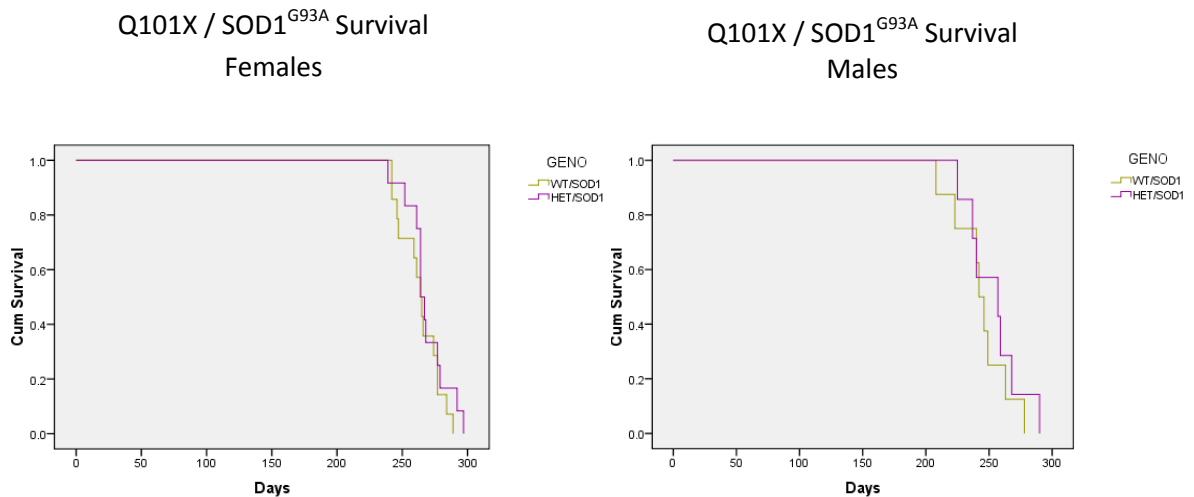
Figure 3.45: Double Q101X / SOD1^{G93A} survival. Survival plot showing the Q101X / SOD1^{G93A} phenotyping cohort survival. Animals included were those that died due to health (SOD1^{G93A} induced paralysis to humane end point) or severe weight loss (more than 20%). Mice that were culled due to reasons such as fight wounds from other mice were not included. N = 22 WT / SOD1^{G93A}, 19 HET / SOD1^{G93A}. p = 0.227, Log rank statistic, Kaplan Meier Analysis.

Mice were culled when they lost 20% of maximum body weight or became paralysed, in accordance with Home Office license conditions. SOD1^{G93A} mice showed a significant decrease in weight near end stage and this was overtly seen in male mice (Figure 3.46). Q101X HET /

SOD1^{G93A} weights were not significantly different to Q101X WT / SOD1^{G93A} littermate controls (p = 0.227 Log rank statistic).
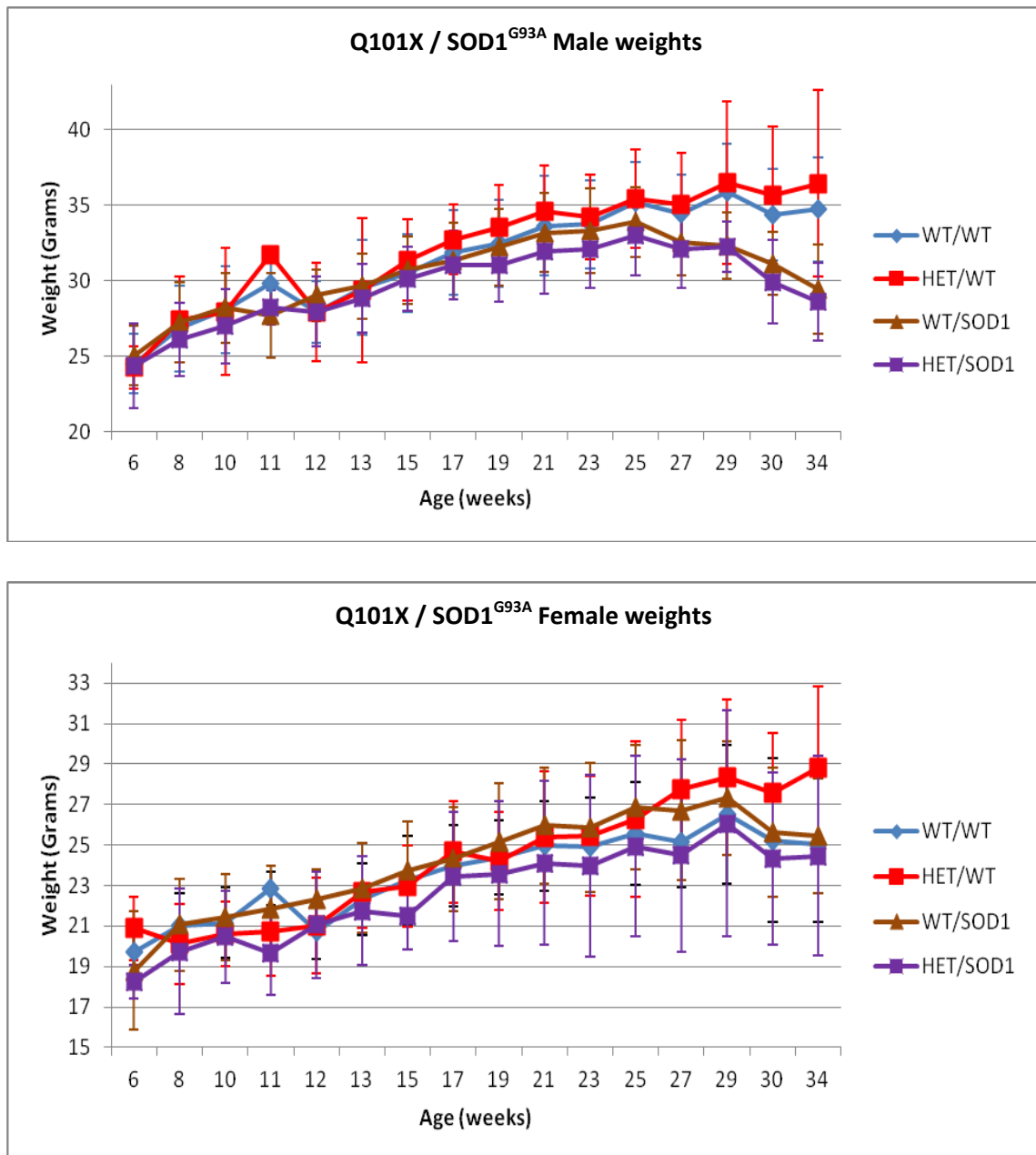
Figure 3.46: Q101X / SOD1^{G93A} weights. Male and female phenotyping cohorts aged until SOD1^{G93A} induced end stage, being weighed up to 34 weeks. WT / SOD1^{G93A} and Q101X HET / SOD1^{G93A} mice show a significant reduction in weight near end stage (versus WT / WT, p = 0.002 and 0.004 respectively, Univariate GLM Bonferroni post hoc). No significant differences in WT / SOD1^{G93A} versus Q101X HET / SOD1^{G93A} are observed. Error bars show standard deviation.

3.8.2. Q101X / SOD1^{G93A} SHIRPA

Body tone

When assessing body tone, Q101X HET / SOD1^{G93A} mice showed softer body tone versus WT / SOD1^{G93A} littermates (p = 0.042). This was expected due to characterisation of the Q101X heterozygotes in other lines which show a soft body tone phenotype. When comparing Q101X HET / WT mice to Q101X HET / SOD1^{G93A} mice, there was no significant difference in the proportion of mice showing soft body tone (p = 0.982, Figure 3.47). This shows that this TDP43 induced phenotyped is not modified by the SOD1^{G93A} transgene.
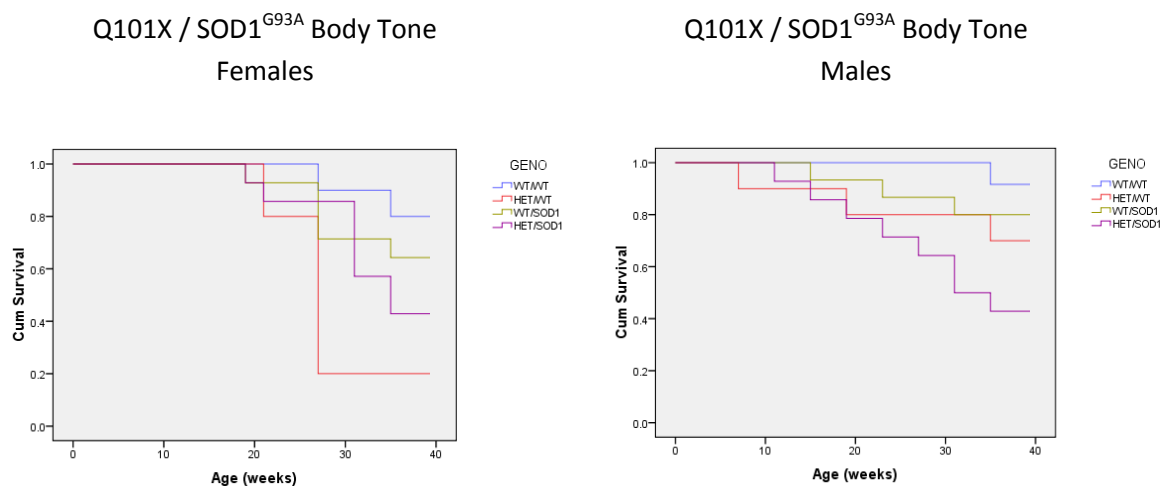
Figure 3.47: Q101X / SOD1^{G93A} Body tone. Onset plots showing softer body tone in the SHIRPA test, through time. Plots shown by sex. Y axis shows proportion of mice with lines decreasing from 1, where no mice show the phenotype. N = female WT / WT 10, Q101X HET / WT 5, WT / SOD1^{G93A} 14, Q101X HET / SOD1^{G93A} 14. N = male WT / WT 12, Q101X HET / WT 10, WT / SOD1^{G93A} 15, Q101X HET / SOD1^{G93A} 14. Mean age at which body tone was shown for both sexes combined was WT / WT no phenotype, Q101X HET / WT 32 (more than 50% of females), WT / SOD1^{G93A} no phenotype, Q101X HET / SOD1^{G93A} 26 (50% for both sexes). WT / SOD1^{G93A} versus Q101X HET / SOD1^{G93A} p = 0.042, Q101X HET / WT versus Q101X HET / SOD1^{G93A} p = 0.982, WT / WT versus HET / WT p = 0.006 Kaplan Meier Log Rank Statistic. Overall p = 0.008 with no significant differences between sexes within genotypes (p > 0.05).

Negative geotaxis

Mice were assessed on the negative geotaxis challenge. Near end stage, 50% of WT / SOD1^{G93A} male mice were significantly slipping on the negative geotaxis, with 90% of Q101X HET /

SOD1^{G93A} mice slipping (Figure 3.48). Most females did not slip on the negative geotaxis however more than 50% of Q101X HET / SOD1^{G93A} did slip.

Q101X / SOD1^{G93A} Negative geotaxis Females

Q101X / SOD1^{G93A} Negative geotaxis Males
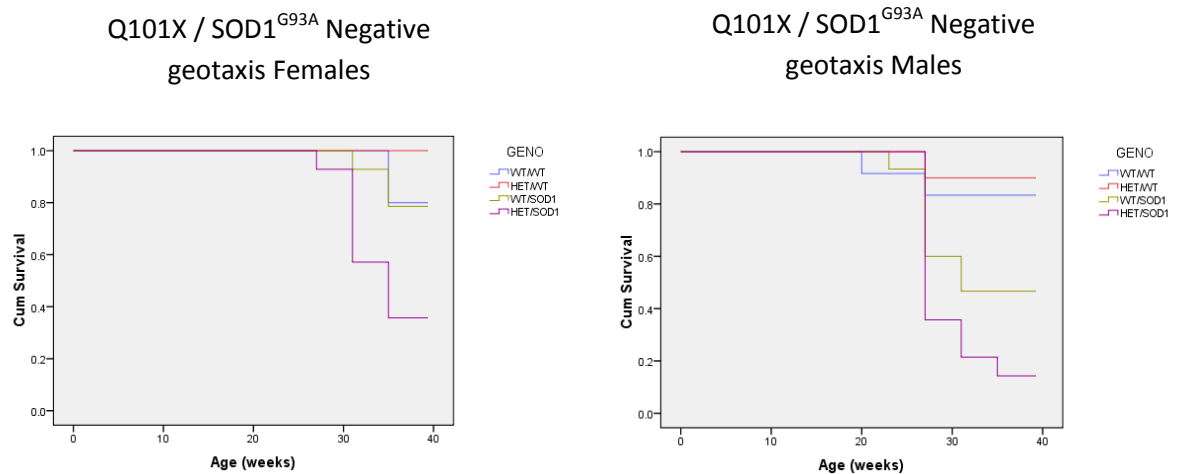
Figure 3.48: Q101X / SOD1^{G93A} Negative geotaxis. Onset plots showing slipping on negative geotaxis in the SHIRPA test through time. Plots shown by sex. Y axis shows proportion of mice with lines decreasing from 1, where no mice show the phenotype. N = female WT / WT 10, Q101X HET / WT 5, WT / SOD1^{G93A} 14, Q101X HET / SOD1^{G93A} 14. N = male WT / WT 12, Q101X HET / WT 10, WT / SOD1^{G93A} 15, Q101X HET / SOD1^{G93A} 14. Mean age at which negative geotaxis was shown for both sexes combined was WT / WT = no phenotype, Q101X HET / WT = no phenotype, WT / SOD1^{G93A} = 35 (50% of males), Q101X HET / SOD1^{G93A} = 32 (more than 50% of both sexes). WT / SOD1^{G93A} versus Q101X HET / SOD1^{G93A} p = 0.005, Kaplan Meier Log Rank Statistic. Overall p < 0.001 with a significant difference in male and female Q101X HET / SOD1^{G93A} mice presenting the phenotype (p = 0.025).

3.8.3. Startle response and open field

Startle response was assessed at 10, 18 and 22 weeks. Reduced startle response in SOD1^{G93A} mice has been shown previously (Acevedo-Arozena *et al.*, 2011). Smaller cohorts were also assessed at 28 and 34 weeks. At 10 weeks, no significant differences in startle or pre-pulse inhibition were observed (n = WT-WT 21, Q-Het-WT 17, WT-SOD1^{G93A} 25, Q-Het-SOD1^{G93A} 26). No significant differences were seen at 18 weeks (n = WT-WT 16, Q-Het-WT 13, WT-SOD1^{G93A} 25, Q-Het-SOD1^{G93A} 17) or at 22 weeks, with WT / SOD1^{G93A} versus Q101X HET / SOD1^{G93A} p = 0.073, Figure 3.49. Smaller cohorts were assessed at 28 and 34 weeks with no significant differences in startle response (28 weeks n = WT-WT 9, Q-Het-WT 11, WT-SOD1^{G93A} 9, Q-Het-SOD1^{G93A} 8, 34 weeks n = WT-WT 11, Q-Het-WT 7, WT-SOD1^{G93A} 4, Q-Het-SOD1^{G93A} 6). There were no significant differences in pre-pulse inhibition at any time points or differences due to sex.
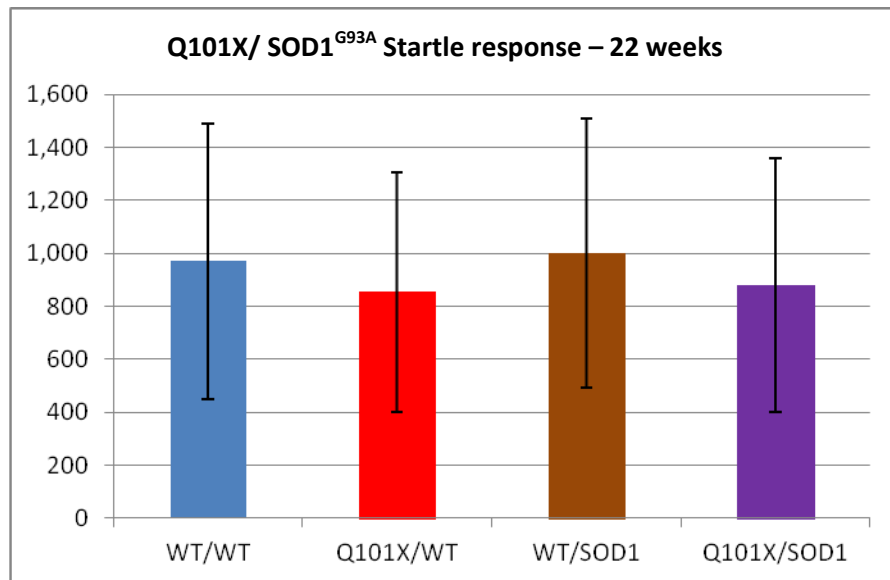
Figure 3.49: Q101X / SOD1^{G93A} Startle response at 22 weeks. Bar chart showing the relative startle response to a 110 dB tone, quantitatively measured. Error bars represent standard deviation. N = WT / WT 20, Q101X HET / WT 19, WT / SOD1^{G93A} 27, Q101X HET / SOD1^{G93A} 23. Average startle response was WT / WT = 971.67, Q101X HET / WT = 855.69, WT / SOD1^{G93A} = 1000.63, Q101X HET / SOD1^{G93A} = 878.49. WT / SOD1^{G93A} versus Q101X HET / SOD1^{G93A} p = 0.073, Multivariate GLM Bonferroni post hoc.

Open field was assessed at 14 and 30 weeks. At 14 weeks, SOD1^{G93A} mice were pre-symptomatic, reflected in the open field where there are no significant differences in activity compared to wild-type controls. At 14 weeks, there was a trend for reduced Q101X HET / SOD1^{G93A} movement duration, WT / SOD1^{G93A} versus Q101X HET / SOD1^{G93A} p = 0.088, Figure 3.50. There were no significant differences due to sex.
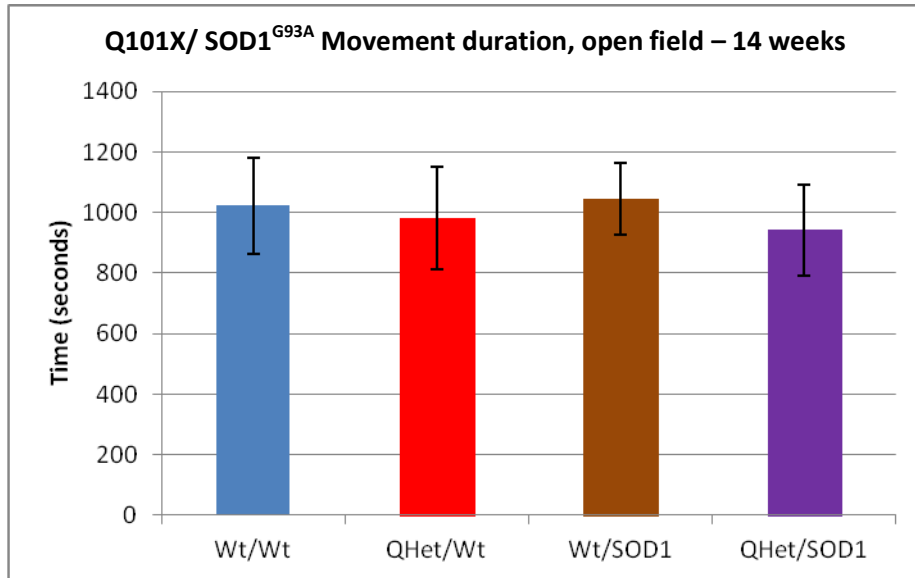
Figure 3.50: Q101X / SOD1^{G93A} Open field at 14 weeks. Bar chart showing movement duration (seconds) from a total of 1800 seconds in the arena, measured using Noldus Ethovision software. Error bars represent standard deviation. N = WT / WT 20, Q101X HET / WT 11, WT / SOD1^{G93A} 24, Q101X HET / SOD1^{G93A} 24. Movement duration average was WT / WT = 1022.60, Q101X HET / WT = 982.34, WT / SOD1^{G93A} = 1045.66, Q101X HET / SOD1^{G93A} = 941.80. WT / SOD1^{G93A} versus Q101X HET / SOD1^{G93A} p = 0.088, Multivariate GLM Bonferroni post hoc.

3.8.4. Rotarod and grip strength

Rotarod was assessed at selected time points, as shown in Figure 3.51. From 8 weeks through to 36 weeks, no significant differences in time on the rotating rod were observed as well as no differences by sex. No prior training regime and a large variation in performance have masked an expected decline in WT / SOD1^{G93A} performance.
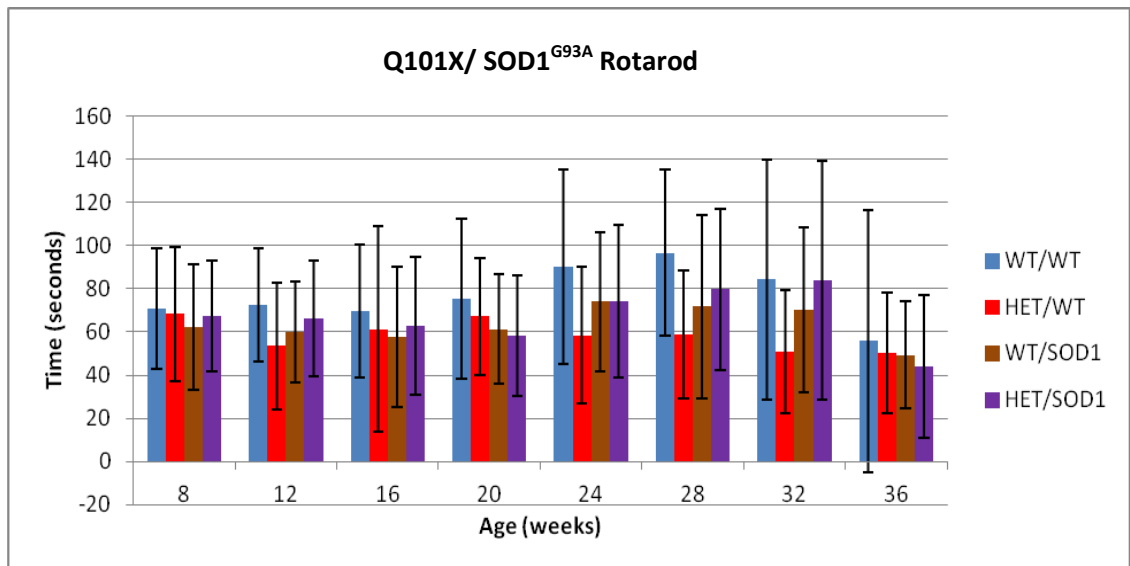
Figure 3.51: Q101X / SOD1^{G93A} longitudinal rotarod. Graph showing average time on the accelerating rotarod, with error bars representing standard deviation. Rotarod measurements were taken in triplicate over three days (nine values per mouse), with the average of total performance taken. There are no consistently significant differences in rotarod performance between genotypes observed up to 64 weeks (p > 0.05, Repeated measures ANOVA wherever possible and Standard GLM).

As well as rotarod, grip strength was assessed from 8 weeks though to 36 weeks. By 36 weeks, Q101X WT / SOD1^{G93A} mice show significantly reduced grip strength versus wild-type littermate controls (Figure 3.52). At this stage, WT / SOD1^{G93A} versus Q101X HET / SOD1^{G93A} grip strength was not significantly different (p = 0.529). Sex was not significantly different between genotypes (p > 0.05).
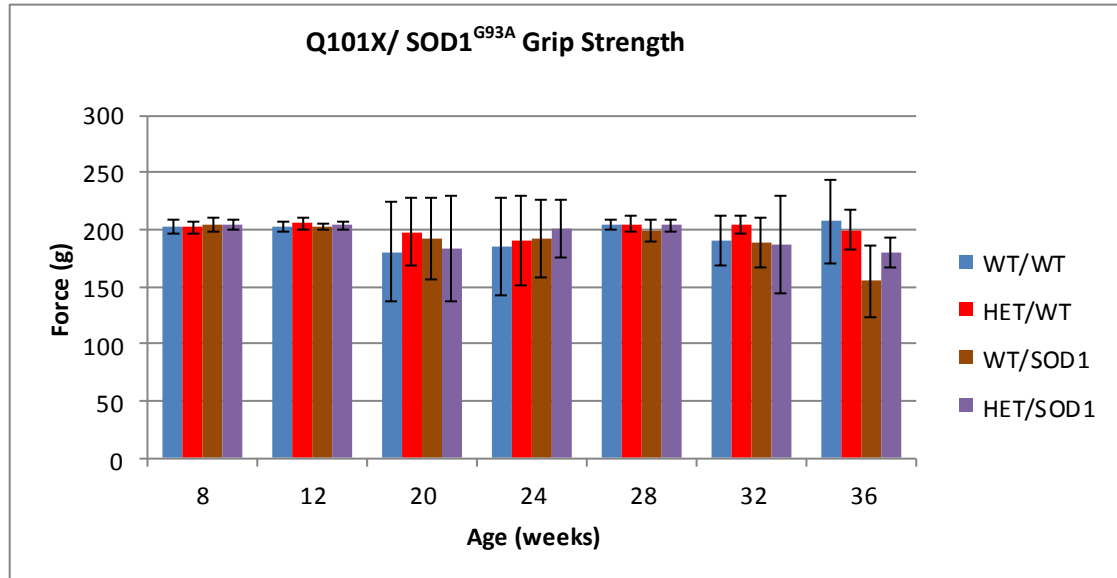
Figure 3.52: Q101X / SOD1^{G93A} longitudinal grip strength. Graph showing average grip strength, with error bars representing standard deviation. Measurements represent average force (g) generated in duplicate over four limbs. There are no significant differences in grip strength between genotypes observed up to 32 weeks with males and females. There is a reduction in force at 36 weeks as a result of the SOD1^{G93A} induced ALS phenotype in these mice (p = 0.008), but WT / SOD1^{G93A} versus Q101X HET / SOD1^{G93A} mice are not significantly different (p = 0.529, ANOVA 1 way Bonferroni post hoc).

3.9. Results discussion

3.9.1. Introduction

In this chapter the Q101X and K160R mutations identified from the MRC Harwell ENU archive have been characterised *in vivo*. An extensive longitudinal behavioural screen has been completed to determine whether these mutations are functional. This study identified that Q101X is homozygous lethal as was subsequently published in knock out studies (Kraemer *et al.*, 2010; Sephton *et al.*, 2010; Wu *et al.*, 2010). Q101X heterozygous mice are viable and show *in vivo* TDP43 protein auto-regulation to retain protein levels equivalent to those of wild-type mice. These mice also show significant alterations in the SHIRPA assessment.

Mice which are homozygous for K160R are viable. A phenotyping cohort of more than ten mice per sex per genotype was generated with a phenotyping regime matching that of the Q101X line. Significant changes in SHIRPA, consistent with the Q101X heterozygotes were seen. Finally, compound mutants for *Tardbp*$^{Q101X/K160R}$ were generated, to assess the impact of the

K160R allele having to auto-regulate itself. These compound mutants show the SHIRPA phenotypes that Q101X heterozygous and K160R homozygous mutants show generally with an earlier onset. *Tardbp*^Q101X/K160R mice also show EM pathology not seen in Q101X heterozygotes. Finally, these mice show preliminary anxiety and emotionality phenotypes not observed in any other genotype.

Q101X heterozygotes were crossed to low copy SOD1^G93A transgenic mice to assess for potential modifying effects. With a defined disease course as a result of the SOD1^G93A transgene, mice were phenotyped for phenotypic deviations from this baseline. Q101X HET / SOD1^G93A mice did show phenotypic deviations in the negative geotaxis test in the SHIRPA, by slipping more. A potential trend in reduced movement duration in open field at 14 weeks and trend towards reduced startle response at 22 weeks were not replicated at alternative time points. This shows that there is no overt impact on the SOD1^G93A phenotype from the TDP43 Q101X mutation, arguing no significant interaction between the genotypes in this context.

3.9.2. Q101X, K160R and Compound *Tardbp*^Q101X/K160R mutants

Q101X viability and auto-regulation

Q101X is homozygous lethal without any embryos being detected at E6.5 dpc (Table 3.1). Whilst studying these mice three knock out publications have shown that homozygous TDP43 knockout mice die between E3.5 – 6.5 / 8.5 dpc (Kraemer *et al.*, 2010; Sephton *et al.*, 2010; Wu *et al.*, 2010). Assessment in development from these papers supports lethality being the result of impaired inner cell mass proliferation. It is likely that the Q101X mutation is lethal through the same mechanism as homozygous knock outs although this has not been assessed directly. These results support Q101X being a null allele.

In heterozygous knock outs, all three studies show that TDP43 levels auto-regulate to wild-type levels *in vivo*. This is confirmed in Q101X heterozygotes which at young and aged stages show wild-type protein levels. In aged mice up to 18 months, no significant differences in Q101X heterozygote protein levels have been shown.

Out of the three published knockout mice generated two show no significant phenotypes in knock out heterozygous mice (Sephton *et al.*, 2010; Wu *et al.*, 2010). The third study (Kraemer *et al.*, 2010) which aged mice beyond the first two studies (over one year) shows motor

phenotypes in aged mice despite no reduction in TDP43 levels or TDP43 pathology. Only beyond one year do motor phenotypes emerge in this knock out model. These mice showed reduced grip strength and when upside down on a grid, held on for a significantly reduced time. These phenotypes emerge with age but were not progressive. They were also unable to detect any overt pathology in brain, spinal cord and selected muscle. The authors speculate that subtle non-structural abnormalities may be driving the phenotype, such as changes in metabolism.

The knock out data supports that Q101X is a null allele, mirroring the knock out generated mice. The inability to detect Q101X protein by Western blot and the down regulation of the transcript relative to the wild-type allele, indicate that the Q101X protein is unlikely to be translated. If translated, the Q101X protein is likely to be degraded rapidly. Applying a proteasome inhibitor would allow for translation assessment. As with published knock out studies, despite a potential trend for reduced protein levels in Q101X heterozygotes, no reduction in protein levels versus wild-type was detected by Western blotting. A subtle reduction in protein levels may support a mild loss of function driving the observed motor phenotypes in heterozygous knock outs and the non-motor phenotypes in Q101X heterozygotes.

Q101X and K160R lines: survival and weights

Female cohorts of Q101X, K160R and compound mutants were aged to end stage. In the Q101X and K160R cohorts no significant differences were seen between wild-type and mutant survival. In the compound heterozygote cohort, both Q101X heterozygotes and compound (*Tardbp*$^{Q101X/K160R}$) heterozygotes died significantly earlier than littermate controls (Figure 3.6). wild-type mean survival was 749 days, where Q101X heterozygotes and compound heterozygotes showed a mean survival of 693 and 689 days respectively. Where possible, samples have been collected from all end stage mice for post mortem analysis. The cause of death continues to be determined and is being investigated. So far a mixture of phenotypes have been observed including lymphomas, however no genotype specific phenotypes have been identified. This shows that compound heterozygotes may be more susceptible to common causes of death in mice at this age versus wild-type mice. As aged mice die for a number of reasons, if there is no genotype specific cause then this mutation may result in an age dependent susceptibility to natural causes of death. The number of Q101X heterozygotes in the survival study was six, which is small. In the Q101X heterozygote specific colony there

was a significantly larger number of mice in the survival study, fifteen. In this study, Q101X heterozygous mice did not die earlier than littermate controls. This data therefore supports only compound heterozygous mice showing shortened survival, but the six Q101X heterozygous littermate controls are a more appropriate control than the Q101X heterozygote colony with their respective littermate controls due to the genetic similarity of the mice. Genetic background may contribute to why an earlier end point is seen for Q101X heterozygotes in one line over another, supporting a potential lethality-susceptibility phenotype for Q101X heterozygotes on the compound heterozygote genetic background.

Weights were measured throughout the lifespan of phenotyped mice from 5 to 7 weeks of age onwards. Differences in weight are an important phenotype potentially reflecting metabolic or structural changes. TDP43 alterations have also been shown to result in weight phenotypes and body fat metabolism alterations (Chiang *et al.*, 2010). No significant differences in weight were seen in Q101X and K160R lines. In the compound heterozygote colony, female compound heterozygote mice were significantly smaller than littermate controls from 28 weeks onwards (Figure 3.9). Weight loss was also seen in conditional TDP43 knockout mice which altered levels of *Tbc1d1*, a gene controlling fat metabolism and leanness (Chiang *et al.*, 2010). A potential loss of function in compound mice may affect *Tbc1d1* in a similar way to the conditional knockout out, ultimately altering fat metabolism resulting specifically in reduced fat mass. Levels of *Tbc1d1* could be measured to assess this as well as generating further mice for fat analysis.

SHIRPA: Q101X and K160R

Gait

In Q101X and compound heterozygote lines, significant differences in gait were seen. Gait was visually assessed in the SHIRPA arena. Abnormal gait was associated with low pelvic elevation, pronounced limb movement and loss of fluidity. In the Q101X cohort, less than 30% of heterozygotes showed abnormal gait in both sexes. In the compound heterozygotes line, more than 50% of Q101X heterozygotes and compound heterozygotes showed an abnormal gait, indicating that on this background the gait phenotype was more penetrant for Q101X heterozygotes. Overall, gait abnormalities are often associated with motor alterations. Gait could more quantitatively be assessed using Treadscan gait analysis systems / software. The sensitivity of the software to this subtle gait change may be limiting. In assessing these mice, gait was variable due to the genetic background, compared to assessing gait in congenic mice. Mutants have been scored for a non-fluid gait and this is statistically significant, however

further alterations in other phenotypes may have been expected and fully quantitative assessment is required. Strong gait abnormalities seen in other ALS models such as SOD1[G93A] are the result of motor unit loss and severe degeneration. The gait phenotype here was a more subtle phenotype where mice had lost the fluidity of their movement, potentially indicating a finer loss in motor coordination which may have both neuronal and muscular causes.

Limb grasp

Limb grasping was seen in Q101X, K160R and compound heterozygote lines. In the Q101X heterozygote line (Figure 3.12), limb grasping was mainly seen in females with more than 50% limb grasping at 80 weeks. In the K160R line, more than 50% homozygote mice limb grasped at 45 weeks, which was matched in the compound line by compound heterozygous mice. With large proportions of mutant mice all limb grasping, this supports that both the Q101X and K160R mutations cause limb grasping. As a phenotype, many mutant mice have shown limb grasping however the underlying mechanism is poorly characterised. With the general motor capabilities of these mice being relatively normal, this implies a limb grasping response being driven by a nervous system alteration rather than a muscular defect. These alterations are difficult to identify, however this could be anticipated considering TDP43's role in neurodegeneration and neuronal function across organisms. A poor understanding of the causative mechanism for limb grasping limits the ability to understand the causative molecular change.

Body tone and severe body tone

Body tone was commonly softer in all three TDP43 lines. This was measured by feeling the rear body of the mouse and assessing muscular tone and elicited tonal response to touch. In the Q101X cohort, more than 50% Q101X heterozygotes showed at softer body tone by 30 weeks, with a severely softer body tone by 90 weeks, showing a progressive phenotype. In the K160R cohort, 50% homozygotes showed a softer body tone by 35 weeks, with a severely softer body tone by 65 weeks. In the compound heterozygotes, more than 50% compound *Tardbp*[Q101X/K160R] mice had a softer body tone by 20 weeks, with a severely softer tone by 40 weeks. There was also a trend in compound heterozygotes versus Q101X heterozygote littermates for this occurring earlier with higher prevalence in the compound mutants ($p = 0.105$). The high penetrance of this phenotype across cohorts provides strong support that it is induced by both Q101X and K160R mutations. This phenotype was also seen in the Q101X HET / SOD1[G93A]

cohort of mice. By being present in lines carrying different ENU induced point mutations it supports that the body tone phenotype is caused by the Q101X and K160R TDP43 mutations and not by alternative ENU mutations. Body tone itself, is a phenotype which is very poorly represented in the literature (Ingman *et al.*, 2004; Messaoudi *et al.*, 2005; Duysen *et al.*, 2007). Mice require extensive handling to be settled to assess true body tone, which may contribute to it not being frequently assessed and reported. With no data indicating the pathological or mechanistic changes which drive this reduction in tone, muscle was dissected for neuromuscular junction assessment by Dr Gonzalo Blanco and Dr Abraham Acevedo. External oblique muscle, internal oblique muscle and transversus abdominis muscles overlay where the body tone is felt and the response elicited. Neuromuscular junction staining of compound heterozygous mice with soft body tone versus wild-type littermates with normal body tone, showed no overt abnormalities. Further characterisation of the muscles is required however this result supports this being a non-muscular based phenotype. There may be a potential sensory defect in eliciting the tone response or a higher central nervous system processing defect. Cohorts of mice are currently being generated for sensory assessment and brain imaging to further delineate this poorly defined phenotype. Results support no sensory deficits.

Negative geotaxis

The final SHIRPA endophenotype commonly affected was slipping on the negative geotaxis challenge. In the Q101X cohort, more than 50% Q101X heterozygotes slipped at 50 weeks. More than 50% K160R homozygotes showed slipping at 25 weeks and this was matched by compound heterozygote mutants. Slipping was observed in control mice as this is a significantly difficult challenge for wild-type mice. With mutants slipping on the negative geotaxis challenge at an earlier age this supports a subtle age associated reduction in controlled movement down the grid, but does not support a motor deficit on its own.

Startle and open field

Startle response and pre-pulse inhibition were assessed in the Q101X, K160R and compound heterozygote lines at multiple time points. In the Q101X and K160R lines, no significant differences in startle response or pre-pulse inhibition were seen at 10 and 22 weeks. In the compound line, there was a trend towards reduced startle response for compound

heterozygotes versus wild-type controls (p = 0.06) at 22 weeks (Figure 3.27). Overall, the startle response test provides a fully quantitative assessment of reflexive nervous function. There is significant variation in the response in these lines, probably due to the mixed genetic background of the mice tested. Mice were not retested at older time points as with a large C57BL/6J background, loss of hearing due to the age-related hearing (AHL) locus would potentially interfere with the results (Gates *et al.*, 1999; Keithley *et al.*, 2004). The AHL locus contributes towards age related hearing loss and in C57BL/6J mice this locus results in cochlear degeneration and hearing loss around mid-life.

Open field assessment showed no significant differences in Q101X and K160R cohorts. The initial assessment at 14 weeks was used to assess locomotor activity, neophobia, agoraphobia, exploratory drive and aspects of anxiety and fear. At the repeated time point, as the mice were no longer naive to the test, assessment focused purely on locomotor activity. In the *Tardbp*$^{Q101X/K160R}$ line, K160R heterozygous littermates showed increased maximum distance travelled per ambulation, compared to littermate controls (Figure 3.28). The number of K160R heterozygotes is low, so this should be viewed as a preliminary result. K160R heterozygotes from the K160R line did not show this phenotype, supporting that this is unlikely to be a significant difference.

Rotarod and grip strength

In all three lines, rotarod and grip strength were assessed. No significant differences were observed. For the rotarod, the mice were not trained in advance of the test and as a result many mice consistently performed badly on the test. This resulted in a low average running time on the rod with large variation between those that successfully ran versus mice that could not or would not. The result is that subtle to medium differences may be masked by the variation resulting in a loss of sensitivity to differences. Training mice in advance of the test can significantly increase mean time on the rod and reduce variation. In training, mice are continuously replaced to achieve a high baseline time on the rod in advance of being tested, which they more effectively maintain in future runs. This has since been applied to other lines in the laboratory.

There were no significant differences for grip strength within the three lines assessed. There was low variation in grip strength readings supporting a sensitive detection for potential loss of

grip strength. This supports that these mutant mice do not showing significant motor deficits in their grip strength.

Pathology

Samples from one year old males were assessed for pathology at the light microscope level. Results from Dr Sebastian Brandner show that there was no overt pathology in the brains of mutant mice. Samples from end stage two year mice have been collected and will be assessed. At the EM level in the spinal cord, Dr Julian Thorpe showed small aggregates of TDP43 in the cytoplasm of neurons in compound heterozygote mice. Further samples at end stage have been collected to see if this phenotype progresses. Interestingly, at the Society for Neuroscience conference in 2011, unpublished data presented by Dr Gitcho (Washington Univ. Sch. of Med) from an Alzheimer's transgenic mouse (APP-PS1), showed similar structures in spinal cord cytoplasm, labelled with anti-TDP43-phospho (Cosmo) at eight months. This result may indicate that these structures are associated with a general neural process which under certain conditions, potentially stress induced in the Alzheimer's model, promotes TDP43 mini aggregate formation in the cytoplasm. Further investigation is required using antibodies against phosphorylated and non-phosphorylated TDP43. Overall the data from the compound heterozygous mice support a subtle intracellular change at the EM level which is not reflected as overt pathology at the light microscopy level.

Protein levels

Q101X heterozygote protein levels match those of wild-type levels in young and aged mice (Figure 3.37). This is consistent with the *in vivo* auto-regulation seen in knockout mice. In the compound heterozygote line, there may be a trend to reduced $Tardbp^{Q101X/K160R}$ protein levels. This is seen in three month brain, in one year brain and in eighteen month old brain (Figure 3.39, Figure 3.40 and Figure 3.41). Littermate Q101X heterozygotes and K160R heterozygotes do not show any differences either. K160R homozygote protein levels have not been assessed due to time constraints.

Q101X and K160R summary

The Q101X and K160R mutations have been characterised independently and together as compound mutants. They show common phenotypes in the SHIRPA surrounding body tone softness and limb grasp.

The compound heterozygotes (*Tardbp*$^{Q101X/K160R}$) show the strongest phenotypes. The body tone phenotype has an earlier mean onset than in Q101X heterozygotes or K160R homozygotes, with an earlier onset trend versus a small cohort of Q101X heterozygote littermate controls. Compound heterozygote mice also show significantly reduced survival and females are significantly smaller than littermate controls from 28 weeks. At 22 weeks, there is a trend towards reduced startle response. These behavioural changes are not seen in Q101X heterozygotes and K160R homozygotes (not accounting for genetic differences between lines) and support more pronounced phenotypes in the compound heterozygotes. This is matched by a trend towards reduced protein levels versus wild-type controls and EM pathology seen at 8 months. The enhanced changes in compound heterozygotes are the result of summing the effects of the Q101X and K160R alleles. Q101X heterozygotes show *in vivo* auto-regulation of TDP43 but still show phenotypes. K160R homozygotes also show similar behavioural phenotypes however the compound mutants show these phenotypes more overtly. As a preliminary result, this is seen in *Sort1* splicing and also in cognitive behavioural tests. The enhanced and novel phenotypes may be the result of Q101X auto-regulation accentuating a mild functional deficit in the K160R mutation, which with two functional K160R alleles is less pronounced.

The commonality of phenotypes between Q101X and K160R mutants supports similar effects. Although at the level detectable by Western blots there is no significant difference, if protein levels are subtly reduced in Q101X heterozygotes, this would support a loss of function driving observed phenotypes. K160R homozygotes also show phenotypes, with heterozygotes usually showing no phenotype. This would further support a potential partial loss of function, as heterozygotes still have one wild-type allele and the K160R allele me be mildly hypomorphic. *Sort1* splicing in aged homozygous K160R brain was not significantly different to the wild-type allele, so it is not hypomorphic for this splicing function. However in the compound mutant, *Tardbp*$^{Q101X/K160R}$, there was reduced *Sort1* splicing function. This result needs further repeating with other target genes.

Although the mechanisms behind softer body tone and limb grasp phenotypes are poorly defined, assessment of muscle and motor performance in the phenotyping tests show normal

motor capability in all lines. This supports a neurological cause driving these reflexive phenotypes as there is no data for muscular force generation deficits (although direct assessment of the relevant muscles has not been completed). Overt pathology has not been identified at the light microscopy level in these mutants in the brain. In the compound mutants, EM pathology has been observed in eight month old spinal cord. Overall, both the Q101X and K160R mutations are functional, with data here supporting mild loss of function. Q101X heterozygotes show body tone and limb grasping phenotypes which are not classical motor phenotypes. Out of the three knock out TDP43 mice generated, one shows motor phenotypes as a grip strength deficit. This may be because these mice were assessed by pooling results across multiple ages (Kraemer *et al.*, 2010). Phenotypes indicative of neurological defects are present in limb grasping and body tone in compound $Tardbp^{Q101X/K160R}$ mice, supporting these mutations having clear impacts on mouse reflexes at a behavioural level.

3.9.3. TDP43 Q101X / SOD1^{G93A}

Q101X heterozygotes were crossed to low copy SOD1^{G93A} transgenic mice to generate double mutants. The aim was to assess whether there was any interactive effect. With a defined disease course induced by SOD1^{G93A}, the phenotyping regime focused on searching for phenodeviants from the SOD1^{G93A} induced baseline phenotype.

Q101X HET / SOD1^{G93A} mice did not show altered survival or weight loss versus WT / SOD1^{G93A} mice (Figure 3.45 and Figure 3.46). Q101X HET / SOD1^{G93A} mice slipped more on the negative geotaxis test, with more than 50% slipping by 30 weeks where as 50% of WT / SOD1^{G93A} mice did not slip. There were also trends for reduced startle response at 22 weeks and reduced movement duration in the open field at 30 weeks (Figure 3.49 and Figure 3.50). These phenotypes could potentially support a mild reduction in motor capabilities of Q101X HET / SOD1^{G93A} versus WT / SOD1^{G93A} mice. Rotarod and quantitative grip strength were not significantly different. Overall, subtle alterations in Q101X HET / SOD1^{G93A} may be present; however there is no significant alteration in the SOD1^{G93A} or Q101X induced phenotypes. This supports no accentuation of phenotypes between the Q101X and SOD1^{G93A} mutations. This does not rule out potential interactions between SOD1 and TDP43 overall, however in this genetic cross no overt interaction was observed.

CHAPTER 4

Results:

Functional assessment of an allelic series of TDP43 mutations *in vitro*

4.   Results: Functional assessment of an allelic series of TDP43 mutations *in vitro*

4.1.   Introduction

The aim of the work in this chapter is to assess the functional effects of an allelic series of mutations identified in mouse TDP43 (as discussed in Chapter 1), using an established *in vitro* system. This work was carried out in the laboratory of Dr Emanuele Buratti / Professor Francisco Baralle as part of an EMBO sponsored short term fellowship. The cystic fibrosis transmembrane regulator (CFTR) add-back assay was used in order to provide a functional assessment of each mutation on TDP43 splicing activity. In humans, CFTR exon 9 skipping is regulated by TDP43 through its binding to UG repeats at the 3' splice site of exon 9. This mechanism of CFTR exon 9 skipping and the TDP43 binding site were previously characterised by Dr Buratti / Professor Baralle (Niksic *et al.*, 1999; Buratti & Baralle, 2001; Buratti *et al.*, 2001; Pagani *et al.*, 2003a; Pagani *et al.*, 2003b; Buratti *et al.*, 2004; Ayala *et al.*, 2006; Buratti *et al.*, 2007). Following binding to the target sequence, TDP43 interacts with other heterogeneous nuclear ribonucleoproteins (hnRNPs) to promote exclusion of exon 9 from the RNA transcript.

Professor Baralle's laboratory have created multiple constructs with a mini-gene containing CFTR exon 9 where the ratio of exon skipping, regulated through TDP43 binding, is controlled by the binding sequence motifs (Pagani *et al.*, 2003a). In the mini-gene, exon 9 skipping activity is dominantly driven by the action of TDP43. Characterised mutations in the target binding sequence of the mini-gene alter TDP43's binding and subsequent action in promoting exon 9 skipping. For this assay the mini-gene construct $C_{155}T$ $TG_{11}T_5$ (D'Ambrogio *et al.*, 2009) was used, where endogenous HeLa TDP43 promotes approximately 50% exon skipping. A summary schematic of the mini-gene is shown below (Figure 4.1).
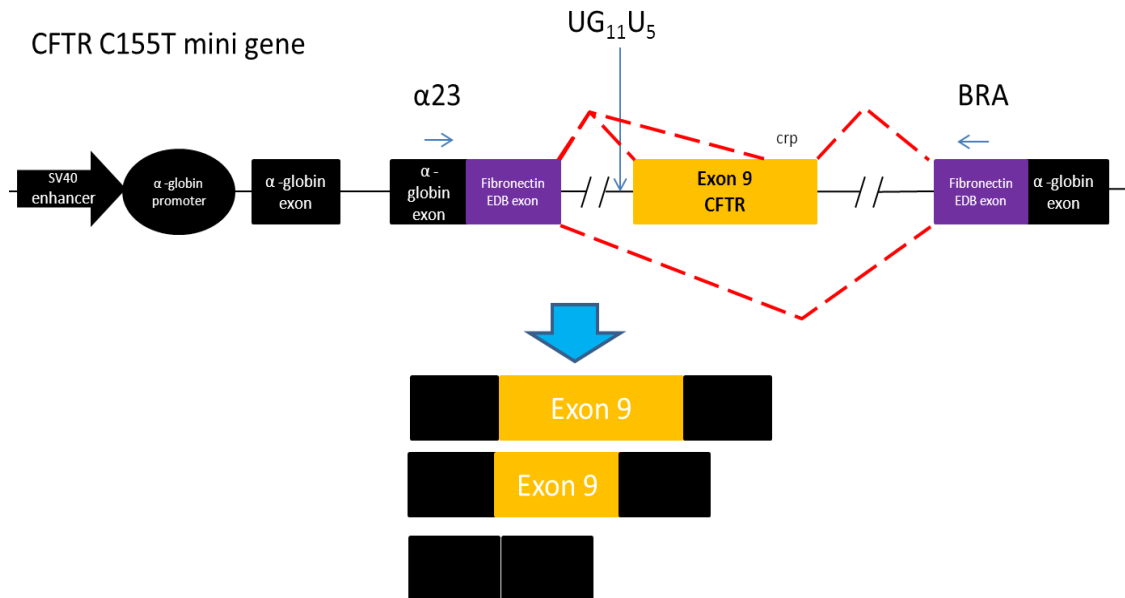
Figure 4.1: Mini-gene construct with splicing outcomes. The schematic shows the CFTR mini-gene construct used in the add-back assay. The mini-gene contains an α-globin promoter, α-globin exons (black boxes), Fibronectin extra domain B (EDB) exons (purple boxes) and CFTR exon 9 (orange box). The marked UG sequence is the regulatory region that TDP43 binds, subsequently promoting exon 9 skipping (skipping outcomes indicated below blue arrow and by dotted red lines). Altering the $UG_{11}U_5$ sequence with the C155T mutation alters the activity of TDP43 in driving exon skipping. There is an intermediary outcome for partial exon 9 skipping which also occurs through a cryptic splice site. 24 hours post transfection; RNA was extracted from harvested cells and converted to cDNA. The degree of exon skipping was determined by PCR using primers α23 and BRA, in the indicated exon regions with horizontal blue arrows. PCR product was then run on an agarose gel with ethidium bromide staining for visualisation. Band intensity was measured using ImageJ software.

Each of the missense TDP43 mutations were assessed for their ability to complete mini-gene exon 9 skipping in an equivalent fashion to the wild-type protein, assessing whether there was a loss or gain of function. The aim was to compare the effects of each of the mutations on splicing output of the reporter mini-gene versus wild-type TDP43. This would provide an assessment for each of the mutations on TDP43's functional role in splicing. Each of the mutations and their conservation is given in the introduction, Figure 1.1.

4.2.   Mouse TDP43 can complete CFTR mini-gene splicing

CFTR exon 9 is not spliced by TDP43 in the mouse, instead, exon 9 splicing is regulated through an alternative mechanism (Buratti *et al.*, 2001). This is due to the absence of a polymorphic regulatory sequence thought to have developed specifically in humans during evolution, which is not present in mouse CFTR (Rozmahel *et al.*, 1997; Kazazian & Moran, 1998). Furthermore, it had never been shown that mouse TDP43 could promote exon 9 skipping in the mini-gene, despite proof that the relatively poorly conserved Drosophila homolog, TBPH, could (D'Ambrogio *et al.*, 2009). In order to confirm this ability, the add-back assay was first completed, comparing human TDP43 and mouse TDP43 rescue.

For the add-back assay, HeLa cells were seeded and grown in 6 well plates, before being treated with 40 mM siRNA targeted against endogenous TDP43, for two successive days. Following this, a flag tagged human siRNA resistant construct (pFLAG TDP), or V5 / HIS mouse (pcDNA 3.1 TDP43) construct, was co-transfected into the siRNA treated cells with the CFTR mini-gene. The mouse TDP43 construct sequence is two bases different to the endogenous HeLa cell TDP43 siRNA targeted sequence (Figure 4.2), therefore this experiment initially assessed whether the siRNA degraded the mouse construct transcript. Only if the mouse construct expression was not inhibited by the siRNA, could the allelic series of expressed proteins be functionally assessed.

Exon 4 | Exon 5

t aat tct aag caa agc caa gat gag cct   Human sequence

  N   S   K   Q   S   Q   D   E   P   Encoded amino acids

t aat tct aag ca**g tcc** ca**g** gat gag cct   Human siRNA resistant sequence

  N   S   K   Q   S   Q   D   E   P   Encoded amino acids

c aa**c** tct aag caa agc c**c**a ga**c** gag cct   Mouse sequence in siRNA region

  N   S   K   Q   S   **P**   D   E   P   Encoded amino acids

(dTdT) c guu ucg guu cua cuc gga   siRNA
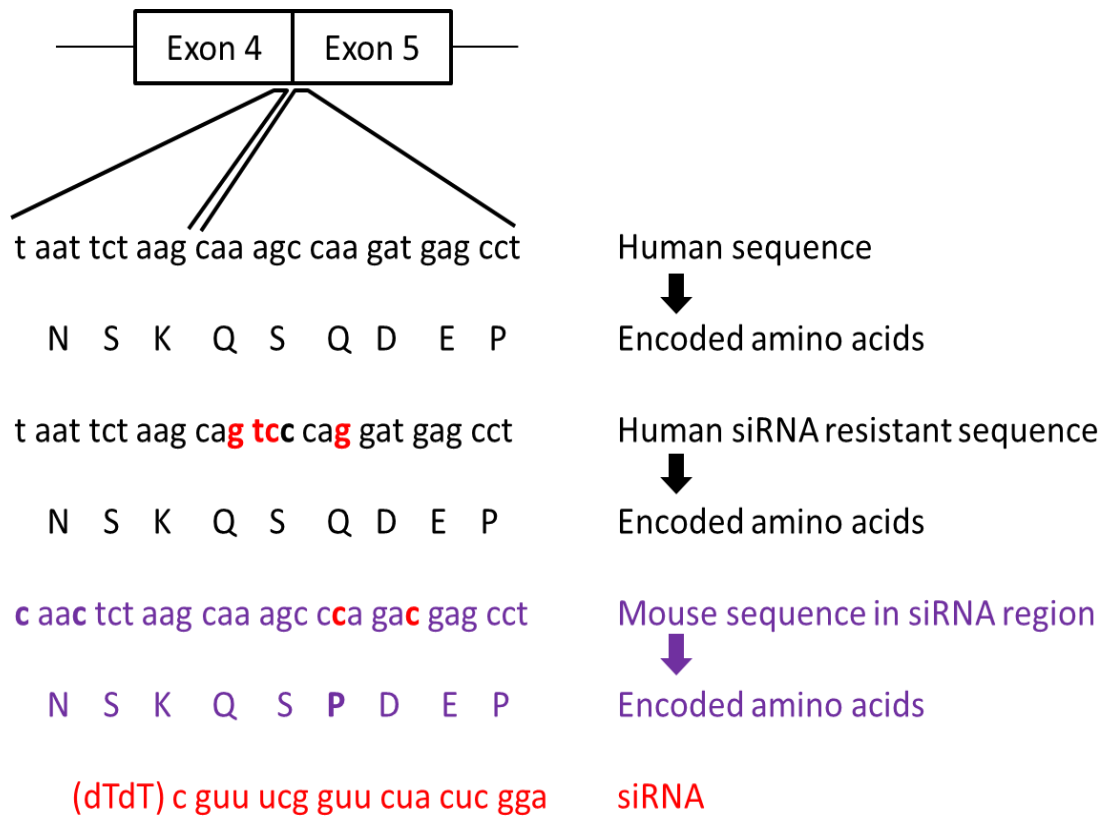
Figure 4.2: siRNA sequence. The schematic shows the TDP43 cDNA sequence in human and mouse as well as encoded protein spanning exons 4 and 5. siRNA (red) was targeted against this sequence with 4 differences engineered in the human resistant construct (from Buratti / Baralle lab). The mouse constructs contained two base differences to the siRNA targeted sequence.

Following 24 hours post co-transfection cells were pelleted for RNA and protein extraction. RNA was converted to cDNA and amplified using α23 and BRA primers (primers targeted to the mini-gene exons), before band assessment. Protein was extracted from cell pellets and analysed by Western blot to confirm successful down regulation of endogenous protein and transfected plasmid expression. The add-back assay is summarised in Figure 4.3.
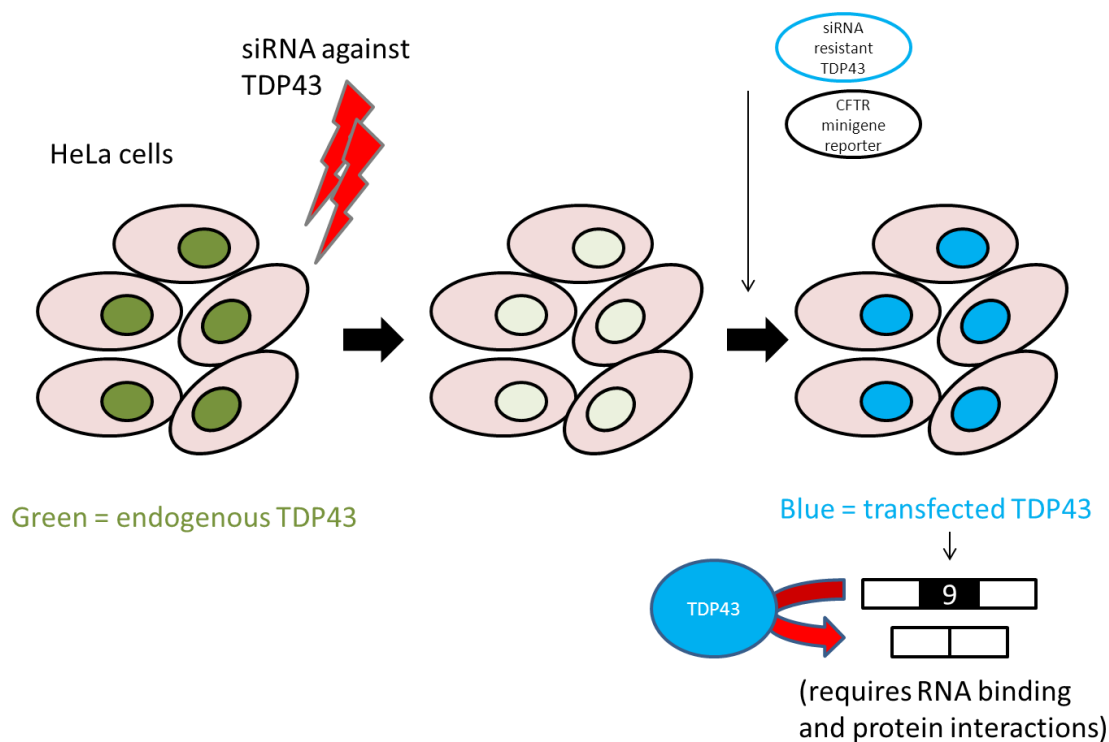
Figure 4.3: **Schematic showing the add-back assay**. HeLa cells expressing predominantly nuclear TDP43 are treated with successive rounds of siRNA to reduce endogenous TDP43 expression to almost non-existent levels, routinely greater than 90% (Ayala *et al.*, 2008a) . siRNA resistant mouse TDP43 constructs alongside the CFTR reporter mini-gene are then transfected into the HeLa cells, which now express exogenous TDP43 to promote exon skipping in the reporter mini-gene.

There is strong expression of the mouse V5 / HIS tagged TDP43 proteins as labelled by their V5 tags (anti-V5, 377500, Invitrogen), Figure 4.4 panel C. Results show (Figure 4.4) that the mouse TDP43 exogenous transcript is not degraded by the endogenous TDP43 targeted siRNA.

Wild-type mouse TDP43 is able to rescue exon 9 skipping in the HeLa cell add-back assay. Without siRNA treatment, HeLa cells promote 43.9% CFTR mini-gene exon 9 inclusion. Treating the cells with siRNA significantly reduces endogenous TDP43 (as confirmed by almost complete protein band absence in Figure 4.4 panel C), resulting in exon 9 inclusion increasing to 93.8%. Following siRNA treatment, where siRNA resistant human TDP43 is added back, exon 9 skipping function is rescued, restoring exon 9 inclusion to 41.9%. Wild-type mouse TDP43 protein also rescues skipping to 52.1% inclusion (not significantly different to human TDP43, p = 0.603 1 Way ANOVA). This experiment was replicated at least three independent times for

each construct (Figure 4.4). Mouse TDP43 was unable to rescue exon 9 skipping following siRNA treatment, when amino acid residues F147 / F149 were mutated as a loss of function control. This was expected through the characterisation that these phenylalanines in the first RNA recognition motif (RRM1) are critical for human TDP43 RNA-binding (Buratti & Baralle, 2001; Ayala *et al.*, 2005), which has now been confirmed for mouse TDP43.
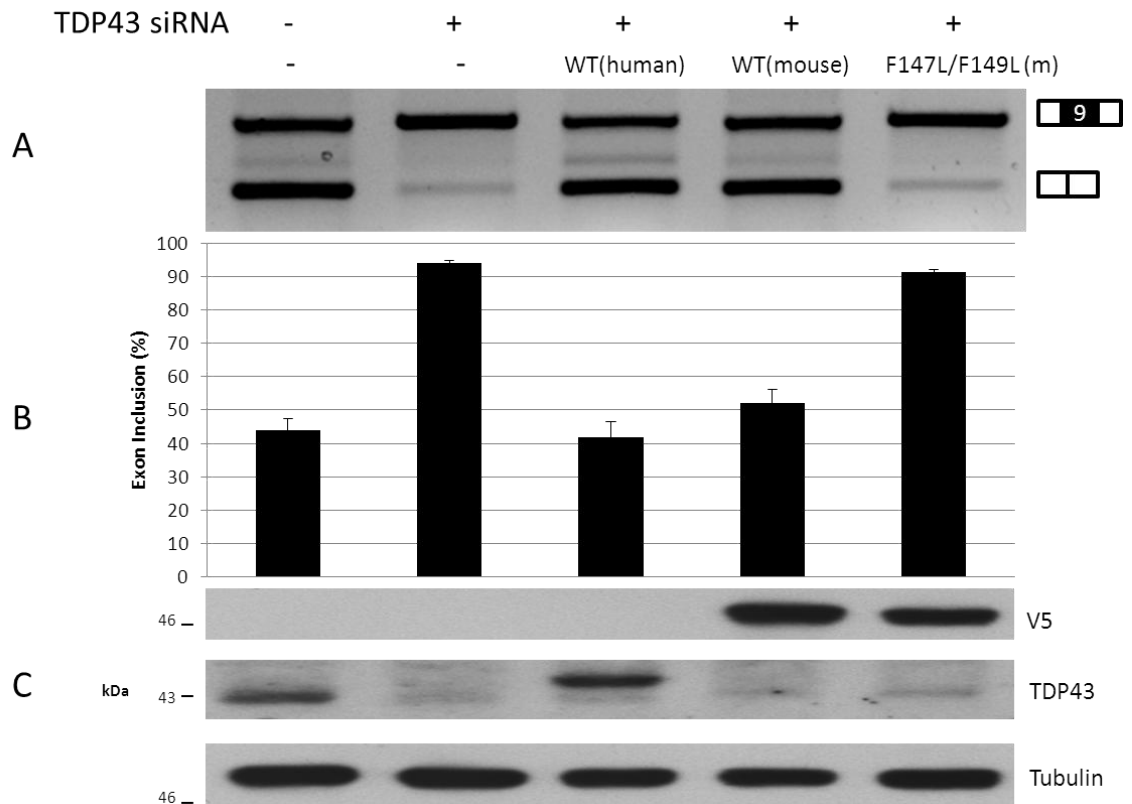
Figure 4.4: Mouse CFTR mini-gene rescue. Add-back assay showing mouse TDP43 can rescue exon 9 skipping, as in human TDP43 rescue. Panel A shows cDNA PCR product with CFTR specific PCR primers. Band intensity was quantified using ImageJ software. Panel B shows bar chart of exon inclusion measured as a percentage of exon included band versus total (included + excluded) band intensity. The cryptic splice site band in between full exon 9 inclusion and exclusion bands was not included as part of the measurement. Error bars represent standard error of the mean. Panel C shows Western blots with anti V5 (Invitrogen) labelling mouse TDP43 constructs, anti-TDP43 (in house Buratti laboratory antibody) being specific for human TDP43 only and anti-Tubulin control (in house Buratti laboratory antibody).

4.3. Assessment of TDP43 mutations in the add-back assay

Wild-type mouse TDP43 protein is able to rescue exon 9 CFTR mini-gene skipping function. TDP43 V5 / HIS tagged constructs carrying all mutations in the allelic series were assessed in the add-back assay, shown in Figure 4.5. This was completed in six well dishes. For each six well dish, 180,000 cells were plated per well. In the experiment, one well each contained: no siRNA, siRNA alone and siRNA with wild-type TDP43 rescue. In the remaining three wells, siRNA with mutant construct rescue (a different mutation per well) was completed. Mutants were then compared to wild-type rescue per six well dish to minimise variation between dishes. This was repeated for each mutant at least three independent times. There was a significant reduction in exon skipping as expected following siRNA knock down of TDP43 (versus non siRNA treated $p < 0.0001$, 1 Way ANOVA). Out of all mutations tested, F210I showed a significantly reduced ability to rescue exon skipping resulting in higher exon inclusion overall (versus wild-type mouse TDP43 rescue $p = 0.011$, 1 Way ANOVA). This implies a functional deficit where F210I is unable to promote efficient exon skipping (Figure 4.5). Control Western blots were run for all samples to confirm that all V5 / HIS plasmids expressing each of the mutant proteins were to approximately an equal level and that the siRNA had successfully downregulated the endogenous HeLa TDP43.
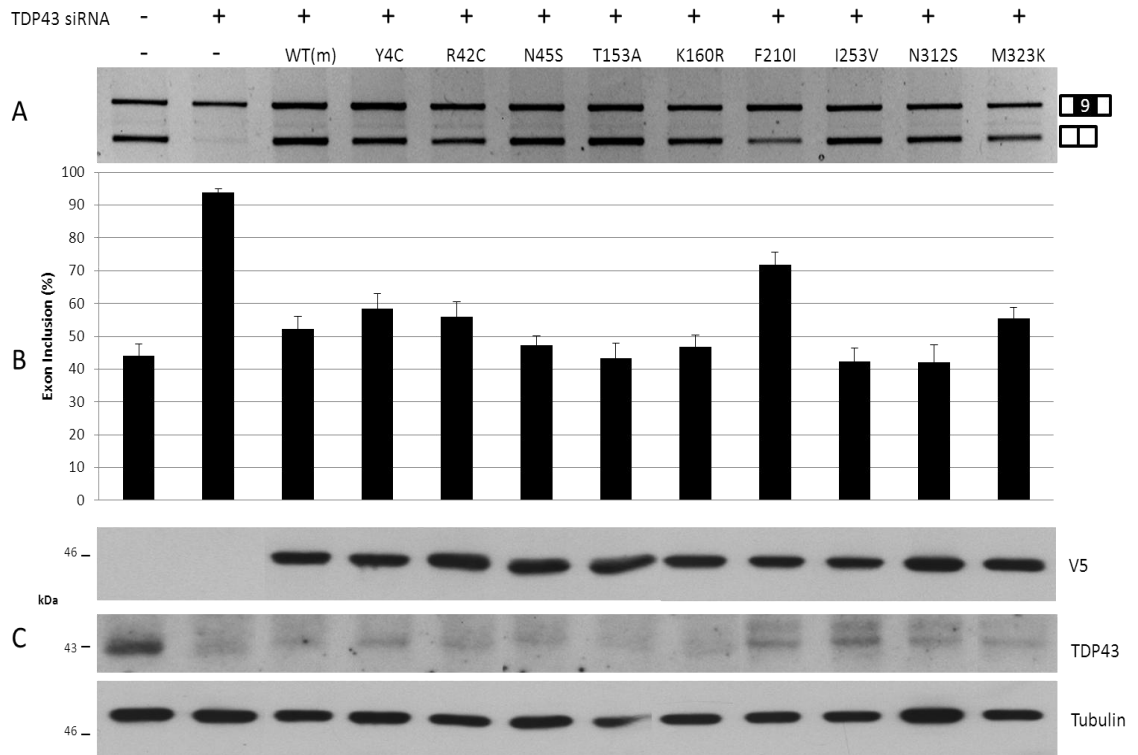
Figure 4.5: Allelic series add-back assay. Panel A shows reverse transcription PCR bands with exon 9 inclusion / exclusion, following siRNA treatment and TDP43 WT or mutant rescue. Panel B bar chart represents exon 9 inclusion, as a percentage of total included / excluded band intensity (as measured by ImageJ software). Panel C shows transfected protein expression (anti V5, Invitrogen), endogenous protein levels (in house anti TDP43) and Tubulin loading control levels (in house anti Tubulin). All missense mutations in the allelic series were transfected into siRNA treated HeLa cells, alongside the CFTR mini-gene reporter. When assessing exon skipping recovery versus WT TDP43 (Figure 4.5 panel A and B), F210I shows a significant inability to promote exon skipping. Western blot analysis shows that all mutant constructs were expressed approximately equally and that endogenous TDP43 was heavily downregulated by siRNA.

Wild-type TDP43 rescue of exon 9 skipping was 52.1% (Figure 4.5). Excluding F210I, mutant rescue from all other constructs was not significantly different to wild-type rescue. When comparing F210I rescue to wild-type rescue from the same six well plates, F210I rescue (71.7% inclusion) was significantly reduced compared to wild-type rescue ($p = 0.011$, 1 Way ANOVA).

4.4. F210I localisation

As F210I was the only mutation to show a loss of ability to rescue exon 9 skipping function it was further investigated *in vitro*. Protein localisation was assessed in order to deconstruct the potential mechanism through which the F210I allele is unable to recover mini-gene exon 9 skipping in the add-back assay (Figure 4.5). HeLa cells were transfected with V5 / HIS tagged Wild-type or F210I TDP43 and after 24 hours incubation; cells were pelleted for biochemical fractionation using lysis buffers and centrifugation into nuclear and cytoplasmic fractions (Figure 4.6). They were then analysed by Western blotting.

TDP43 is predominantly (approximately 95%) localised to the nucleus as is transfected wild-type mouse TDP43 in HeLa cells. Transfected F210I TDP43 also localises to the nucleus indicating that the nuclear versus cytoplasmic localisation is unaffected (Figure 4.6). This experiment was repeated independently three times.
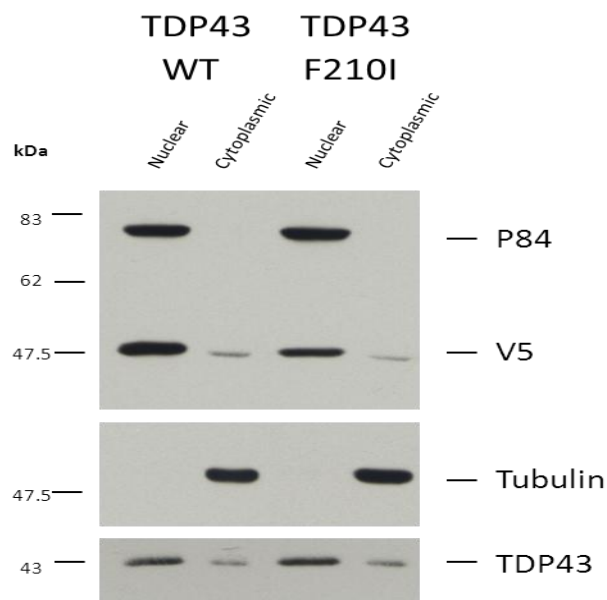
Figure 4.6: F210I nuclear versus cytoplasmic localisation. HeLa cells transfected with WT or F210I TDP43 were harvested 24 hours post transfection and fractionated into nuclear and cytoplasmic compartments. P84, a nuclear matrix protein, and Tubulin, were used to label nuclear and cytoplasmic fractions to confirm successful fractionation. V5 labelling against the tagged mouse proteins shows no overt differences between WT and F210I. Endogenous human TDP43 (as labelled with a human specific in house antibody generated by the Buratti / Baralle laboratory) shows a similar pattern.

4.5. F210I GST Overlay (far Western)

In order to complete CFTR mini-gene exon skipping, TDP43 must successfully interact with a number of proteins, including characterised interactions with hnRNP family members (D'Ambrogio *et al.*, 2009). To assess whether major TDP43 protein interactions are affected by F210I, a GST overlay experiment was completed. Utilising wild-type and F210I GST tagged plasmids; BL-21 bacterial cells were transformed to express the GST tagged proteins for subsequent protein purification. HeLa cell nuclear and cytoplasmic fractions were run on a 12% acrylamide gel before being transferred to a PVDF membrane in the standard Western blot protocol. The membranes were either incubated with wild-type or F210I recombinant GST protein (2 µg) purified as described in Chapter 2. Standard incubation followed with a GST primary antibody (anti GST, Healthcare) and a HRP (Goat) secondary antibody. The binding pattern for this experiment has been previously published for human TDP43 (D'Ambrogio *et al.*, 2009), allowing for comparison to this result (Figure 4.7). There is no overt difference in the protein binding pattern between wild-type and F210I TDP43. The mouse versus human binding pattern to HeLa extract is also identical. This experiment was repeated three independent times, using purified protein extracted from independent bacterial transformations.
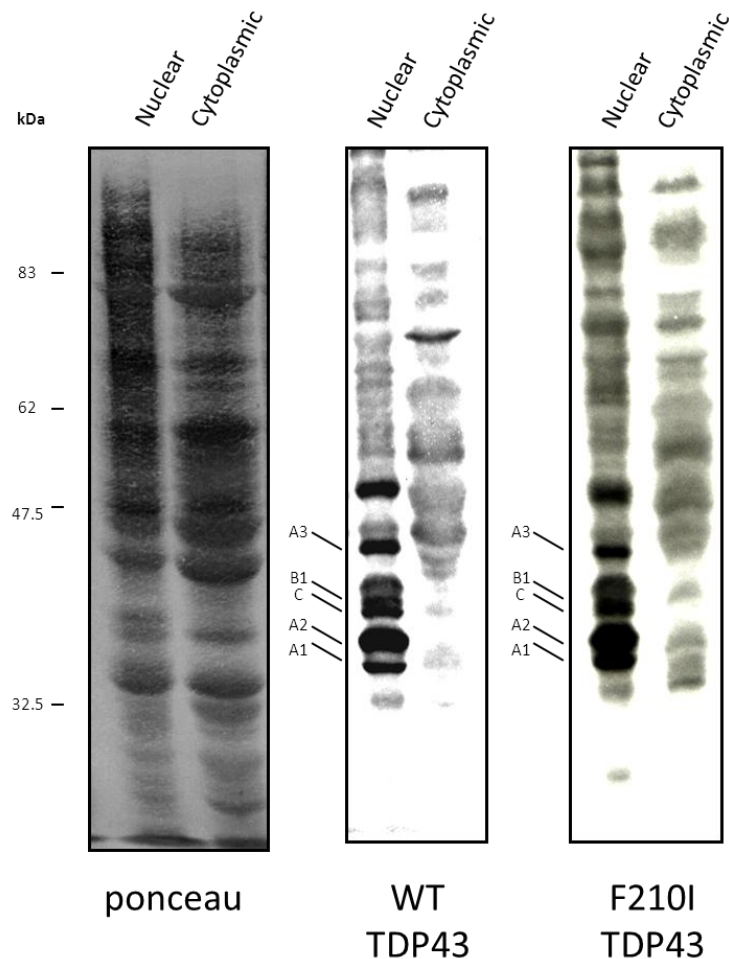
Figure 4.7: F210I GST overlay. HeLa cell extracts (nuclear and cytoplasmic) were run on acrylamide gels before transfer to PVDF membranes. GST overlay was completed using GST purified WT and F210I TDP43 protein. The binding pattern of the WT and F210I mouse proteins, to human HeLa extracts, is similar to the published human binding pattern. Indicated bands, are hnRNP family binding members as characterised by the Buratti / Baralle laboratory (D'Ambrogio *et al.*, 2009). Band presence / absence is similar for WT and F210I TDP43. Ponceau staining shows the smear of proteins at all molecular weights indicative of the extracted protein array from the nuclear and cytoplasmic fractions. Binding patterns were visualised following antibody incubation with ECL.

Wild-type TDP43 predominantly binds a cluster of hnRNPs, shown to bind human TDP43 (Figure 4.7). These include hnRNPs A3, B1, C, A2 and A1 (D'Ambrogio *et al.*, 2009). F210I TDP43 also binds these hnRNPs with a similar binding pattern, representing the major affinity interactions for TDP43 with HeLa cell extracted nuclear and cytoplasmic proteins.

166

4.6. F210I band shift with UG repeats

An electrophoretic mobility shift assay (EMSA) experiment was completed to assess whether F210I shows normal binding affinity to UG_6 repeats. Binding to UG repeats is required for the CFTR exon 9 skipping function with the EMSA *in vitro* assessing direct binding affinity to labelled UG_6 repeats. Recombinant GST purified wild-type and F210I TDP43 were added to radioactively labelled UG_6 repeats at increasing concentrations and run on 5% acrylamide gels. The gels were then dried onto filter paper and visualised by Cyclone (Packard) exposure. F210I TDP43 shows a strongly reduced ability to bind UG_6 repeats (Figure 4.8) compared to wild-type TDP43.
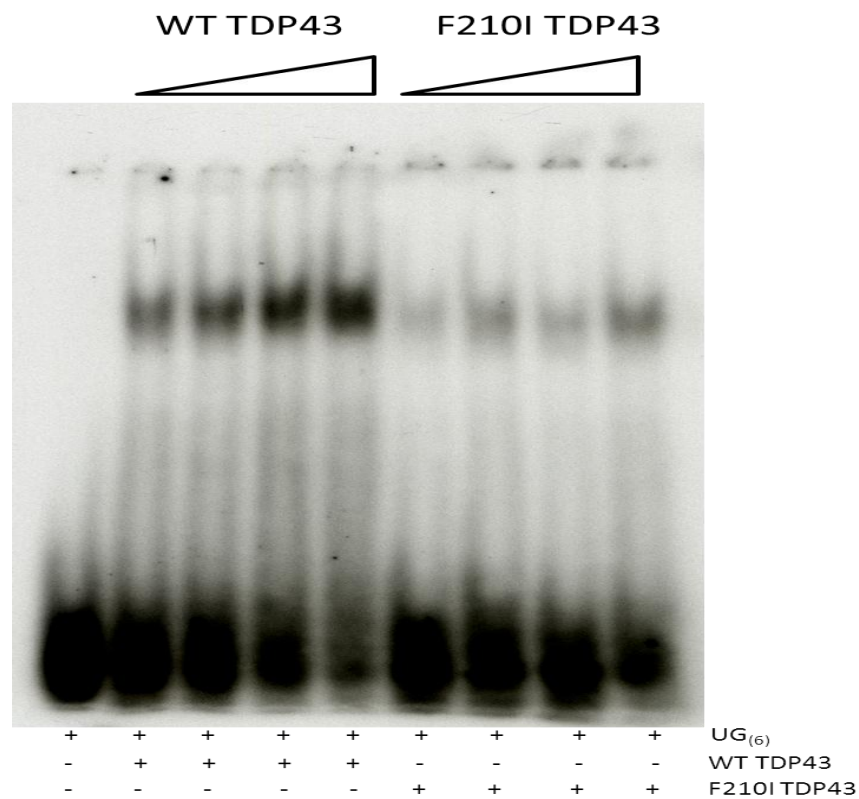
Figure 4.8: F210I band shift. Radioactively labelled UG_6 repeats were loaded onto an EMSA 5% acrylamide gel. With no binding protein added, a smeared band is seen at the bottom of the gel. As increasing amounts of WT TDP43 are added, the protein binds the free UG_6 repeats and forms a band shifted complex. Likewise, the amount of free labelled RNA decreases as more is bound to TDP43. Conversely, F210I TDP43 shows a strong loss of ability in forming the band shift complex. A basal band of low intensity is formed however this is highly reduced compared to WT TDP43, with additional F210I TDP43 protein not significantly increasing the formation of the band shift complex.

4.7.   Results discussion

The mechanism behind CFTR exon 9 splicing has been well characterised (Buratti & Baralle, 2001; Buratti *et al.*, 2001; Pagani *et al.*, 2003a; Pagani *et al.*, 2003b). In humans, TDP43 plays an important role in regulating exon 9 skipping in CFTR. The add-back assay with a CFTR exon 9 mini-gene was used to assess the functional capability of the allelic array of mouse TDP43 mutations.

Like human TDP43, mouse TDP43 is able to rescue CFTR exon 9 mini-gene skipping (Figure 4.4). Human TDP43 rescue was 41.9% whereas the mouse rescue was increased by 10% (52.1%), but this is not significantly different, $p = 0.603$, 1 Way ANOVA. This shows a 10% reduction in the ability TDP43 to promote exon 9 skipping, compared to human TDP43 rescue. This may be affected by the transfection efficiency of the different plasmids. However this does not affect the purpose of this assay, in assessing the functional capability of the mutant mouse forms versus wild-type TDP43. A recovery rate of 52.1% also provides a sufficiently clear baseline from which to assess potential gain of skipping function, below 52.1%, or loss of function above 52.1%.

Mutating two critical phenylalanines in the first RRM of TDP43 (F147L / F149L) abolishes the RNA-binding capability of TDP43 to UG repeats and results in the loss of TDP43's ability to promote exon skipping (Buratti & Baralle, 2001). These phenylalanines are conserved across species as well as in the mouse. As a result, mouse TDP43 F147L / F149L was unable to promote exon skipping (siRNA only treated cells showed 93.8% inclusion, siRNA with F147L / F149L showed 91.2% inclusion). This initial experiment showed that the mouse TDP43 constructs are resistant to the siRNA used to knock down endogenous TDP43. The sequence of the siRNA and mouse sequence differs by only two bases and this is sufficient for the constructs to express the V5 / HIS tagged TDP43 proteins (Figure 4.4 and Figure 4.5) without being significantly degraded at the RNA level.

Having established TDP43 rescue in the add-back assay, all missense mutant constructs were assessed for their ability to rescue exon 9 skipping. All mutant TDP43 alleles were successfully able to recover exon 9 skipping, excluding F210I ($p = 0.011$, 1 Way ANOVA). When comparing the five wild-type add-back experiments completed versus the five F210I add-back results (with these runs completed in the same six well dishes), wild-type recovery showed an exon inclusion average of 52.15%, versus F210I recovery at 71.77% exon 9 skipping. siRNA only

treated cells without construct rescue show 93.86% exon 9 inclusion. Therefore, F210I recovery is approximately 50% between wild-type recovery levels and no recovery. This *in vitro* result implies a potential reduction in exon 9 skipping function of 50%.

With F210I showing a reduced ability to rescue exon 9 skipping function, protein localisation was assessed. Biochemical fractionation of transfected HeLa cells showed that both wild-type and F210I TDP43 predominantly localised to the nucleus as expected. This matches the endogenous pattern of localisation. This result implies that the F210I mutation does not affect subcellular localisation of TDP43. Sub nuclear localisation of TDP43 in chromatin fractions has not been assessed for F210I, as described for the RRM1 mutant (Ayala *et al.*, 2008b). This result implies that F210I TDP43 is not mislocalised and is free to promote exon 9 skipping, however further characterisation for sub nuclear localisation could be assessed.

To further characterise potential differences between wild-type TDP43 and F210I *in vitro* in HeLa cells, a GST overlay was completed to assess protein interactions. When HeLa nuclear and cytoplasmic extract were exposed to GST purified TDP43 protein, the binding pattern was not overtly different between wild-type and F210I proteins. The binding pattern had previously been established between human TDP43 and HeLa fractions (D'Ambrogio *et al.*, 2009) with this result now characterising the mouse protein binding pattern. The two patterns are identical and this may be expected considering the 96% amino acid conservation between human and mouse TDP43. Both wild-type and F210I TDP43 have a high affinity for binding other hnRNP family members, with the same banding patterns visualised. This indicates that TDP43's major protein interactions are not affected by the F210I mutation. This may be expected, as the highly characterised protein binding region in TDP43 lies in the C-terminus, downstream of the F210I mutation. Furthermore, a recent paper has identified a binding region in the N terminus (Swarup *et al.*, 2011b). There is minimal information on the importance of the second RNA recognition motif (RRM2) and within it the F210I region as having roles in binding to other proteins. It is established in the literature (Buratti *et al.*, 2005; D'Ambrogio *et al.*, 2009) that the C-terminus mediates most known protein interactions and it is the C-terminus that is critical for binding to many hnRNP family members (Buratti *et al.*, 2005; D'Ambrogio *et al.*, 2009), making this region potentially less likely to be affected by the F210I mutation.

The GST overlay is a powerful technique which assesses major protein interactions. It is not quantitative as band intensity can vary significantly between repeat runs. A band presence / absence assessment effectively identifies whether a new binding partner is present or a major existing binding partner is lost. The major bands identified represent the protein binding

partners with the highest affinity for TDP43. There are hundreds of other characterised protein interactions for TDP43, which have been established and validated through techniques including co-immunoprecipitation. The majority of these binding partners are not represented here and this characterisation would require alternative approaches which are more quantitative, such as immunoprecipitation. As such, it is possible that F210I may affect TDP43's protein interactions in ways that the GST overlay is not able to detect. This result shows that major interactions with hnRNP family members are not lost as a result of the F210I mutation.

The final *in vitro* assessment of the F210I mutation confirmed that this mutation affects the ability of TDP43 to bind UG_6 repeats. TDP43 has a high affinity for binding UG repeats (Kuo *et al.*, 2009), binding a minimum of six repeats. The binding affinity also increases with more repeats (Buratti & Baralle, 2001). There was a striking inability for F210I to match the wild-type binding to UG_6 repeats. This *in vitro* assessment conclusively shows that F210I has highly reduced UG_6 RNA-binding ability.

Phenylalanine 210 lies in the second RRM. At position 211 there is a second phenylalanine with both residues being conserved from human through to zebra fish. The 210 residue is not conserved in Drosophila however the 211 residue is. Mutating F210 to an isoleucine creates a mutation that may fit an RNA-binding deficient model, considering the mutation lies in the second RRM. The *in vitro* data presented in this chapter further supports that the deficit in promoting exon 9 skipping, is likely to be the result of an inability to efficiently bind UG repeats in the mini-gene transcript. Major protein interactions seem unaffected and F210I TDP43 successfully localises to the nucleus, however correct sub nuclear localisation has not been shown. F210I TDP43 shows a clear functional inability to promote exon 9 skipping.

There is clear data that F147 / F149 in the first RRM are critical in enabling TDP43 to bind UG repeats and RNA in general (Figure 4.4). For both human and mouse TDP43, further data has supported the first RRM being necessary and sufficient for human TDP43 binding to RNA (Buratti & Baralle, 2001), with deletion of the second RRM not inhibiting RNA-binding (Buratti & Baralle, 2001). As such, it was anticipated that mutations affecting general protein structure, or the missense mutations in the first RRM (T153A and K160R), might be the most likely candidates to affect CFTR skipping function. Surprisingly, F210I, in the second RRM, shows an inability to complete wild-type function. The 50% loss of rescue ability *in vitro* indicates a strongly hypomorphic effect on RNA-binding and skipping function.

The mechanism through which F210I causes an RNA-binding deficiency remains to be determined. RRM2 may play a more important role in RNA-binding than previously thought.

Alternatively this specific mutation may impact on RNA-binding in a dimer specific manner. TDP43 is thought to function as a dimer (Kuo *et al.*, 2009). F210 could be a critical residue in the dimer which physically binds RNA or it may affect the binding of other phenylalanines such as 147 / 149. A direct effect on the impact of physical RNA-binding is more likely considering the nature of the mutation; however other aspects of TDP43 biology could also be affected. This could range through effects on protein structure and stability, subtle protein localisation or interactions but this is not supported by the EMSA. Initial assessment of the structure of mouse F210I TDP43 could be achieved through modelling the mutational change, circular dichroism and running native gels to assess dimer formation. Alternative effects could be tested through techniques such as chromatin fractionation to assess nuclear protein localisation or through assessing protein turnover rates. Considering these hypotheses, it still remains that a mutation in RRM2 affects TDP43's binding to UG_6 repeats and its functional ability to promote exon 9 mini-gene skipping. The nature of the mutation implies a direct effect on the physical interaction with RNA explaining both phenotypes and establishes the importance of RRM2 in affecting TDP43's functional ability to bind UG_6 repeats and promote CFTR mini-gene exon 9 skipping.

CHAPTER 5

Results:

In vivo F210I characterization

5.   Results: *In vivo* F210I characterization

5.1.   Introduction

In Chapter 4 it was shown *in vitro* that F210I is highly inefficient at promoting mini-gene exon 9 skipping. This chapter will describe how this phenotype translates *in vivo*. Following the finding that F210I is strongly hypomorphic for UG_6 RNA-binding and promoting exon 9 skipping, heterozygous F210I mice were imported from RIKEN Japan into MRC Harwell. After a period in quarantine, the mice are now available and have continued to be backcrossed to C57BL/6J (from an original DBA / C57BL/6J background). A cohort of mice (backcross 5, BC5, to C57BL/6J) has been generated for phenotyping as well as timed matings to assess the F210I mutation *in vivo*. This chapter utilizes mice of BC2-4 to preliminarily characterize the cellular and molecular changes driven by F210I TDP43 *in vivo*. A summary schematic of the mice used is shown below (Figure 5.1).
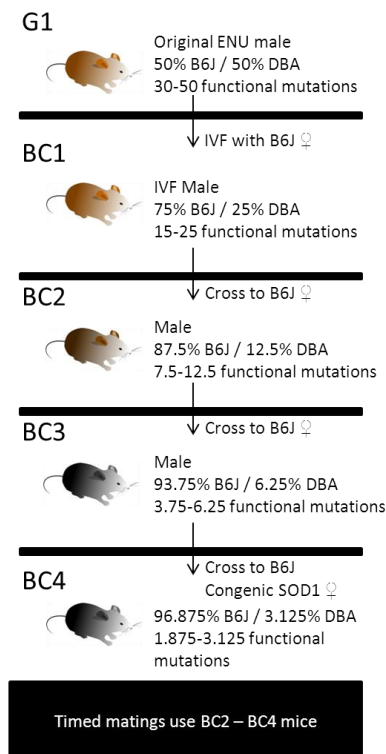
Figure 5.1: F210I mouse genetics. Figure shows original G1 mouse carrying the F210I mutation, with its sperm from an ENU archive being used to produce BC1 mice. The background of the IVF mouse is 50% C57BL/6J / 50% DBA. This line has been backcrossed continuously with C57BL/6J with inter crosses at various generations used for timed matings.

Upon receiving the mice and completing two generations of backcross to C57BL/6J, intercross matings were set up to obtain Mouse Embryonic Fibroblasts (MEFs). The initial aim for MEF culture was to replicate the findings in HeLa cells, by electroporating the CFTR mini-gene into MEFs. This cellular system allows assessment of exon skipping *ex vivo* in wild-type, heterozygous and homozygous F210I MEFs.

MEFs were harvested to assess protein and RNA changes. The aim was to confirm *ex vivo* that F210I is a hypomorphic allele for RNA-binding function. In parallel, whole embryonic head from the same embryo that the MEFs were generated from was used for protein and RNA analysis. Samples of brain, liver and spinal cord from BC2 adult wild-type and heterozygous F210I mice (12 weeks of age) were also harvested with the purpose of protein and RNA analysis.

Following the *in vitro* identification of F210I, in early 2011, two publications (Ayala *et al.*, 2011; Polymenidou *et al.*, 2011) characterized the impacts on the transcriptome when TDP43 is downregulated. They showed that TDP43 auto-regulates its protein levels through binding its own 3'UTR. It also has critical roles in RNA metabolism affecting more than 6,000 genes in the murine transcriptome when downregulated in the striatum of adult mice (many of these changes being potentially direct or indirect). Considering the established *in vitro* effects of F210I on RNA-binding, both auto-regulation and the effects on target genes were assessed to characterize F210I as a potential hypomorphic *in vivo* model for RNA-binding function.

The model of auto-regulation proposed from the Buratti / Baralle laboratory (Ayala *et al.*, 2011) hypothesizes that when there is excess TDP43 in the cell, it binds a CLIP (Cross Linking and immunoprecipitation) identified sequence in its 3' UTR. It binds this CLIP identified sequence with a lower affinity than UG repeats. The binding of TDP43 subsequently affects recognition of multiple poly adenylation sites, affecting the ratio of read through for varying transcripts. This leads to exosome mediated decay of the transcript encoding for further full length TDP43 production. This model was established in stably transfected HEK293 cells expressing a single copy of tagged human TDP43 with a tetracycline inducible promoter (Ayala *et al.*, 2011). Shortly after this publication, the Cleveland laboratory published a model with similar principles (Polymenidou *et al.*, 2011) but not based on exosome mediated decay being the driving force to protein encoding transcript degradation. Instead, TDP43 binds its own 3' UTR in the CLIP identified sequence and then promotes the inclusion of an exon within the 3' UTR, targeting the RNA for nonsense mediated decay (NMD). These models are not antagonistic, with both mechanisms likely to be occurring to a certain degree. With these models in place, the F210I allele *in vivo* may be an ideal model in which to assess auto-

regulation being dependent on an RNA-binding event, considering the established *in vitro* loss of function. The initial aim was to assess whether F210I can bind the TDP43 3' UTR CLIP identified sequence as efficiently as the wild-type protein (through band shift). This was completed by Dr Mauricio Budini in Professor Baralle's laboratory (shown in Figure 5.6). Following this, characterization of changes in *Tardbp* transcripts at the RNA level and TDP43 at the protein level were completed in multiple tissues.

Alongside proposed auto-regulation models which may be relevant to TDP43 pathology in humans, the Cleveland laboratory (Polymenidou *et al.*, 2011) knocked down endogenous TDP43 in adult brain. They assessed the consequences across the murine transcriptome through RNA sequencing and exon microarrays. The striatum of young adult mice was injected with antisense oligonucleotide (ASO) targeted against the *Tardbp* encoded transcripts. This ASO downregulated the TDP43 encoding transcript by forming double stranded RNA recognized by RNAse H which in turn completes pre-mRNA degradation. Two weeks after ASO treatment, the striatum, now containing highly downregulated levels of TDP43, was harvested for protein and RNA extraction. RNA sequencing was completed and in response to TDP43 down regulation, changes across 30% of the murine transcriptome were observed. In particular, large effects were seen with 601 mRNA level changes and 965 splicing pattern changes. Many of these changes were then validated by PCR and quantitative real time PCR. This was the first example showing the extent of TDP43's role in RNA metabolism across the transcriptome, which has subsequently been replicated in other models or has been assessed using similar methods (Chiang *et al.*, 2010; Shan *et al.*, 2010; Sephton *et al.*, 2011; Tollervey *et al.*, 2011). With this in mind, F210I mice are being used to assess the impact of this mutation by performing RNA sequencing and proteomics to detect changes across the transcriptome and proteome. The preliminary results from these experiments are not presented as part of the work in this thesis. However, the results from the Cleveland group identified multiple RNAs which are regulated by TDP43. This provided specific targets to assess the degree of loss of function in F210I MEFs and tissues for RNA level and splicing changes, which are presented here.

To assess the effects of the F210I allele on RNA levels and splicing, target genes were selected based on published changes. RNA was harvested and converted to cDNA. Primers were designed spanning introns and the included / excluded target exon. PCR was completed to produce non saturated PCR bands for band quantification and comparison. Likewise, cDNA was used in real time PCRs to quantify transcript levels using SYBR Green. All primers used for real

time PCRs were assessed for band amplification purity with primers being optimized to optimal amplification efficiency (as indicated in methods).

5.2. CFTR mini-gene rescue in F210I MEFs

It was established *in vitro* in Chapter 4 (Figure 4.5) when transfected in HeLa cells that F210I shows a 50% reduction in its ability to promote CFTR exon 9 skipping. This was next assessed *ex vivo* in MEFs derived from E14.5 dpc embryos. MEFs were harvested and cultured as described in Chapter 2. At passage 2 (P2), wild-type, heterozygous and homozygous F210I MEFs were cultured and electroporated with the CFTR mini-gene. Negative controls included electroporation with no mini-gene, or no buffer. From three independent runs, results show that F210I heterozygous and homozygous MEFs are less efficient than wild-type in promoting exon skipping (Figure 5.2).
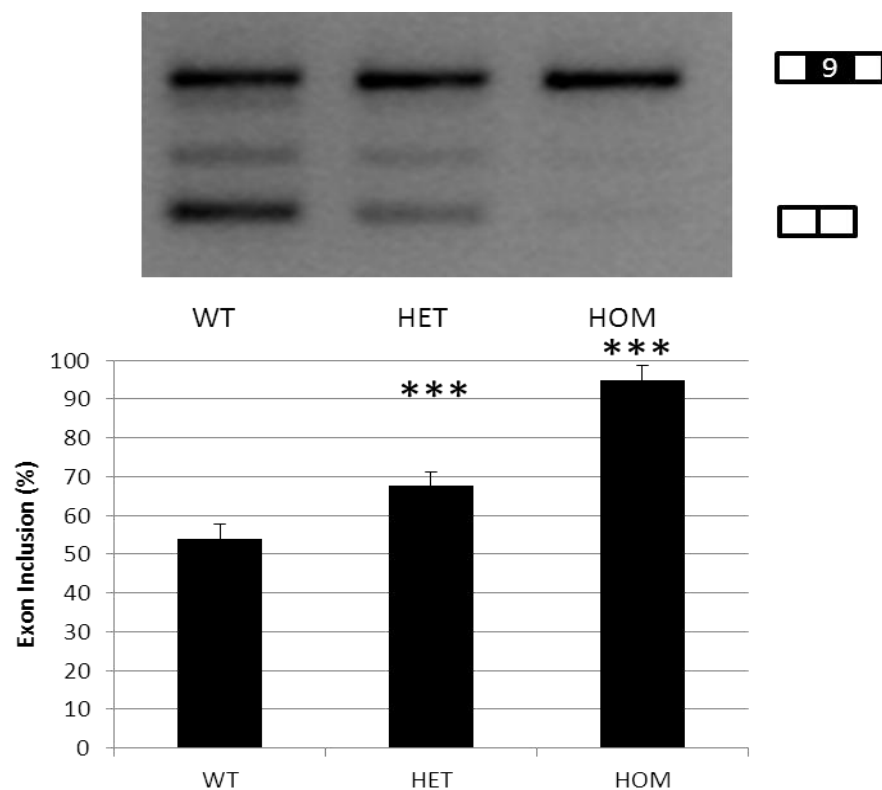
Figure 5.2: F210I MEFs electroporated with the CFTR mini-gene. P2 MEFs were electroporated with the CFTR mini-gene with RNA harvested following 24 hours. As in Chapter 4, RNA was extracted and converted to cDNA. BRA and α23 primers were used to amplify the CFTR exon 9 region and determine exon 9 skipping. Wild-type MEFs promote approximately 50% exon 9 skipping whereas heterozygous and homozygous MEFs show a significantly reduced ability to promote exon 9 skipping. Top panel shows PCR product run on a 1.8% acrylamide gel stained with ethidium bromide. Exon 9 included is the top band and excluded the bottom band. The intermediary band is the

result of a cryptic splice site as discussed in Chapter 4. Bar chart shows exon inclusion as a percentage of included / excluded total. Bands were quantified using ImageJ software. N = 5 WT, 6 heterozygous, 3 homozygous. Error bars show the standard deviation.

Wild-type MEFs show 54.0% exon 9 inclusion of the mini-gene. Heterozygous F210I MEFs have a significantly reduced ability to promote exon skipping with 67.7% exon 9 inclusion (p < 0.001 1 Way ANOVA). Homozygous MEFs show an almost complete loss of ability in promoting exon 9 skipping, with 94.8% exon inclusion (versus wild-type and heterozygous MEFs p <0.0001 1 Way ANOVA). This shows a clear dosage effect from normal CFTR exon 9 mini-gene splicing in the wild-type MEFs, to an intermediary loss of ability to promote skipping in the heterozygous MEFs (approximately 13% increased exon 9 inclusion). Finally, the homozygous MEFs show an almost complete inability to promote exon 9 skipping.

5.3. MEFs immunofluorescence

As in Chapter 4, protein localisation was assessed in MEFs. The aim was to determine whether the F210I mutation *in vivo*, impacts upon its nuclear versus cytoplasmic localisation. Further to the biochemical fractionation done *in vitro*, the labelling pattern within the nucleus was assessed by immunofluorescence *ex vivo*. Wild-type, heterozygous and homozygous P2 MEFs were grown and stained by immunofluorescence using anti-TDP43 and DAPI labelling.
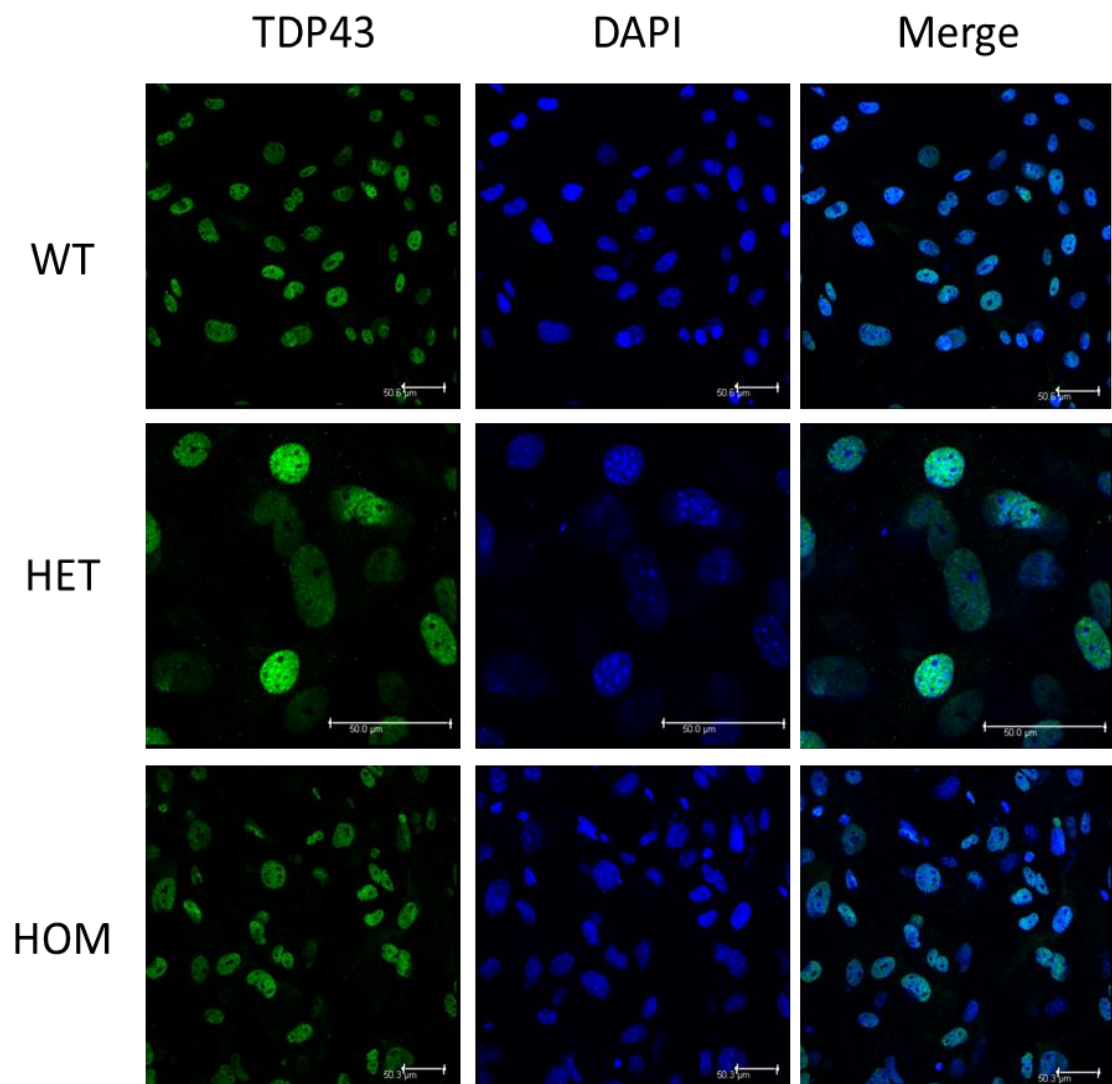
Figure 5.3: TDP43 stained F210I MEFs. P3 MEFs were grown on cover slips and fixed with 4% PFA followed by membrane permeabilization. MEFs were stained using primary anti-TDP43 (Protein Tech) with an AlexaFluor 488 conjugated secondary. DAPI staining shows that TDP43 localises predominantly to the nucleus in MEFs and that F210I does not appear to overtly affect protein localisation *ex vivo*. Scale bar is 50 μm.

F210I heterozygous and homozygous MEFs do not appear to show mislocalisation of TDP43 compared to wild-type MEFs (Figure 5.3). MEFs were stained on three independent runs and assessed visually using a confocal microscope (Leica SP5) with Z stack imaging to assess for variation through visual planes. No overt visual differences were observed although this was not quantified.

5.4. F210I homozygote lethality

Intercross matings were set up to assess F210I homozygote mouse viability. This has been assessed with females from all backcrosses from the DBA / C57BL/6J founder background through to BC5 C57BL/6J mice (Figure 5.1). Data presented represent BC 2-4 mice.

From intercross litters, a preliminary result of 20 wild-type mice and 23 heterozygous mice were born with no homozygotes at weaning. The expected Mendelian ratio is 1 wild-type: 2 heterozygotes: 1 homozygote. This was assessed using the Chi squared test. No homozygotes have been genotyped making the Chi squared significantly different to that expected. Furthermore, from heterozygous intercross matings a ratio of 1 wild-type: 2 heterozygous mice born are expected, with a trend to fewer heterozygous mice than expected (Table 5.1).

Category	Observed	Observed (%)	Expected	Expected (%)
WT	20	46.51%	10.75	25%
HET	23	53.49%	21.5	50%
HOM	0	0%	10.75	25%

X^2 = 18.814, 2 DoF, two tailed p = 0.0001

Category	Observed	Observed (%)	Expected	Expected (%)
WT	20	46.51%	14.33	33.3%
HET	23	53.49%	28.66	66.67%

X^2 = 3.365, 1 DoF, two tailed p = 0.066

Table 5.1: F210I viability. Tables showing the numbers of genotyped mice at weaning from F210I heterozygous inter cross matings. Left table shows Chi squared using all three genotypes and right table assumes homozygous mice not to be viable. A general policy of collecting newly born pups that die immediately after birth for genotyping has been adopted; however there have been no abnormal numbers of post natal deaths and no samples genotyped have been homozygotes (data not shown).

There are significant differences in the expected ratio of wild-type versus homozygous mice born and genotyped from inter cross matings. There is a trend to fewer heterozygous mice

born than expected and no homozygous mice have been identified at birth or weaning. As homozygous mice are not viable, male heterozygotes were crossed to C57BL/6J wild-type congenic females to generate a phenotyping colony. From these crosses, a wild-type versus heterozygote ratio of 1:1 is expected. Heterozygous males used have been BC2 to BC4. Results show that there is no significant difference (p = 0.1835 χ^2 test) in the ratio of wild-type versus heterozygous mice across males and females (Table 5.2).

Category	Observed	Observed (%)	Expected	Expected (%)
WT Female	69	22.19%	77.75	25%
HET Female	76	24.43%	77.75	25%
WT Male	94	30.23%	77.75	25%
HET Male	72	23.15%	77.75	25%

X^2 = 4.846, 3 DoF, two-tailed p = 0.1835

Table 5.2: F210I backcross ratios. Table showing the Chi square test for mice genotyped at weaning using F210I heterozygous males crossed to congenic C57BL/6J WT females. There is no significant difference when accounting for all four genotype / sex combinations with an expected ratio of 1:1:1:1 from 311 mice. When assessing males only, X^2 = 2.916 with 1 degrees of freedom, p = 0.0877.

5.5. F210I homozygous embryos

Despite homozygote lethality, F210I homozygous embryos remain alive at E14.5 dpc and as such, primary cells such as MEFs have been cultured. Timed matings were set up to identify the stages at which homozygous embryos are viable and the potential causes of embryonic lethality. Embryos were harvested at E14.5 dpc and dissected for assessment of overt morphological abnormalities. Representative images of a normal heterozygous versus homozygous E14.5 dpc F210I embryos are shown below (Figure 5.4 and Figure 5.5).

HET   **HOM**

Figure 5.4: F210I homozygous embryo photo. F210I heterozygous versus littermate homozygous E14.5 dpc embryo side image. Photo of heterozygous embryo alongside a littermate homozygous embryo. The photo was taken in PBS in a petri dish, following dissection from the embryo sack. The homozygous embryo is around a third smaller, with spinal oedema. The eyes also appear less developed however this embryo is still alive. The red staining pattern observed in the homozygous embryo is not thought to be a significant phenotype, observed intermittently in all homozygous embryos assessed. No scale bar was taken at the time of this photograph.

HET   **HOM**

Figure 5.5: F210I homozygous embryo photo (zoomed in). F210I heterozygous versus littermate homozygous E14.5 dpc embryo. Zoomed in example photo of heterozygous versus homozygous embryo taken on a light microscope. The heterozygous embryo appears completely normal for this stage of development. The homozygous embryo shows holoprosencephaly and overt oedema. No scale bar was taken at the time of this photograph.

Dissection of three homozygous F210I E14.5 dpc embryos identified holoprosencephaly in two embryos, under developed eyes in two embryos and oedema in all three embryos. A dissection of these embryos assessed all major organs, including heart, liver, gonads and lungs. Heterozygous embryos showed completely normal development as did wild-type embryos (four assessed per genotype). Homozygous embryos appeared to have formed all major organs correctly but the size of the organs was significantly smaller, all proportional to the overall embryo size. All homozygous embryos displayed oedema most easily visible in the spinal cord area and are smaller in size by approximately a third, as in Figure 5.4. Having dissected more than twenty embryos whilst culturing MEFs (and not for pure morphological dissection), the holoprosencephaly and retarded eye development appear to have a low penetrance (both observed from five in twenty) in homozygous embryos however the spino-oedema is observed in all homozygotes.

5.6. Q101X / F210I

As F210I homozygotes are not viable, the aim was to assess whether $Tardbp^{F210I/Q101X}$ mice would be viable by crossing F210I heterozygous males to Q101X heterozygous females. F210I homozygotes have two F210I alleles whereas in the compound mutant $Tardbp^{F210I/Q101X}$ there is one F210I allele which must auto-regulate, as discussed in Chapter 3, for Q101X crossed to K160R. Crosses to generate the compound mutant $Tardbp^{F210I/Q101X}$ were set up. The aim was to see whether this compound mutant would progress in development to a different stage versus F210I homozygotes, considering the compound mutant has one F210I allele. Having one F210I and no wild-type allele also provides an *in vivo* model in which to assess the effects of F210I on auto-regulation versus the increased dosage of F210I homozygotes.

Although F210I is hypomorphic for RNA-binding function, it is possible that the mutation confers some toxic gain of function. It is hypothesized that the Q101X allele may reduce F210I expression (if auto-regulation is inefficient) and may rescue the phenotype in development, versus being homozygous for F210I. Preliminary crosses indicated that $Tardbp^{F210I/Q101X}$ is not viable at birth (Table 5.3).

WT	Q101X / +	F210I / +	F210I / Q101X
9	3	1	0

Table 5.3: F210I / Q101X compound mouse viability. Results from three litters indicating that $Tardbp^{F210I/Q101X}$ mice are unlikely to be viable.

As shown in Table 5.3 although the numbers are very low, Q101X / F210I compound homozygotes preliminarily, are not viable at birth. Timed matings were therefore set up to assess whether compound homozygous mutants were viable across embryonic development. No double homozygotes were found at E14.5 dpc however double mutants were found at E11.5 dpc, as shown in Table 5.4.

WT	Q101X / +	F210I / +	F210I / Q101X
9	10	11	8

X^2 = 0.526, 3 DoF, two-tailed p = 0.9131

Table 5.4: F210I / Q101X E11.5 dpc timed matings. Six timed matings at E11.5 dpc were harvested to assess $Tardbp^{F210I/Q101X}$ viability. Compound mutants were genotyped with genotype ratios not significantly different to the expected Mendelian ratio of 1:1:1:1.

All of the eight compound heterozygotes observed (Table 5.4) were significantly smaller than their littermate embryos, with five showing visible signs of resorption. No $Tardbp^{F210I/Q101X}$ embryos were visibly normal compared to littermate controls. Overall this supports that compound $Tardbp^{F210I/Q101X}$ die earlier than $Tardbp^{F210I/F210I}$ mutants, which are alive at E14.5 dpc.

5.7. F210I levels / Auto-regulation

Auto-regulation was assessed *in vitro* and *in vivo*. Following the identification of the CLIP identified sequence (Ayala *et al.*, 2011) which TDP43 binds in its own 3' UTR to auto-regulate its protein levels, the binding capability of F210I to this sequence was assessed. This experiment was completed by Dr Mauricio Budini in the Buratti / Baralle laboratory. In an identical fashion to the band shift experiment completed by myself, Dr Budini used the same constructs and protocol to assess binding to the TDP43 3' UTR CLIP identified sequence.

Alongside this run (repeated three independent times), he also repeated my UG_6 band shift experiment (which had also already been repeated three independent times) (Figure 5.6).
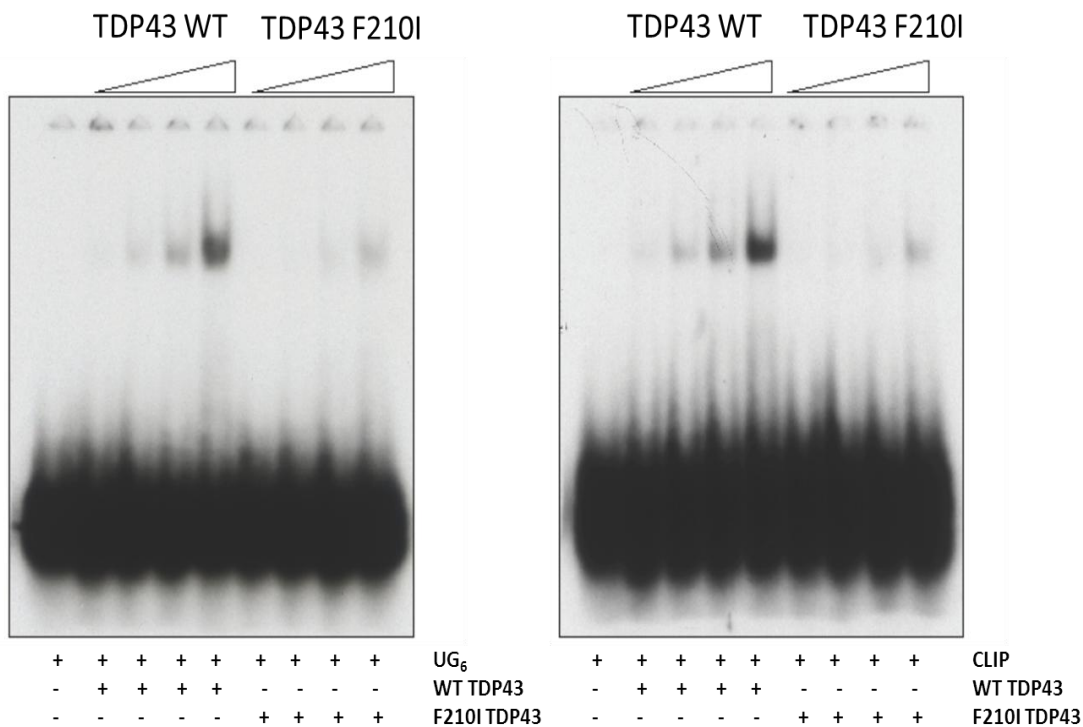
Figure 5.6: UG_6 and CLIP band shift EMSA. Following the protocol completed in Chapter 4, GST purified WT and F210I TDP43 was run on a 5% acrylamide gel to assess binding affinity to radioactively labeled RNA. With equal amounts of protein, the inability of F210I TDP43 to efficiently bind UG_6 repeats, as shown by a lack of the band shifted complex, is repeated (left panel). The right panel shows WT versus F210I TDP43 binding to the CLIP identified sequence, with F210I showing a highly reduced binding affinity compared to WT TDP43.

F210I TDP43 shows a reduced ability to bind both UG_6 and the CLIP identified 3' UTR RNA sequences (Figure 5.6). TDP43 has a higher binding affinity to UG_6 over the CLIP identified sequence (Ayala *et al.*, 2011) reflected in Figure 5.6 where more CLIP sequence RNA is loaded to form the band shift complex versus UG_6 where the free RNA band is greater for the CLIP sequence to form the band shift.

In order to address reduced 3' UTR CLIP identified sequence binding *ex vivo*, TDP43 MEFs were grown for RNA and protein harvest (n = 3:3:3 per genotype). The RNA was converted to cDNA and primers were designed to assess *Tardbp* transcript splicing and levels (through PCR and real time PCR).

NMD2 (*Tardbp* targeted) primers were designed to amplify transcript *Tardbp*-001 (1106bp) and *Tardbp*-002 (147 bp). NMD2 stands for nonsense mediated decay and these primers were designed to amplify *Tardbp* translation and degradation transcripts based on a proposed

model of degradation (Polymenidou *et al.*, 2011). Although the amplicon lengths between the two transcripts are significantly different, the aim was to compare the ratio of the two bands between wild-type, heterozygous and homozygous MEFs to assess potential differences in transcript lengths (Figure 5.7).
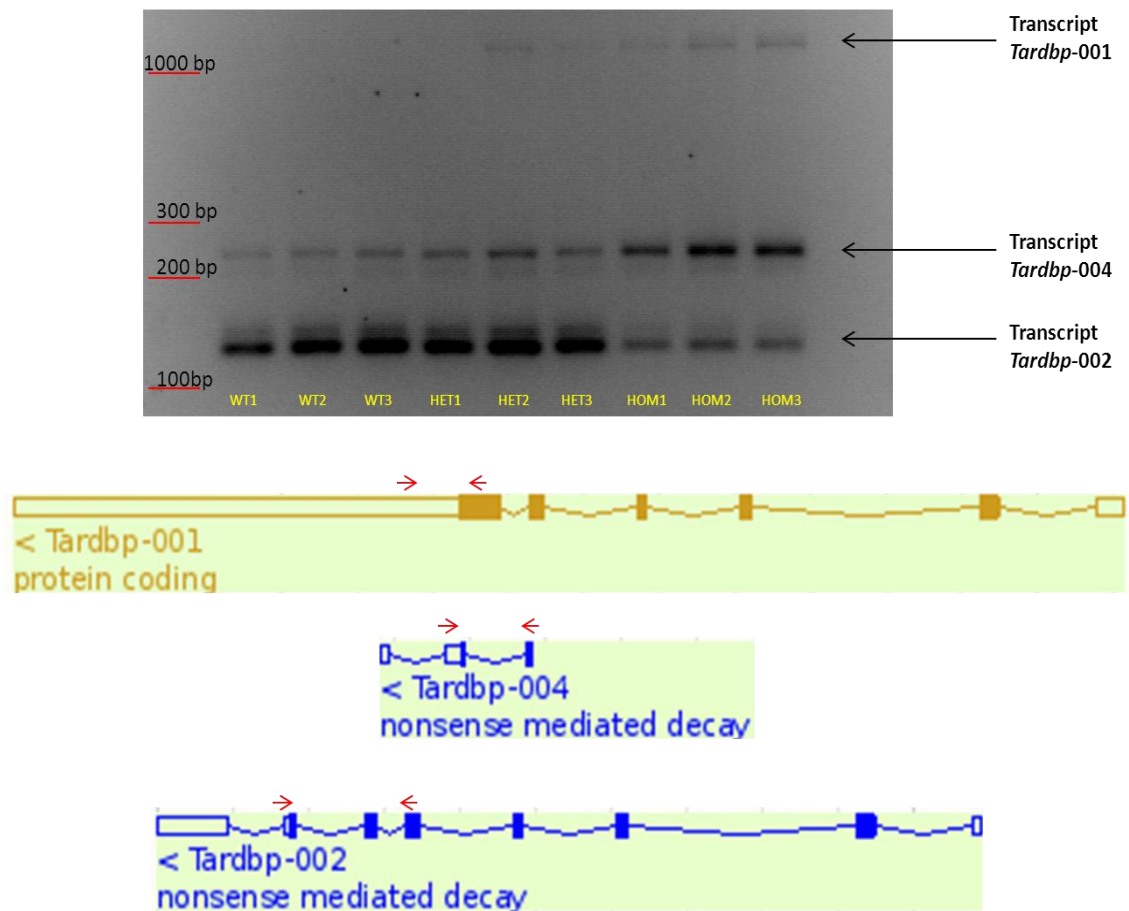
Figure 5.7: NMD2 primer amplification in MEFs. RNA harvested from WT, heterozygous and homozygous F210I MEFs, was converted to cDNA and amplified using primers NMD2. PCR product was run on a 3.5% NuSieve 3:1 agarose gel, stained with ethidium bromide. Expected amplification products include *Tardbp*-001 at 1106 bp and *Tardbp*-002 at 147 bp. A further PCR product was observed at 250 bp, which was gel purified with Sanger sequencing identifying an annotated transcript, *Tardbp*-004. Transcript schematic taken from www.ensembl.org showing NMD2 primer locations (red arrows) for each of the amplified transcripts.

There is an increase in the presence of transcript *Tardbp*-002 in heterozygous and wild-type MEFs compared to homozygous MEFs. This increase is not fully quantitative due to the nature of the PCR however it is qualitative (as equal amounts of cDNA were used in the PCR). Transcript *Tardbp*-001 is not present in high abundance. This is due to the transcript being too large and unable to compete with the smaller amplification products. There is some detection of *Tardbp*-001 in the homozygote samples and potentially some heterozygote samples. The

NMD2 primers also amplified an intermediary band at 250 bases. This band was gel purified and sent for Sanger sequencing (by GATC). Alignment of the sequence with the annotated transcripts on www.ensembl.org showed that this is a small annotated non coding transcript, *Tardbp*-004. This amplified transcript was not identified by similarly positioned primers in other studies (Polymenidou *et al.*, 2011) due to the exact positions of the primers.

RNA was also extracted from embryonic head (E14.5 dpc) and 12 week old adult brain. Reverse transcription PCR using NMD2 primers with these samples showed the presence of transcript *Tardbp*-002 however there was almost no detection of transcript *Tardbp*-001 at 1106 bp (Figure 5.8) or transcript *Tardbp*-004.
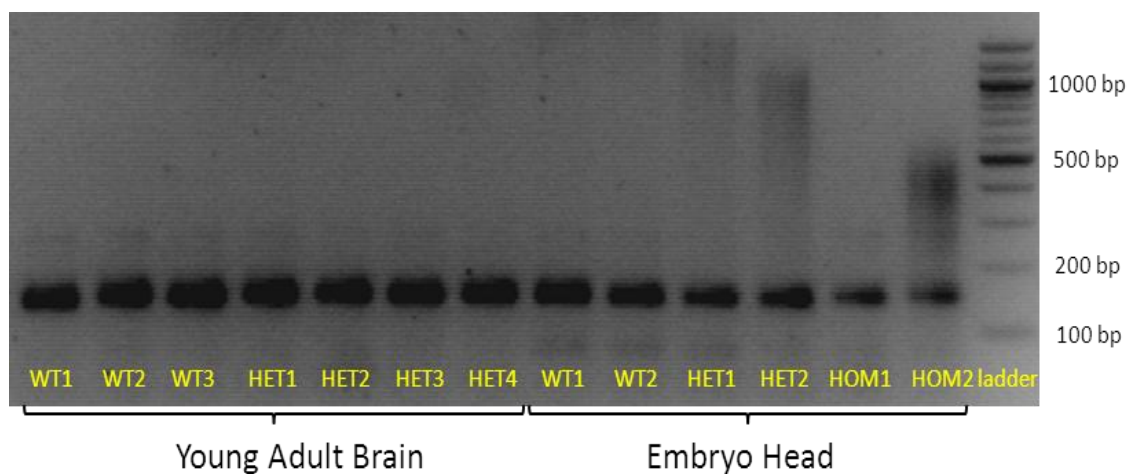
Figure 5.8: NMD2 primer amplification in embryonic head and adult brain. As in Figure 5.7, cDNA generated from RNA extracted from embryonic head and adult brain was amplified in a PCR using NMD2 primers. PCR product was run on 3.5% NuSieve 3:1 agarose gel. *Tardbp*-002 is detected at 147 bp, with *Tardbp*-001 at 1106 being undetected.

Transcript *Tardbp*-002, at 147 bp, is present in wild-type, heterozygous and homozygous samples in MEFs, embryonic head and adult brain (Figure 5.7 and Figure 5.8). In Figure 5.8, there is a trend for increasing band intensity from homozygous to heterozygous and wild-type samples for transcript *Tardbp*-002. This is also observed in MEFs (Figure 5.7). However in embryonic head and young adult brain, there is almost complete absence of transcript *Tardbp*-001, which was barely present in some homozygous and heterozygous samples in MEFs (Figure 5.7), likely due to it being too large to compete as a PCR with transcript *Tardbp*-002. Transcript *Tardbp*-004 observed in MEFs may be lowly present in E14.5 dpc head and adult brain (250bp band in Figure 5.8).

In order to further characterize alterations in TDP43 encoding transcripts, real time PCR was completed on cDNA extracted from wild-type, heterozygous and homozygous embryonic head (n = 5:5:5 per genotype). Primers in *Tardbp* exons 2 (F) / 3 (R) were used to assess levels of all mRNA transcripts containing these exons. This was quantified against control gene *S16*, a ribosomal protein whose levels have never been shown to be altered by the effects of TDP43 knock down in any known publication. The primers were assessed prior to the experiment for optimal amplification efficiency without significant differences between the *Tardbp* and *S16* primers. Exon 2F / 3R *Tardbp* primer based amplification showed significant differences in levels between wild-type, heterozygous and homozygous samples (Figure 5.9).
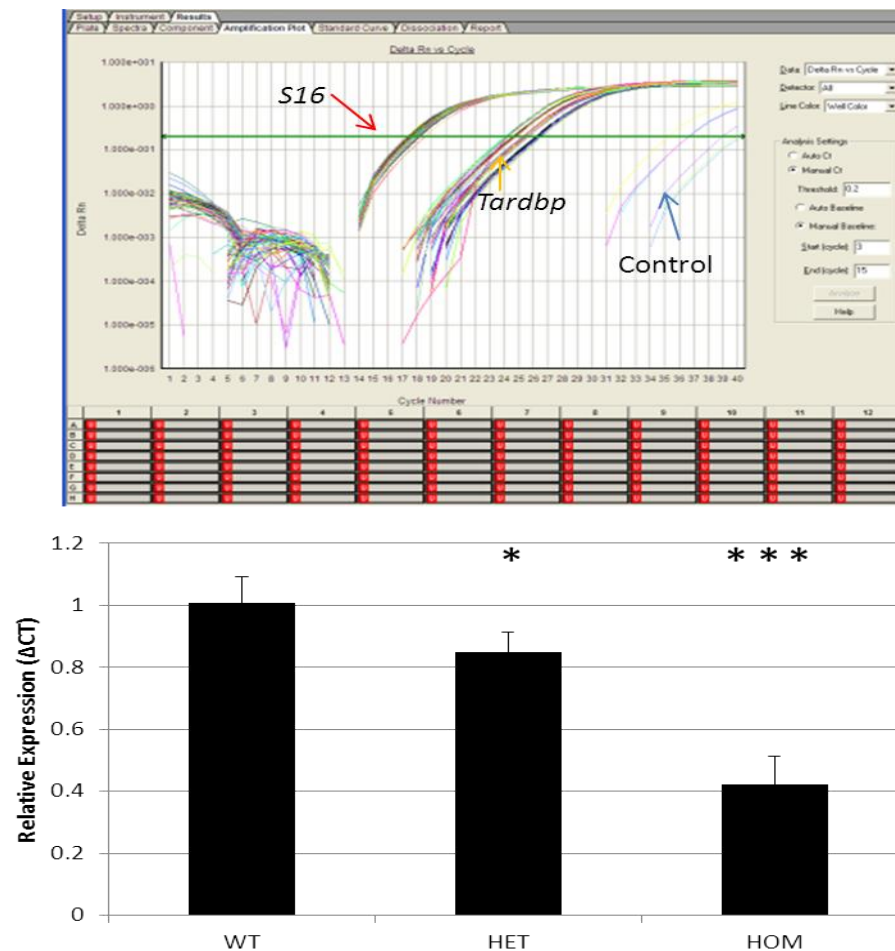
Figure 5.9: *Tardbp* **exon 2F / 3R real time PCR from E14.5 dpc embryonic head**. Top panel: Window from Applied Bio systems real time PRC programme, showing PCR amplification run as measured by SYBR Green. Red arrow shows *S16* amplification, yellow arrow shows *Tardbp* amplification and blue arrow shows control samples with no RNA used in RT reaction and H$_2$O controls. All samples were run in triplicate with a 0.1 CT value replication range, showing a consistent level of pipetting. Bottom panel: bar chart showing the relative levels of WT, heterozygous and homozygous exon 2-3 transcript levels as calculated from the CT values by ΔΔCT (n = 5:5:5). WT versus heterozygous p = 0.027, WT versus homozygous p < 0.0001, ANOVA with Bonferroni post hoc analysis. Error bars shown are standard deviation.

Levels of exon 2F / 3R *Tardbp* transcripts are significantly reduced in heterozygous and homozygous embryonic head (Figure 5.9). Heterozygous exon 2F / 3R transcript is significantly lower than wild-type levels, 1.00 versus 0.85 ($p = 0.027$, ANOVA Bonferroni post hoc) with homozygous levels highly reduced, 1.00 versus 0.422 ($p < 0.001$, ANOVA Bonferroni post hoc).

With significant differences in *Tardbp* RNA transcript exon 2F / 3R levels, protein levels were assessed. Initially, protein was extracted from wild-type, heterozygous and homozygous MEFs, n = 3:3:3 per genotype (Figure 5.10).
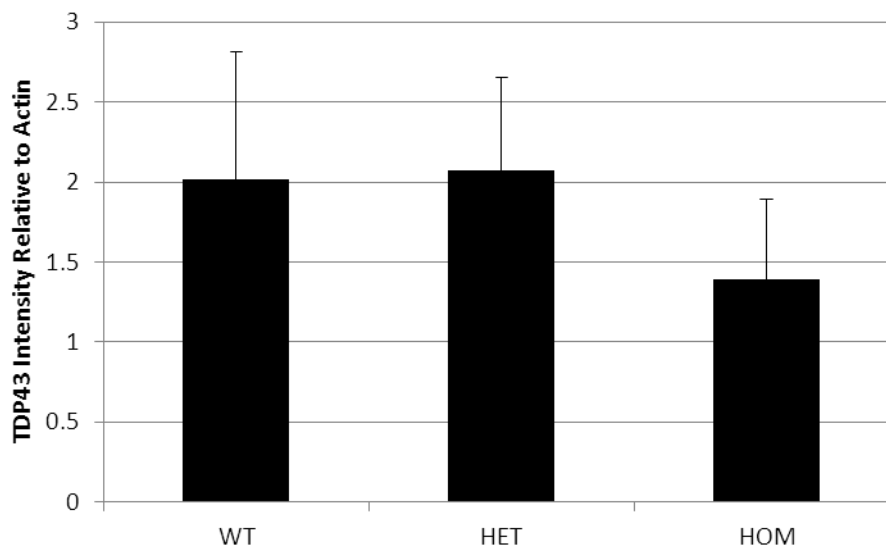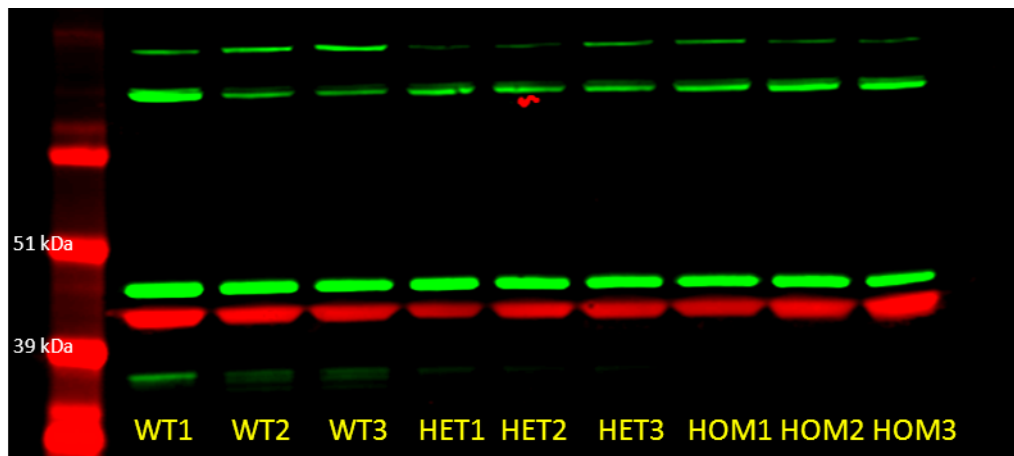
Figure 5.10: TDP43 F210I protein levels in MEFs. Western blot analysis was carried out by electrophoresis on Invitrogen 10% bis-tris gels and transferred onto low fluorescence PVDF membrane (IPFL10100 Millipore).Top panel: Western blot image taken on Li-Cor Odyssey system, with anti-TDP43 (ProteinTech) in green, and anti-actin (Invitrogen) in red, detected by anti-mouse red secondary and anti-green rabbit secondary (Li-Cor). Bottom panel: quantification of TDP43 levels as measured by Odyssey software, relative to actin levels. There are no significant differences in TDP43 soluble levels, WT versus homozygous p = 0.817 (ANOVA Bonferroni post hoc). Error bars represent standard deviation.

Figure 5.10 shows no significant difference in protein levels between wild-type, heterozygous and homozygous MEFs. Further protein was extracted from new wild-type, heterozygous and homozygous MEF samples (n = 5:5:4 per genotype) and 12 week old adult brain (Figure 5.11) as there was a potential trend to a reduction in homozygous levels.
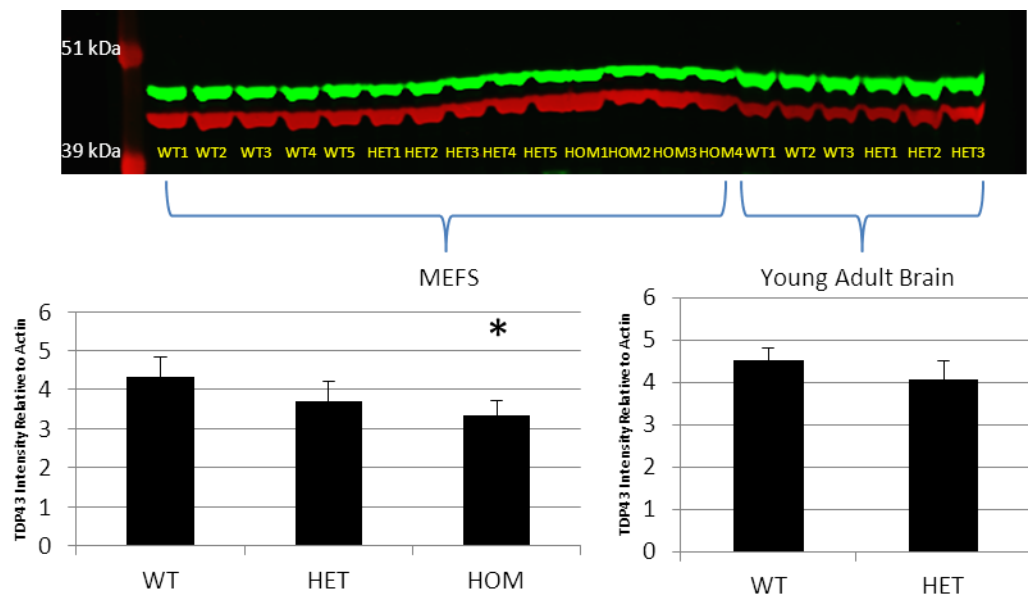
Figure 5.11: F210I protein levels in MEFs and adult brain. Western blot was run on an Invitrogen 10% bis-tris gel and transferred onto low fluorescence PVDF membrane. Top panel: Western blot image taken using Li-Cor Odyssey system. Green = anti-TDP43 (ProteinTech), Red = anti-actin (Invitrogen), using Li-Cor secondary antibodies. Band intensity was measured using Odyssey software, with TDP43 levels (relative to actin) shown in bar charts. In MEFs, WT versus homozygous TDP43 levels are significantly different: p = 0.033, with a trend in WT versus heterozygous p = 0.22 (ANOVA Bonferroni post hoc). There is no significant difference in WT versus heterozygous adult brain levels (p = 0.22). Error bars show standard deviation.

Figure 5.11 shows that there is a significant difference in TDP43 protein levels in wild-type versus homozygous MEFs (p = 0.033 ANOVA Bonferroni post hoc). There is also a trend to reduced levels in heterozygous MEFs (p = 0.22) There are no significant differences in adult brain when comparing wild-type versus heterozygous adult brain (p = 0.22, Students two tailed T test).

With significant differences observed in MEFs, using aliquots from the same extracted samples; this result was repeated. However, no significant difference in protein levels was observed (Figure 5.12). These samples were re-run five times, however there was no replicated difference between wild-type, heterozygous and homozygous TDP43 protein levels.

Figure 5.12 shows one of multiple repeats aimed at determining whether there is significant difference in F210I TDP43 protein levels.
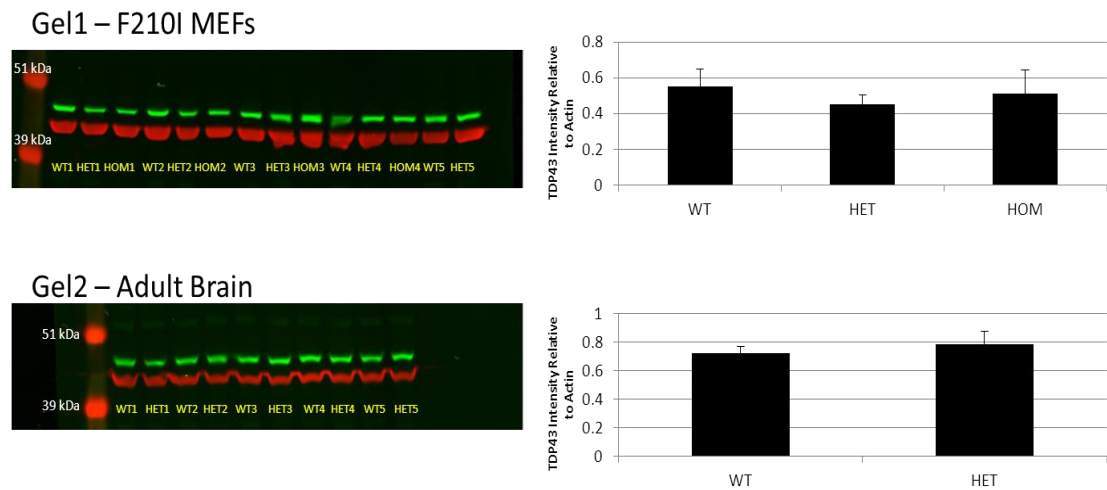
Figure 5.12: F210I Western repeat. Repeated Western blot from Figure 5.11 with additional adult brain samples. In MEFs, protein levels are not significantly different when normalized against actin (Gel 1). WT versus heterozygous p = 0.358, WT versus homozygous p = 1 (ANOVA Bonferroni post hoc). Adult brain protein levels were re-run with brains from two additional mice per genotype, however there is no significant difference in TDP43 protein levels, p = 0.24 (students two tailed T test, gel 2). Error bars show standard deviation.

5.8.   TDP43 target splicing changes

TDP43 down regulation affects approximately 30% of the murine transcriptome (Polymenidou *et al.*, 2011) through direct and indirect mechanisms. When knocked down in mouse adult brain, the splicing pattern of approximately 965 mRNAs is altered. With these changes having been characterized, the aim was to assess whether F210I is strongly hypomorphic and mimics the changes that occur when TDP43 is knocked down.

Primer sequences from the Cleveland laboratory (Polymenidou *et al.*, 2011) were requested and ordered. Genes selected were Pyruvate dehydrogenase phosphatase catalytic subunit 1 (*Pdp1*), DnaJ (Hsp40) homolog, subfamily C, member 5 (*Dnajc5*), Polymerase (DNA-directed), delta interacting protein 3 (*Poldip3*) and Sortilin 1 (*Sort1*). These genes show large differences in splicing when TDP43 is knocked down. RNA was extracted from wild-type, heterozygous and homozygous E14.5 dpc head and converted to cDNA for PCR as described in methods. The results showed that there are significant differences in splicing patterns of all genes assessed, where the ratio of the spliced band was in a reasonable range to detect differences. They are

all differentially spliced in E14.5 dpc head in F210I mutants, compared to wild-type controls (Figure 5.13, Figure 5.14, Figure 5.15 and Figure 5.16).

Figure 5.13 shows that the ratio of *Pdp1* splicing is different when comparing MEFs to adult brain. TDP43 promotes exon 1 inclusion and when knocked down there is more exon 1 exclusion. In heterozygous E14.5 dpc head there is a strong trend towards more exon 1 exclusion (p = 0.073 ANOVA Bonferroni post hoc). This is clearly visualized when assessing the excluded band which is more faintly present in the heterozygous lanes compared to wild-type. This band is almost completely absent in homozygous samples which show a significant increase in the proportional amount of exon 1 inclusion (p < 0.001 ANOVA Bonferroni post hoc).

Figure 5.13: *Pdp1* **splicing in embryonic head**. Top panel is an image taken from (Polymenidou *et al.*, 2011), showing that when TDP43 is knocked down, there is more exclusion of *Pdp1* exon1. In the schematic, blue boxes show exons, orange box is the spliced exon and purple box indicates UG repeats where TDP43 may bind. Bar chart shows normal splicing pattern (blue bar) and TDP43 knocked down pattern (red bar). This change was seen in the F210I mutants, with a significant increase in exon 1 inclusion in homozygous embryo head (p < 0.001 Bonferroni post hoc). Heterozygous embryos show a trend to increased exon 1 inclusion (p = 0.073 ANOVA Bonferroni post hoc). Middle panel shows PCR product from identical primers to Don Cleveland's study, with exon included and excluded bands expected between 300 bp and 200 bp (methods contain exact amplicon lengths). Bar chart represents exon inclusion as a percentage of the total included versus excluded band intensity. Error bars represent standard deviation. N = 5:5:5.

The splicing pattern of *Dnajc5* is significantly different when comparing wild-type, heterozygous and homozygous embryonic head samples. Wild-type exon inclusion is 28.54%,

however this is significantly increased in both heterozygous (45.13%) and homozygous (76.19%) samples (wild-type versus heterozygous p = 0.005, wild-type versus homozygous p < 0.001 ANOVA Bonferroni post hoc). This matches the changes observed in adult brain knock down (Polymenidou *et al.*, 2011) showing that within E14.5 dpc heterozygous and homozygous head there is ineffective skipping compared to wild-type littermates as shown in Figure 5.14.
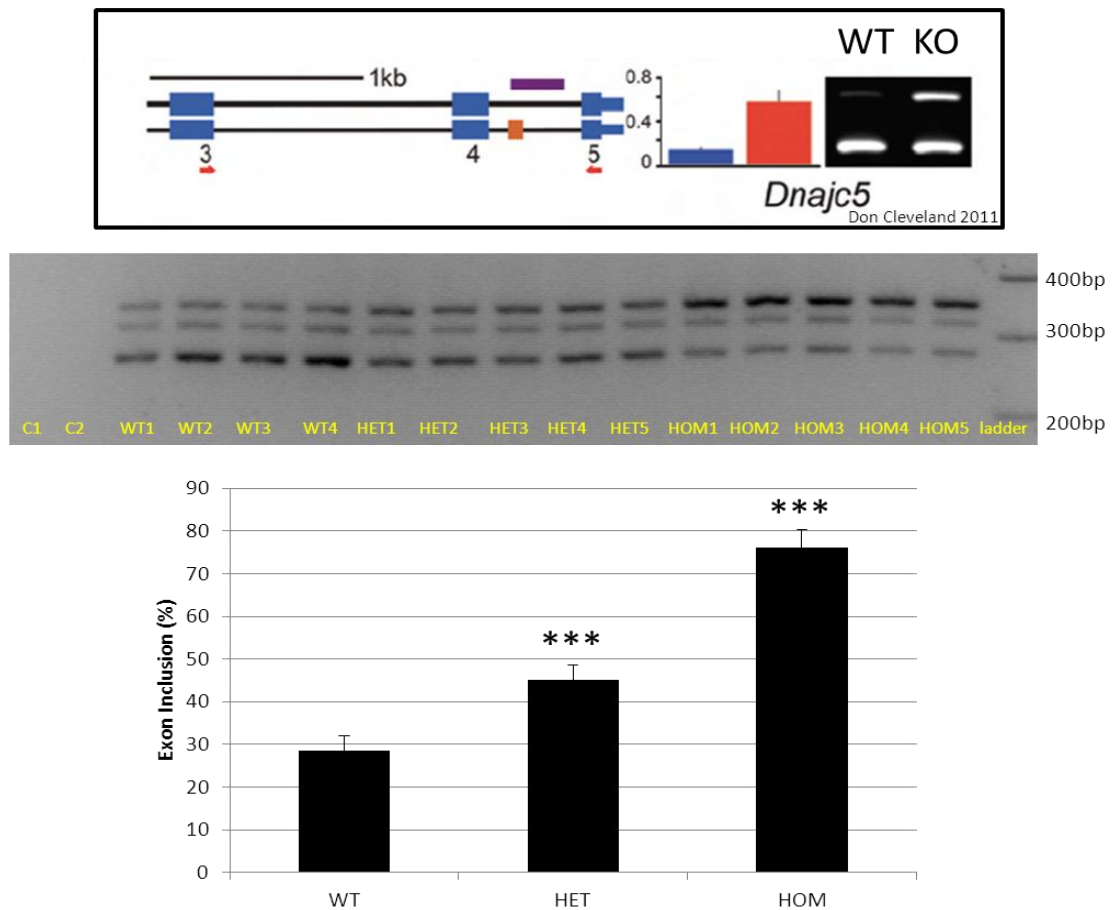
Figure 5.14: ***Dnajc5* splicing in embryonic head**. Top panel is an image taken from (Polymenidou *et al.*, 2011), showing that when TDP43 is knocked down, there is more inclusion of the partial exon between 4 and 5. This was also seen in the F210I mutants, with a significant increase in exon 4.5 inclusion in heterozygous and homozygous embryo head (WT versus heterozygous p = 0.005, WT versus homozygous p < 0.001 ANOVA Bonferroni post hoc). Bar chart represents exon inclusion as a percentage of the total included versus excluded band intensity. C1 is a control with no RNA used in the reverse transcriptase reaction and C2 is a PCR water control. Error bars represent standard deviation. N = 5:5:5.

TDP43 promotes *Poldip3* exon 3 inclusion in RNA transcripts. When knocked down, there is a loss in *Poldip3* inclusion in adult brain (Polymenidou *et al.*, 2011). In E14.5 dpc head, there is also a significant loss in exon 3 inclusion in heterozygous and homozygous samples (wild-type versus heterozygous p = 0.009, wild-type versus homozygous p < 0.0001 ANOVA Bonferroni post hoc, Figure 5.15). Heterozygous samples show an intermediary phenotype between wild-type and homozygous states.
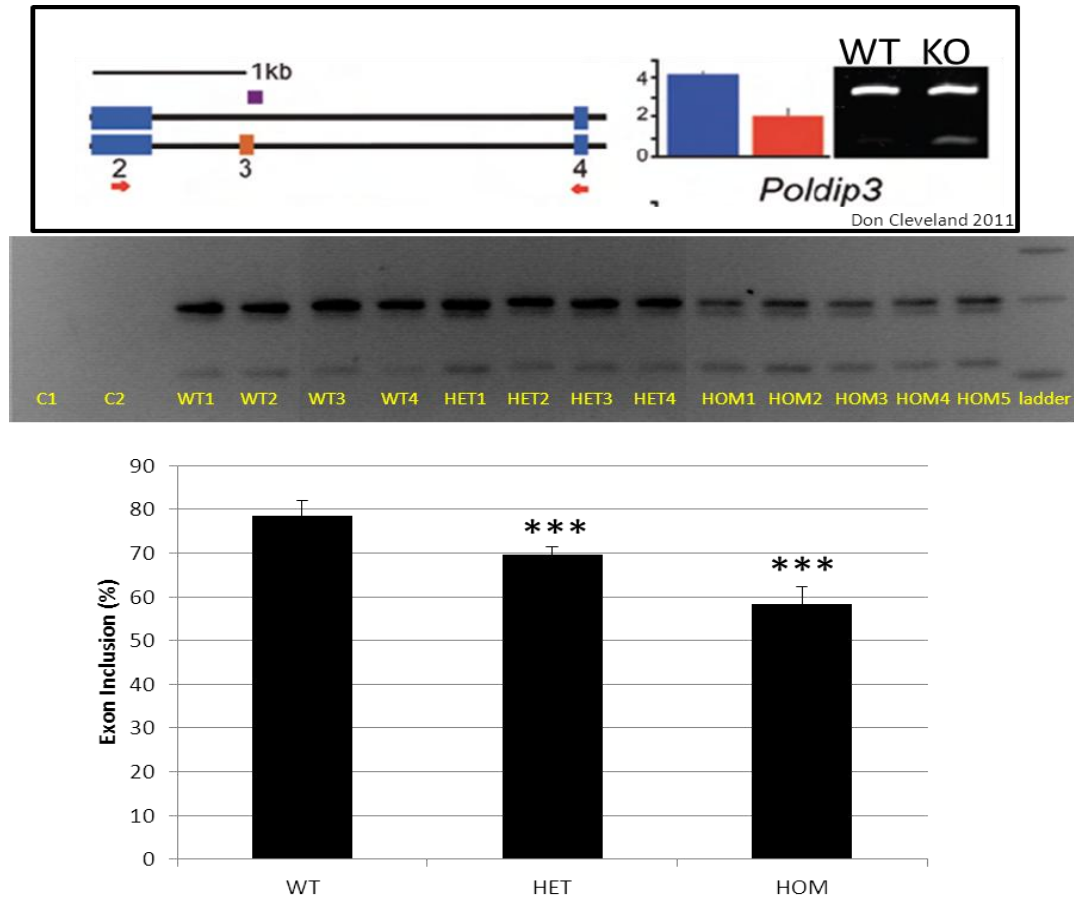
Figure 5.15: *Poldip3* splicing in embryonic head. Top panel is an image taken from (Polymenidou *et al.*, 2011), showing that when TDP43 is knocked down, there is more exclusion of exon 3. This was also seen in the F210I mutants, with a significant increase in exon 3 exclusion in heterozygous and homozygous embryo head (WT versus heterozygous p = 0.009, WT versus homozygous p < 0.0001 ANOVA Bonferroni post hoc). Bar chart represents exon inclusion as a percentage of the total included versus excluded band intensity. Error bars represent standard deviation. N = 4 WT: 4 heterozygote: 5 homozygote.

TDP43 promotes skipping of *Sort1* exon 18 (Polymenidou *et al.*, 2011). When assessed in F210I embryonic head, there is a significant decrease in exon 18 skipping in heterozygote and homozygote samples (p < 0.001 1 Way ANOVA Bonferroni post hoc, for both). In wild-type

head, exon 18 is included in 30.06% of mRNA transcripts, however in heterozygotes this increases to 65.28% and in homozygote samples it goes up to 92.00%. There is a striking difference in the splicing pattern with a dose dependent effect, matching the result from the Cleveland group (Figure 5.16).
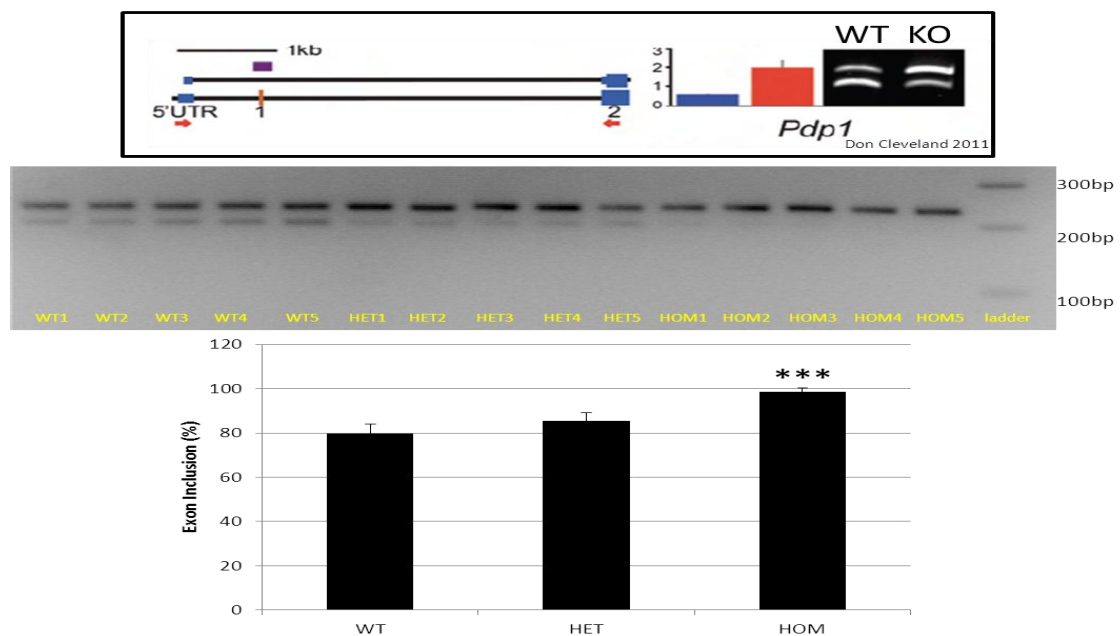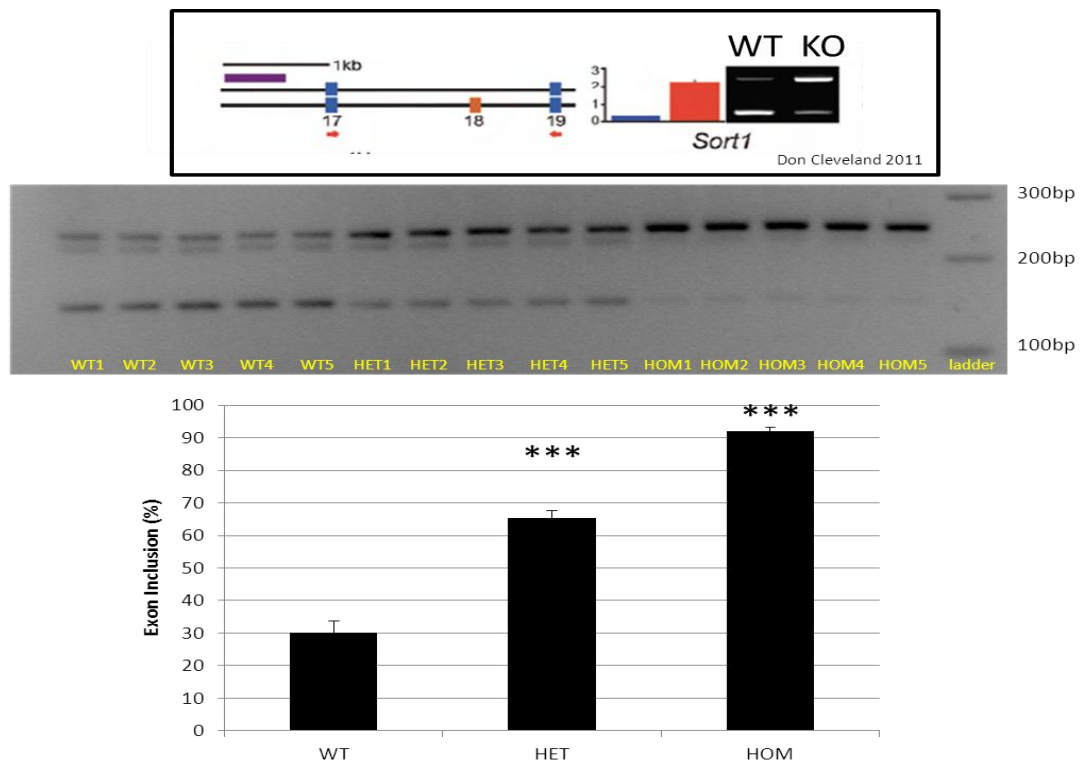

Figure 5.16: *Sort1* splicing in embryonic head. Top panel is an image taken from (Polymenidou *et al.*, 2011), showing that when TDP43 is knocked down, there is more inclusion of exon 18. This was also seen in the F210I mutants, with a significant increase in exon 18 inclusion in heterozygous and homozygous embryo head (p < 0.001 for both ANOVA Bonferroni post hoc). Bar chart represents exon inclusion as a percentage of the total included versus excluded band intensity. Error bars represent standard deviation. N = 5:5:5.

Sort1 exon skipping is reduced in F210I heterozygous and homozygous E14.5 dpc head. To assess whether this loss of skipping occurs in other tissues, MEFs and adult brain samples were harvested. RNA was extracted from MEFs and adult brain using the same protocol as embryonic head. Results show that *Sort1* exon inclusion in MEFs and adult brain is significantly higher in heterozygous and homozygous F210I (Figure 5.17 and Figure 5.18).
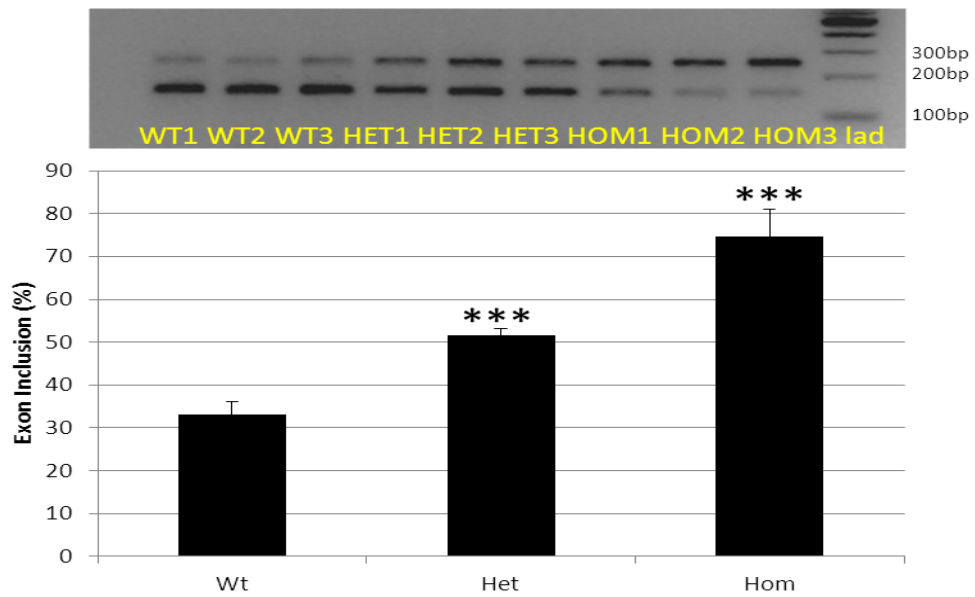
Figure 5.17: *Sort1* splicing in MEFs. Top panel shows reverse transcription PCR using *Sort1* primers to amplify exon 18 included / excluded transcripts. Heterozygous and homozygous F210I MEFs show significantly increased exon 18 inclusion as shown relatively by the bar chart, representing percentage of total exon inclusion. Bands were measured using ImageJ software. Error bars show standard deviation. N = 3:3:3.

Sort1 splicing assessed in MEFs (Figure 5.17) shows a similar pattern to E14.5 dpc head (Figure 5.16). Wild-type exon inclusion (33.19%) increases to 51.58% in heterozygous and 74.54% in homozygous MEFs (p < 0.001 ANOVA Bonferroni post hoc). This altered splicing is also observed in adult F210I brain (Figure 5.18).
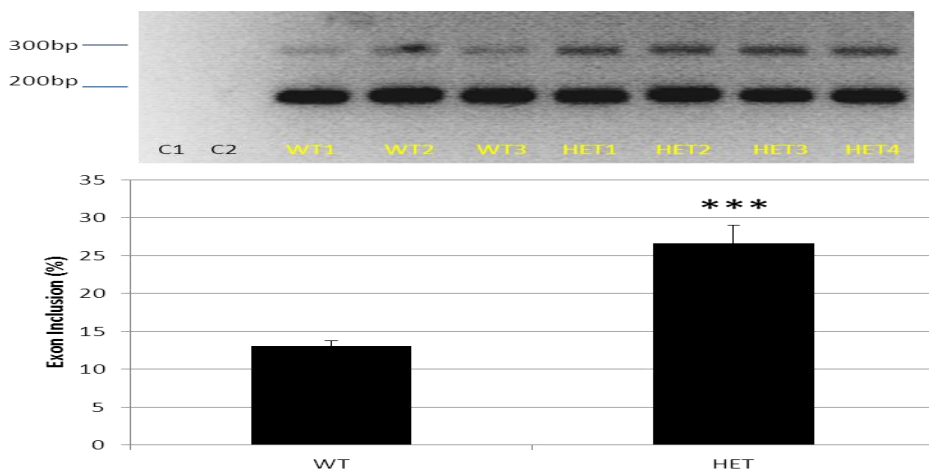
Figure 5.18: *Sort1* splicing in adult brain. Top panel shows reverse transcription PCR using primers to amplify exon 18 included / excluded transcripts. C1 and C2 are controls with no RNA used in the reverse transcription reaction and water used in PCR reaction. Heterozygous F210I splicing in adult brain (12 weeks) is significantly increased as shown relatively by the bar chart. Bands were measured using ImageJ software. Error bars show standard deviation. N = 3 WT: 4 heterozygotes.

As shown in Figure 5.18, heterozygous F210I adult brain shows increased levels of *Sort1* exon 18 included transcript. Compared to wild-type littermate levels (13.06%), proportional levels in heterozygous brains are 26.56% (p < 0.001 students two tailed T test). In brain, the exon excluded transcript is dominantly present; this remains as a significant increase in heterozygous brains of over 10%.

5.9.   TDP43 target RNA level changes

Alongside assessing changes in splicing patterns for TDP43 target genes, changes in mRNA levels were also assessed. Knock down of TDP43 in adult striatum leads to alterations in the levels of 601 mRNAs, as determined by RNA sequencing (Polymenidou *et al.*, 2011). To address this in the context of F210I, genes were chosen with large differences or those relevant to amyotrophic lateral sclerosis (ALS). Fused in sarcoma (*Fus*), progranulin (*Grn*), Ca^{++}-dependent secretion activator (*Cadps*) and cyclin dependent kinase 6 (*Cdk6*) were all assessed. *Fus*, *Grn*, and *Cadps* were chosen as they have been shown to be highly altered by the Cleveland lab, with *Fus* and *Grn* being especially relevant to TDP43 pathology. *Cdk6* was chosen as knock down of TDP43 in HeLa cells altered *Cdk6* levels ten-fold (Ayala *et al.*, 2008a).

Mutations in *FUS* are causative of ALS (Kwiatkowski *et al.*, 2009; Vance *et al.*, 2009). When TDP43 is knocked down (Polymenidou *et al.*, 2011) levels of *Fus* mRNA are reduced to half of those in wild-type brain. As a result, *Fus* levels were assessed by real time PCR in E14.5 dpc head from wild-type, heterozygous and homozygous F210I embryos (Figure 5.19). Real time PCR shows no significant differences in the relative expression of *Fus* in any genotype. Relative expression remains consistent at approximately wild-type levels.

Fus mRNA quantitative PCR
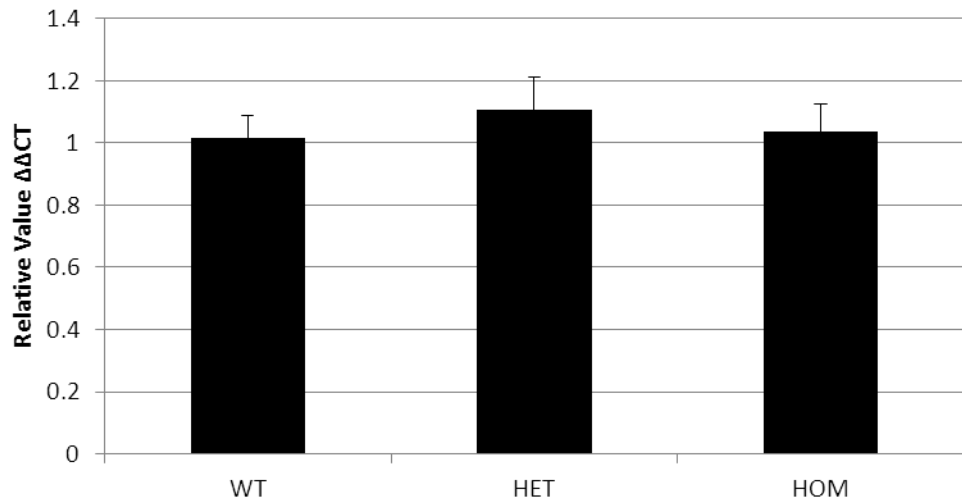
Figure 5.19: *Fus* **RNA expression**. Transcript levels of *Fus* were determined in WT, heterozygous and homozygous E14.5 head (n = 5:5:5 per genotype). Bar chart shows relative expression following real time PCR, through calculating ΔΔCT values. Control gene was *S16*. There is no significant difference in the relative expression of *Fus* between WT, heterozygous and homozygous E14.5 dpc head (p > 0.05 ANOVA Bonferroni post hoc). Error bars show standard deviation.

Grn levels were also assessed by real time PCR. When TDP43 is knocked down in adult striatum, *Grn* mRNA levels increase six-fold. However, in F210I embryonic head, there is a trend to reduced levels of *Grn* (wild-type versus heterozygous p = 0.187, wild-type versus homozygous p = 0.386, ANOVA Bonferroni post hoc) (Figure 5.20). *Grn* levels in heterozygous and homozygous F210I embryonic head appear to show a trend which opposes the expected response to TDP43 knock down in striatum.

Grn mRNA quantitative PCR
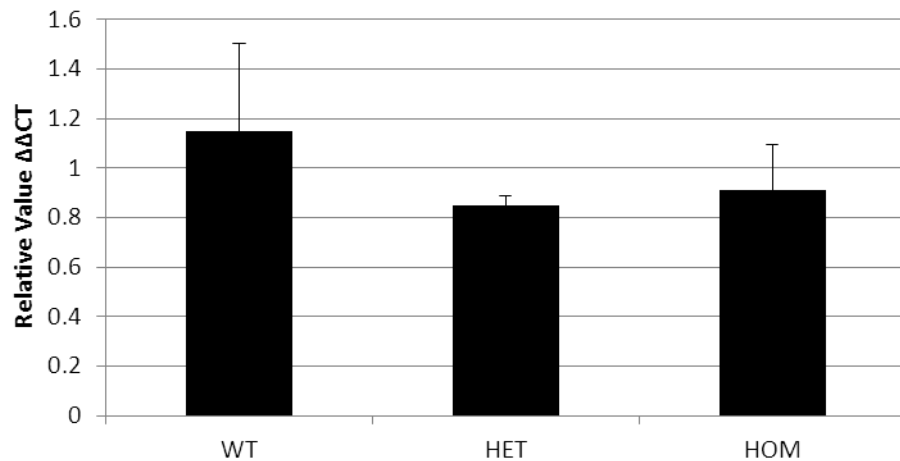
Figure 5.20: *Grn* RNA expression. Transcript levels of *Grn* were determined in WT, heterozygous and homozygous E14.5 head (n = 5:5:5 per genotype). Bar chart shows relative expression following real time PCR, through calculating ΔΔCT values. Control gene was *S16*. There is no significant difference in the relative expression of *Grn* between WT, heterozygous and homozygous E14.5 dpc head. Error bars show standard deviation.

Cadps mRNA levels decrease versus wild-type, when TDP43 is knocked down (Polymenidou *et al.*, 2011). Levels were assessed in F210I wild-type, heterozygous and homozygous embryonic head with a significant decrease in homozygous head versus wild-type (Figure 5.21).

Cadps mRNA quantitative PCR
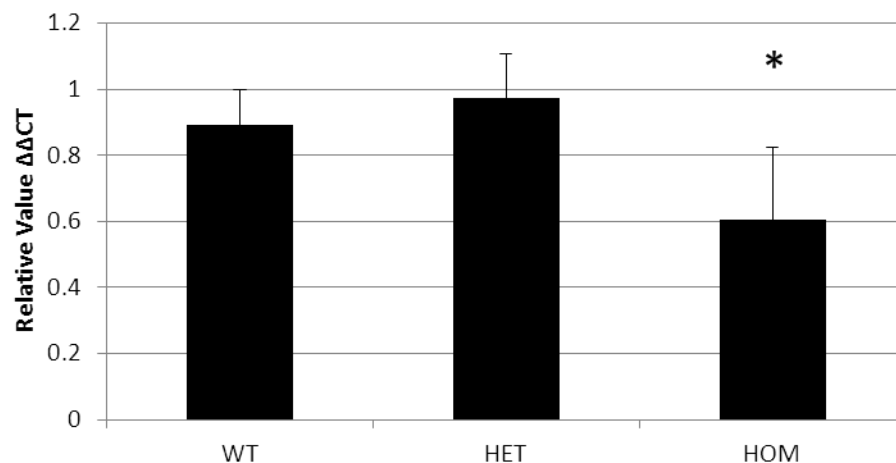
Figure 5.21: *Cadps* RNA expression. Transcript levels of *Cadps* were determined in WT, heterozygous and homozygous E14.5 head (n = 5:5:5 per genotype). Bar chart shows relative expression following real time PCR, through calculating ΔΔCT values. Control gene was *S16*. Error bars show standard deviation.

Cadps levels are significantly reduced in homozygous versus wild-type head (p = 0.046, ANOVA Bonferroni post hoc). Relative expression decreases from 0.89 in wild-type, to 0.60 in

homozygous samples. This reduction is mild compared to the decrease observed in TDP43 knocked down striatum (Polymenidou *et al.*, 2011).

Having assessed three targets identified in mouse TDP43 knock down, an alternative target observed in HeLa cells was assessed (Ayala *et al.*, 2008a). Upon TDP43 depletion in HeLa cells, levels of *Cdk6* increase tenfold. This was assessed in F210I MEFs. Figure 5.22 shows that there is no significant difference in *Cdk6* mRNA levels between wild-type and F210I mutant embryonic head. However, there is a trend to increasing *Cdk6* levels in homozygous versus wild-type embryonic head (p = 0.16, ANOVA Bonferroni post hoc) which would mimic the human cellular based result (Ayala *et al.*, 2008a).
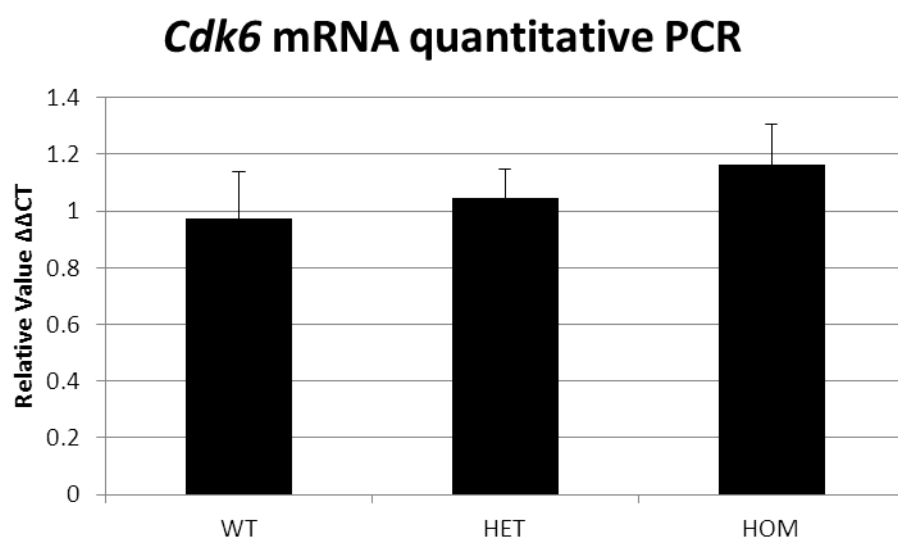
Figure 5.22: *Cdk6* **RNA expression**. Transcript levels of *Cdk6* were determined in WT, heterozygous and homozygous E14.5 head (n = 5:5:5 per genotype). Bar chart shows relative expression following real time PCR, through calculating ΔΔCT values. Control gene was *S16*. There is no significant difference in the relative expression of *Cdk6* between WT, heterozygous and homozygous E14.5 dpc head, despite a potential trend for an increase in homozygous E14.5 head. Error bars show standard deviation.

Summary tables for TDP43 target splicing and level changes are given (Table 5.5 and Table 5.6).

Target Gene	Does TDP43 affect splicing	Does TDP43 promote exon skipping	Pheno in knockout	F210I Heterozygote Pheno	F210I Homozygote Pheno	Knock out system
Pdp1	Yes	Yes	Less skipping	Reduced skipping	Highly reduced skipping	ASO in mouse
Dnajc5	Yes	Yes	Less skipping	Reduced skipping	Highly reduced skipping	ASO in mouse
Poldip3	Yes	No	More skipping	More skipping	Highly increased skipping	ASO in mouse
Sort1	Yes	Yes	Less skipping	Reduced skipping	Highly reduced skipping	ASO in mouse

Table 5.5: TDP43 RNA targets - splicing. When TDP43 is knocked down, splicing changes observed are all matched in heterozygote and homozygote F210I samples which are hypomorphic for splicing function. In all genes assessed, heterozygote samples show an intermediate loss of function and homozygote samples show a more extreme loss of function.

Target Gene	Does TDP43 affect levels	Does TDP43 stabilize / destabilise RNA	Pheno in knockout	F210I Heterozygote Pheno	F210I Homozygote Pheno	Knock out system
Fus	Yes	stabilize	Reduce to 0.5	No change	No Change	ASO in mouse
Grn	Yes	destabilize	6 fold increase	No change (trend to reduce)	No change (trend to reduce)	ASO in mouse
Cadps	Yes	stabilize	Reduce to 0.32	No change	Reduce to 0.67	ASO in mouse
Cdk6	Yes	destabilize	10 fold increase in cells	No change	No change (trend to increase)	siRNA in HEK293 cells

Table 5.6: TDP43 RNA targets – mRNA levels. Shows the effects of F210I on target mRNA levels, as determined by quantitative real time PCR. Changes in target genes do not generally match changes in knock down systems. However, changes in *Cadps* and *Cdk6* homozygotes trend towards loss of function, matching the knock down models.

5.10. Results discussion

Overall, the work in this chapter confirms the F210I *in vitro* loss of RNA-binding function *in vivo*, showing that F210I is a strongly hypomorphic allele affecting TDP43's roles in RNA metabolism. Changes in *Tardbp* transcripts show F210I to be an *in vivo* tool that will be used to delineate the mechanisms of auto-regulation. Significantly large alterations are observed in splicing and may be detected to varying degrees in other TDP43 functions.

CFTR splicing assessment in MEFs

In Chapter 4, the identification of F210I was described *in vitro* as being unable to promote efficient mini-gene CFTR exon 9 skipping with highly reduced UG_6 RNA-binding. The aim of the work described in this chapter was to characterise whether this deficit translated *in vivo* and to characterise the mutation in heterozygous and homozygous forms whilst generating a colony for phenotypic assessment.

In order to confirm the *in vitro* results from Chapter 4, wild-type, heterozygous and homozygous MEFs were cultured and electroporated with the CFTR mini-gene. Results showed a clear loss of exon skipping ability in heterozygous and homozygous MEFs with a dosage effect. Wild-type levels of exon inclusion (54.05%) significantly increased in heterozygous (67.71%) and homozygous (94.85%) MEFs (Figure 5.2). The homozygous MEFs show almost no exon 9 skipping with heterozygous MEFs showing an intermediary phenotype.

The add-back assay in HeLa cells implied an approximate 50% reduction in the ability of F210I to promote exon 9 skipping. This was calculated based on wild-type recovery as the maximum baseline for exon 9 skipping and F147L / F149L skipping as complete loss of function, due to complete loss of RNA-binding. The observed result *in vitro* is much more severe in homozygous MEFs *in vivo*, where the amount of exon skipping at 94.85% is more similar to the F147L / F149L complete loss of function. The differences observed between the *in vitro* and *in vivo* results are likely to be the result of the signal to noise ratio within the two systems. The *in vitro* study is likely to be noisier considering the added complexity of siRNA and co-transfection. With a more extreme loss of function shown *in vivo*, all mutations from the allelic TDP43 ENU allelic array should be assessed in MEFs, to address more sensitively whether there is a functional deficit in any of these mutations for RNA based functions. This would be more

accurate than the HeLa assay. However, this experiment is practically limited by re deriving the mice carrying these mutations to generate the MEFs.

MEFs immunofluorescence

Having confirmed the *in vitro* results from Chapter 4 *in vivo*, MEFs were stained with anti-TDP (ProteinTech) and DAPI to compare protein localisation. Confocal microscopy (Figure 5.3) showed no overt differences in the subcellular distribution of TDP43 in wild-type, heterozygous and homozygous F210I MEFs. This matches the overexpression results in HeLa cells (Chapter 4, Figure 4.6), implying no overt effects on protein localisation caused by F210I. As discussed in Chapter 4, sub nuclear localisation has not been assessed. This result shows that alterations in RNA-binding are not due to protein mislocalisation to the cytoplasm.

F210I homozygote viability

Alongside MEF characterisation, matings were also established to assess homozygous F210I mouse viability. Results show that homozygous F210I mice are not viable (Table 5.1). Dissections at E14.5 dpc show that at this stage of development, homozygous embryos remain alive; however all observed showeded overt phenotypes indicating that they will not survive to birth. Homozygous embryos are typically a third smaller in size than littermate heterozygous and wild-type embryos, all displaying oedema (particularly visible as spino-oedema). Other phenotypes (holoprosencephaly and less developed eyes) have also been observed with low penetrance. All major organs assessed appear normally formed and importantly, without obvious developmental delay, but they are smaller. Further investigation into the cause of lethality is required by assessing homozygous embryos through developmental time points (from E10.5 dpc to E18.5 dpc) to characterise the changes that occur through time. Delineating a potential cause of death is potentially difficult considering the diversity of interactions and roles TDP43 appears to have. Arguably, affecting 30% of the murine transcriptome would provide multiple potential mechanisms through which F210I TDP43 could be inducing homozygote lethality. Although oedema is preliminarily the consistently observed phenotype in homozygous E14.5 dpc embryos, further assessment is required. Determining to what stage some survive is required alongside continued dissections to establish the frequency of phenotypes observed.

Many F210I homozygous mutants remain alive at E14.5 dpc, which is significantly later than TDP43 knock out mouse models and the Q101X homozygotes, which die between E3.5 to E6.5 dpc (Kraemer *et al.*, 2010; Sephton *et al.*, 2010). In these models which have early lethality, there is a complete loss of TDP43 function. F210I is strongly hypomorphic for RNA-binding as described throughout Chapter 4 and this Chapter. Assuming there is no gain of function associated with F210I, the differences in which F210I and Q101X survive in embryonic development are likely to be the result of the degree of loss of function. Q101X likely results in 100% loss of RNA-binding function as with knockouts, confirming TDP43 function is required in the early stages of development up to E6.5 dpc. However, F210I homozygotes, while showing a strong loss of function in CFTR mini-gene splicing and endogenous target splicing, are able to proceed in development until at least E14.5 dpc. From *in vitro* band shift results, a strong loss of RNA-binding is expected *in vivo*, potentially driving the described results in this chapter. With a strong loss of RNA-binding function, F210I homozygous embryos continue in development beyond knockout and Q101X lethal stages remaining alive. The presence of F210I protein versus its absence in the knockout may be necessary with a non RNA-binding function being required during early development. Alternatively, the minimal RNA-binding from F210I may be enough to proceed in early embryonic development.

Observed F210I mutant numbers

F210I homozygous mice are not viable. From heterozygous inter crosses; the numbers of heterozygous mice genotyped trends towards not being double the wild-type number. When assessing the ratio of heterozygous versus wild-type mice with male heterozygous F210I mice crossed to wild-type C57BL/6J female mice, the ratio of born mice is not significantly different to the expected 1:1. This result shows that in heterozygous inter crosses, homozygous mice are not viable and there is a trend towards heterozygous mice not being born at the expected ratio of 2:1 versus wild-type. This could imply some maternal driven interaction for heterozygous females and their litters, as when heterozygous males are crossed to wild-type females, the expected ratio of genotypes 1:1 is observed. In order to further determine a maternal genotype interaction, the ratio of mice born from female F210I heterozygotes crossed to male wild-type mice could be assessed. Overall, this is a preliminary result and the numbers need to be increased.

Q101X / F210I rescue attempt

Although there is strong data for F210I being hypomorphic for RNA-binding function, there remains the possibility that F210I may confer elements of gain of function. In an attempt to rescue F210I homozygote lethality and address a potential gain of function, compound mutants between F210I and Q101X were generated. This cross also provides an *in vivo* model in which to assess F210I auto-regulation in the context of the Q101X allele. It was anticipated that in the Q101X allele context, the F210I allele may be expressed at a lower level, if it is not efficiently able to auto-regulate. A reduction in a potential toxic gain of function allele may reduce the toxicity in the developing embryo. Compound *Tardbp*$^{Q101X/F210I}$ mice are not viable (Table 5.3). Compound embryos were observed at E11.5 dpc (Table 5.4) however they were either dead or in an unhealthy condition, such that they would be resorbed. These preliminary results indicate that compound *Tardbp*$^{Q101X/F210I}$ mice die earlier than F210I homozygous embryos and that if the compound heterozygotes have reduced F210I levels versus F210I homozygotes, this may be the cause of earlier lethality. Embryos were kept for protein extraction. However, many of the compound heterozygotes (*Tardbp*$^{F210I/Q101X}$) were so small or at a resorption stage that extracting enough protein for analysis was challenging. This experiment could be completed by dissecting embryos at an earlier time point and pooling samples by genotype to extract enough protein. It is anticipated that *Tardbp*$^{F210I/Q101X}$ protein levels would be reduced compared to *Tardbp*$^{F210I/F210I}$ levels, which would confirm *in vivo* an auto-regulation deficit in F210I and also further support F210I loss of function driving embryonic lethality. In this case, the compound mutants dying earlier than F210I homozygotes would be explained by reduced TDP43 protein levels and increased loss of function. Further confirmation is required to support this hypothesis.

Auto-regulation in vivo

Assessment of *Tardbp* transcript splicing was next assessed *in vivo* from MEFs, embryonic head and adult brain. Figure 5.7 shows NMD2 primers designed to amplify full length transcript *Tardbp*-001 and nonsense mediated decay *Tardbp*-002, thought to be the full length encoding protein transcript and a nonsense mediated decay transcript respectively. According to one proposed model (Polymenidou *et al.*, 2011), if TDP43 binding to the 3' UTR CLIP identified sequence is required to convert transcript *Tardbp*-001 to *Tardbp*-002, then less *Tardbp*-002

should be present in F210I homozygous samples. TDP43 binds the 3' UTR CLIP identified sequence promoting the inclusion of an exon in the 3' UTR which forms transcript *Tardbp*-002 which is targeted for NMD. If F210I TDP43 does not promote this efficiently, less of this transcript will be present and more of the unconverted *Tardbp*-001 is expected, which would also result in increased protein levels. This expected pattern was observed with more of transcript *Tardbp*-002 (Figure 5.7 and Figure 5.8) being present in heterozygous and wild-type samples. This needs to be further quantitatively shown by designing real time primers amplifying each transcript specifically. Reciprocally, more of *Tardbp*-001 was expected in homozygous samples. In MEFs, there is a faint *Tardbp*-001 band present, which is absent in heterozygous and wild-type samples. With the amplicon length between the two transcripts being more than 800 bp, the amplification efficiency of this large transcript explains its poor presence, as the PCR for this band is unable to compete with the shorter bands. As a result, quantification of the bands relative to each other is not possible and this is further limited by the poor band intensity of *Tardbp*-001. This data implies that the transcript ratios in the F210I homozygotes match that of the proposed nonsense mediated decay auto-regulation model (Polymenidou *et al.*, 2011). However, the presence of the various transcripts is best quantified through Northern blotting or real time PCR. Assuming the Cleveland model is correct this result is expected to be driven by the binding of TDP43 to the 3' UTR CLIP identified sequence, which is significantly reduced by F210I *in vitro* with this result supporting this to be the case *in vivo*.

The NMD2 primers also amplified a third transcript, almost exclusively in the MEF samples. This transcript appears to increase in heterozygous and more so in homozygous MEFs compared to wild-type. The band was sequenced and identified as annotated transcript *Tardbp*-004, a short processed transcript. It contains elements of the 3'UTR and final exon encoding TDP43; however it has no characterised roles (as assessed at www.ensembl.org). RACE needs to be completed to determine whether the whole transcript in MEFs matches that which is annotated as well as its potential roles in MEFs. With increasing band intensity from wild-type through heterozygous to homozygous MEFs (although Figure 5.7 is not quantitative), this implies that the levels of this transcript are directly affected by the F210I mutation in a dose dependent manner in MEFs. Further experimentation would be required to examine the roles of this transcript in TDP43 auto-regulation and the relevance of tissue specific expression of the transcript.

The variation between transcript *Tardbp*-004 levels in wild-type, heterozygous and homozygous MEFs shows that the regulation of this transcript is potentially dependent on TDP43 binding to its 3' UTR. This binding suppresses the presence of this transcript, which

F210I is unable to efficiently complete resulting in increased levels in heterozygous and homozygous MEFs. This transcript is also absent in embryonic head and adult brain indicating its presence is regulated cell specifically. *Tardbp*-004 may have multiple roles and may be critical in the process of auto-regulation. Further investigation into the impacts of altered *Tardbp*-004 levels on auto-regulation, transcript and protein processes are required.

With potential alterations in splicing characterised in F210I heterozygous and homozygous mutants, general transcript levels were quantified by real time PCR using primers in *Tardbp* exons 2F / 3R. These primers amplify ten annotated transcripts excluding transcripts *Tardbp*-004 and *Tardbp*-005. As a result, they do not distinguish between transcripts destined for protein translation or decay, as defined by current models (Ayala *et al.*, 2011; Polymenidou *et al.*, 2011). The levels of these transcripts are significantly reduced in heterozygous and homozygous embryonic head, compared to wild-type littermate controls (Figure 5.9). Relative expression significantly deceases from 1 (wild-type) to 0.85 (heterozygous) to 0.42 (homozygous). General transcript levels are reduced in heterozygous and homozygous embryonic head compared to wild-type, with potential *Tardbp* mediated deregulation. Further deconstruction of the alterations in the 3' UTR are required in a tissue specific manner, to delineate the mechanism through which these changes occur. However, there is data supporting that this mechanism occurs through TDP43 binding to RNA. In the case of F210I TDP43, there is significantly restricted ability to complete this RNA binding. Therefore, this is likely to be the cause of these changes with F210I providing an *in vivo* model to assess alterations driven through a strongly hypomorphic allele for RNA-binding.

TDP43 protein levels were next assessed to detect whether the changes identified at the RNA level affected protein levels. From the splicing results for *Tardbp*, there may be increasing levels of transcript *Tardbp*-001 in heterozygous and homozygous F210I MEFs with reduced non-protein coding *Tardbp*-002 levels. According to proposed models (Ayala *et al.*, 2011; Polymenidou *et al.*, 2011), this should result in increased full length TDP43 protein levels in heterozygous and homozygous F210I, in a dosage dependent manner. Western blots with protein samples from various tissues have shown inconsistent results. A reduction in TDP43 levels in homozygous MEFs has been shown, but this has not been replicated (Figure 5.11). No significant difference in adult wild-type versus heterozygous brain protein has been observed (Figure 5.12). Overall, the lack of consistency in detecting protein level changes is a limiting factor but this will be repeated with an increased sample size. If levels are different, they may be subtle or potentially not detectable by Western blot. Despite these difficulties further support for lower protein levels in F210I homozygous MEFs comes from a preliminary run

doing stable isotope labelling by amino acids in cell culture (SILAC) experiments on F210I MEFs, where protein levels are reduced to 0.69 of wild-type levels (unpublished results from the laboratory).This experiment now needs to be replicated. Alternative anti-TDP43 antibodies could also be tried for re-quantification. Overall, it is not possible to say that protein levels between wild-type, heterozygous and homozygous samples are significantly different, indicating that phenotypes observed in heterozygous and homozygous samples are the result of the hypomorphic effects of F210I, rather than a reduction in the levels of overall protein. All these protein studies have analysed RIPA soluble protein. RIPA insoluble protein will also be assessed as a change in solubility is thought to be critical with regards to TDP43 pathology. Overall, it is certainly apparent that F210I protein levels are not increased in heterozygous and homozygous F210I samples, as is predicted based on auto-regulation models.

According to the Cleveland model (Polymenidou *et al.*, 2011) when considering F210I as a hypomorphic allele, changes at the RNA and protein level are expected. At the RNA level, the NMD2 transcripts show a potential increase in *Tardbp*-001 and decrease in *Tardbp*-002 in homozygous F210I samples. This is matched by a general reduction in *Tardbp* transcripts with the exon 2F / 3R primers. The splicing changes match the proposed model and the general reduction in transcripts is indicative of F210I being unable to efficiently regulate *Tardbp* RNAs. However, the model proposes increased TDP43 protein levels in homozygous and to a lesser degree heterozygous samples. This result is not observed, particularly with non-replicated trends to reductions in TDP43 levels in both. This could potentially be the result of F210I affecting the protein at a level independent of RNA, such as increasing the rate of protein degradation. Alternatively, the mechanism of auto-regulation is likely to be more complex and there may be potential redundancy from other factors. Further RNA and protein characterisation is required, however F210I is an allele hypomorphic for RNA-binding and can be used *in vivo* as a tool to understand the mechanisms of TDP43 auto-regulation.

TDP43 transcriptome targets

Having characterised changes in *Tardbp* encoding transcripts, endogenous targets were assessed to confirm the hypomorphic effects of F210I, as characterised for TDP43 knock down (Polymenidou *et al.*, 2011). In embryonic head, significant differences in splicing were observed in *Pdp1*, *Dnajc5*, *Poldip3* and *Sort1* (Figure 5.13, Figure 5.14, Figure 5.15 and Figure 5.16), with heterozygous head showing an intermediary phenotype. *Sort1* splicing was also

assessed in MEFs and adult brain (Figure 5.18 and Figure 5.19) confirming the altered patterns of splicing despite different levels of wild-type basal splicing in different tissues. These results mirror those when TDP43 was knocked down in adult striatum (Polymenidou *et al.*, 2011) and show F210I as a hypomorphic allele affecting splicing function. Through affecting the splicing patterns potentially of 965 mRNAs, F210I is likely to impact on multiple pathways, with those relevant to ALS yet to be determined. This can be determined in cells using homozygous F210I cultures, as well as in adult heterozygous mice. It remains to be determined whether the degree of change characterised in the heterozygotes will be sufficient to affect processes at the level of the organism. RNA sequencing and exon microarrays from F210I samples would provide transcriptome-wide data as to the degree of RNA changes versus the TDP43 knock down model, with potential phenotypes being analysed in this context providing a powerful tool.

With TDP43 affecting 30% of the murine transcriptome either directly or indirectly, the challenge is to determine which interactions are critical to pathology in diseases such as ALS or FTLD-TDP. One such potential interaction is *Sort1*, a multi-ligand receptor. TDP43 affects splicing of *Sort1*, a neuronally expressed protein, which acts as a receptor for *Grn* (Hu *et al.*, 2010; Zheng *et al.*, 2011). Mutations in *GRN* are causative of frontotemporal Dementia (FLTD) (Baker *et al.*, 2006), part of the spectrum of disease with ALS (Liscic *et al.*, 2008). It has also been shown that, following neuronal injury, the levels of TDP43 and Grn are inversely related (Moisse *et al.*, 2009b), and this is shown when knocking down TDP43 in the striatum, where levels of *Grn* shoot upwards six fold (Polymenidou *et al.*, 2011). These three proteins may be critical to neuronal health and as such, the initial impacts of TDP43 splicing on *Sort1* must be addressed. If the splicing changes are validated at the protein level, selected targets like *Sort1* can be assessed for altered activity. This has already been shown from an identified TDP43 target *Poldip3* / SKAR (Fiesel *et al.*, 2011). Here, the splicing change is reflected at the level of the protein, with *Poldip3* splicing also being altered in F210I (Figure 5.15). While the reduction in exon inclusion is lower in embryonic head compared to the knock down model (Polymenidou *et al.*, 2011), the changes in protein should remain and a comparison of adult heterozygous F210I striatum splicing with wild-type controls may be a more accurate predictor of the degree of protein change expected as this will compare alterations from the same tissue.

With endogenous targets of TDP43 showing altered splicing patterns, consistent with F210I being a strongly hypomorphic allele, changes in target mRNA was also characterised. Based on TDP43 knock down, target transcripts for *Fus* and *Cadps* were expected to be significantly

reduced, with *Grn* significantly increased. *Cdk6* was also expected to increase based on cellular TDP43 data (Ayala *et al.*, 2008a). These changes were generally not observed (Figure 5.19, Figure 5.20, Figure 5.21 and Figure 5.22). Levels of *Fus* and *Grn* in heterozygous and homozygous embryonic head were not significantly different from wild-type levels, with a potential trend for reduced *Grn* levels compared to wild-type (heterozygous p = 0.187, homozygous p = 0.386 ANOVA Bonferroni post hoc). *Cadps* levels were expected to decrease with a significant reduction in homozygous versus wild-type levels (p = 0.046 ANOVA Bonferroni post hoc) but with no difference between heterozygous and wild-type levels. The decrease in the knock down model was 0.32 versus wild-type, but the F210I homozygous decrease was 0.87 versus wild-type, being milder. The difference may be explained by the varying degrees of loss of function between F210I and knock down within mice, or tissue specificity. When TDP43 is knocked down in HeLa cells *Cdk6* levels increase ten-fold (Ayala *et al.*, 2008a). In F210I embryonic head there is a trend to increased levels but it is not significant (wild-type versus homozygotes p = 0.16 ANOVA Bonferroni post hoc). Overall, expected mRNA level changes were not observed in F210I embryonic head to the expected degree. Inevitably, tissue specificity and the context of the developing head versus adult injected striatum may be heavily contributing factors to differences observed. Alternatively the F210I allele may have varying impacts on some aspects of RNA regulation over others potentially affecting some genes more than others. This requires further characterisation. Determining changes in target genes shows which roles F210I results in loss of function and provides an understanding of what model F210I provides.

Concluding remarks

Changes in TDP43 RNA and protein as well as target genes have been characterised using MEFs, embryonic head and adult brain. Where complete data from embryonic head has been collected, there is a potential caveat in whether there are secondary consequences on gene changes within the head as a result of abnormal development for F210I homozygotes. However, there are phenotypes in target genes that are not significantly altered in these heads at the harvested stage and confirmation of other changes (such as *Sort1* splicing) has been validated in MEFs and adult brain. The adult brain, MEFs and embryonic head provide accessible samples in which to characterise changes in TDP43 and target genes, with comparisons providing valuable information regarding tissue specificity differences (such as transcript *Tardbp*-004 expression exclusively in MEFs). Further characterisation is required in

these and other tissues including primary cortical and embryonic motor neurons. In trying to address TDP43's role in pathology and neuronal health, brain, spinal cord and specific neural cultures (cortical and embryonic motor neuron) will provide potentially more relevant *in vivo* models. F210I provides a powerful allele in which to assess these changes in heterozygote and homozygote states, where knockout and Q101X mutants are unable to due to their early lethality.

Overall, F210I provides a strong *in vitro* and *in vivo* hypomorphic allele to deconstruct TDP43 biology. Data from this chapter supports F210I being strongly hypomorphic. F210I heterozygotes and homozygotes provide *in vivo* models that will establish the consequences of a strongly hypomorphic allele with or without a wild-type allele. There are clear impacts on *Tardbp* transcripts and potential impacts on TDP43 protein. Further investigation into how F210I alters TDP43 protein properties is required. It is clear that this allele significantly impacts on *Tardbp* transcript processing and auto-regulation. Assessment of endogenous TDP43 targets shows a clear impact on splicing. All genes assessed show a significantly altered splicing pattern in line with a loss of function, most severely seen in homozygotes. Further characterisation is required for F210I's effects on target mRNA levels as well as the potential impact F210I may have on other known roles including RNA editing, stress granules, RNA translocation and miRNA formation. Further characterisation of F210I protein steady state levels, potential effects on solubility and degradation rates also need to be determined.

CHAPTER 6

Discussion and Conclusions

6.   Discussion and Conclusions

6.1.   Main findings and contribution to field

6.1.1.   Introduction

One nonsense and nine missense mutations were identified spanning all major domains of mouse TDP43. These mutations, generated by ENU mutagenesis, are expressed in endogenous TDP43 with a normal spatio-temporal expression pattern as expected for wild-type TDP43. Multiple TDP43 models have been generated across species and phyla including cell lines, yeast and non-human primates. In all of these systems the aims have been to model aspects of pathology and create tools to further understand TDP43 function and dysfunction in pathology. Across research groups both knock out and transgenic approaches have been employed, with significant data supporting both loss and gain of function elements contributing to neuronal health and pathology. In the mouse, homozygous knockout mice are not viable and in general transgenic overexpression lines there is a clear dose-dependent toxicity with wild-type and mutant human TDP43. The mutations identified as part of the work in this thesis provide an opportunity to assess the importance of different domains of mouse TDP43 in its normal function and potential impact on pathology. The aim was to characterise the functional nature of each mutation, to determine which mutations could be used as tools to understand TDP43 function and potential pathobiology. From the alleles that have been analysed to date, at the mouse behavioural level all mutations are functional. They do not model motor neuron disease but they have other phenotypes potentially indicative of neurological defects. Furthermore, *in vitro* and *in vivo* characterisation has identified F210I as a novel mouse hypomorphic allele for RNA-binding.

6.1.2.   Q101X

The Q101X mutation occurs N-terminally before all major characterised domains of TDP43. Q101X homozygous mice are not viable and die during embryonic development, before E6.5 dpc. This supports the Q101X mutation being a null allele, as an alternative model alongside

published homozygous knockout mice which die at the same stages of development. Q101X heterozygotes also show normal protein levels due to auto-regulation by TDP43 of its protein product. As well as this, Q101X heterozygotes show behavioural phenotypes not seen in published knockouts. Although motor phenotypes are not observed in these mice, other endophenotypes including limb grasping and a softer body tone are detected which support potential neuronal perturbations. It is worth noting that out of three studies using TDP43 heterozygous knockout mice, only one has identified motor phenotypes in aged mice (Kraemer *et al.*, 2010). Knockout TDP43 mice may also share the phenotypes seen in the Q101X heterozygotes as the published mice have not been assessed for limb grasping and body tone phenotypes. Considering the Q101X heterozygote phenotypes, no overt TDP43 pathology is seen at one year at the light level or six months at the EM level with normal protein levels in aged heterozygote mice up to eighteen months. These assessments were made in the brain and spinal cord, indicating that the cause behind these phenotypes may be located elsewhere. Alternatively, TDP43 auto-regulation may be more subtly affected in specific cell populations resulting in altered TDP43 levels. This may not be reflected when assessing samples at the whole brain or spinal cord level.

Within the literature there is little characterisation underlying the causes of limb grasping and body tone. Limb grasping is a phenotype observed in multiple mouse models and is thought to be the result of neurological or muscular perturbations. Under Mouse Genome Informatics (www.informatics.jax.org), limb grasping is classed as an abnormal reflex linked to abnormal motor and / or sensory capabilities. The muscular force in tests such as grip strength and activity of Q101X heterozygotes appears normal indicating a neurological cause. Likewise with body tone, there is a basal muscular tone with a reflexive elicited response. Loss of this tone may be due to relevant muscular alterations or a neuronal cause eliciting this response. The neuromuscular junctions (NMJs) have been assessed in the potentially relevant muscles with no overt differences. These muscles are the external oblique, internal oblique and transversus abdominis muscles. Causative overt pathology in the brain has not been observed and identifying the specific neuronal centres responsible for these phenotypes has not been shown in the literature previously. The physical change in body tone may also be associated with altered metabolism. Factors that could be assessed which may be relevant could include detecting allocations of fat - muscle ratio versus mass, alterations in types of fat such as lean fat and hormonal effects on body composition.

These phenotypes are also specific in that using traditional tests may not identify relevant mechanisms. For example, if there is a sensory component to loss of body tone, assessing

mouse performance on a hot plate may not be appropriate to the phenotype observed for body tone. Locating and testing the appropriate muscles and neuronal innervations for these phenotypes is a significant challenge. If a sensory component is involved in either of these phenotypes this would match TDP43's established role in neuronal maintenance. In flies, alterations in sensory neuron branching have been observed when overexpressing TBPH (Lu *et al.*, 2009). This may not be expected as these mice represent a potential endogenous mild loss of function versus overexpression in flies. The overall data across species supports TDP43 playing important roles in multiple aspects of neuronal function and these phenotypes while elusive in their cause, may be indicative of neuronal perturbations.

6.1.3.   K160R and compound (*Tardbp*$^{Q101X/K160R}$) mutants

The K160R mutation lies in the first RNA recognition motif (RRM1). Homozygous mice are viable and display a number of phenotypes in common with the Q101X heterozygous mice, including limb grasping and a softer body tone. This supports that the K160R mutation exerts a similar effect as Q101X, causing a potential reduction in function of TDP43 for these endophenotypes. The commonality of phenotypes in limb grasping and softer body tone, with each line carrying different alternative ENU mutations, further supports these phenotypes being the result of the TDP43 mutations. These results support the Q101X mutation in heterozygosis and K160R mutation in homozygosis resulting in common neurological relevant phenotypes with an earlier onset in K160R homozygotes when comparing to Q101X heterozygotes.

Compound mutants between Q101X and K160R (*Tardbp*$^{Q101X/K160R}$) also show these behavioural phenotypes with a higher penetrance and earlier onset. These mice also show novel phenotypes. The compound (*Tardbp*$^{Q101X/K160R}$) mutants reach end stage significantly earlier than littermate controls. In this line however, Q101X heterozygote littermates also reach end stage earlier, but in the original Q101X cohort they do not. *Tardbp*$^{Q101X/K160R}$ female mice are significantly smaller from 28 weeks of age. As with K160R homozygotes, most *Tardbp*$^{Q101X/K160R}$ mutant mice limb grasped when suspended and slipped on the negative geotaxis test and mean onset of 40 weeks of age. However, they showed a softer body tone phenotype with an earlier onset and a higher penetrance compared to K160R homozygotes. An array of cognitive tests on six month old female animals also showed that only compound mutants have anxiety

and lower emotionality phenotypes. This was detected using the light-dark box and black-white alley tests. K160R homozygotes and Q101X heterozygotes did not show these anxiety phenotypes. The numbers of mice assessed were not greater than ten per genotype and a second cohort has been generated to repeat these tests. At the EM level, compound (*Tardbp*$^{Q101X/K160R}$) mutants at six months had small TDP43 cytoplasmic structures in the cytoplasm neurons in the spinal cord. These structures were not seen in any of the other TDP43 mutants. At a molecular level there was also a trend for reduced TDP43 protein levels. This has been assessed in young mice through to aged mice and in all cases a trend towards reduced levels was observed, but not consistently shown. Where significant differences were seen, they were not replicated. This may support a mild reduction in protein levels that is not detectable at the Western blot level, using the Protein Tech TDP43 antibody.

The compound (*Tardbp*$^{Q101X/K160R}$) mutants share phenotypes of respective Q101X heterozygote and K160R homozygote mice with an earlier onset. This supports an increased effect where being compound heterozygous enhances phenotype onset and prevalence not seen in other genotypes. Furthermore, an interactive or potential additive effect is also observed which is not present in other genotypes. With compound females being significantly smaller in adulthood, formation of mini aggregate like structures at the EM level and cognitive phenotypes in the light-dark box and black-white alley test, these mice model alterations not seen in Q101X heterozygotes and K160R homozygotes. This may be due to an interactive effect between the Q101X and K160R alleles or alternatively it may be due to having only one K160R allele compared to being heterozygous or homozygous for the K160R allele. At the protein level, western blots supporting a trend in reduced levels in the compound heterozygotes (*Tardbp*$^{Q101X/K160R}$) which may be the result of a single K160R allele having to auto-regulate protein levels to match those when having two alleles. An enhanced reduction in protein levels in these mice may sufficiently alter processes relevant to weight, EM alterations and cognitive behaviour not seen in Q101X heterozygotes and K160R homozygotes.

Further to the existing behavioural characterisation of the compound mice the end stage samples for pathological assessment have yet to be completed. Therefore the final stages in the complete characterisation of these mice are a work in progress. Determining if there is a specific cause behind them reaching end stage earlier than wild-type controls remains to be defined.

The reduced weight may support a subtle loss of function in compound (*Tardbp*$^{Q101X/K160R}$) mice. This may model a process similar to the rapid weight loss in a conditional TDP43

knockout mouse model (Chiang *et al.*, 2010). This could be assessed in these mice as to whether a similar process is occurring more subtly or there is an alternative mechanism mediating weight loss. The EM phenotype of cytoplasmic deposition has not been reported in other transgenic TDP43 mouse models. Mini-aggregation structures in the cytoplasm may support a loss of endogenous TDP43 localisation and function or a gain of function in a novel cytoplasmic area. This may be relevant to the phenotypes that are unique to the compound mice including being smaller and cognitive alterations. The anxiety and emotionality phenotypes may also be indicative of TDP43's role in human dementia (FTLD-TDP) by showing that a mild loss of function affects cognitive aspects of mouse behaviour in anxiety. This result will be confirmed with a second cohort of mice to conclusively support TDP43's role in cognition, which may be partially modelled in these compound heterozygotes. In humans with anxiety disorders the forebrain and hippocampus are often highly affected areas (Simpson, 2010) and this would be particularly relevant to TDP43's role in FTLD-TDP where there is degeneration in the forebrain. A more enhanced assessment for pathology in the forebrain may be required. Multiple anxiety disorders also show alterations in neurotransmitters such as noradrenaline, serotonin and gamma-aminobutyric acid (GABA), which provide targets for future assessment. A cohort of $Tardbp^{Q101X/K160R}$ mice is also being assessed by magnetic resonance imaging for structural abnormalities in the brain.

6.1.4. Q101X / SOD1^{G93A}

TDP43 Q101X heterozygote mice were crossed to SOD1^{G93A} low copy transgenic mice (Acevedo-Arozena *et al.*, 2011) to assess for interactive effects. In human ALS pathology, TDP43 and SOD1 appear to show independence in inclusion formation although it has been shown in sporadic ALS that misfolded SOD1 is present (Bosco *et al.*, 2010). When SOD1 causes ALS, mutant SOD1 is found in protein inclusions however in most ALS cases with or without TDP43 mutations, TDP43 is pathologically altered and is a component of inclusions. Although inclusions are thought to contain exclusively SOD1 or TDP43, mutations in both genes converge, both resulting in selective motor neuron degeneration and ALS. As such, it was decided to create double mutants to assess a possible interaction in a longitudinal study to end stage which is induced by the SOD1^{G93A} transgene at 31 − 38 weeks. There were no major interactive effects induced by either SOD1^{G93A} or TDP43 Q101X. There were significant motor performance differences in the negative geotaxis test with Q101X HET / SOD1^{G93A} mice slipping

more than WT / SOD1^{G93A} mice, but these differences did not translate quantitatively to grip strength measurements. There were also consistent trends for reduced startle response in Q101X HET / SOD1^{G93A} mice, which has been shown to be due to motor neuron degeneration in SOD1^{G93A} mice (Acevedo-Arozena *et al.*, 2011) however this trend was not significant. This data supports a mild change in the SHIRPA with a trend in reduced startle but overall there appear to be no interactive effects between these two genes / mutations in this context. This does not conclusively rule out interactive effects.

6.1.5.   F210I

The work completed in this thesis on F210I supports that it is a novel hypomorphic allele for TDP43 RNA-binding. This is corroborated by the general characterisation of the F210I mutation in Chapters 4 and 5 as well as the earlier lethality seen in *Tardbp*$^{Q101X/F210I}$ compound mutants. F210I is not a complete null for TDP43 function, as is evident by the survival of homozygous embryos to a much later embryonic stage (E14.5 dpc) than knockout (up to E8.5 dpc) or Q101X homozygous mutants (E6.5 dpc). In inter-cross matings there is also preliminary data that F210I heterozygotes may not be born at the Mendelian expected ratio. Further intercross matings are required to increase the numbers assessed and a comparison to female F210I heterozygote females crossed to wild-type males is also required to compare inheritance of the F210I allele from maternal and paternal sources. Overall, F210I is a novel RNA-binding loss of function system that can be studied to assess TDP43 RNA-binding function in multiple processes as has been already shown to be altered in MEFs and mice for auto-regulation and RNA metabolism.

The data for loss of TDP43 function *in vitro* is shown in F210I deficient RNA-binding to UG$_6$ and CLIP identified TDP43 3' UTR binding sequences. *In vivo* there is a reduction in splicing function with a dosage dependent effect. Crosses to generate *Tardbp*$^{Q101X/F210I}$ compound mutants preliminarily show that these mutants die earlier. As the Q101X allele requires the F210I allele to auto-regulate to a greater degree than having two F210I alleles, earlier lethality supports increased loss of function for auto-regulation due to F210I being less able to bind the 3' UTR identified CLIP sequence. If F210I were predominantly a gain of toxic function allele, it would be hypothesized that the compound *Tardbp*$^{Q101X/F210I}$ allele may survive longer in development if there was an auto-regulation deficit. This would be due to a dose dependent effect where

the *Tardbp*$^{Q101X/F210I}$ mice have one allele, which would be less toxic than two alleles. Assessment of protein levels in these embryos will also be used to confirm F210I's inability to auto-regulate *in vivo*. Considering this, with TDP43's splicing and RNA metabolic functions, there is no data so far for a gain of function in F210I although this cannot be ruled out.

Within the literature, it has been shown that RRM1 is necessary and sufficient for RNA-binding. RRM2, which has an RNA-binding affinity two orders of magnitude lower than that of RRM1 is thought to have alternative roles (Buratti & Baralle, 2001; Kuo *et al.*, 2009). The results from the work described in this thesis for F210I contradict deletion experiments supporting RRM2 as not being critical for RNA-binding. This work shows that the F210I point mutation in the second RRM has a significant impact on RNA-binding and function. Assessing the nature through which F210I has this effect is discussed in future work with regards to the experiments that could be completed to identify this. The mutation of a phenylalanine in losing a benzene ring is likely to indicate the loss of a residue which physically binds RNA. This would be expected as the phenylalanines 147 / 149 in the first RRM are critical for physically interacting with RNA. The second RRM has also been hypothesised to be important for TDP43 dimerization for normal function and this mutation may in some way impact on this dimerization. Irrespective of the mechanism through which F210I confers this hypomorphic effect, F210I TDP43 is less able to bind RNA targets including its highest affinity UG repeats which are central to TDP43's roles in RNA metabolism. As such, F210I is a novel allele re-affirming the importance of an RRM2 point mutation on murine TDP43 RNA function.

F210I in homozygosis is embryonic lethal. The full causes of embryonic lethality continue to be characterised with an oedema phenotype being consistently observed as a potential causal factor. With TDP43 having such diverse roles in RNA metabolism, F210I homozygous lethality may be the result of multiple developmental problems accumulating to cause death, rather than failure in development of an individual organ or system. By being lethal at a later stage of development (later than E14.5 dpc), F210I provides a hypomorphic allele that can be compared to Q101X or knockout lethality which occurs much earlier. Later survival supports minimal RNA-binding function being required earlier in development or a non RNA-binding requirement for TDP43. Later developmental stages may be more reliant on TDP43's RNA-binding roles. F210I is a novel model to study TDP43's role in development at stages in the mouse where currently no other model exists to do this.

F210I survival to E14.5 dpc in homozygosis also allows for culture of MEFs and primary neuronal cells (both cortical and embryonic motor neurons can be cultured at this stage). This

is not possible from knock out models due to early lethality. The unpublished transgenic RNAi mice (Prof Xu, SfN 2011) provide a complementary model to culture these neurons as well. By growing and assessing these neurons the impact of a strong loss of function on post mitotic neurons can be assessed using the F210I model. This provides a novel cellular model in which to assess TDP43 function and dysfunction. Exploiting the progress made since the discovery of TDP43 mutations in ALS / FTLD-TDP, this cellular model will be used to understand TDP43 basal function as well as function in response to stress to show the impact of loss of endogenous TDP43 RNA-binding function on mouse neurons. This may model aspects of human pathology and provide further insight into the roles of TDP43 in these neuronal cells.

F210I heterozygous mice are viable and at a molecular level show reduced RNA-binding function. This reflects an underlying molecular phenotype in which a cohort of mice will be behaviourally phenotyped in the future as has been done for the Q101X and K160R mutations. F210I heterozygous mice provide an *in vivo* model to assess a mild loss of RNA-binding function in the context of a wild-type allele. This provides a novel model to assess changes in TDP43 and the relationship between loss of function and pathology. Both homozygous and heterozygous F210I cellular and animal models provide RNA-binding specific loss of function tools to delineate TDP43 biology in the mouse. Whether it is in development, post mitotic neurons or at the level of the whole animal, hypotheses relating to auto-regulation and the impact on RNA transcripts can be assessed using F210I. As complete knock outs do not survive they have not been able to assess many of the questions it is expected that F210I will, considering the auto-regulation in knock out heterozygotes. Likewise, transgenic mice overexpress human TDP43 in the context of wild-type endogenous mouse TDP43. The degree of endogenous mouse protein down regulation in the different models varies depending on exogenous protein overexpression levels. By crossing F210I to these models, these double mutants may delineate the importance of loss of endogenous function versus overexpressed human TDP43, if they rescue F210I homozygous lethality.

6.2. Future work

6.2.1. Q101X / K160R

The assessment of all mutations is a work in progress. For the Q101X and K160R mutations all behavioural characterisation has been completed. Final assessment from end stage samples is

required for RNA and protein levels as well as pathology assessment. Separate compound heterozygote cohorts ($Tardbp^{Q101X/K160R}$) of mice with littermate controls have been generated to confirm the cognitive deficits in the light-dark box test and the black-white alley test. Cohorts have also been sent for sensory testing by Dr David Bennet (KCL) with results indicating no overt sensory deficits. Tests applied were Hargreaves reflex withdrawal to radiant heat, Von Frey withdrawal threshold, Randall Sellito and cold plate test. These tests measure various sensory mediated pain and mechanical response thresholds but are not specific to body tone muscles. Another cohort has also being sent to Dr Mark Lythgoe (UCL) to image the brains using MRI. This is being completed to assess for alterations that may link to any of the observed phenotypes in the compound heterozygotes.

For the Q101X, K160R and compound mutants it is critical to further assess RNA and protein levels. Particularly in the compound heterozygotes, samples need to be re-extracted to determine if there is a significant reduction in protein levels. If this is the case it would show that a reduction in protein levels is causing the observed phenotypes. In all cases, only RIPA soluble protein has been assessed. When re-quantifying newly extracted samples, RIPA insoluble fractions should also be assessed as a shift in solubility is a hallmark of TDP43 pathogenicity. Likewise, preliminary characterisation of a reduction in *Sort1* splicing needs to be assessed with an increased number of samples and in other genes, as well as assessment of *Tardbp* transcripts. Further in depth analysis on the compound mutants is required in the forebrain region and hippocampus particularly, to search for pathology or structural alterations that may be associated with the anxiety phenotype.

For the compound heterozygotes, further post mortem assessment is required in order to determine the causes of death. Post mortems are being carried out by Dr Michael Cheeseman (MRC Harwell) with preliminary results showing a number of causes of death across all genotypes. It is anticipated that there will be no mutant specific causes indicating that these mice are more susceptible to age related end stage associated with their genetic background.

Overall, the aim for the Q101X and K160R mutants is to further understand the limb grasp and body tone phenotypes at a molecular or structural level. Pathology can be a challenging criterion to identify with the immediate muscles that form body tone requiring a more extensive analysis than the neuromuscular junction measurement that has been completed. Variations in these muscles or the nervous system immediately contacting / innervating them are potentially where the most obvious differences may be found. If body tone is a reflexive response assessment here as well as higher order nervous system centres is required.

6.2.2.　F210I

F210I is an exciting novel allele that has been identified and characterised as part of the work described in this thesis. As it is a RNA-binding hypomorphic allele, future work can be broken down into three further areas: continued characterisation of the degree of loss of function, model assessment for pathology and rescuing the homozygous lethality phenotype.

Continued characterisation of the mutation can take place both *in vitro* and *in vivo*. The striking loss of RNA-binding function has already been shown. Further work is required to understand how F210I causes loss of RNA-binding function and ruling out any potential gain of function mechanisms associated with the mutation. Basic biology from protein turnover (by blocking the ubiquitin proteasome system using chemicals such as MG132) to more complicated structural alterations and dimerization (such as circular dichroism or native Western blotting) need to be applied.

Beyond potential structural alterations induced by F210I, preliminary characterisation has shown that there are significant impacts on endogenous functional targets and auto-regulation. Disruption of both of these processes, as discussed in the introduction, is hypothesised to be critical to TDP43 pathology in humans. F210I provides an ideal *in vivo* tool to assess this. Experiments already being undertaken in the group include RNA sequencing, exon arrays and stable isotope labelling by amino acids in cell culture (SILAC). RNA sequencing and exon arrays will provide fully quantitative changes in the transcriptome for mRNA levels and splicing, showing the degree of loss of function impact in the heterozygous and homozygous F210I states. SILAC will provide complementary data for changes across the proteome providing an excess of data for changes *in vivo* induced by F210I. Extensive data from multiple models, in particular the unpublished transgenic RNAi mice (Prof Xu, UMass, presented at Society for Neuroscience 2011) shows that loss of function is critical to neuronal health and results in pathology with progressive motor neuron degeneration. The degree to which characterised pathology in the mouse models the human condition is yet to be determined but motor phenotypes and selectively progressive neurodegeneration are relevant to the human condition.

F210I provides an *in vivo* tool to characterise the mechanisms of auto-regulation. Although to date the mechanism is controversial, F210I has been shown *in vitro* to bind its own 3' UTR

inefficiently. Transcript levels are altered as well as the splicing pattern of individual 3' UTR transcripts. These RNA changes need to be characterised in a tissue specific manner, as differences by tissue type have been shown as part of the work described in this thesis. The F210I allele has a reduced ability *in vivo* to maintain normal auto-regulation at the RNA level, as shown by altered splicing and exon 2F / 3R transcript levels. This needs to be confirmed at the protein level, but this can also be assessed at a cellular level in homozygous cells (MEFs and embryonic motor neurons) and in adult tissue. With proposed models of auto-regulation, the individual mechanisms (such as exosome mediated decay versus nonsense mediated decay) can be tested in the F210I model *in vivo* (Ayala *et al.*, 2011; Polymenidou *et al.*, 2011). These models predict which transcripts are sent for decay and which encode full length TDP43 protein. In particular, transcript *Tardbp*-001 is thought to encode full length TDP43 and this transcript needs to be quantified by real time PCR in wild-type and F210I mutant samples. If the levels inversely correlate with *Tardbp*-002 (based on proposed models) F210I heterozygous and homozygous samples should show a dose dependent increase in protein levels which is not anticipated based on preliminary Western blot results. Therefore, the F210I allele can assess the proposed models of auto-regulation *in vivo* in a cell specific manner, to characterise the mechanism of auto-regulation and assess its relevance to pathology in the mouse.

A cohort of F210I mice has been generated for behavioural assessment. In homozygosis F210I is embryonic lethal. Only mice carrying the F210I mutation in heterozygosis, in the context of the wild-type allele, will be phenotyped. These mice will be aged and characterised to end stage. While aging this cohort, the preliminary characterisation from these mice at a molecular level has shown that *Sort1* splicing as well as splicing in other target genes is significantly affected at 12 weeks in brain. This is likely to reflect multiple alterations in TDP43 RNA functions across the murine transcriptome. The question now remains as to whether the changes occurring at the molecular level in F210I heterozygotes will be enough to induce behavioural phenotypes in the relatively short lifespan of the mouse. Further assessment in human patients is also required to assess whether TDP43 shows functional changes in disease. With the production of aggregates and sequestration of TDP43 from the nucleus in ALS, a loss of TDP43 function is expected to cause or contribute to the disease process. If this is validated, it can be compared to the F210I allele in the mouse which is strongly hypomorphic for many roles in RNA metabolism.

Alongside molecular and behavioural characterisation of F210I as a model, alternative data from *in vitro* models can be assessed *in vivo*. One such model has been to knockdown TDP43 in HEK293 cells, resulting in changes in cell cycle genes impacting on the morphology of cells

(Ayala *et al.*, 2008a). This can be assessed in the F210I loss of function model. Taking into account the varying degrees of loss of function in the two models, whether F210I homozygous MEFs or other primary cells are affected in an identical fashion can be assessed. A model to consider is that TDP43 unable to bind RNA (F147L / F149L) has been shown to form large nuclear structures in the nucleus in cellular models (Ayala *et al.*, 2008b; Wang *et al.*, 2012). These structures may be the result of increased TDP43 self-aggregation and this can be assessed in the context of F210I.

F210I is homozygous lethal. Future work will focus on establishing the cause of lethality in embryonic development. With knockout mice and Q101X homozygotes dying early in development (before E8.5 dpc) F210I already provides an allele in which to tease out degrees of potential loss of function at different stages of development. Establishing the cause of death will further delineate TDP43's roles in development. F210I homozygotes assessed so far show consistent spino-oedema phenotypes indicating a critical role for TDP43 in mouse heart development. The lower penetrant retarded eye development and holoprosencephaly phenotypes also show alternative potential functions for TDP43 in development. Characterising these roles will further enhance understanding of TDP43 function but may also provide insight into pathogenesis in TDP43 proteinopathies. Mutations affecting developmental processes may impact on adult disease course in later life.

As F210I is homozygous lethal, it can only be studied at a cellular level, or in embryonic development up to E14.5 dpc. To further utilise F210I in homozygosity, transgenic BAC TDP43 mice (Swarup *et al.*, 2011a) have been imported into Harwell with the aim of rescuing the lethality phenotype. In transgenic rodent mice published, there is inconsistency in the degree of nuclear clearance of endogenous TDP43 protein. If the endogenous F210I allele in homozygosis can be rescued in the context of a BAC transgene then F210I may represent a loss of function in the nucleus shown by protein clearance. It will be interesting to see if this alters transgene disease course, indicating a significant role for endogenous protein levels in the pathology seen in transgenic mice, as indicated by one study (Igaz *et al.*, 2011). The cross to a BAC transgenic TDP43 model where disease course is slow, mimicking the human condition more effectively provides an ideal model in which to compare F210I induced changes. This model may also show reduced endogenous F210I down regulation due to the nature of the transgene being lowly overexpressed.

Another key element in human pathology and modelling TDP43's role is stress. In the human condition, many patients are normal up until mid-life and from symptom onset there is a rapid

decline. One of the future directions for F210I is to characterise its functional ability to cope with various forms of stress. This can be achieved at multiple levels. In cells stress granule formation in response to oxidative, heat shock or other stresses can be measured, in particular assessing TDP43 localisation to stress granules as this may be an RNA-binding dependent event. Likewise in animals, stresses can be achieved through processes such as axotomies. Overall, F210I at a cellular and animal level provides an *in vivo* model to assess if loss of function can lead to pathology. The field needs to be monitored for the most relevant hypotheses regarding RNA functions. As such, any of these hypotheses can be tested in F210I post mitotic neurons in homozygosis and mice in heterozygosis to also use the F210I allele to deconstruct TDP43's normal functions. These hypotheses may also be tested in potential rescued F210I homozygotes.

6.2.3.   Future work all mutations

All mutations have been assessed in the CFTR mini-gene assay *in vitro*. Since 2006, there has been a large expansion in our understanding of TDP43's roles in cell biology. This provides an opportunity to further develop assays to assess all remaining TDP43 point mutations for potential functional effects. As it is costly and time consuming to rederive mice carrying all mutations for assessment, if further *in vitro* assays are developed they could be used to assess the allelic array of mutations. In the case of the CFTR assay it would be ideal to rederive MEFs for all lines to assess each mutation, considering the increased sensitivity *ex vivo*.

An alternative screen to assess the allelic series of mutations could also be to overexpress constructs carrying each of the mutations in various cell lines. The impacts on survival, TDP43 localisation, protein solubility and response to stress could all be used as markers to assess the series of mutations. This experiment would also be relatively quick to complete.

Experiments to delineate the functionality of an allelic series of ENU mutations in any gene are most effectively achieved when known functions of that gene can be assayed. In the CFTR context, TDP43's role in splicing has been assayed and F210I was successfully identified. TDP43 plays multiple roles in RNA metabolism with deficits in splicing likely to link to deficits in other RNA metabolism roles. Much remains unknown regarding domains such as the N terminus and the second RRM. Multiple roles are speculated, such as RRM2 being important for dimerization and chromatin organisation. The allelic series of mutations needs to be functionally validated

in each case and can provide future tools in which to assess these functions. Mutations in different domains may have large impacts on protein folding and biology or may subtly affect a specific function of that domain.

Characterisation of the allelic series of mutations continues as a work in progress. F210I was identified through the CFTR assay which also missed that M323K shows a gain of splicing function (shown *in vivo*, data not presented). As such, while new assays need to be applied relating to alternative aspects of TDP43 function and dysfunction, their limitations must also be recognised. It is likely that many more of the missense mutations identified are functional considering the highly conserved nature of TDP43. Interestingly, in human screens there are no reports of amino acid changes in control patients or in affected patients outside the C-terminal region (excluding one case). As such, these mutations warrant further investigation to provide *in vivo* mouse tools to delineate TDP43 function.

CHAPTER 7

Bibliography

7.   Bibliography

Acevedo-Arozena, A., Kalmar, B., Essa, S., Ricketts, T., Joyce, P., Kent, R., Rowe, C., Parker, A., Gray, A., Hafezparast, M., Thorpe, J.R., Greensmith, L. & Fisher, E.M. (2011) A comprehensive assessment of the SOD1G93A low-copy transgenic mouse, which models human amyotrophic lateral sclerosis. *Disease models & mechanisms*, **4**, 686-700.

Acevedo-Arozena, A., Wells, S., Potter, P., Kelly, M., Cox, R.D. & Brown, S.D. (2008) ENU mutagenesis, a way forward to understand gene function. *Annual review of genomics and human genetics*, **9**, 49-69.

Acharya, K.K., Govind, C.K., Shore, A.N., Stoler, M.H. & Reddi, P.P. (2006) cis-requirement for the maintenance of round spermatid-specific transcription. *Developmental biology*, **295**, 781-790.

Aizawa, H., Sawada, J., Hideyama, T., Yamashita, T., Katayama, T., Hasebe, N., Kimura, T., Yahara, O. & Kwak, S. (2010) TDP-43 pathology in sporadic ALS occurs in motor neurons lacking the RNA editing enzyme ADAR2. *Acta neuropathologica*, **120**, 75-84.

Al-Chalabi, A., Andersen, P.M., Nilsson, P., Chioza, B., Andersson, J.L., Russ, C., Shaw, C.E., Powell, J.F. & Leigh, P.N. (1999) Deletions of the heavy neurofilament subunit tail in amyotrophic lateral sclerosis. *Human molecular genetics*, **8**, 157-164.

Alexander, G.M., Erwin, K.L., Byers, N., Deitch, J.S., Augelli, B.J., Blankenhorn, E.P. & Heiman-Patterson, T.D. (2004) Effect of transgene copy number on survival in the G93A SOD1 transgenic mouse model of ALS. *Brain research. Molecular brain research*, **130**, 7-15.

Arai, T., Hasegawa, M., Akiyama, H., Ikeda, K., Nonaka, T., Mori, H., Mann, D., Tsuchiya, K., Yoshida, M., Hashizume, Y. & Oda, T. (2006) TDP-43 is a component of ubiquitin-positive tau-negative inclusions in frontotemporal lobar degeneration and amyotrophic lateral sclerosis. *Biochemical and biophysical research communications*, **351**, 602-611.

Ash, P.E., Zhang, Y.J., Roberts, C.M., Saldi, T., Hutter, H., Buratti, E., Petrucelli, L. & Link, C.D. (2010) Neurotoxic effects of TDP-43 overexpression in C. elegans. *Human molecular genetics*, **19**, 3206-3218.

Avemaria, F., Lunetta, C., Tarlarini, C., Mosca, L., Maestri, E., Marocchi, A., Melazzini, M., Penco, S. & Corbo, M. (2011) Mutation in the senataxin gene found in a patient affected by familial ALS with juvenile onset and slow progression. *Amyotrophic lateral*

sclerosis : official publication of the World Federation of Neurology Research Group on Motor Neuron Diseases, **12**, 228-230.

Ayala, Y.M., De Conti, L., Avendano-Vazquez, S.E., Dhir, A., Romano, M., D'Ambrogio, A., Tollervey, J., Ule, J., Baralle, M., Buratti, E. & Baralle, F.E. (2011) TDP-43 regulates its mRNA levels through a negative feedback loop. *The EMBO journal*, **30**, 277-288.

Ayala, Y.M., Misteli, T. & Baralle, F.E. (2008a) TDP-43 regulates retinoblastoma protein phosphorylation through the repression of cyclin-dependent kinase 6 expression. *Proceedings of the National Academy of Sciences of the United States of America*, **105**, 3785-3789.

Ayala, Y.M., Pagani, F. & Baralle, F.E. (2006) TDP43 depletion rescues aberrant CFTR exon 9 skipping. *FEBS letters*, **580**, 1339-1344.

Ayala, Y.M., Pantano, S., D'Ambrogio, A., Buratti, E., Brindisi, A., Marchetti, C., Romano, M. & Baralle, F.E. (2005) Human, Drosophila, and C.elegans TDP43: nucleic acid binding properties and splicing regulatory function. *Journal of molecular biology*, **348**, 575-588.

Ayala, Y.M., Zago, P., D'Ambrogio, A., Xu, Y.F., Petrucelli, L., Buratti, E. & Baralle, F.E. (2008b) Structural determinants of the cellular localization and shuttling of TDP-43. *Journal of cell science*, **121**, 3778-3785.

Baker, M., Mackenzie, I.R., Pickering-Brown, S.M., Gass, J., Rademakers, R., Lindholm, C., Snowden, J., Adamson, J., Sadovnick, A.D., Rollinson, S., Cannon, A., Dwosh, E., Neary, D., Melquist, S., Richardson, A., Dickson, D., Berger, Z., Eriksen, J., Robinson, T., Zehr, C., Dickey, C.A., Crook, R., McGowan, E., Mann, D., Boeve, B., Feldman, H. & Hutton, M. (2006) Mutations in progranulin cause tau-negative frontotemporal dementia linked to chromosome 17. *Nature*, **442**, 916-919.

Bielas, J.H. & Heddle, J.A. (2000) Proliferation is necessary for both repair and mutation in transgenic mouse cells. *Proceedings of the National Academy of Sciences of the United States of America*, **97**, 11391-11396.

Bosco, D.A., Morfini, G., Karabacak, N.M., Song, Y., Gros-Louis, F., Pasinelli, P., Goolsby, H., Fontaine, B.A., Lemay, N., McKenna-Yasek, D., Frosch, M.P., Agar, J.N., Julien, J.P., Brady, S.T. & Brown, R.H., Jr. (2010) Wild-type and mutant SOD1 share an aberrant conformation and a common pathogenic pathway in ALS. *Nature neuroscience*, **13**, 1396-1403.

Bose, J.K., Wang, I.F., Hung, L., Tarn, W.Y. & Shen, C.K. (2008) TDP-43 overexpression enhances exon 7 inclusion during the survival of motor neuron pre-mRNA splicing. *The Journal of biological chemistry*, **283**, 28852-28859.

Braun, R.J., Sommer, C., Carmona-Gutierrez, D., Khoury, C.M., Ring, J., Buttner, S. & Madeo, F. (2011) Neurotoxic 43-kDa TAR DNA-binding protein (TDP-43) triggers mitochondrion-dependent programmed cell death in yeast. *The Journal of biological chemistry*, **286**, 19958-19972.

Buratti, E. & Baralle, F.E. (2001) Characterization and functional implications of the RNA binding properties of nuclear factor TDP-43, a novel splicing regulator of CFTR exon 9. *The Journal of biological chemistry*, **276**, 36337-36343.

Buratti, E., Brindisi, A., Giombi, M., Tisminetzky, S., Ayala, Y.M. & Baralle, F.E. (2005) TDP-43 binds heterogeneous nuclear ribonucleoprotein A/B through its C-terminal tail: an important region for the inhibition of cystic fibrosis transmembrane conductance regulator exon 9 splicing. *The Journal of biological chemistry*, **280**, 37572-37584.

Buratti, E., Brindisi, A., Pagani, F. & Baralle, F.E. (2004) Nuclear factor TDP-43 binds to the polymorphic TG repeats in CFTR intron 8 and causes skipping of exon 9: a functional link with disease penetrance. *American journal of human genetics*, **74**, 1322-1325.

Buratti, E., De Conti, L., Stuani, C., Romano, M., Baralle, M. & Baralle, F. (2010) Nuclear factor TDP-43 can affect selected microRNA levels. *The FEBS journal*, **277**, 2268-2281.

Buratti, E., Dork, T., Zuccato, E., Pagani, F., Romano, M. & Baralle, F.E. (2001) Nuclear factor TDP-43 and SR proteins promote in vitro and in vivo CFTR exon 9 skipping. *The EMBO journal*, **20**, 1774-1784.

Buratti, E., Stuani, C., De Prato, G. & Baralle, F.E. (2007) SR protein-mediated inhibition of CFTR exon 9 inclusion: molecular characterization of the intronic splicing silencer. *Nucleic acids research*, **35**, 4359-4368.

Caccamo, A., Majumder, S., Deng, J.J., Bai, Y., Thornton, F.B. & Oddo, S. (2009) Rapamycin rescues TDP-43 mislocalization and the associated low molecular mass neurofilament instability. *The Journal of biological chemistry*, **284**, 27416-27424.

Chaudhury, A., Chander, P. & Howe, P.H. (2010) Heterogeneous nuclear ribonucleoproteins (hnRNPs) in cellular processes: Focus on hnRNP E1's multifunctional regulatory roles. *RNA*, **16**, 1449-1462.

Chen, H.J., Anagnostou, G., Chai, A., Withers, J., Morris, A., Adhikaree, J., Pennetta, G. & de Belleroche, J.S. (2010) Characterization of the properties of a novel mutation in VAPB in familial amyotrophic lateral sclerosis. *The Journal of biological chemistry*, **285**, 40266-40281.

Chen, Y.Z., Bennett, C.L., Huynh, H.M., Blair, I.P., Puls, I., Irobi, J., Dierick, I., Abel, A., Kennerson, M.L., Rabin, B.A., Nicholson, G.A., Auer-Grumbach, M., Wagner, K., De

Jonghe, P., Griffin, J.W., Fischbeck, K.H., Timmerman, V., Cornblath, D.R. & Chance, P.F. (2004) DNA/RNA helicase gene mutations in a form of juvenile amyotrophic lateral sclerosis (ALS4). *American journal of human genetics*, **74**, 1128-1135.

Chiang, P.M., Ling, J., Jeong, Y.H., Price, D.L., Aja, S.M. & Wong, P.C. (2010) Deletion of TDP-43 down-regulates Tbc1d1, a gene linked to obesity, and alters body fat metabolism. *Proceedings of the National Academy of Sciences of the United States of America*, **107**, 16320-16324.

Choleris, E., Thomas, A.W., Kavaliers, M. & Prato, F.S. (2001) A detailed ethological analysis of the mouse open field test: effects of diazepam, chlordiazepoxide and an extremely low frequency pulsed magnetic field. *Neuroscience and biobehavioral reviews*, **25**, 235-260.

Colombrita, C., Zennaro, E., Fallini, C., Weber, M., Sommacal, A., Buratti, E., Silani, V. & Ratti, A. (2009) TDP-43 is recruited to stress granules in conditions of oxidative insult. *Journal of neurochemistry*, **111**, 1051-1061.

Corrado, L., Carlomagno, Y., Falasco, L., Mellone, S., Godi, M., Cova, E., Cereda, C., Testa, L., Mazzini, L. & D'Alfonso, S. (2011) A novel peripherin gene (PRPH) mutation identified in one sporadic amyotrophic lateral sclerosis patient. *Neurobiology of aging*, **32**, 552 e551-556.

Corrado, L., Del Bo, R., Castellotti, B., Ratti, A., Cereda, C., Penco, S., Soraru, G., Carlomagno, Y., Ghezzi, S., Pensato, V., Colombrita, C., Gagliardi, S., Cozzi, L., Orsetti, V., Mancuso, M., Siciliano, G., Mazzini, L., Comi, G.P., Gellera, C., Ceroni, M., D'Alfonso, S. & Silani, V. (2010) Mutations of FUS gene in sporadic amyotrophic lateral sclerosis. *Journal of medical genetics*, **47**, 190-194.

Crawley, J.N. & Paylor, R. (1997) A proposed test battery and constellations of specific behavioral paradigms to investigate the behavioral phenotypes of transgenic and knockout mice. *Hormones and behavior*, **31**, 197-211.

D'Ambrogio, A., Buratti, E., Stuani, C., Guarnaccia, C., Romano, M., Ayala, Y.M. & Baralle, F.E. (2009) Functional mapping of the interaction between TDP-43 and hnRNP A2 in vivo. *Nucleic acids research*, **37**, 4116-4126.

Da Cruz, S. & Cleveland, D.W. (2011) Understanding the role of TDP-43 and FUS/TLS in ALS and beyond. *Current opinion in neurobiology*, **21**, 904-919.

Daoud, H., Belzil, V., Martins, S., Sabbagh, M., Provencher, P., Lacomblez, L., Meininger, V., Camu, W., Dupre, N., Dion, P.A. & Rouleau, G.A. (2011) Association of long ATXN2 CAG repeat sizes with increased risk of amyotrophic lateral sclerosis. *Archives of neurology*, **68**, 739-742.

DeJesus-Hernandez, M., Mackenzie, I.R., Boeve, B.F., Boxer, A.L., Baker, M., Rutherford, N.J., Nicholson, A.M., Finch, N.A., Flynn, H., Adamson, J., Kouri, N., Wojtas, A., Sengdy, P., Hsiung, G.Y., Karydas, A., Seeley, W.W., Josephs, K.A., Coppola, G., Geschwind, D.H., Wszolek, Z.K., Feldman, H., Knopman, D.S., Petersen, R.C., Miller, B.L., Dickson, D.W., Boylan, K.B., Graff-Radford, N.R. & Rademakers, R. (2011) Expanded GGGGCC hexanucleotide repeat in noncoding region of C9ORF72 causes chromosome 9p-linked FTD and ALS. *Neuron*, **72**, 245-256.

Del Bo, R., Tiloca, C., Pensato, V., Corrado, L., Ratti, A., Ticozzi, N., Corti, S., Castellotti, B., Mazzini, L., Soraru, G., Cereda, C., D'Alfonso, S., Gellera, C., Comi, G.P. & Silani, V. (2011) Novel optineurin mutations in patients with familial and sporadic amyotrophic lateral sclerosis. *Journal of neurology, neurosurgery, and psychiatry*, **82**, 1239-1243.

Deng, H.X., Chen, W., Hong, S.T., Boycott, K.M., Gorrie, G.H., Siddique, N., Yang, Y., Fecto, F., Shi, Y., Zhai, H., Jiang, H., Hirano, M., Rampersaud, E., Jansen, G.H., Donkervoort, S., Bigio, E.H., Brooks, B.R., Ajroud, K., Sufit, R.L., Haines, J.L., Mugnaini, E., Pericak-Vance, M.A. & Siddique, T. (2011) Mutations in UBQLN2 cause dominant X-linked juvenile and adult-onset ALS and ALS/dementia. *Nature*, **477**, 211-215.

Deng, H.X., Hentati, A., Tainer, J.A., Iqbal, Z., Cayabyab, A., Hung, W.Y., Getzoff, E.D., Hu, P., Herzfeldt, B., Roos, R.P. & et al. (1993) Amyotrophic lateral sclerosis and structural defects in Cu,Zn superoxide dismutase. *Science*, **261**, 1047-1051.

Devon, R.S., Orban, P.C., Gerrow, K., Barbieri, M.A., Schwab, C., Cao, L.P., Helm, J.R., Bissada, N., Cruz-Aguado, R., Davidson, T.L., Witmer, J., Metzler, M., Lam, C.K., Tetzlaff, W., Simpson, E.M., McCaffery, J.M., El-Husseini, A.E., Leavitt, B.R. & Hayden, M.R. (2006) Als2-deficient mice exhibit disturbances in endosome trafficking associated with motor behavioral abnormalities. *Proceedings of the National Academy of Sciences of the United States of America*, **103**, 9595-9600.

Dewey, C.M., Cenik, B., Sephton, C.F., Dries, D.R., Mayer, P., 3rd, Good, S.K., Johnson, B.A., Herz, J. & Yu, G. (2011) TDP-43 is directed to stress granules by sorbitol, a novel physiological osmotic and oxidative stressor. *Molecular and cellular biology*, **31**, 1098-1108.

Dormann, D., Capell, A., Carlson, A.M., Shankaran, S.S., Rodde, R., Neumann, M., Kremmer, E., Matsuwaki, T., Yamanouchi, K., Nishihara, M. & Haass, C. (2009) Proteolytic processing of TAR DNA binding protein-43 by caspases produces C-terminal fragments with disease defining properties independent of progranulin. *Journal of neurochemistry*, **110**, 1082-1094.

Dreumont, N., Hardy, S., Behm-Ansmant, I., Kister, L., Branlant, C., Stevenin, J. & Bourgeois, C.F. (2010) Antagonistic factors control the unproductive splicing of SC35 terminal intron. *Nucleic acids research*, **38**, 1353-1366.

Dreyfuss, G., Kim, V.N. & Kataoka, N. (2002) Messenger-RNA-binding proteins and the messages they carry. *Nature reviews. Molecular cell biology*, **3**, 195-205.

Duysen, E.G., Li, B., Darvesh, S. & Lockridge, O. (2007) Sensitivity of butyrylcholinesterase knockout mice to (--)-huperzine A and donepezil suggests humans with butyrylcholinesterase deficiency may not tolerate these Alzheimer's disease drugs and indicates butyrylcholinesterase function in neurotransmission. *Toxicology*, **233**, 60-69.

Elden, A.C., Kim, H.J., Hart, M.P., Chen-Plotkin, A.S., Johnson, B.S., Fang, X., Armakola, M., Geser, F., Greene, R., Lu, M.M., Padmanabhan, A., Clay-Falcone, D., McCluskey, L., Elman, L., Juhr, D., Gruber, P.J., Rub, U., Auburger, G., Trojanowski, J.Q., Lee, V.M., Van Deerlin, V.M., Bonini, N.M. & Gitler, A.D. (2010) Ataxin-2 intermediate-length polyglutamine expansions are associated with increased risk for ALS. *Nature*, **466**, 1069-1075.

Faber, P.W., Barnes, G.T., Srinidhi, J., Chen, J., Gusella, J.F. & MacDonald, M.E. (1998) Huntingtin interacts with a family of WW domain proteins. *Human molecular genetics*, **7**, 1463-1474.

Feiguin, F., Godena, V.K., Romano, G., D'Ambrogio, A., Klima, R. & Baralle, F.E. (2009) Depletion of TDP-43 affects Drosophila motoneurons terminal synapsis and locomotive behavior. *FEBS letters*, **583**, 1586-1592.

Fiesel, F.C., Voigt, A., Weber, S.S., Van den Haute, C., Waldenmaier, A., Gorner, K., Walter, M., Anderson, M.L., Kern, J.V., Rasse, T.M., Schmidt, T., Springer, W., Kirchner, R., Bonin, M., Neumann, M., Baekelandt, V., Alunni-Fabbroni, M., Schulz, J.B. & Kahle, P.J. (2010) Knockdown of transactive response DNA-binding protein (TDP-43) downregulates histone deacetylase 6. *The EMBO journal*, **29**, 209-221.

Fiesel, F.C., Weber, S.S., Supper, J., Zell, A. & Kahle, P.J. (2011) TDP-43 regulates global translational yield by splicing of exon junction complex component SKAR. *Nucleic acids research*.

Figlewicz, D.A., Krizus, A., Martinoli, M.G., Meininger, V., Dib, M., Rouleau, G.A. & Julien, J.P. (1994) Variants of the heavy neurofilament subunit are associated with the development of amyotrophic lateral sclerosis. *Human molecular genetics*, **3**, 1757-1761.

Fuentealba, R.A., Udan, M., Bell, S., Wegorzewska, I., Shao, J., Diamond, M.I., Weihl, C.C. & Baloh, R.H. (2010) Interaction with polyglutamine aggregates reveals a Q/N-rich domain in TDP-43. *The Journal of biological chemistry*, **285**, 26304-26314.

Gates, G.A., Couropmitree, N.N. & Myers, R.H. (1999) Genetic associations in age-related hearing thresholds. *Archives of otolaryngology--head & neck surgery*, **125**, 654-659.

Gellera, C., Colombrita, C., Ticozzi, N., Castellotti, B., Bragato, C., Ratti, A., Taroni, F. & Silani, V. (2008) Identification of new ANG gene mutations in a large cohort of Italian patients with amyotrophic lateral sclerosis. *Neurogenetics*, **9**, 33-40.

Geser, F., Lee, V.M. & Trojanowski, J.Q. (2010) Amyotrophic lateral sclerosis and frontotemporal lobar degeneration: a spectrum of TDP-43 proteinopathies. *Neuropathology : official journal of the Japanese Society of Neuropathology*, **30**, 103-112.

Geser, F., Martinez-Lage, M., Robinson, J., Uryu, K., Neumann, M., Brandmeir, N.J., Xie, S.X., Kwong, L.K., Elman, L., McCluskey, L., Clark, C.M., Malunda, J., Miller, B.L., Zimmerman, E.A., Qian, J., Van Deerlin, V., Grossman, M., Lee, V.M. & Trojanowski, J.Q. (2009) Clinical and pathological continuum of multisystem TDP-43 proteinopathies. *Archives of neurology*, **66**, 180-189.

Geyer, M.A. (1999) Assessing prepulse inhibition of startle in wild-type and knockout mice. *Psychopharmacology*, **147**, 11-13.

Geyer, M.A., Swerdlow, N.R., Lehmann-Masten, V., Teschendorf, H.J., Traut, M. & Gross, G. (1999) Effects of LU-111995 in three models of disrupted prepulse inhibition in rats. *The Journal of pharmacology and experimental therapeutics*, **290**, 716-724.

Giordana, M.T., Piccinini, M., Grifoni, S., De Marco, G., Vercellino, M., Magistrello, M., Pellerino, A., Buccinna, B., Lupino, E. & Rinaudo, M.T. (2010) TDP-43 redistribution is an early event in sporadic amyotrophic lateral sclerosis. *Brain Pathol*, **20**, 351-360.

Gitcho, M.A., Baloh, R.H., Chakraverty, S., Mayo, K., Norton, J.B., Levitch, D., Hatanpaa, K.J., White, C.L., 3rd, Bigio, E.H., Caselli, R., Baker, M., Al-Lozi, M.T., Morris, J.C., Pestronk, A., Rademakers, R., Goate, A.M. & Cairns, N.J. (2008) TDP-43 A315T mutation in familial motor neuron disease. *Annals of neurology*, **63**, 535-538.

Gitcho, M.A., Bigio, E.H., Mishra, M., Johnson, N., Weintraub, S., Mesulam, M., Rademakers, R., Chakraverty, S., Cruchaga, C., Morris, J.C., Goate, A.M. & Cairns, N.J. (2009) TARDBP 3'-UTR variant in autopsy-confirmed frontotemporal lobar degeneration with TDP-43 proteinopathy. *Acta neuropathologica*, **118**, 633-645.

Gitler, A.D. & Shorter, J. (2011) RNA-binding proteins with prion-like domains in ALS and FTLD-U. *Prion*, **5**, 179-187.

Godena, V.K., Romano, G., Romano, M., Appocher, C., Klima, R., Buratti, E., Baralle, F.E. & Feiguin, F. (2011) TDP-43 regulates Drosophila neuromuscular junctions growth by modulating Futsch/MAP1B levels and synaptic microtubules organization. *PloS one*, **6**, e17808.

Graves, M.C., Fiala, M., Dinglasan, L.A., Liu, N.Q., Sayre, J., Chiappelli, F., van Kooten, C. & Vinters, H.V. (2004) Inflammation in amyotrophic lateral sclerosis spinal cord and brain is mediated by activated macrophages, mast cells and T cells. *Amyotrophic lateral sclerosis and other motor neuron disorders : official publication of the World Federation of Neurology, Research Group on Motor Neuron Diseases*, **5**, 213-219.

Greenway, M.J., Andersen, P.M., Russ, C., Ennis, S., Cashman, S., Donaghy, C., Patterson, V., Swingler, R., Kieran, D., Prehn, J., Morrison, K.E., Green, A., Acharya, K.R., Brown, R.H., Jr. & Hardiman, O. (2006) ANG mutations segregate with familial and 'sporadic' amyotrophic lateral sclerosis. *Nature genetics*, **38**, 411-413.

Gros-Louis, F., Lariviere, R., Gowing, G., Laurent, S., Camu, W., Bouchard, J.P., Meininger, V., Rouleau, G.A. & Julien, J.P. (2004) A frameshift deletion in peripherin gene associated with amyotrophic lateral sclerosis. *The Journal of biological chemistry*, **279**, 45951-45956.

Guo, W., Chen, Y., Zhou, X., Kar, A., Ray, P., Chen, X., Rao, E.J., Yang, M., Ye, H., Zhu, L., Liu, J., Xu, M., Yang, Y., Wang, C., Zhang, D., Bigio, E.H., Mesulam, M., Shen, Y., Xu, Q., Fushimi, K. & Wu, J.Y. (2011) An ALS-associated mutation affecting TDP-43 enhances protein aggregation, fibril formation and neurotoxicity. *Nature structural & molecular biology*, **18**, 822-830.

Gurney, M.E., Pu, H., Chiu, A.Y., Dal Canto, M.C., Polchow, C.Y., Alexander, D.D., Caliendo, J., Hentati, A., Kwon, Y.W., Deng, H.X. & et al. (1994) Motor neuron degeneration in mice that express a human Cu,Zn superoxide dismutase mutation. *Science*, **264**, 1772-1775.

Hadano, S., Hand, C.K., Osuga, H., Yanagisawa, Y., Otomo, A., Devon, R.S., Miyamoto, N., Showguchi-Miyata, J., Okada, Y., Singaraja, R., Figlewicz, D.A., Kwiatkowski, T., Hosler, B.A., Sagie, T., Skaug, J., Nasir, J., Brown, R.H., Jr., Scherer, S.W., Rouleau, G.A., Hayden, M.R. & Ikeda, J.E. (2001) A gene encoding a putative GTPase regulator is mutated in familial amyotrophic lateral sclerosis 2. *Nature genetics*, **29**, 166-173.

Hafezparast, M., Klocke, R., Ruhrberg, C., Marquardt, A., Ahmad-Annuar, A., Bowen, S., Lalli, G., Witherden, A.S., Hummerich, H., Nicholson, S., Morgan, P.J., Oozageer, R., Priestley, J.V., Averill, S., King, V.R., Ball, S., Peters, J., Toda, T., Yamamoto, A., Hiraoka, Y., Augustin, M., Korthaus, D., Wattler, S., Wabnitz, P., Dickneite, C., Lampel, S., Boehme, F., Peraus, G., Popp, A., Rudelius, M., Schlegel, J., Fuchs, H., Hrabe de Angelis, M., Schiavo, G., Shima, D.T., Russ, A.P., Stumm, G., Martin, J.E. & Fisher, E.M. (2003) Mutations in dynein link motor neuron degeneration to defects in retrograde transport. *Science*, **300**, 808-812.

Haidet-Phillips, A.M., Hester, M.E., Miranda, C.J., Meyer, K., Braun, L., Frakes, A., Song, S., Likhite, S., Murtha, M.J., Foust, K.D., Rao, M., Eagle, A., Kammesheidt, A., Christensen, A., Mendell, J.R., Burghes, A.H. & Kaspar, B.K. (2011) Astrocytes from familial and sporadic ALS patients are toxic to motor neurons. *Nature biotechnology*, **29**, 824-828.

Hanson, K.A., Kim, S.H., Wassarman, D.A. & Tibbetts, R.S. (2010) Ubiquilin modifies TDP-43 toxicity in a Drosophila model of amyotrophic lateral sclerosis (ALS). *The Journal of biological chemistry*, **285**, 11068-11072.

Hasegawa, M., Arai, T., Nonaka, T., Kametani, F., Yoshida, M., Hashizume, Y., Beach, T.G., Buratti, E., Baralle, F., Morita, M., Nakano, I., Oda, T., Tsuchiya, K. & Akiyama, H. (2008) Phosphorylated TDP-43 in frontotemporal lobar degeneration and amyotrophic lateral sclerosis. *Annals of neurology*, **64**, 60-70.

Hattula, K. & Peranen, J. (2000) FIP-2, a coiled-coil protein, links Huntingtin to Rab8 and modulates cellular morphogenesis. *Current biology : CB*, **10**, 1603-1606.

Hewitt, C., Kirby, J., Highley, J.R., Hartley, J.A., Hibberd, R., Hollinger, H.C., Williams, T.L., Ince, P.G., McDermott, C.J. & Shaw, P.J. (2010) Novel FUS/TLS mutations and pathology in familial and sporadic amyotrophic lateral sclerosis. *Archives of neurology*, **67**, 455-461.

Hirano, A. (1996) Neuropathology of ALS: an overview. *Neurology*, **47**, S63-66.

Hu, F., Padukkavidana, T., Vaegter, C.B., Brady, O.A., Zheng, Y., Mackenzie, I.R., Feldman, H.H., Nykjaer, A. & Strittmatter, S.M. (2010) Sortilin-mediated endocytosis determines levels of the frontotemporal dementia protein, progranulin. *Neuron*, **68**, 654-667.

Igaz, L.M., Kwong, L.K., Chen-Plotkin, A., Winton, M.J., Unger, T.L., Xu, Y., Neumann, M., Trojanowski, J.Q. & Lee, V.M. (2009) Expression of TDP-43 C-terminal Fragments in Vitro Recapitulates Pathological Features of TDP-43 Proteinopathies. *The Journal of biological chemistry*, **284**, 8516-8524.

Igaz, L.M., Kwong, L.K., Lee, E.B., Chen-Plotkin, A., Swanson, E., Unger, T., Malunda, J., Xu, Y., Winton, M.J., Trojanowski, J.Q. & Lee, V.M. (2011) Dysregulation of the ALS-associated gene TDP-43 leads to neuronal death and degeneration in mice. *The Journal of clinical investigation*, **121**, 726-738.

Igaz, L.M., Kwong, L.K., Xu, Y., Truax, A.C., Uryu, K., Neumann, M., Clark, C.M., Elman, L.B., Miller, B.L., Grossman, M., McCluskey, L.F., Trojanowski, J.Q. & Lee, V.M. (2008) Enrichment of C-terminal fragments in TAR DNA-binding protein-43 cytoplasmic inclusions in brain but not in spinal cord of frontotemporal lobar degeneration and amyotrophic lateral sclerosis. *The American journal of pathology*, **173**, 182-194.

Iguchi, Y., Katsuno, M., Niwa, J., Yamada, S., Sone, J., Waza, M., Adachi, H., Tanaka, F., Nagata, K., Arimura, N., Watanabe, T., Kaibuchi, K. & Sobue, G. (2009) TDP-43 depletion induces neuronal cell damage through dysregulation of Rho family GTPases. *The Journal of biological chemistry*, **284**, 22059-22066.

Ilieva, H., Polymenidou, M. & Cleveland, D.W. (2009) Non-cell autonomous toxicity in neurodegenerative disorders: ALS and beyond. *The Journal of cell biology*, **187**, 761-772.

Ingman, K., Sallinen, J., Honkanen, A. & Korpi, E.R. (2004) Comparison of deramciclane to benzodiazepine agonists in behavioural activity of mice and in alcohol drinking of alcohol-preferring rats. *Pharmacology, biochemistry, and behavior*, **77**, 847-854.

Johnson, B.S., Snead, D., Lee, J.J., McCaffery, J.M., Shorter, J. & Gitler, A.D. (2009) TDP-43 is intrinsically aggregation-prone, and amyotrophic lateral sclerosis-linked mutations accelerate aggregation and increase toxicity. *The Journal of biological chemistry*, **284**, 20329-20339.

Johnson, J.O., Mandrioli, J., Benatar, M., Abramzon, Y., Van Deerlin, V.M., Trojanowski, J.Q., Gibbs, J.R., Brunetti, M., Gronka, S., Wuu, J., Ding, J., McCluskey, L., Martinez-Lage, M., Falcone, D., Hernandez, D.G., Arepalli, S., Chong, S., Schymick, J.C., Rothstein, J., Landi, F., Wang, Y.D., Calvo, A., Mora, G., Sabatelli, M., Monsurro, M.R., Battistini, S., Salvi, F., Spataro, R., Sola, P., Borghero, G., Galassi, G., Scholz, S.W., Taylor, J.P., Restagno, G., Chio, A. & Traynor, B.J. (2010) Exome sequencing reveals VCP mutations as a cause of familial ALS. *Neuron*, **68**, 857-864.

Joyce, P.I., Fratta, P., Fisher, E.M. & Acevedo-Arozena, A. (2011) SOD1 and TDP-43 animal models of amyotrophic lateral sclerosis: recent advances in understanding disease toward the development of clinical treatments. *Mammalian genome : official journal of the International Mammalian Genome Society*, **22**, 420-448.

Justice, M.J., Noveroske, J.K., Weber, J.S., Zheng, B. & Bradley, A. (1999) Mouse ENU mutagenesis. *Human molecular genetics*, **8**, 1955-1963.

Kabashi, E., Lin, L., Tradewell, M.L., Dion, P.A., Bercier, V., Bourgouin, P., Rochefort, D., Bel Hadj, S., Durham, H.D., Vande Velde, C., Rouleau, G.A. & Drapeau, P. (2010) Gain and loss of function of ALS-related mutations of TARDBP (TDP-43) cause motor deficits in vivo. *Human molecular genetics*, **19**, 671-683.

Kabashi, E., Valdmanis, P.N., Dion, P., Spiegelman, D., McConkey, B.J., Vande Velde, C., Bouchard, J.P., Lacomblez, L., Pochigaeva, K., Salachas, F., Pradat, P.F., Camu, W., Meininger, V., Dupre, N. & Rouleau, G.A. (2008) TARDBP mutations in individuals with sporadic and familial amyotrophic lateral sclerosis. *Nature genetics*, **40**, 572-574.

Kasai, T., Tokuda, T., Ishigami, N., Sasayama, H., Foulds, P., Mitchell, D.J., Mann, D.M., Allsop, D. & Nakagawa, M. (2009) Increased TDP-43 protein in cerebrospinal fluid of patients with amyotrophic lateral sclerosis. *Acta neuropathologica*, **117**, 55-62.

Kawahara, Y. & Mieda-Sato, A. (2012) TDP-43 promotes microRNA biogenesis as a component of the Drosha and Dicer complexes. *Proceedings of the National Academy of Sciences of the United States of America*.

Kazazian, H.H., Jr. & Moran, J.V. (1998) The impact of L1 retrotransposons on the human genome. *Nature genetics*, **19**, 19-24.

Keays, D.A., Clark, T.G. & Flint, J. (2006) Estimating the number of coding mutations in genotypic- and phenotypic-driven N-ethyl-N-nitrosourea (ENU) screens. *Mammalian genome : official journal of the International Mammalian Genome Society*, **17**, 230-238.

Keithley, E.M., Canto, C., Zheng, Q.Y., Fischel-Ghodsian, N. & Johnson, K.R. (2004) Age-related hearing loss and the ahl locus in mice. *Hearing research*, **188**, 21-28.

Kocerha, J., Kouri, N., Baker, M., Finch, N., DeJesus-Hernandez, M., Gonzalez, J., Chidamparam, K., Josephs, K.A., Boeve, B.F., Graff-Radford, N.R., Crook, J., Dickson, D.W. & Rademakers, R. (2011) Altered microRNA expression in frontotemporal lobar degeneration with TDP-43 pathology caused by progranulin mutations. *BMC genomics*, **12**, 527.

Kraemer, B.C., Schuck, T., Wheeler, J.M., Robinson, L.C., Trojanowski, J.Q., Lee, V.M. & Schellenberg, G.D. (2010) Loss of murine TDP-43 disrupts motor function and plays an essential role in embryogenesis. *Acta neuropathologica*, **119**, 409-419.

Kuhnlein, P., Sperfeld, A.D., Vanmassenhove, B., Van Deerlin, V., Lee, V.M., Trojanowski, J.Q., Kretzschmar, H.A., Ludolph, A.C. & Neumann, M. (2008) Two German kindreds with familial amyotrophic lateral sclerosis due to TARDBP mutations. *Archives of neurology*, **65**, 1185-1189.

Kuo, P.H., Doudeva, L.G., Wang, Y.T., Shen, C.K. & Yuan, H.S. (2009) Structural insights into TDP-43 in nucleic-acid binding and domain interactions. *Nucleic acids research*, **37**, 1799-1808.

Kwiatkowski, T.J., Jr., Bosco, D.A., Leclerc, A.L., Tamrazian, E., Vanderburg, C.R., Russ, C., Davis, A., Gilchrist, J., Kasarskis, E.J., Munsat, T., Valdmanis, P., Rouleau, G.A., Hosler, B.A., Cortelli, P., de Jong, P.J., Yoshinaga, Y., Haines, J.L., Pericak-Vance, M.A., Yan, J., Ticozzi, N., Siddique, T., McKenna-Yasek, D., Sapp, P.C., Horvitz, H.R., Landers, J.E. & Brown, R.H., Jr. (2009) Mutations in the FUS/TLS gene on chromosome 16 cause familial amyotrophic lateral sclerosis. *Science*, **323**, 1205-1208.

Kwong, L.K., Uryu, K., Trojanowski, J.Q. & Lee, V.M. (2008) TDP-43 proteinopathies: neurodegenerative protein misfolding diseases without amyloidosis. *Neuro-Signals*, **16**, 41-51.

Lagier-Tourenne, C., Polymenidou, M. & Cleveland, D.W. (2010) TDP-43 and FUS/TLS: emerging roles in RNA processing and neurodegeneration. *Human molecular genetics*, **19**, R46-64.

Laird, A.S., Van Hoecke, A., De Muynck, L., Timmers, M., Van den Bosch, L., Van Damme, P. & Robberecht, W. (2010) Progranulin is neurotrophic in vivo and protects against a mutant TDP-43 induced axonopathy. *PloS one*, **5**, e13368.

Landers, J.E., Leclerc, A.L., Shi, L., Virkud, A., Cho, T., Maxwell, M.M., Henry, A.F., Polak, M., Glass, J.D., Kwiatkowski, T.J., Al-Chalabi, A., Shaw, C.E., Leigh, P.N., Rodriguez-Leyza, I., McKenna-Yasek, D., Sapp, P.C. & Brown, R.H., Jr. (2008) New VAPB deletion variant and exclusion of VAPB mutations in familial ALS. *Neurology*, **70**, 1179-1185.

Lanson, N.A., Jr., Maltare, A., King, H., Smith, R., Kim, J.H., Taylor, J.P., Lloyd, T.E. & Pandey, U.B. (2011) A Drosophila model of FUS-related neurodegeneration reveals genetic interaction between FUS and TDP-43. *Human molecular genetics*, **20**, 2510-2523.

Lee, E.B., Lee, V.M. & Trojanowski, J.Q. (2012) Gains or losses: molecular mechanisms of TDP43-mediated neurodegeneration. *Nature reviews. Neuroscience*, **13**, 38-50.

Li, Y., Ray, P., Rao, E.J., Shi, C., Guo, W., Chen, X., Woodruff, E.A., 3rd, Fushimi, K. & Wu, J.Y. (2010) A Drosophila model for TDP-43 proteinopathy. *Proceedings of the National Academy of Sciences of the United States of America*, **107**, 3169-3174.

Liachko, N.F., Guthrie, C.R. & Kraemer, B.C. (2010) Phosphorylation promotes neurotoxicity in a Caenorhabditis elegans model of TDP-43 proteinopathy. *The Journal of neuroscience : the official journal of the Society for Neuroscience*, **30**, 16208-16219.

Ling, S.C., Albuquerque, C.P., Han, J.S., Lagier-Tourenne, C., Tokunaga, S., Zhou, H. & Cleveland, D.W. (2010) ALS-associated mutations in TDP-43 increase its stability and promote TDP-43 complexes with FUS/TLS. *Proceedings of the National Academy of Sciences of the United States of America*, **107**, 13318-13323.

Liscic, R.M., Grinberg, L.T., Zidar, J., Gitcho, M.A. & Cairns, N.J. (2008) ALS and FTLD: two faces of TDP-43 proteinopathy. *European journal of neurology : the official journal of the European Federation of Neurological Societies*, **15**, 772-780.

Liu-Yesucevitz, L., Bilgutay, A., Zhang, Y.J., Vanderweyde, T., Citro, A., Mehta, T., Zaarur, N., McKee, A., Bowser, R., Sherman, M., Petrucelli, L. & Wolozin, B. (2010) Tar DNA binding protein-43 (TDP-43) associates with stress granules: analysis of cultured cells and pathological brain tissue. *PloS one*, **5**, e13250.

Lomen-Hoerth, C., Murphy, J., Langmore, S., Kramer, J.H., Olney, R.K. & Miller, B. (2003) Are amyotrophic lateral sclerosis patients cognitively normal? *Neurology*, **60**, 1094-1097.

Lu, Y., Ferris, J. & Gao, F.B. (2009) Frontotemporal dementia and amyotrophic lateral sclerosis-associated disease protein TDP-43 promotes dendritic branching. *Molecular brain*, **2**, 30.

Mackenzie, I.R., Baborie, A., Pickering-Brown, S., Du Plessis, D., Jaros, E., Perry, R.H., Neary, D., Snowden, J.S. & Mann, D.M. (2006) Heterogeneity of ubiquitin pathology in frontotemporal lobar degeneration: classification and relation to clinical phenotype. *Acta neuropathologica*, **112**, 539-549.

Mackenzie, I.R., Bigio, E.H., Ince, P.G., Geser, F., Neumann, M., Cairns, N.J., Kwong, L.K., Forman, M.S., Ravits, J., Stewart, H., Eisen, A., McClusky, L., Kretzschmar, H.A., Monoranu, C.M., Highley, J.R., Kirby, J., Siddique, T., Shaw, P.J., Lee, V.M. & Trojanowski, J.Q. (2007) Pathological TDP-43 distinguishes sporadic amyotrophic lateral sclerosis from amyotrophic lateral sclerosis with SOD1 mutations. *Annals of neurology*, **61**, 427-434.

Mackenzie, I.R., Neumann, M., Baborie, A., Sampathu, D.M., Du Plessis, D., Jaros, E., Perry, R.H., Trojanowski, J.Q., Mann, D.M. & Lee, V.M. (2011) A harmonized classification system for FTLD-TDP pathology. *Acta neuropathologica*, **122**, 111-113.

Majounie, E., Renton, A.E., Mok, K., Dopper, E.G., Waite, A., Rollinson, S., Chio, A., Restagno, G., Nicolaou, N., Simon-Sanchez, J., van Swieten, J.C., Abramzon, Y., Johnson, J.O., Sendtner, M., Pamphlett, R., Orrell, R.W., Mead, S., Sidle, K.C., Houlden, H., Rohrer, J.D., Morrison, K.E., Pall, H., Talbot, K., Ansorge, O., Hernandez, D.G., Arepalli, S., Sabatelli, M., Mora, G., Corbo, M., Giannini, F., Calvo, A., Englund, E., Borghero, G., Floris, G.L., Remes, A.M., Laaksovirta, H., McCluskey, L., Trojanowski, J.Q., Van Deerlin, V.M., Schellenberg, G.D., Nalls, M.A., Drory, V.E., Lu, C.S., Yeh, T.H., Ishiura, H., Takahashi, Y., Tsuji, S., Le Ber, I., Brice, A., Drepper, C., Williams, N., Kirby, J., Shaw, P., Hardy, J., Tienari, P.J., Heutink, P., Morris, H.R., Pickering-Brown, S. & Traynor, B.J. (2012) Frequency of the C9orf72 hexanucleotide repeat expansion in patients with amyotrophic lateral sclerosis and frontotemporal dementia: a cross-sectional study. *Lancet neurology*, **11**, 323-330.

Manfredi, G. & Xu, Z. (2005) Mitochondrial dysfunction and its role in motor neuron degeneration in ALS. *Mitochondrion*, **5**, 77-87.

Maruyama, H., Morino, H., Ito, H., Izumi, Y., Kato, H., Watanabe, Y., Kinoshita, Y., Kamada, M., Nodera, H., Suzuki, H., Komure, O., Matsuura, S., Kobatake, K., Morimoto, N., Abe, K., Suzuki, N., Aoki, M., Kawata, A., Hirai, T., Kato, T., Ogasawara, K., Hirano, A., Takumi, T., Kusaka, H., Hagiwara, K., Kaji, R. & Kawakami, H. (2010) Mutations of optineurin in amyotrophic lateral sclerosis. *Nature*, **465**, 223-226.

Mercado, P.A., Ayala, Y.M., Romano, M., Buratti, E. & Baralle, F.E. (2005) Depletion of TDP 43 overrides the need for exonic and intronic splicing enhancers in the human apoA-II gene. *Nucleic acids research*, **33**, 6000-6010.

Messaoudi, M., Rozan, P., Nejdi, A., Hidalgo, S. & Desor, D. (2005) Behavioural and cognitive effects of oligofructose-enriched inulin in rats. *The British journal of nutrition*, **93 Suppl 1**, S27-30.

Miguel, L., Frebourg, T., Campion, D. & Lecourtois, M. (2011) Both cytoplasmic and nuclear accumulations of the protein are neurotoxic in Drosophila models of TDP-43 proteinopathies. *Neurobiology of disease*, **41**, 398-406.

Miller, R.G., Mitchell, J.D., Lyon, M. & Moore, D.H. (2007) Riluzole for amyotrophic lateral sclerosis (ALS)/motor neuron disease (MND). *Cochrane Database Syst Rev*, CD001447.

Mishra, M., Paunesku, T., Woloschak, G.E., Siddique, T., Zhu, L.J., Lin, S., Greco, K. & Bigio, E.H. (2007) Gene expression analysis of frontotemporal lobar degeneration of the motor neuron disease type with ubiquitinated inclusions. *Acta neuropathologica*, **114**, 81-94.

Moisse, K., Mepham, J., Volkening, K., Welch, I., Hill, T. & Strong, M.J. (2009a) Cytosolic TDP-43 expression following axotomy is associated with caspase 3 activation in NFL-/- mice: support for a role for TDP-43 in the physiological response to neuronal injury. *Brain research*, **1296**, 176-186.

Moisse, K., Volkening, K., Leystra-Lantz, C., Welch, I., Hill, T. & Strong, M.J. (2009b) Divergent patterns of cytosolic TDP-43 and neuronal progranulin expression following axotomy: implications for TDP-43 in the physiological response to neuronal injury. *Brain research*, **1249**, 202-211.

Moreland, R.J., Dresser, M.E., Rodgers, J.S., Roe, B.A., Conaway, J.W., Conaway, R.C. & Hanas, J.S. (2000) Identification of a transcription factor IIIA-interacting protein. *Nucleic acids research*, **28**, 1986-1993.

Mori, F., Tanji, K., Zhang, H.X., Nishihira, Y., Tan, C.F., Takahashi, H. & Wakabayashi, K. (2008) Maturation process of TDP-43-positive neuronal cytoplasmic inclusions in amyotrophic lateral sclerosis with and without dementia. *Acta neuropathologica*, **116**, 193-203.

Munch, C., Sedlmeier, R., Meyer, T., Homberg, V., Sperfeld, A.D., Kurt, A., Prudlo, J., Peraus, G., Hanemann, C.O., Stumm, G. & Ludolph, A.C. (2004) Point mutations of the p150 subunit of dynactin (DCTN1) gene in ALS. *Neurology*, **63**, 724-726.

Nagai, M., Re, D.B., Nagata, T., Chalazonitis, A., Jessell, T.M., Wichterle, H. & Przedborski, S. (2007) Astrocytes expressing ALS-linked mutated SOD1 release factors selectively toxic to motor neurons. *Nature neuroscience*, **10**, 615-622.

Neumann, M. (2009) Molecular neuropathology of TDP-43 proteinopathies. *International journal of molecular sciences*, **10**, 232-246.

Neumann, M., Sampathu, D.M., Kwong, L.K., Truax, A.C., Micsenyi, M.C., Chou, T.T., Bruce, J., Schuck, T., Grossman, M., Clark, C.M., McCluskey, L.F., Miller, B.L., Masliah, E., Mackenzie, I.R., Feldman, H., Feiden, W., Kretzschmar, H.A., Trojanowski, J.Q. & Lee, V.M. (2006) Ubiquitinated TDP-43 in frontotemporal lobar degeneration and amyotrophic lateral sclerosis. *Science*, **314**, 130-133.

Niksic, M., Romano, M., Buratti, E., Pagani, F. & Baralle, F.E. (1999) Functional analysis of cis-acting elements regulating the alternative splicing of human CFTR exon 9. *Human molecular genetics*, **8**, 2339-2349.

Nishimoto, Y., Ito, D., Yagi, T., Nihei, Y., Tsunoda, Y. & Suzuki, N. (2010) Characterization of alternative isoforms and inclusion body of the TAR DNA-binding protein-43. *The Journal of biological chemistry*, **285**, 608-619.

Nishimura, A.L., Mitne-Neto, M., Silva, H.C., Richieri-Costa, A., Middleton, S., Cascio, D., Kok, F., Oliveira, J.R., Gillingwater, T., Webb, J., Skehel, P. & Zatz, M. (2004) A mutation in the vesicle-trafficking protein VAPB causes late-onset spinal muscular atrophy and amyotrophic lateral sclerosis. *American journal of human genetics*, **75**, 822-831.

Nonaka, T., Kametani, F., Arai, T., Akiyama, H. & Hasegawa, M. (2009) Truncation and pathogenic mutations facilitate the formation of intracellular aggregates of TDP-43. *Human molecular genetics*, **18**, 3353-3364.

O'Neill, J.P. (2000) DNA damage, DNA repair, cell proliferation, and DNA replication: how do gene mutations result? *Proceedings of the National Academy of Sciences of the United States of America*, **97**, 11137-11139.

Ou, S.H., Wu, F., Harrich, D., Garcia-Martinez, L.F. & Gaynor, R.B. (1995) Cloning and characterization of a novel cellular protein, TDP-43, that binds to human immunodeficiency virus type 1 TAR DNA sequence motifs. *Journal of virology*, **69**, 3584-3596.

Ouagazzal, A., Grottick, A.J., Moreau, J. & Higgins, G.A. (2001a) Effect of LSD on prepulse inhibition and spontaneous behavior in the rat. A pharmacological analysis and comparison between two rat strains. *Neuropsychopharmacology : official publication of the American College of Neuropsychopharmacology*, **25**, 565-575.

Ouagazzal, A.M., Jenck, F. & Moreau, J.L. (2001b) Drug-induced potentiation of prepulse inhibition of acoustic startle reflex in mice: a model for detecting antipsychotic activity? *Psychopharmacology*, **156**, 273-283.

Pagani, F., Buratti, E., Stuani, C. & Baralle, F.E. (2003a) Missense, nonsense, and neutral mutations define juxtaposed regulatory elements of splicing in cystic fibrosis transmembrane regulator exon 9. *The Journal of biological chemistry*, **278**, 26580-26588.

Pagani, F., Stuani, C., Zuccato, E., Kornblihtt, A.R. & Baralle, F.E. (2003b) Promoter architecture modulates CFTR exon 9 skipping. *The Journal of biological chemistry*, **278**, 1511-1517.

Parker, S.J., Meyerowitz, J., James, J.L., Liddell, J.R., Crouch, P.J., Kanninen, K.M. & White, A.R. (2012) Endogenous TDP-43 localized to stress granules can subsequently form protein aggregates. *Neurochemistry international*.

Paubel, A., Violette, J., Amy, M., Praline, J., Meininger, V., Camu, W., Corcia, P., Andres, C.R. & Vourc'h, P. (2008) Mutations of the ANG gene in French patients with sporadic amyotrophic lateral sclerosis. *Archives of neurology*, **65**, 1333-1336.

Petrucelli, L. & Dawson, T.M. (2004) Mechanism of neurodegenerative disease: role of the ubiquitin proteasome system. *Annals of medicine*, **36**, 315-320.

Polymenidou, M., Lagier-Tourenne, C., Hutt, K.R., Huelga, S.C., Moran, J., Liang, T.Y., Ling, S.C., Sun, E., Wancewicz, E., Mazur, C., Kordasiewicz, H., Sedaghat, Y., Donohue, J.P., Shiue, L., Bennett, C.F., Yeo, G.W. & Cleveland, D.W. (2011) Long pre-mRNA depletion and RNA missplicing contribute to neuronal vulnerability from loss of TDP-43. *Nature neuroscience*, **14**, 459-468.

Puls, I., Jonnakuty, C., LaMonte, B.H., Holzbaur, E.L., Tokito, M., Mann, E., Floeter, M.K., Bidus, K., Drayna, D., Oh, S.J., Brown, R.H., Jr., Ludlow, C.L. & Fischbeck, K.H. (2003) Mutant dynactin in motor neuron disease. *Nature genetics*, **33**, 455-456.

Quwailid, M.M., Hugill, A., Dear, N., Vizor, L., Wells, S., Horner, E., Fuller, S., Weedon, J., McMath, H., Woodman, P., Edwards, D., Campbell, D., Rodger, S., Carey, J., Roberts, A., Glenister, P., Lalanne, Z., Parkinson, N., Coghill, E.L., McKeone, R., Cox, S., Willan, J., Greenfield, A., Keays, D., Brady, S., Spurr, N., Gray, I., Hunter, J., Brown, S.D. & Cox, R.D. (2004) A gene-driven ENU-based approach to generating an allelic series in any gene. *Mammalian genome : official journal of the International Mammalian Genome Society*, **15**, 585-591.

Rademakers, R. (2012) C9orf72 repeat expansions in patients with ALS and FTD. *Lancet neurology*, **11**, 297-298.

Renton, A.E., Majounie, E., Waite, A., Simon-Sanchez, J., Rollinson, S., Gibbs, J.R., Schymick, J.C., Laaksovirta, H., van Swieten, J.C., Myllykangas, L., Kalimo, H., Paetau, A., Abramzon, Y., Remes, A.M., Kaganovich, A., Scholz, S.W., Duckworth, J., Ding, J., Harmer, D.W., Hernandez, D.G., Johnson, J.O., Mok, K., Ryten, M., Trabzuni, D.,

Guerreiro, R.J., Orrell, R.W., Neal, J., Murray, A., Pearson, J., Jansen, I.E., Sondervan, D., Seelaar, H., Blake, D., Young, K., Halliwell, N., Callister, J.B., Toulson, G., Richardson, A., Gerhard, A., Snowden, J., Mann, D., Neary, D., Nalls, M.A., Peuralinna, T., Jansson, L., Isoviita, V.M., Kaivorinne, A.L., Holtta-Vuori, M., Ikonen, E., Sulkava, R., Benatar, M., Wuu, J., Chio, A., Restagno, G., Borghero, G., Sabatelli, M., Heckerman, D., Rogaeva, E., Zinman, L., Rothstein, J.D., Sendtner, M., Drepper, C., Eichler, E.E., Alkan, C., Abdullaev, Z., Pack, S.D., Dutra, A., Pak, E., Hardy, J., Singleton, A., Williams, N.M., Heutink, P., Pickering-Brown, S., Morris, H.R., Tienari, P.J. & Traynor, B.J. (2011) A hexanucleotide repeat expansion in C9ORF72 is the cause of chromosome 9p21-linked ALS-FTD. *Neuron*, **72**, 257-268.

Robertson, J., Sanelli, T., Xiao, S., Yang, W., Horne, P., Hammond, R., Pioro, E.P. & Strong, M.J. (2007) Lack of TDP-43 abnormalities in mutant SOD1 transgenic mice shows disparity with ALS. *Neuroscience letters*, **420**, 128-132.

Rosen, D.R. (1993) Mutations in Cu/Zn superoxide dismutase gene are associated with familial amyotrophic lateral sclerosis. *Nature*, **364**, 362.

Rozmahel, R., Heng, H.H., Duncan, A.M., Shi, X.M., Rommens, J.M. & Tsui, L.C. (1997) Amplification of CFTR exon 9 sequences to multiple locations in the human genome. *Genomics*, **45**, 554-561.

Russell, W.L., Kelly, E.M., Hunsicker, P.R., Bangham, J.W., Maddux, S.C. & Phipps, E.L. (1979) Specific-locus test shows ethylnitrosourea to be the most potent mutagen in the mouse. *Proceedings of the National Academy of Sciences of the United States of America*, **76**, 5818-5819.

Sampathu, D.M., Neumann, M., Kwong, L.K., Chou, T.T., Micsenyi, M., Truax, A., Bruce, J., Grossman, M., Trojanowski, J.Q. & Lee, V.M. (2006) Pathological heterogeneity of frontotemporal lobar degeneration with ubiquitin-positive inclusions delineated by ubiquitin immunohistochemistry and novel monoclonal antibodies. *The American journal of pathology*, **169**, 1343-1352.

Schymick, J.C., Scholz, S.W., Fung, H.C., Britton, A., Arepalli, S., Gibbs, J.R., Lombardo, F., Matarin, M., Kasperaviciute, D., Hernandez, D.G., Crews, C., Bruijn, L., Rothstein, J., Mora, G., Restagno, G., Chio, A., Singleton, A., Hardy, J. & Traynor, B.J. (2007) Genome-wide genotyping in amyotrophic lateral sclerosis and neurologically normal controls: first stage analysis and public release of data. *Lancet neurology*, **6**, 322-328.

Seelaar, H., Rohrer, J.D., Pijnenburg, Y.A., Fox, N.C. & van Swieten, J.C. (2011) Clinical, genetic and pathological heterogeneity of frontotemporal dementia: a review. *Journal of neurology, neurosurgery, and psychiatry*, **82**, 476-486.

Sephton, C.F., Cenik, C., Kucukural, A., Dammer, E.B., Cenik, B., Han, Y., Dewey, C.M., Roth, F.P., Herz, J., Peng, J., Moore, M.J. & Yu, G. (2011) Identification of neuronal RNA

targets of TDP-43-containing ribonucleoprotein complexes. *The Journal of biological chemistry*, **286**, 1204-1215.

Sephton, C.F., Good, S.K., Atkin, S., Dewey, C.M., Mayer, P., 3rd, Herz, J. & Yu, G. (2010) TDP-43 is a developmentally regulated protein essential for early embryonic development. *The Journal of biological chemistry*, **285**, 6826-6834.

Shan, X., Chiang, P.M., Price, D.L. & Wong, P.C. (2010) Altered distributions of Gemini of coiled bodies and mitochondria in motor neurons of TDP-43 transgenic mice. *Proceedings of the National Academy of Sciences of the United States of America*, **107**, 16325-16330.

Shaw, P.J. & Ince, P.G. (1997) Glutamate, excitotoxicity and amyotrophic lateral sclerosis. *Journal of neurology*, **244 Suppl 2**, S3-14.

Simpson, C.L., Lemmens, R., Miskiewicz, K., Broom, W.J., Hansen, V.K., van Vught, P.W., Landers, J.E., Sapp, P., Van Den Bosch, L., Knight, J., Neale, B.M., Turner, M.R., Veldink, J.H., Ophoff, R.A., Tripathi, V.B., Beleza, A., Shah, M.N., Proitsi, P., Van Hoecke, A., Carmeliet, P., Horvitz, H.R., Leigh, P.N., Shaw, C.E., van den Berg, L.H., Sham, P.C., Powell, J.F., Verstreken, P., Brown, R.H., Jr., Robberecht, W. & Al-Chalabi, A. (2009) Variants of the elongator protein 3 (ELP3) gene are associated with motor neuron degeneration. *Human molecular genetics*, **18**, 472-481.

Simpson, H.B. (2010) Anxiety disorders theory, research, and clinical perspectives. Cambridge University Press,, Cambridge, UK ; New York, pp. 1 online resource (xv, 378 p.).

Sreedharan, J., Blair, I.P., Tripathi, V.B., Hu, X., Vance, C., Rogelj, B., Ackerley, S., Durnall, J.C., Williams, K.L., Buratti, E., Baralle, F., de Belleroche, J., Mitchell, J.D., Leigh, P.N., Al-Chalabi, A., Miller, C.C., Nicholson, G. & Shaw, C.E. (2008) TDP-43 mutations in familial and sporadic amyotrophic lateral sclerosis. *Science*, **319**, 1668-1672.

Stallings, N.R., Puttaparthi, K., Luther, C.M., Burns, D.K. & Elliott, J.L. (2010) Progressive motor weakness in transgenic mice expressing human TDP-43. *Neurobiology of disease*, **40**, 404-414.

Strong, M.J. & Volkening, K. (2011) TDP-43 and FUS/TLS: sending a complex message about messenger RNA in amyotrophic lateral sclerosis? *The FEBS journal*, **278**, 3569-3577.

Suraweera, A., Lim, Y., Woods, R., Birrell, G.W., Nasim, T., Becherel, O.J. & Lavin, M.F. (2009) Functional role for senataxin, defective in ataxia oculomotor apraxia type 2, in transcriptional regulation. *Human molecular genetics*, **18**, 3384-3396.

Swarup, V., Phaneuf, D., Bareil, C., Robertson, J., Rouleau, G.A., Kriz, J. & Julien, J.P. (2011a) Pathological hallmarks of amyotrophic lateral sclerosis/frontotemporal lobar

degeneration in transgenic mice produced with TDP-43 genomic fragments. *Brain : a journal of neurology*, **134**, 2610-2626.

Swarup, V., Phaneuf, D., Dupre, N., Petri, S., Strong, M., Kriz, J. & Julien, J.P. (2011b) Deregulation of TDP-43 in amyotrophic lateral sclerosis triggers nuclear factor kappaB-mediated pathogenic pathways. *The Journal of experimental medicine*, **208**, 2429-2447.

Talbot, K. & Ansorge, O. (2006) Recent advances in the genetics of amyotrophic lateral sclerosis and frontotemporal dementia: common pathways in neurodegenerative disease. *Human molecular genetics*, **15 Spec No 2**, R182-187.

Tollervey, J.R., Curk, T., Rogelj, B., Briese, M., Cereda, M., Kayikci, M., Konig, J., Hortobagyi, T., Nishimura, A.L., Zupunski, V., Patani, R., Chandran, S., Rot, G., Zupan, B., Shaw, C.E. & Ule, J. (2011) Characterizing the RNA targets and position-dependent splicing regulation by TDP-43. *Nature neuroscience*, **14**, 452-458.

Tsai, K.J., Yang, C.H., Fang, Y.H., Cho, K.H., Chien, W.L., Wang, W.T., Wu, T.W., Lin, C.P., Fu, W.M. & Shen, C.K. (2010) Elevated expression of TDP-43 in the forebrain of mice is sufficient to cause neurological and pathological phenotypes mimicking FTLD-U. *The Journal of experimental medicine*, **207**, 1661-1673.

Turner, B.J., Baumer, D., Parkinson, N.J., Scaber, J., Ansorge, O. & Talbot, K. (2008) TDP-43 expression in mouse models of amyotrophic lateral sclerosis and spinal muscular atrophy. *BMC neuroscience*, **9**, 104.

Uchida, A., Sasaguri, H., Kimura, N., Tajiri, M., Ohkubo, T., Ono, F., Sakaue, F., Kanai, K., Hirai, T., Sano, T., Shibuya, K., Kobayashi, M., Yamamoto, M., Yokota, S., Kubodera, T., Tomori, M., Sakaki, K., Enomoto, M., Hirai, Y., Kumagai, J., Yasutomi, Y., Mochizuki, H., Kuwabara, S., Uchihara, T., Mizusawa, H. & Yokota, T. (2012) Non-human primate model of amyotrophic lateral sclerosis with cytoplasmic mislocalization of TDP-43. *Brain : a journal of neurology*.

Udan, M. & Baloh, R.H. (2011) Implications of the prion-related Q/N domains in TDP-43 and FUS. *Prion*, **5**, 1-5.

van Blitterswijk, M., van Vught, P.W., van Es, M.A., Schelhaas, H.J., van der Kooi, A.J., de Visser, M., Veldink, J.H. & van den Berg, L.H. (2012) Novel optineurin mutations in sporadic amyotrophic lateral sclerosis patients. *Neurobiology of aging*, **33**, 1016 e1011-1017.

Van Damme, P., Veldink, J.H., van Blitterswijk, M., Corveleyn, A., van Vught, P.W., Thijs, V., Dubois, B., Matthijs, G., van den Berg, L.H. & Robberecht, W. (2011) Expanded ATXN2 CAG repeat size in ALS identifies genetic overlap between ALS and SCA2. *Neurology*, **76**, 2066-2072.

van Swieten, J.C. & Heutink, P. (2008) Mutations in progranulin (GRN) within the spectrum of clinical and pathological phenotypes of frontotemporal dementia. *Lancet neurology*, **7**, 965-974.

Vance, C., Rogelj, B., Hortobagyi, T., De Vos, K.J., Nishimura, A.L., Sreedharan, J., Hu, X., Smith, B., Ruddy, D., Wright, P., Ganesalingam, J., Williams, K.L., Tripathi, V., Al-Saraj, S., Al-Chalabi, A., Leigh, P.N., Blair, I.P., Nicholson, G., de Belleroche, J., Gallo, J.M., Miller, C.C. & Shaw, C.E. (2009) Mutations in FUS, an RNA processing protein, cause familial amyotrophic lateral sclerosis type 6. *Science*, **323**, 1208-1211.

Vilarino-Guell, C., Wider, C., Soto-Ortolaza, A.I., Cobb, S.A., Kachergus, J.M., Keeling, B.H., Dachsel, J.C., Hulihan, M.M., Dickson, D.W., Wszolek, Z.K., Uitti, R.J., Graff-Radford, N.R., Boeve, B.F., Josephs, K.A., Miller, B., Boylan, K.B., Gwinn, K., Adler, C.H., Aasly, J.O., Hentati, F., Destee, A., Krygowska-Wajs, A., Chartier-Harlin, M.C., Ross, O.A., Rademakers, R. & Farrer, M.J. (2009) Characterization of DCTN1 genetic variability in neurodegeneration. *Neurology*, **72**, 2024-2028.

Voigt, A., Herholz, D., Fiesel, F.C., Kaur, K., Muller, D., Karsten, P., Weber, S.S., Kahle, P.J., Marquardt, T. & Schulz, J.B. (2010) TDP-43-mediated neuron loss in vivo requires RNA-binding activity. *PloS one*, **5**, e12247.

Waibel, S., Neumann, M., Rabe, M., Meyer, T. & Ludolph, A.C. (2010) Novel missense and truncating mutations in FUS/TLS in familial ALS. *Neurology*, **75**, 815-817.

Wang, H.Y., Wang, I.F., Bose, J. & Shen, C.K. (2004) Structural diversity and functional implications of the eukaryotic TDP gene family. *Genomics*, **83**, 130-139.

Wang, I.F., Chang, H.Y., Hou, S.C., Liou, G.G., Way, T.D. & James Shen, C.K. (2012) The self-interaction of native TDP-43 C terminus inhibits its degradation and contributes to early proteinopathies. *Nature communications*, **3**, 766.

Wang, I.F., Wu, L.S., Chang, H.Y. & Shen, C.K. (2008) TDP-43, the signature protein of FTLD-U, is a neuronal activity-responsive factor. *Journal of neurochemistry*, **105**, 797-806.

Wang, J.W., Brent, J.R., Tomlinson, A., Shneider, N.A. & McCabe, B.D. (2011) The ALS-associated proteins FUS and TDP-43 function together to affect Drosophila locomotion and life span. *The Journal of clinical investigation*, **121**, 4118-4126.

Wegorzewska, I., Bell, S., Cairns, N.J., Miller, T.M. & Baloh, R.H. (2009) TDP-43 mutant transgenic mice develop features of ALS and frontotemporal lobar degeneration. *Proceedings of the National Academy of Sciences of the United States of America*, **106**, 18809-18814.

Wils, H., Kleinberger, G., Janssens, J., Pereson, S., Joris, G., Cuijt, I., Smits, V., Ceuterick-de Groote, C., Van Broeckhoven, C. & Kumar-Singh, S. (2010) TDP-43 transgenic mice develop spastic paralysis and neuronal inclusions characteristic of ALS and frontotemporal lobar degeneration. *Proceedings of the National Academy of Sciences of the United States of America*, **107**, 3858-3863.

Wu, D., Yu, W., Kishikawa, H., Folkerth, R.D., Iafrate, A.J., Shen, Y., Xin, W., Sims, K. & Hu, G.F. (2007) Angiogenin loss-of-function mutations in amyotrophic lateral sclerosis. *Annals of neurology*, **62**, 609-617.

Wu, L.S., Cheng, W.C., Hou, S.C., Yan, Y.T., Jiang, S.T. & Shen, C.K. (2010) TDP-43, a neuro-pathosignature factor, is essential for early mouse embryogenesis. *Genesis*, **48**, 56-62.

Xu, Y.F., Gendron, T.F., Zhang, Y.J., Lin, W.L., D'Alton, S., Sheng, H., Casey, M.C., Tong, J., Knight, J., Yu, X., Rademakers, R., Boylan, K., Hutton, M., McGowan, E., Dickson, D.W., Lewis, J. & Petrucelli, L. (2010) Wild-type human TDP-43 expression causes TDP-43 phosphorylation, mitochondrial aggregation, motor deficits, and early mortality in transgenic mice. *The Journal of neuroscience : the official journal of the Society for Neuroscience*, **30**, 10851-10859.

Yan, J., Deng, H.X., Siddique, N., Fecto, F., Chen, W., Yang, Y., Liu, E., Donkervoort, S., Zheng, J.G., Shi, Y., Ahmeti, K.B., Brooks, B., Engel, W.K. & Siddique, T. (2010) Frameshift and novel mutations in FUS in familial amyotrophic lateral sclerosis and ALS/dementia. *Neurology*, **75**, 807-814.

Yang, Y., Hentati, A., Deng, H.X., Dabbagh, O., Sasaki, T., Hirano, M., Hung, W.Y., Ouahchi, K., Yan, J., Azim, A.C., Cole, N., Gascon, G., Yagmour, A., Ben-Hamida, M., Pericak-Vance, M., Hentati, F. & Siddique, T. (2001) The gene encoding alsin, a protein with three guanine-nucleotide exchange factor domains, is mutated in a form of recessive amyotrophic lateral sclerosis. *Nature genetics*, **29**, 160-165.

Zhang, Y.J., Xu, Y.F., Cook, C., Gendron, T.F., Roettges, P., Link, C.D., Lin, W.L., Tong, J., Castanedes-Casey, M., Ash, P., Gass, J., Rangachari, V., Buratti, E., Baralle, F., Golde, T.E., Dickson, D.W. & Petrucelli, L. (2009) Aberrant cleavage of TDP-43 enhances aggregation and cellular toxicity. *Proceedings of the National Academy of Sciences of the United States of America*, **106**, 7607-7612.

Zhang, Y.J., Xu, Y.F., Dickey, C.A., Buratti, E., Baralle, F., Bailey, R., Pickering-Brown, S., Dickson, D. & Petrucelli, L. (2007) Progranulin mediates caspase-dependent cleavage of TAR DNA binding protein-43. *The Journal of neuroscience : the official journal of the Society for Neuroscience*, **27**, 10530-10534.

Zheng, Y., Brady, O.A., Meng, P.S., Mao, Y. & Hu, F. (2011) C-terminus of progranulin interacts with the beta-propeller region of sortilin to regulate progranulin trafficking. *PloS one*, **6**, e21023.

Zhou, H., Huang, C., Chen, H., Wang, D., Landel, C.P., Xia, P.Y., Bowser, R., Liu, Y.J. & Xia, X.G. (2010) Transgenic rat model of neurodegeneration caused by mutation in the TDP gene. *PLoS genetics*, **6**, e1000887.